THE BIOMECHANICAL AND BEHAVIORAL SIGNIFICANCE OF THE NEANDERTHAL FEMUR

by

Kelli Hamm Tamvada

A Dissertation

Submitted to the University at Albany, State University of New York

in Partial Fulfillment of

the Requirements for the Degree of

Doctor of Philosophy

College of Arts and Sciences

Department of Anthropology

2015

The Biomechanical and Behavioral Significance of the Neanderthal Femur

by

Kelli Hamm Tamvada

Abstract

The Neanderthal (*Homo neanderthalensis*) femur is distinct from that of recent modern humans (*Homo sapiens*). Broadly speaking, the Neanderthal femur is more "robust", meaning that it appears to be biomechanically stronger, and it is more curved, which may enhance the predictability of the stresses and strains experienced by the bone. It has been hypothesized that the Neanderthal morphology is an adaptation to withstand elevated and repetitive loads associated with increased mobility. This study tests the mobility hypothesis using comparative and biomechanical methods. Specifically, this study sought to test the mobility hypothesis by a) determining whether or not a relationship exists between skeletal variables and day range (a surrogate for mobility) in living primates, and b) using finite element analysis to quantify differences in biomechanical strength between Neanderthals and modern humans while simulating loads associated with bipedal walking, traumatic loads, and stumbling.

The hypothesis that extant primates with longer day ranges exhibit more robust and more curved bones, used here as an indication of predictability of deformation, is rejected. The hypothesis that Neanderthal femora are as strong as or stronger than recent modern human femora is partially rejected. Under loading regimes simulating normal walking, it is unclear which femur is stronger. The human femur is stronger under simulated traumatic loads. The Neanderthal femur is stronger under loads simulating stumbling. The human femur is more predictable along the neck and at midshaft; the Neanderthal femur is more predictable along proximal and distal diaphyseal sections. The femoral neck is the weakest location on the modern human femur, whereas the distal lateral metaphysis is typically the weakest location on the Neanderthal femur.

Although a relationship between curvature and robusticity variables could not be confirmed using an extant primate sample, the unexpected results of the Neanderthal/human femur comparisons suggest that because regions of peak stress differ considerably between the species as a result of the differences in morphology, each may be adapted to the specific and typical demands imposed by their respective habitats and lifestyles.

Dedication

I dedicate this dissertation to my family and friends who have been supportive of this endeavor from the beginning and I would like to thank each of them for their continued encouragement and understanding.

My parents, Phil and Marie, fostered in me a love of learning for as long as I can remember, and still do. To my husband, Arvind Tamvada, who never failed to understand when deadlines took precedence, and to my son, Jaxon, who is too young to understand. I hope that one day you will and will be inspired to make your own educational journey, whatever that may be.

Finally, I dedicate this dissertation to Dr. Douglas E. Jones, whom I met as a collections assistant at the Alabama Museum of Natural History; he was an inspiration.

Acknowledgements

Although a doctoral dissertation is an individual effort, it is not written without the support of others. I would like to take this space to acknowledge the people and institutions who have aided me in this effort.

First and foremost, my advisor, Dr. David Strait, deserves an immense measure of gratitude because of his never-ending guidance and encouragement. Even prior to officially becoming his student, he began the advising process, and has never quit. Insightful comments and academic direction are a necessary component of advisement, but managing a person is a talent. Thank you, David.

I would like to thank the other members of my doctoral committee, Dr. Adam Gordon and Dr. Sharon DeWitte, for the time and effort each invested in the creation of this dissertation.

I am most grateful for the National Science Foundation (BCS 1060835) for providing the funds that allowed me to collect data at The Powell-Cotton Museum in Birchington, United Kingdom, the American Museum of Natural History in New York City, the National Museum of Natural History in Washington, D. C., and the Cleveland Museum of Natural History in Cleveland, Ohio; and to the staff at these museums for their assistance in coordinating arrangements, providing database access, and allowing me the privilege of working with their primate collections.

The BioMesh Workshop at the University of Massachusetts provided a wonderful education in finite element analysis that facilitated finite element model creation and analysis, and the instructors have continued to be helpful through the years.

Table of Contents

List of Tables

List of Figures

CHAPTER I

INTRODUCTION

The study of human evolution is an important component of anthropology. Paleoanthropologists seek to connect living humans to past populations of humans or other hominins through the study of their physical form. The concept of biological continuity states that there is a common biological thread of descent that connects all living organisms; the study of diversity among hominins and the adaptations that shaped their skeletons provides a comparative perspective to the platform on which we, ourselves, are situated. Understanding the biology of extinct hominins allows us to not only understand our extinct relatives, but also to better understand ourselves and how the physical form that we inhabit came to be. Evolution is a natural process that acts on all living organisms, not excluding modern humans, and a more complete anthropological perspective aids our understanding of the interplay between all of the participants in our global ecosystem. This research focuses on a small aspect of human variation: how Neanderthal and human femoral morphology varies, what the biomechanical consequences of that variation are, and what the biomechanical consequences tell us about differences in behavior between these closely related species. Ultimately, Neanderthals became extinct while modern humans proliferated and have reached a level of global colonization and technical sophistication quite unique among mammals. While this research does not seek to understand why Neanderthals became extinct as modern humans flourished, by contributing to our knowledge of differences in behavior and the selective pressures that lead to skeletal adaptations, it does also help to answer that question.

Paleoanthropological studies of Neanderthals, *Homo neanderthalensis*, and earlier members of the genus *Homo* add an important temporal depth to our understanding of skeletal variation, thus representing an essential element of the literature investigating human variation. Neanderthal skeletal morphology is interesting in its own right, but particularly so because Neanderthals are the closest relatives of modern humans. Thus, inquiries regarding the differences between Neanderthals and modern humans can be narrower in scope than comparisons between humans and other taxa, such as the great apes. Because it is impossible to directly observe Neanderthal behavior, we rely on analyses of their fossilized skeletal material and archaeological remains to gain insights into their behavior. In addition to being the closest relatives of modern humans, Neanderthals are also significant for study because they are the only well-represented hominins that existed sympatrically and contemporaneously with early modern humans, which means that Neanderthal skeletal morphology can be compared to early modern humans without temporal depth being a confounding factor.

Neanderthals have a distinct skeletal morphology that has been described as adaptive for various purposes. The Neanderthal femur is one such skeletal element that exhibits considerable differences from modern human femora (Anthony and Rivet 1907; Boule 1911-1913; Heim 1982; Patte 1955; Schwalbe 1919; Trinkaus 1983; Trinkaus 1993). It is distinct from *recent* modern human femora in that it has 1) a larger degree of antero-posterior curvature, 2) a smaller neck-shaft angle, 3) large articular surfaces relative to limb length, 4) round as opposed to elliptical diaphyseal cross-sectional geometry (i.e., the shape of a bone when viewed as a transverse cross-section), and 5) thicker diaphyseal cortices, or medullary stenosis. Bone tissue is capable of adapting to

changes in applied external forces (Goodship et al. 1979; Jones et al. 1977; Krolner and Toft 1963; Lanyon 1987; Lanyon and Bourn 1979; Lanyon et al. 1982; Lanyon et al. 1979; Nordstrom et al. 1996; Paul 1971a; Ruff 2005; Ruff et al. 2006; Skerry 2000; Taylor et al. 1996a; Tilton et al. 1980; Woo 1981). So, the fact that early anatomically modern humans such as Skhul and Qafzeh, who were approximately equally technologically sophisticated as Neanderthals, express some of these "Neanderthal characteristics" but not all of them (Boule et al. 1934; Sladek et al. 2000; Vandermeersch 1981), suggests that differences between Neanderthal and human femora could result from behavioral differences accrued through way of life (e.g. mobility level) or environmental differences (e.g. topography or relief of terrain), whereas others are likely genetically determined (e.g. cold-adapted body proportions). Each of these variables is capable of altering the mechanical environment in which the femur is loaded, thereby affecting shape.

In this study, I seek to understand the biomechanical significance of different femoral shapes, specifically in regards to Neanderthal and recent human femora. Each of the separate skeletal variables is worthy of investigation, but the femur, like any other bone, is an integrated structure (Bertram and Biewener 1988; Currey 2002) rather than merely a collection of discrete characteristics (e.g. diaphyseal curvature, cross-sectional robusticity or geometry) independently grouped together. In other words, longitudinal curvature occurs inseparably with particular diaphyseal geometries and cortex thicknesses, all of which are responsive to changes in mechanical environments.

Human Femoral Variation during the Pleistocene

Behavior may be inferred from studies of fossil specimens insofar as mechanical loading during life (i.e. through mobility, activity level, subsistence strategies, etc.) affects bone remodeling (Cullinane and Einhorn 2002; Ruff 2005). The effects of externally applied stimuli on bone are discussed in detail in Chapter II, and are consistent across mammalian species; however, it should be noted that at least one study (Abbott et al. 1996) indicates that osteons are smaller in Neanderthal and other early *Homo* species than in recent humans, and also that bone formation rates may be lower among these groups, reminding us that although Neanderthals and modern humans are closely related, there may be physiological differences between the species in addition to gross morphological differences.

Recall that the Neanderthal femur has been described as distinct from anatomically modern human femora in that it has 1) round as opposed to elliptical diaphyseal cross-sectional geometry, 2) a smaller neck-shaft angle, 3) large articular surfaces relative to limb length, 4) a larger degree of anteroposterior curvature, and 5) thicker diaphyseal cortices. As will be discussed below, not all of these differences persist once body mass is taken into consideration or temporal trends are considered. The historical descriptions in the literature, however, have prompted interest in understanding the form of the Neanderthal femur and advances in paleoanthropological methods have led to improvements in techniques of studying these characteristics.

Robusticity

Trinkaus and Ruff (1999) and Trinkaus et al. (1999a) analyzed cross-sectional geometric data for Neanderthals from the Near East and Europe, and early anatomically

modern human (EAMH) femora in an attempt to detect differences in mechanical loads experienced by Neanderthals and EAMHs during life, as a means of interpreting behavioral patterns. Their analyses include adult specimens from Near Eastern (Amud, Kebara, Shanidar, Tabun) and European (La Chapelle-aux-Saints 1, La Ferrassie 1 and 2, Fond-de-Foret 1, Krapina, Neanderthal 1, and Spy 2) Neanderthal sites, and the EAMH sites of Qafzeh and Skhul. They recorded values for total area, cortical area, maximum second moment of area, and the polar moment of area. Cortical area gives an indication of resistance to axial loading, and when compared to total area, indicates diaphyseal robusticity; second moments of area are measures of rigidity relative to bending; and polar moment of area characterizes an object's ability to resist torsion (Trinkaus and Ruff 1999).

Results indicate that percent cortical area (cortical area relative to total area) is only slightly different between Neanderthals and EAMHs, with Neanderthal specimens tending to be more robust, although not significantly so (Trinkaus and Ruff 1999). However, comparisons of cortical areas and polar moments of area to femoral lengths revealed significant differences between Neanderthals and EAMHs. This suggests that Neanderthal femora are absolutely stronger than EAMH femora, which leads to the suggestion that there could be habitual differences in load levels during locomotion. However, previous estimates of body mass related to geographic locale suggest that Neanderthals have hyper-arctic cold-adapted body forms, whereas EAMHs are estimated to have more linear body forms, like their ancestors in Africa (Ruff 1994). When body mass is taken into account, the differences between the two groups becomes insignificant. Neither group is different from Upper Paleolithic modern humans used in the

comparative sample when body mass is considered. Thus, although Neanderthals have absolutely stronger femora according to this analysis, the differences between groups seem to be the result of differences in body mass as opposed to differences in locomotor activities.

Diaphyseal geometry

Differences between Neanderthal and EAMH diaphyseal shape are apparent at mid-distal, mid-shaft, and mid-proximal levels of the femoral diaphysis. All Neanderthal femora in the sample of Trinkaus and Ruff (1999) are more rounded in cross-section than contemporaneous EAMH femora, which have a more elliptical shape. Early anatomically modern humans are characterized by a concavity or flatness on either side of the linea aspera, which is located on a pronounced pilaster of bone (Trinkaus and Ruff 1999). There are differences within the Neanderthal sample regarding orientation of the major axis (i.e., the longest diameter of an ellipse). For instance, the major axis of Shanidar 5 is more antero-posteriorly aligned; Tabun 1 is primarily oriented medio-laterally; and Amud 1 and Tabun 3 exhibit antero-lateral and postero-medial alignment, respectively. Early anatomically modern humans, by contrast, are less variable in this aspect and have generally antero-posteriorly defined major axes. Overall, the diaphyseal cross-sectional shape is distinctively different between the two groups (Trinkaus and Ruff 1999).

Second moments of area are measures of a beam's capacity to resist bending. When Trinkaus and Ruff (1999) compared the second moment of area at mid-shaft (standardized by body mass times bone length), they found that the Neanderthals are slightly more gracile relative to EAMHs in the antero-posterior dimension, but not

significantly more so. However, along the medio-lateral dimension, the Neanderthals are more robust than EAMHs. This is probably due to the circular shape of the Neanderthal femur making it more resistant to bending in the medio-lateral direction than the elliptical shape of the EAMH femur. What this difference implies about the behavior of Neanderthals versus EAMHs is debated. One suggestion is that Neanderthals were more consistently involved in activities that would require them to resist greater medio-lateral bending forces (Trinkaus 1986). Analysis of Neanderthal proximal pedal phalanges lends support to differences in medio-lateral loading patterns between Neanderthals and later humans (Trinkaus and Hilton 1996). A second suggestion is that differences in mid-shaft medio-lateral strength are primarily due to changing hip and pelvic proportions, which would affect bending at mid-shaft (Ruff 1995). Thus, the Neanderthal pelvis must be considered in relation to the EAMH pelvis as there are anatomical distinctions that could have ramifications for bending moments of the femur.

Neanderthals have broad pelves with flaring ilia and medio-laterally long pubic bones (Rak 1991; Trinkaus 1983; Trinkaus 1984), whereas EAMHs have narrow pelves with ilia exhibiting little flare, and medio-laterally short pubic bones (Vandermeersch 1981). The shape of the Neanderthal pelvis is such that the ilio-tibial tract (fibrous reinforcement of the fascia lata originating at the crest of the ilium and running down the femur to insert on the lateral condyle of the tibia) is in a more lateral position relative to that of EAMHs, which may more effectively reduce medio-lateral bending in the femur. Also, the high femoral neck-shaft angles of EAMHs could reduce medio-lateral bending more than lower neck-shaft angles of Neanderthals, meaning the two groups had differing means of compensating for medio-lateral bending.

Femoral curvature

In addition to variation in femoral diaphyseal cross-sectional properties, individuals within the genus *Homo* also vary in the extent to which their femora display anterero-posterior diaphyseal curvature. Among recent modern humans, African femora are typically the straightest and Native American femora are typically the most curved, yet intra- and inter-group variation exists. Neanderthals are described as having femora more curved than modern humans. In fact, with the initial discovery of a Neanderthal femur, controversy arose as to whether the specimen was pathological or normal (Schackelford and Trinkaus 2002). Since then and with the discovery of additional Neanderthal skeletal remains, it has become clear that the characteristic femoral curvature is not pathological. Other theories were proposed in attempts to explain variation in femoral curvature, including race (Stewart 1962), culture/activity (Walensky 1965), muscular insertions (Bertram and Biewener 1988) and hip morphology (Ruff et al. 1993).

Femoral curvature generally sorts into categories of race, implying that some aspect of femoral curvature is genetically controlled (Walensky 1965). Based on results from a study of 874 femora sorted into white, black, Eskimo, and American Indian racial groups, Walensky states that race provides the genetic template and sets developmental limits on how much curvature is modified by function. Accordingly, femoral curvature (in combination with other variables) is widely used in forensic science to help identify human remains (Ballard and Trudell 1999). However, femoral curvature does vary within groups and between sexes, implying that some source of curvature is plastic, responding to mechanical stimuli or the extrinsic environment encountered by the organism over the course of its development and lifespan. In fact, Gilbert (1976) even questions the

accepted practice of using femoral curvature to identify an individual's race. By increasing the number of races investigated by Stewart (1962) and Walensky (1965) to include two South American groups from Ecuador and Peru, Gilbert provides evidence that the interpretation of a genetic basis of femoral curvature is actually a plastic response to body weight, as indicated by the positive correlation between ponderal index and curvature. Most terrestrial mammals exhibit longitudinal curvature in their long bones; this is not specifically a human phenomenon (Bertram and Biewener 1988; Biewener 1983). Perhaps the best experimental evidence of the plastic nature of bone curvature comes from Lanyon's (1980) study of rat tibiae. In this experiment, tibiae of growing rats were deprived of their normal mechanical environment by severance of the sciatic nerve. Although tibiae attained a normal length, they failed to achieve normal weight, thickness, cross sectional shape, or typical longitudinal curvature. The tibiae were straighter than rat tibiae allowed to develop normally according to the demands of the mechanical environment to which they would normally be subjected. Thus, based on studies of differences in femoral curvature associated with specific racial groups (Ballard and Trudell 1999; Stewart 1962; Walensky 1965), it is plausible that some amount of femoral curvature is based in genetics and some is a function of the interplay between force transmission through the bone and the mechanical environment to which a bone is exposed during growth and activity (Gilbert 1976; Lanyon 1980). The exact nature of this relationship is not fully understood.

A study by Shackelford and Trinkaus (2002) compared the degree of longitudinal curvature among and between four groups of hominins. European and Near Eastern Neanderthals (Amud 1, Fond-de-Foret, La Ferrassie 1 & 2, Neanderthal 1, and Spy 2),

EAMHs (Qafzeh 9, Skhul 4 and 6), Early to Middle Upper Paleolithic humans (Cro-Magnon 4322 & 4325; Dolni Vestonice 3, 13, 14, & 16; Nazlet Khater 1; Ohalo 2; Paviland 1; Pavlov 1; and Predmosti 4) and Late Upper Paleolithic to Mesolithic humans (Bruniquel 24; Cap Blanc 1; Gough's Cave 1; Obercassel 1 & 2; Tagliente 1; Tam Hang 534, 537, 538, & 540) comprise the fossil groups. Three samples of recent modern human femora were also used. These are composed of Jomon, Neolithic, and Japanese individuals, representing both gracile and robust groups.

In this analysis, information was gathered on anterior femoral chord length (a measure of diaphysis length that excludes proximal and distal ends), subtense (a measure of curvature defined as the perpendicular distance from the chord to the most anterior point on the femoral diaphysis), and point of maximum curvature (measured as the distance from the proximal origin of the chord to the point of maximum curvature) (Shackelford and Trinkaus 2002). Results indicate that in recent modern human samples, chord length and subtense are not significantly correlated ($p = 0.301$), which indicates that femoral curvature does not correlate well with size. Also, among the recent sample, point of maximum curvature did not significantly correlate with chord length ($p = 0.194$).

However, results from the pooled fossil groups show that femoral length and curvature do significantly correlate ($p < 0.001$), which could be due, in part, to extremes in size within this sample (Shackelford and Trinkaus 2002). The pooled fossil group also shows a significant relationship between point of maximum curvature and chord length ($p < 0.001$). These significant relationships are obviously different than what was observed for the recent samples. Furthermore, the EAMH and Neanderthal groups show more distal points of maximum curvature compared to later fossil humans. Interestingly, t-tests

and p-values of comparisons between Neanderthals and the other groups indicate that Neanderthals and EAMHs are statistically indistinguishable from one another regarding amount of curvature, as are Neanderthals and Early/Middle Upper Paleolithic humans (Shackelford and Trinkaus 2002). However, Neanderthals, EAMHs, and Early/Middle Upper Paleolithic humans are significantly different from Late Upper Paleolithic/Mesolithic and recent humans in their degree of curvature. Finally, Shackelford and Trinkaus (2002) performed pairwise correlations between subtense and body size, femoral angulation, and sagittal knee dimensions. They state that although p-values indicate some statistically significant relationships, the explanatory value of these variables was low (<10%), meaning that "variation in curvature…is not strongly influenced by body size or lower-limb articular positioning" (Shackelford and Trinkaus 2002, pp 367).

This study primarily demonstrates two things: 1) there is only a very weak relationship between femoral curvature and diaphyseal length, and 2) Neanderthals, while having often been touted as exhibiting marked femoral curvature, are indistinguishable from EAMHs as well as Middle and Upper Paleolithic humans regarding this characteristic (Shackelford and Trinkaus 2002). Differences in femoral curvature are only shown between the early fossil hominins and recent modern humans. The point of maximum curvature is also different between early and later groups, being more distally located in Neanderthals and EAMHs. Interestingly, degree of curvature does not correlate with body mass, whereas previous studies have shown that diaphyseal cross-sectional robusticity does correlate with body mass (Trinkaus and Ruff 1999). It is further apparent that there is a temporal trend of decreasing femoral curvature and

robusticity, which some have suggested is associated with decreased mobility beginning in the Late Upper Paleolithic and continuing with the transition to more sedentary horticulturalist and agricultural lifestyles (Holt et al. 2000).

Activity Levels and Predictability

There are several characteristics of the femur that differ between Neanderthals and humans, and may be related to activity level. These include the neck-shaft angle (Trinkaus 1993), diaphyseal cross-sectional morphology and robusticity (i.e. biomechanical strength) (Ruff et al. 1993; Trinkaus and Ruff 1999; Trinkaus et al. 1999b), and diaphyseal curvature (Bertram and Biewener 1988; De Groote 2008; Ruff 1995; Shackelford and Trinkaus 2002).

Given the plastic nature of these traits in sub-adults, they may be indicative of activity levels during development (Cowgill 2010; Cowgill 2014b; Cowgill et al. 2010; Trinkaus 1993). For example, human infants are born with high neck-shaft angles, but as load bearing begins, the angle decreases. Modern humans have a higher neck-shaft angle than Neanderthals, and this difference in angle will affect the transmission of body mass forces through the acetabulum to the femoral diaphysis.

Diaphyseal robusticity is related to activity levels in that frequent loading induces bony changes meant to reinforce the strength of the bone, usually through bone deposition on the periosteal surface, e.g., (Goodship et al. 1979; Hert et al. 1971; Hert et al. 1972; Lanyon and Baggott 1976; Lanyon et al. 1979). When elevated activity levels are a consequence of locomotion, those activity levels may be associated with increased mobility. Studies of femoral robusticity indicate that Neanderthals have an absolutely

stronger femoral shaft than modern humans and there is a trend in decreasing robusticity through time that is associated with technological sophistication (Ruff et al. 1993).

Aspects of shape, such as cross-sectional geometry and longitudinal curvature, serve to elevate and influence the predictability of stress transmission through the shaft by (Bertram and Biewener 1988). A trade-off exists between a bone's strength and its predictability in bending (Jade et al. 2014). Although load carrying capacity and curvature are inversely related, bending predictability and curvature are positively correlated, and predictability of stress transmission may be an important adaptation to resisting eccentrically directed loads which could lead to bone failure (Bertram and Biewener 1988; Biewener et al. 1983). Neanderthal femora display a more circular as opposed to elliptical diaphyseal cross-section, whereas modern humans have an antero-posteriorly elongated diaphyseal cross-section, but Neanderthal femora are more longitudinally curved than modern human femora. The consequences of these shape differences could represent different means of providing structural support.

There are three means by which a bone may reinforce itself: overall size, cross-sectional shape, and longitudinal curvature. Therefore, Neanderthal and human femora, encompassing differences in each of these three categories, in addition to differences in neck-shaft angle, must be analyzed as composite, integrated structures.

Structure of dissertation and hypotheses

This dissertation seeks to answer questions regarding the biomechanical significance of shape and size differences between Neanderthal and modern human femora using a novel, multifaceted approach. Initially, the reader will be introduced to

bone on the molecular, cellular, tissue, and organ level in Chapter II: Bone Biology. This chapter details how bone is organized on different levels and how it is initially formed and then maintained throughout the life of an organism. Experiments conducted on mammalian bone will be reviewed in order to establish the adaptive nature of bone, that is, how and why bone tissue responds to the mechanical environment in which it is habitually exposed in order to maintain an ideal compromise between the physiological investment of an organism and strength against catastrophic failure that could result in death or reduced fitness. Given this characteristic of bone tissue, Chapter II also includes a discussion on the roles of robusticity (strength) and predictability in preventing bone failure, as well as an introduction to specialized terminology that will be used throughout the entire dissertation. That bone tissue changes according to its mechanical environment has important ramifications insofar as the differences between modern human and Neanderthal femora elucidated in the preceding pages of this chapter have been attributed to differences in mobility levels. It stands to reason that more mobile species would be detectable by either increased femoral robusticity, or femora that respond to variable or eccentric loads in a more predictable manner. Thus, Chapter III: An Inter-generic Comparative Primate Study, documents the relationship between mobility and long bone strength/predictability. Humeri and femora of five primate genera were examined and a correlation between skeletal variables and mobility was sought in order to test the hypotheses that animals that range farther have 1) stronger, more robust bones and 2) bones that behave in a more predictable way (using longitudinal curvature as an indicator of predictability) compared to animals with more limited ranges. Finite element analysis is the method used to conduct many experiments in this dissertation, therefore Chapter

IV: A Validation Study, introduces the reader to finite element analysis as a method, and also documents the validation experiment conducted to test the biological accuracy of the human femur model used to carry out the experiments of Chapter V. Chapter V: FEA of a Human and Neanderthal Femur, reports on strength and predictability of human and Neanderthal femora, specifically, as evidenced through a sophisticated series of experiments designed to test predictions associated with size and shape differences between the two species. These experiments test the null hypotheses that Neanderthal and modern human femora are 1) equally robust, and 2) deform equally predictably in the face of loads associated with normal bipedal walking, trauma, and stumbling. The final chapter summarizes the findings of the and contextualizes it in relation to a very old idea in paleoanthropology, that the Neanderthal femur is highly robust and "designed" to withstand elevated activity levels associated with increased mobility due, perhaps, to less technological and/or biological sophistication relative to modern humans.

CHAPTER II

BONE BIOLOGY

A description of femoral variation during the Mid-Upper Pleistocene and the hypotheses that have been proposed to explain these differences were discussed in the preceding chapter; however, in order to better understand the rationale behind many of these ideas, one must consider the material properties of bone tissue and how it reacts to external stimuli. This chapter explains basic principles of bone biology, including bone composition, bone material properties, animal studies indicating the adaptive nature of bone tissue, and a discussion of beam theory and ideas that have been proposed to explain the role of bone curvature in mammalian limbs.

Bone composition and material properties

Living human bone tissue is primarily composed of a fibrous protein structure made of collagen that is surrounded by the inorganic mineral calcium phosphate. Calcium phosphate crystals and water fill the spaces within the collagen structure. Additionally, there are noncollagenous proteins that account for approximately 10 to 15 percent of protein found in bones. Together, these parts are known as bone matrix (Currey 2002).

Bones are composed of living tissue with different kinds of cells, each of which has its own function. Cells line all surfaces of a bone in a continuous sheath. Cells lining the exterior of a bone form a sheath that is known as the periosteum. Conversely, cells that line the interior of a bone, such as the medullary cavity, form a sheath that is called the endosteum. It is from the endosteum that osteoblasts are generated. Osteoblasts

function to create bone by depositing the collagen structure (osteoid) that is subsequently mineralized. Osteocytes are immobile cells that reside in the bone matrix and are derived from osteoblasts. They communicate with periosteal and endosteal cells, as well as other osteocytes, by means of small processes that travel through channels in the bone (canaliculi). The density of osteocytes within bone varies between species and between locations within one individual. A third kind of bone cell is the osteoclast. Osteoclasts are large, multi-nucleated cells derived from precursor cells floating in the bloodstream (Currey 2002). The role of osteoclasts is to destroy bone, which they do by dissolving it and transferring the waste via cellular vesicles to the space above which the underlying bone is dissolved.

Human bone exists in varied forms at different organizational levels. All human bone is either woven, lamellar, parallel-fibered, or some combination of these types, each of which has its own material properties. Woven bone is the form of bone that is initially deposited when bone is being created and is deposited quite rapidly, at a rate of four or more micrometers a day. It is most commonly found as fetal bone and as the bone callus that initially forms in the event of a fracture. It is highly mineralized but quite porous. Woven bone fibers are randomly oriented, with osteocytes loosely encased within.

Lamellar bone differs from woven bone in its rate of deposition, fibril orientation, degree of mineralization, and appearance. Lamellar bone is laid down more slowly than woven bone (about one micrometer per day), and its fibrils are consistently organized in sheets, called lamellae, with alternating thicknesses. Lamellae are composed of small sections of similarly oriented fibrils, and are less mineralized than woven bone.

The last form of bone at this level is parallel-fibered; it is intermediate in organization and form between woven and lamellar bone. Its fibrils are more organized than those of woven bone, but it is more highly mineralized than lamellar bone.

The three forms of bone discussed above can exist in isolation of one another, or in combination. Fibro-lamellar bone is a combination of woven or parallel-fibered bone and lamellar bone. When fibro-lamellar bone is initially being formed, woven or parallel-fibered bone is deposited around blood vessels near the surface of a bone, forming a cavity. Eventually, lamellar bone is laid down on the inside of the cavity within the woven/parallel-fibered bone. Woven/parallel-fibered bone continues to be deposited on the surface and lamellar bone continues to fill the original cavity until primary osteons are formed. This sequence is repeated over many layers with the first layer eventually becoming deep to the bone's surface. Fibro-lamellar bone can be deposited very quickly and is structurally stronger than woven bone, thus its advantage is that it combines the strength properties of lamellar bone with the rapid rate of deposition of woven bone.

Some forms of bone may be remodeled, transitioning from primary to secondary, but not all forms of bone have this capacity. Remodeling can happen in two ways. Either the primary bone is eroded and replaced from the surface of a bone, or Haversian systems can be formed within the bone. Haversian systems (sometimes called secondary osteons) are formed by osteoclasts and osteoblasts as part of the remodeling process. Several osteoclasts join together to form a cutting cone. The cutting cone targets a specific section of bone called a basic multicellular unit and quickly erodes the unit into a cylindrical void that is rapidly filled with new bone by osteoblasts. A cement sheath, or

cement line, through which canaliculi may pass, is formed as osteoclastic activity ceases, but before osteoblastic activity begins. The osteoblasts make the internal surface of the cavity smooth and deposit bone in concentric rings. Blood vessels and nerves are located at the center of the cavity.

The formation of Haversian systems is not the only manner in which primary bone can be changed into secondary bone. In some cases, osteoblasts do not immediately fill the cavity created by the cutting cone. Osteoblasts may only fill one side of the cavity as the cutting cone continues through the bone. This is called a drifting osteon because the central cavity created by the cutting cone "drifts" through the bone leaving behind it a trail of new, secondary bone deposited by osteoblasts. Primary and secondary bone have different mechanical properties; Haversian bone is weaker in loading than is primary bone (Currey 2002). It is unclear if secondary bone that is formed by drifting osteons also has different mechanical properties as it has not been thoroughly studied.

Finally, bone may be either cortical or cancellous (trabecular). In young individuals, cancellous bone is composed of woven or parallel-fibered bone, but in adults this bone has been replaced with either primary lamellar or Haversian bone. Cancellous bone varies between locations in its fine-scale structure, its large-scale structure, and its porosity. The strut-like components of cancellous bone are called trabeculae. Trabeculae can be plate-like or cylindrical and they make connections with other trabeculae, usually at right angles to one another. Cancellous bone can be more or less organized; at simpler levels, trabeculae are cylindrical and randomly oriented, but at more complex levels they exhibit a high degree of anisotropy and are usually more plate-like in structure. The organization of cancellous bone is not strictly limited to one form of trabeculae or the

other; cylindrical and plate-like trabeculae can exist in varying ratios. Finally, cancellous bone can be composed of long sheets of lamellar bone that form tubular structures connected by small openings in the sheets. Small struts of bone orthogonally connect the sheets to one another. The various organizations and structures of cancellous bone are thought to exhibit different mechanical properties. The simpler types of cancellous bone are usually found deep to the surface of bones, thus being farther from the loading surface, while more organized cancellous bone is found just underneath the loaded cortical surface of bones (Currey 2002), as in the distal end of the femur.

As mentioned above, cancellous bone exists with various degrees of porosity. In humans, the space between trabeculae is usually filled by marrow, but in other species this may not be the case. According to Currey (2002), porosity of cancellous bone exists from almost 100 percent to 50 percent, but below 50 percent porosity it is hard to distinguish cancellous bone from cortical bone. Cortical bone is essentially solid lamellar bone with spaces existing only for canaliculi, osteocytes, blood vessels, and in the case of bone undergoing remodeling, erosion cavities. Mechanical properties of bone are considered at two levels, material and structural. Material mechanical properties are defined by characteristics at the tissue level, whereas structural mechanical properties are defined by a bone's characteristics at the organ level; however, the distinction between the two is not always clear and a failure of the tissue may or may not result in failure of the entire structure. Failure of the structure, i.e., when a bone experiences a fracture, necessarily involves tissue failure, meaning that both material and structural mechanical properties were overcome (Cullinane and Einhorn 2002).

Mechanical Terms

In order to understand the following studies of bone remodeling and results generated through hypothesis testing in subsequent chapters, it will be informative to first define some relevant terminology. When a force is applied to an object, the object will experience acceleration and/or deformation. If the object is not allowed to move, due to a constraint, an internal resistance will develop due to the opposing forces the object subsequently receives. This internal resistance is known as *stress*, and can result in deformation, which is quantified as *strain* (Cullinane and Einhorn 2002). Stress is measured as a unit of force (e.g. Newtons (N)) per unit of area (e.g. square meters (m^2)), and is typically given in Pascals (Pa). One Pa equals 1N per $1m^2$, however this dissertation will measure stress in megapascals (MPa); one MPa equals 1,000,000 Pa. There are three primary types of stress; more complex stresses can be broken down into some combination of these types (Cullinane and Einhorn 2002). *Normal stress* is the intensity of a force perpendicular (or normal) to a given plane of material. *Tensile stresses* are normal stresses that cause traction or tension on the surface of a plane and are resisted by intermolecular attractive forces which resist an object being pulled apart, whereas *compressive stresses* are normal stresses that push against the plane and are resisted by interatomic repulsive forces (Cullinane and Einhorn 2002; Popov 1978). *Shearing stress* results when two forces that are parallel but opposite act on a given plane, and can be either linear or rotational (Cullinane and Einhorn 2002; Popov 1978). As stated previously, these three basic types of stress occur in combination with one another and can result in more complex types of deformation: torsion and bending.

Most simply defined, *strain* (ε) is deformation per unit of length as a function of applied force and the resulting stress. Although it is a dimensionless quantity, strain is reported as a percent or as meter per meter units (Popov 1978); thus, ε = (deformed length – original length)/original length (Cullinane and Einhorn 2002).

The product of a force times its lever arm, the distance from the point of in-force to the pivot (or joint), is called the turning force, or *torque.* In bones, torque can result from muscle action or gravity. *Torsion* is the result of torque causing twisting or bending in a shaft. Externally applied torques are balanced by internal resisting torques in the material, thereby making the external and internal torques equal in a static shaft (Hildebrand 1995). The *polar moment of area* is a measure of an object's ability to resist torsion.

Bending forces cause compression on the concave surface of a bent shaft, and tension on the convex surface (Cullinane and Einhorn 2002). The *second moment of area* is a measure of an object's ability to resist bending, and depends not only on the beam's load, but also on its cross-sectional geometry. Material distributed farther from the bending axis has a greater impact on the beam's ability to resist bending than material that is closer to the bending axis. Beams with higher moments of area are better able to resist loads than those with low measures. Both polar moment of area and second moments of area are used to measure robusticity, i.e., strength of bones.

The properties of materials can be characterized in part by examining the characteristic relationship between stress and strain for that material when it is subjected to particular types of loads (axial compression, axial tension, shear, etc.) Conventionally, stress is plotted along the y-axis and strain along the x-axis. When the slope of the stress-

strain curve is linear, the material is behaving elastically; thus once the forces are removed from the material, it will return to its original shape, having undergone no permanent deformation. *Young's modulus (E)* can be calculated by dividing stress by strain at any point along the initial, linear segment of a stress-strain curve. Young's modulus is used to describe an object's stiffness or rigidity, i.e., an object's tendency to deform along an axis when forces are applied along that axis. *Poisson's ratio (ν)* describes how much the sides of an object will contract or expand laterally during tensile or compressive axial loads, respectively. It is calculated as lateral strain divided by axial strain. The quantity that describes a material's stiffness under shear stress is the *modulus of rigidity (G)*, or *shearing modulus of elasticity*. Generally speaking, the modulus of rigidity is the ratio of shear stress to shear strain. When a material undergoes a relatively small elastic deformation, *G* can be defined as shearing stress divided by distortional angle (Blake 1990b). According to Blake (1990b), because of the constant mathematical relationship between *E*, *G*, and *ν*, as the ratio of *G* to *E* decreases, *ν* increases. There is a straightforward relationship between these variables for isotropic materials, but note that bone is an anisotropic material, which means that its elastic properties vary by axis. Whereas isotropic materials exhibit identical *E*, *G*, and *ν* regardless of the axis of load orientation, these variables will differ in bone depending on the load orientation. Determining *E*, *G*, and *ν* in anisotropic materials is not simple. Experimental studies of cranio-facial bone have shown that bone's material properties vary not only between individuals, but also between regions within a single bone (Peterson and Dechow 2003; Wang and Dechow 2006). In fact, *E* is different for each axis in an anisotropic material, as are *G* and *ν*. However, all regions of bone are not equally anisotropic, and in some

areas bone is nearly orthotropic (Wang and Dechow 2006), in which cases the most important elastic properties are E_1, E_2, E_3, G_{12}, G_{31}, G_{32}, v_{12}, v_{13}, and v_{23}. For G and v, the first number of the subscript indicates the axis of the applied load and the second indicates the response direction. In a general anisotropic linear elastic solid, there are 21 independent elastic constants, as derived from reducing stress and strain matrices that indicate the relationship between stress and strain in response to a given load according to Hooke's Law. In order to ease computations needed for modeling bone in FE models, a factor in subsequent chapters of this dissertation, and also because thorough data on anisotropic elastic properties of bone at all locations along a femur do not exist (Wirtz et al. 2000), bone is often modeled simplistically as an isotropic material, although this simplification is not without consequences (Strait et al. 2005). Specifically, comparisons of macaque finite element models with differences in material properties (testing accuracy of both pattern and magnitude of strain) to validation data indicates that finite element models are robust with respect to overall strain patterns, despite differences in material property modeling, but that quantitative comparisons require higher precision. However, it also appears that using material property data from the species of interest and the skeletal element of interest are perhaps more important than modeling the true anisotropic nature of the material (Strait et al. 2005).

The point at which the slope of the stress-strain curve departs from linearity gives the material's elastic limit, or *yield point,* and beyond this point the material will behave plastically, experiencing permanent deformation, even upon the removal of the load (Cullinane and Einhorn 2002). Bone behaves plastically when loaded in its longitudinal

direction, but when subjected to loading in its transverse direction, it does not (Reilly and Burstein 1975).

A material's *strength* can be calculated by finding the maximum stress at the point of failure. This would be called ultimate tensile, compressive, or shear strength depending on the loading conditions bringing about failure. The amount of strain present at the point the material fails indicates the *ductility* of a material. *Strain energy* can be calculated by finding the area under the linear portion of the stress-strain curve, and indicates the material's *toughness*. The amount of energy invested in a material prior to its yield point is recoverable, and indicates the material's r*esilience*, or ability to store elastic energy. The higher the bone's resilience, the more stress it can withstand before changing from elastic to plastic deformation. Although not typical of healthy bone, pathological bone may be brittle. *Brittle* materials fail at the material's elastic limit, or yield point, rather than undergoing plastic deformation. Thus a brittle material's ultimate strength and yield point are the same value (Cullinane and Einhorn 2002).

As stated previously, bone is anisotropic, meaning that its structural elements are not all homogenously organized (Cullinane and Einhorn 2002; Currey 2002). This means that the orientation of forces will greatly affect the ability of bone to resist loads. Typically, bone is strongest in the direction it is most often loaded, and this is certainly true of cortical bone of the femoral diaphysis, where it was found that osteons are longitudinally oriented, providing an indication of the bone's loading history (Hert et al. 1994). Bone is stronger under compressive loads than tensile or shear loads (Currey 2002), thus a femur is better able to resist compressive forces applied along its

longitudinal axis (as happens during normal walking) than forces applied transversely to the shaft.

A study of cortical bone gathered from individuals ranging in age from 19-80 years found the following average values of ultimate strength in humans: ultimate longitudinal strength in tension is $135*10^6$ N/m^2 and in compression is $205*10^6$ N/m^2; ultimate transverse strength in tension is $53*10^6$ N/m^2 and in compression is $131*10^6$ N/m^2; ultimate transverse strength in torsion is $68*10^6$ N/m^2 (Reilly and Burstein 1975). Trabecular bone is less stiff than cortical bone because it is more porous, but it is better able to withstand higher levels of strain (Cullinane and Einhorn 2002); and like cortical bone, it is stronger in compression than tension. The ultimate strength of trabecular bone is location specific. It has been shown that within a specific site, yield strain is uniform, but significant differences exist across sites (Morgan and Keaveny 2001). Additionally, trabecular bone within the femoral neck (n = 27) was found to be stronger than in the greater trochanter (n = 23), proximal tibia (n = 31) or vertebral bodies (n = 61) (based on bone samples from 61 donors ranging in age from 52 to 82 years) (Morgan and Keaveny 2001).

Bone is *viscoelastic*, probably due to its water content (~8%), which means that it experiences material flow under sustained stress. This has important ramifications for bone remodeling in that the rate at which a load is applied will significantly impact bone's behavior. At high loading rates, bone experiences lower ultimate strength, whereas under low loading rates, or a statically applied load, the ultimate stress is much higher, helping to explain the results described below on the importance of strain rate to

remodeling rate (Cullinane and Einhorn 2002; Hert et al. 1969; O'Connor and Lanyon 1982; Turner et al. 1995).

Experiments conducted in later chapters of this dissertation will discuss bone strength in terms of von Mises stress, because it has been shown that von Mises stress is the best indicator of when a ductile material will fail (Blake 1990a; Keyak and Rossi 2000), rather than the more conservative normal stress theory, so it is worthwhile to mention von Mises stress here. Von Mises stress is an index, or equivalent stress, technically termed the *von Mises-Hencky criterion of ductile failure* or *distortion energy theory*. It describes the combination of the three principal stresses acting on a given point of a structure and is calculated according to the formula $[(S1-S2)^2 + (S2-S3)^2 + (S3-S1)^2 = 2Se^2]$, where S1, S2, and S3 are the principal stresses acting along the x, y, and z axes and Se is the equivalent, or von Mises stress (Blake 1990a). Von Mises stress is important because it has been found that even if none of the principal stresses by themselves attain the yield point of a material, the combination of them could result in failure.

Bone: an adaptive tissue

During bone modeling, the entire shape of a bone may be changed, as bone can be either removed or added to the external and internal *surfaces*. Remodeling, however, refers to a slightly different process. Remodeling can affect any region of a bone, not just surfaces, but also the internal bone. The means by which bone senses strain are currently not well understood. Skerry (2000) and Currey (2002) note that theories promoting such explanations as electrical and magnetic influences on cell behavior are controversial and

variable, although others find this avenue of theory more promising (Lanyon and Baggott 1976). It does seem clear, however, that osteocytes register deformation of the matrix and subsequently signal surface osteoblasts, which then initiate bone formation, maintain existing levels of bone, or signal osteoclasts to commence bone resorption (Skerry 2000).

Frost (1987) introduced the concept of a "mechanostat", in which he attempted to explain general changes involved in modeling and remodeling. According to this concept, simple processes lead to higher order changes. First, since modeling generally adds bone over large surfaces, modeling increases bone mass. Bone subjected to strains above the threshold of the minimum effective strain (i.e. the minimum strain required to induce modeling), increases modeling, and thus also increases bone mass. Remodeling, however, does not entirely replace the original bone, thus reducing bone mass. Very low activity levels lead to strains below the minimum effective strain, thereby preventing modeling but increasing remodeling, thus reducing overall bone mass. Bone may also be subjected to stresses that generate strains less than the minimum effective strain but large enough to prevent massive remodeling. In this situation, neither modeling nor remodeling occurs; the bone tissue is in stasis.

Bone remodeling in mammals

Several studies of bone remodeling are reviewed here; however, note that it is important to bear in mind the critique that surgical procedures themselves may have an effect on the remodeling process, so experimental results should be interpreted with that in mind (Ruff et al. 2006). Despite their limitations, these studies undoubtedly provide significant insight into the remodeling process.

Currey (2002) notes that bone can adapt to changes in functional loading in two ways. Either the bone shape (i.e. architecture) can change, or the mechanical properties of the bone (i.e. quality) can change. In two experiments, Woo (1981) explored the possibility of either of these reactions. The first experiment involved surgically attaching either stiff or flexible steel plates to dog femora. After a year's time, the plates were removed and standard sized strips of bone were sampled from control dogs and dogs to which both stiff and flexible plates had been attached. Although the strips of bone were uniform in width and height, the depth of the strip was the entire depth of that particular dog's cortical bone. Results showed that bone with the flexible plate showed no change from control bone in the maximum bending moment and the area under the load-deformation curve (used to measure the amount of energy absorbed before failure), while bone that received the stiff plate treatment was weaker and absorbed less energy. None of the bone in this study, despite the treatment it received, showed any changes in Young's modulus (stiffness) or tensile strength. They found that bone receiving the stiff plate was thinner, and this entirely accounted for changes in the bone's properties. Thus, bone architecture was affected rather than bone quality.

In a second experiment, Woo (1981) sought to observe the effect of increasing activity level. To this end, they trained an experimental group of pigs to trot about 40 kilometers per week for eight months. The control group of pigs was allowed to behave normally. After the eight month period, strips of cortical bone (standard in width and height, but of individual cortex depth) were removed from both the experimental animals as well as the control animals, and the maximum bending moment and area under the load-deformation curve were tested. Results in this experiment were similar to results in

Woo's (1981) first experiment: bone from the experimental group was able to absorb more energy and bear a larger load than bone from the control animals. Again, neither Young's modulus nor tensile strength had been affected. Furthermore, the bone matrix was similar between groups. Woo's (1981) experiments demonstrate that *bone quality does not change* due to additional support for the bone or due to increased loading. Instead, *bone architecture is altered* so as to be better suited for a novel or modified purpose.

Goodship et al. (1979) designed an experiment to manipulate the magnitude of strain experienced by a bone in order to understand its effect. In this case, peak strains were measured in pig radii during normal locomotion and after a portion of the ulna in one forearm was surgically removed. The intact forearm acted as the control. Strains in the radius were measured via strain gauges attached to the surface of the bone. Removing part of the ulna resulted in peak strains on the radius being approximately doubled compared to the control forelimb. Following this procedure, there was rapid growth of woven bone on the radius, which resulted in the radius becoming round rather than elliptical in cross-section and a subsequent lessening of peak strain. Eventually both the control radius and the experimental radius experienced comparable strains. This indicates that bone has the potential to modify itself in order to maintain an acceptable level of strain.

Similarly, Lanyon et al. (1982) performed an experiment on sheep forelimbs whereby they removed a portion of the ulna. Their results indicate that by the end of the trial, the experimental limb exhibited *less* strain than the control limb, with the remodeling process being completed between six and 12 months post-surgery.

Furthermore, bone on the cranial surface (subjected primarily to tension) was less remodeled than bone on the caudal surface (subjected primarily to compression), even though the cranial surface experienced much more strain; a result that they conclude possibly indicates the importance of strain *distribution*, rather than total strain *magnitude*.

Lanyon et al. (1979) conducted a study on sheep forelimbs to determine the relationship of mechanical stress (due to functional activities) to bone remodeling. They attached strain gauges to the cranial (subjected to tensile strains) and caudal (subjected to compressive strains) cortices of 18 adult sheep and recorded data during locomotion. They then analyzed bone segments cut from the radii of these sheep and recorded data for strain rates, ash content, Young's modulus, and amount of remodeling. Results indicate that the peak compressive strain was 1.8 times greater than the peak tensile strain. Furthermore, bone from the caudal surface had a lower elastic modulus and, when burned, had lower ash content. This shows that the bone subjected to compressive strains was less stiff, perhaps due to less mineral content, as indicated by the lower ash content. Increased remodeling in the more highly strained cortex, could account for the decreased mineral content and subsequent lower ash content (Frost 1987).

As the above studies indicate, it is clear that bone responds to external stimuli, but which loading factors (absolute magnitude, rate, frequency, or some combination) are most important to inducing the remodeling process? Hert et al. (1969) designed an apparatus to allow them to subject the tibiae of 20 growing rabbits to bending stress, measure the subsequent curving of the bone and its changes, and regulate an applied force of up to five kilograms. During the experiment, the compressors were adjusted so that at first each tibia was subjected to 1.0 to 1.5 kilograms of force. Force was gradually

increased until the devices were kept at 3.0 to 5.0 kilograms of force. The rabbits were x-rayed at regular intervals and a select group was injected with a chemical that allowed growth intensity and bone reconstruction to be observed. Two rabbits were sacrificed after two months; six were kept for between 135 and 403 days. At the end of the experiments, x-rays showed that while the rabbits were growing, the tibia developed a slight curve due to the enforced bending. After growth ceased, however, the bones developed no further bending deformation. Moreover, histological examinations revealed that after two months there was no change in the rate of endosteal or periosteal apposition due to the loading, and there was no increase in secondary osteon formation between the control and experimental limb. However, after 13 months, they report thinning of the bone on the anterior and posterior surfaces due to surface remodeling and internal reconstruction of the strained portion of bone, which they attribute to atrophy of the relevant muscles in the anterior and posterior aspects of the leg. Hert and colleagues (1969) thus demonstrated two things: 1) application of static loads does not result in significant remodeling; loads must be applied dynamically and 2) growing bone and mature bone do not respond to stimuli to the same degree; growing bone is more responsive.

To further evaluate the importance of factors influencing bone remodeling, a study subjecting rat tibiae to bending was conducted by Turner et al. (1995). In this study, Turner and colleagues (1995) divided 32 mature rats into four groups. Each group was exposed to daily bending of their right tibiae with a peak applied load of 54 Newtons (N) for all groups. Left tibiae were used as controls. The cyclic fraction of the load was varied such that it was zero N in the first group (meaning the applied force was static), 18

N in the second (the force increased from zero to 54 N then decreased by 18 to 36 N before the next cycle began), 36 N in the third (the force increased from zero to 54 N then decreased by 36 to 18 N per cycle), and 54 N in the fourth (the force increased from zero to 54 N each cycle). These parameters were such that the tibiae from the first group would experience zero changes in strain ($\Delta\varepsilon$) per second, the second would experience 0.0013 $\Delta\varepsilon$ per second, the third would experience 0.026 $\Delta\varepsilon$ per second, and the fourth group would experience 0.039 $\Delta\varepsilon$ per second.

The authors (Turner et al. 1995) measured the lamellar-bone-forming-surface, which was used to detect the percentage of the bone surface that was actively forming bone; mineral apposition rate; and lamellar bone formation rate. Results show that bone formation rate was significantly higher in experimental tibiae of groups three and four ($p = 0.01$) and mineral apposition rate was significantly higher in experimental tibiae of groups two through four ($p = 0.02$). However, there was no difference between limbs of any groups in regards to the relative percent of bone surface forming new bone. This means that maximum bone formation was stimulated by maximum strain rate. The groups subjected to the largest changes in applied force were the groups with significantly increased remodeling. This shows that although peak strain magnitude is an important contributing factor to remodeling, the difference between the minimum and maximum strain magnitude in cyclical loading is more important.

Another animal study investigating the role of strain rate on adaptive bone remodeling (O'Connor and Lanyon 1982) corroborates the results of Turner et al. (1995) by demonstrating that the ratio of the maximum rate of change in strains between artificial loading and normal locomotion was the primary cause (68-81 percent explained)

of bone surface remodeling. Regarding the requirement of a dynamic loading regime, the rate at which strains are produced is the primary factor inducing bone remodeling. Thus, it seems that magnitude of strain may not be as important to remodeling as the rate of applied loads, although larger magnitudes of change in strain do produce larger effects than smaller magnitudes of change. The rate and frequency of applied loads are most important in inducing remodeling (O'Connor and Lanyon 1982; Skerry 2000).

Lanyon (1980) designed an experiment in which he sought to understand the influence of mechanical function on the ontogenetic development of bone curvature by depriving an experimental group of young rats of normal mechanical function by severing the sciatic nerve and sectioning the patellar tendon of one of their hindlimbs, thereby inhibiting loading due to muscle activity and weight bearing. A control group of the same age was raised and used for comparative purposes. After the rats had completed growth, their limbs were dissected.

Results showed that there were no contra-lateral differences between limbs of the control animals with regards to muscle weight, bone weight, bone length, bone width, or bone curvature. However, in the experimental group, there were significant differences between the normal hindlimb and the altered one with respect to muscle weight, bone weight, bone width, and bone curvature, but there was no difference in bone length. The tibial cross-section from the control limb was triangular (same as with the control animals), but the tibia from the altered limb was more rounded in cross-section. It seems, then, that a bone's overall shape is genetically determined, but it only achieves its normal shape in the presence of a normal loading environment. Regarding the development of bone curvature, Lanyon (1980) proposes two explanatory hypotheses: 1) the

accommodational hypothesis which states that muscles surrounding the bone exert force on the periosteum that results in longitudinal curvature so as to spatially accommodate muscle bellies and 2) the bone strain hypothesis which suggests that there is a physiological benefit with regards to optimal fluid flow through bone that is only engendered if the bone is curved since curvature increases strain. However, these hypotheses may not be mutually exclusive: muscles exert force on bones resulting in curvature, and curvature is beneficial to fluid flow due to increased strain, but the degree of curvature must not exceed a certain level or strain will increase to near catastrophic levels. In either case, normal curvature is beneficial and only develops in a normal loading environment.

Hert et al. (1969) demonstrated in rabbits, as discussed above, that bone is much more responsive to bending during growth than after growth has ceased. Genetics certainly play a role in proper bone formation, but bones must also be exposed to a normal mechanical environment in order to develop properly. The bones in the hindlimbs of Lanyon's (1980) rats that were deprived of their normal developmental environment lacked the normal curvature and cross-sectional geometry of the control rats. Whether this curvature is due to opposing muscle forces or because there is some physiological benefit of increased fluid flow through bones as a result of bending is not entirely clear. However, the fact that long bones in mammals are normally curved to some extent when allowed to develop in a normal mechanical environment is not debated. Moreover, the ability of bone to adapt to new loading circumstances during life through remodeling proves that mobility levels could affect a bone's size and shape in order to maintain a desired degree of strain.

Bone remodeling and mobility

Because bony responses to mechanical loading, particularly the rate and frequency of loading, are well documented (Goodship et al. 1979; Hert et al. 1971; Hert et al. 1969; Hert et al. 1972; Jones et al. 1977; Krolner and Toft 1963; Lanyon 1987; Lanyon and Bourn 1979; Lanyon et al. 1982; Lanyon et al. 1979; Nordstrom et al. 1996; Paul 1971b; Ruff 2005; Ruff et al. 2006; Skerry 2000; Taylor et al. 1996b; Tilton et al. 1980; Woo 1981), bones are thought to be useful sources of information for understanding activity levels in populations or organisms whose activity cannot be directly observed. The more an animal travels, the more frequently it subjects its skeletal elements (particularly limb bones) to strain resulting from locomotion. This elevation in strain will result in more extensive remodeling relative to that resulting from a more sedentary state. Remodeling can either add or take away bone, of course, but increasing either the frequency or rate of loading will result in more bone being deposited, thus increasing strength. This relationship is a fundamental concern of the present study. However, the relationship is not necessarily a straightforward one, as there are many factors that can impact overall morphology and they are not always simple to determine, let alone quantify and explain. Even the definition of mobility is one that has received much attention lately (Carlson and Marchi 2014) and is shaded with complexity. Whether mobility is defined as linear movement across a landscape (Carlson et al. 2007), or considers vertical and horizontal landscape differences as well, factors such as load magnitude, frequency of travel, and travel intensity (which can be influenced by such things as substrate angle, speed, and terrain unevenness) play a role in determining final bone shape and size. How these factors relate to one another is still being explored.

For instance, Sparacello et al. (2014) cite high rigidity in fibulae of Late Upper Paleolithic, Neolithic, and Iron Age groups as a result of habitual travel over uneven terrain, which may indicate enhanced leg strength due to frequent inversion and eversion of the foot. Conversely, Shackelford (2014) suggests that reduced femoral and tibial strength in a Late Pleistocene Asian sample whose members lived in a location of uneven terrain, compared to a north African sample that lived on flatter terrain, is the result of differences in mechanical efficiency at the hip and knee joints of the Asian individuals. Pearson et al. (2014) and Cowgill (2014a) explore the effect of body shape and activity patterns on lower limb shape indices with slightly different results. Pearson et al. (2014) did not find a strong relationship between femoral midshaft shape and bi-iliac breadth, whereas Cowgill (2014a) found a stronger relationship. Additionally Cowgill (2014a) has found that such indices differentiate earlier in some populations than others, and attributes the differences to differing body proportions. Higgins (2014) studied the metacarpal structure of three bovid groups that were known to range approximately equal distances, but that differed in the unevenness of their habitual terrain (flat, mountainous, and mixed), and found that the mountainous species experienced an increase in both antero-posterior and medio-lateral strength as indicated by midshaft section moduli. Compared to human tibiae, which also exhibit an increase in antero-posterior (but relatively less of an increase in medio-lateral) bending strength, metacarpals of bovids that traversed mountainous terrain also show an increase in medio-lateral bending strength *relative to* antero-posterior bending strength. The suggested explanation is that the fibula in humans functions as a buttress, lending lateral support to the tibia, whereas the bovid metacarpal is unaccompanied by a supporting bone. In addition to boney

responses to vertical changes in landscape, Carlson (2014) documents changes in mice femora associated with increased horizontal landscape complexity. Compared to a control group of mice, and mice whose cages were arranged to promote linear movement, mice whose cages encouraged turning (simulating obstacle avoidance) were found to have more elliptical femoral diaphyses and higher relative rigidity as indicated by I_x/I_y ratios.

In summary, although there are clear correlations between activity and bone strength/shape, there is likely no single mechanism that determines a final outcome, but rather an intricate combination of variables, each of which contributes in some manner. Discovering the causal relationships that determine bone strength and shape will require complex, collaborative research that accounts for confounding factors (e.g., differences in body mass, body proportions, landscape complexity and activity levels), many of which are currently under investigation.

Beam theory and the strength vs. predictability hypothesis

Longitudinal curvature is one variable that differs between modern human and Neanderthal femora. Upon a visual inspection, Neanderthal femora appear to be consistently more curved than modern human femora, which leads to the following questions: What is the biomechanical significance of femoral curvature? How do curvature and cross-sectional geometry relate to one another?

The term "curvature" has been loosely applied in the literature and the methods used to define curvature are not always explicitly stated. For instance, curvature moment arm and radius of curvature (Swartz 1990) are two separate concepts that may

erroneously be used interchangeably. Curvature moment arm refers to the measurement of distance between an axially applied force and the neutral axis. This measurement will vary in objects of different sizes. Radius of curvature, however, refers to the arc of a circle whose perimeter aligns with the arc of interest or neutral axis in a bone. Thus, two curved long bones with the same radius of curvature but different lengths will not have the same curvature moment arm. However, two curved long bones of different lengths and different radii of curvature can exhibit identical curvature moment arms. The manner in which one measures curvature plays a crucial role in interpreting the implications of studies of bone curvature and, for instance, helps explain the results of Shackelford and Trinkaus's (2002) study of femoral curvature in Neanderthals, early anatomical modern humans, and recent modern humans.

There are five primary hypotheses that have been proposed to explain bone curvature. The aim of this study is not to attempt to falsify or verify any of these hypotheses, but is instead to understand the role curvature plays in strength and predictability of long bones. In order to do that, however, it is important to consider why bones exhibit curvature in the first place. Thus, the first hypothesis suggests that curvature functions to offset externally applied bending moments, thereby producing overall levels of low stress (Pauwels 1980). However, bending is an inescapable consequence of locomotion and curvature actually increases bending stress rather than alleviating it. Therefore, it seems that the cause of bone curvature is not the development of an ideal shape for the minimization of stresses.

Similarly, the second hypothesis proposes that curvature in long bones develops so as to minimize bending moments and make certain that the diaphysis is loaded in net

compression rather than tension, since bones are stronger under compressive forces (Frost 1964). However, studies have shown that it cannot be predicted whether a bone is consistently loaded in net tension or net compression based exclusively on the direction of its longitudinal curvature, thereby disputing the explanatory power of this hypothesis too (Lanyon 1980; Lanyon and Bourn 1979).

Lanyon (1980) suggests that two additional hypotheses should be investigated: the accommodational hypothesis, in which bone form develops in order to accommodate adjacent musculature, and a bone-strain hypothesis, in which curvature is developed in order to optimize the level of functional strain in bone tissue. Regarding the accommodational hypothesis, Lanyon (1980) states that a bone's degree of curvature and its cross-sectional shape could be influenced by forces exerted by attached muscles and the need to spatially accommodate large muscle bellies. A study on primate musculature and forelimb curvature indicates that although some evidence supports this hypothesis, the overall data are inconclusive (Swartz 1990). The optimal bone strain hypothesis is based on the observation that longitudinal curvature results in bending, which increases bone strain during axial loading. There are physiological advantages to having a tolerable degree of strain, probably associated with movement of fluid through the bone matrix as well as maintaining an appropriate bone mass through remodeling (Lanyon 1980). Too much strain, however, would result in bone failure (Currey 2002). The physiological advantages resulting from the ideal amount of bending stress are real and important; however, the degree to which this dictates degree of curvature is not clear. Advantages are more likely to be by-products of curvature, rather than the adaptive reason for it.

The fifth hypothesis of the predictable strain environment requires a more detailed explanation and warrants a discussion of beam theory. Cylinders are often used as analogs to long bones because of their roughly comparable shapes. Perfectly straight cylinders, loaded in purely axial compression, are more resistant to fracture as a result of bending than are curved cylinders; curvature weakens bones. However, the direction in which a straight cylinder will fracture when compressive force is too large or when a force is applied eccentrically is much less predictable than that of a curved cylinder. It is not uncommon for bones to experience non-axial forces, and indeed it is quite difficult to maintain a purely axial load. Bertram and Biewener (1988) state that when unpredictable loading environments predominate, such as those experienced by terrestrial mammals, the limitation of load will be determined by a bone's strength during bending, rather than its strength during purely axial compression. Increases in load on a curved bone primarily change the magnitude of stress instead of the magnitude *and* distribution of stress, as would occur in a straight bone. This means that under normal patterns of loading, curved bones will deform (via bending moments) in a predictable pattern along the plane of curvature, whereas it is much more difficult to predict the manner in which a straight bone will deform when force is applied eccentrically: there is "no load at which the pattern of stress changes" in curved structures (Bertram and Biewener 1988, pp 80). Thus, structures of predetermined curvature are less likely to fail due to breaking than straight structures when either is subjected to loads from variable directions.

These observations led Bertram and Biewener (1988) to introduce a model that they use to evaluate the trade-offs between strength and predictability of deformation in bones. They propose that the structural effectiveness of a column, used as a simple proxy

for long bones, will be defined by a function which maximizes the interaction of load-carrying capacity (strength) and predictability. They suggest that the simplest way to express the necessary (insofar as predictability is an important consideration in the design of bones) compromise between predictability and load-carrying capacity is the product of the two. The formula **(f/F) x P_b** plotted against curvature (where **f** is the magnitude of the load, **F** is maximum load, and **P_b** is predictability) will present the optimum values for this compromise (Bertram and Biewener 1988).

More recently, Jade et al. (2014) conducted an experiment to compare the analytical methods of Bertram and Biewener (1988) that are based on a simple beam model to a (more realistic) finite element femur model created from a CT scan of a human femur. Results suggest an excellent correspondence between the two methods: as a long bone's longitudinal shape eccentricity, or curvature, increases, the bending direction of the bone becomes more predictable. Curved bones are least strong under axial loads when the load and plane of curvature are exactly aligned; by moving the load off of the bone's plane of curvature, the eccentricity of the load is reduced and the bone's load carrying capacity increases. Conclusions drawn from both of these studies are clear: femoral curvature reflects a trade-off between bending strength and predictability of bending direction (Jade et al. 2014).

In order to investigate the importance of this model in living organisms, Bertram and Biewener (1988) applied it to mammals. It is presently assumed that animal limb bones are designed in such a way as to be as strong as necessary for most situations encountered by the animal, but with a minimum amount of physiological investment with regards to the material involved in the initial formation of the bone and also the cost

involved in moving the limb during locomotion (Bertram and Biewener 1988; Currey 2002). According to Bertram and Biewener (1988), animal studies support this theory in that bones are more robust than would be necessary if they were straight instead of curved and also because bones possess a means for controlling the patterns of stress to which they are subjected. For example, the horse radius is significantly curved, but the horse metacarpal is straight. By measuring strain at the midshaft of both the radius and metacarpal in horses traveling at variable gaits, Biewener et al. (1983) found that the radius experiences higher strains during locomotion, but resultant bending always occurs along the predetermined curve of the bone. Conversely, the straight metacarpal experiences lower strain during locomotion, but the direction of bending varies across animals. They propose that these patterns correspond to the greater frequency of fracture in (straight) distal elements of the horse forelimb than in (curved) proximal elements. Studies such as this one (Biewener et al. 1983) and others (Biewener and Taylor 1986; Rubin and Lanyon 1982) provide strong evidence that most stress generated in long bones during locomotion is the result of bending, yet long bones of animals consistently develop curvature when exposed to normal mechanical environments. This observation indicates that curvature must play a vital role in optimum design for function, but what factors determine which bones are curved, and to what degree?

Bertram and Biewener (1988) identify factors that contribute to the curvature of long bones, and propose that the best compromise between such factors will determine the final degree of curvature, a proposal supported by the results of Jade et al. (2014). Two factors are loading variability and body size. Biewener (1983) showed that in mammals ranging from small to large, long bone curvature decreases as size increases.

This means that bones in larger animals are straighter, and therefore stronger, but this may also help explain why large animals have restricted variability of movement relative to small animals.

Other factors that could influence curvature are muscle forces. A straight bone becomes curved during locomotion due to muscle forces pulling on the bone's long axis and/or as the result of the normal off-axis orientation of the limb segments relative to the ground reaction force when they are loaded during locomotion (Bertram and Biewener 1988). This is a possible explanation of why the mammalian tibia is straighter than the radius and ulna.

A final factor affecting bone curvature is cross-sectional geometry. If a bone is wider in one cross-sectional dimension (e.g. along the sagittal plane) than another, this will also influence the predictability of bending direction. Although the narrow dimension will be less stable than the wide dimension, if predictability of bending is the primary objective, the result will be the same as that of curvature (Bertram and Biewener 1988).

In summary, it is accepted that bone is able to respond to applied forces through a complex remodeling process. Increased or atypical stimuli can induce the remodeling process. Generally, remodeling results in peak strains experienced by bones returning to normal or pre-experimental values. Experimental studies have shown that in order for bones to develop properly, they must be subjected to a normal mechanical environment during growth. Some properties of bones continue to change throughout the life of an animal, whereas others are primarily determined during growth. A study on the rat tibia deprived of its normal function showed that in the absence of a normal mechanical

environment, the tibia failed to develop normal curvature or cross-sectional geometry (Lanyon 1980). The method used in this study to create a false mechanical environment was non-reversible, so it is undeterminable if the bone would be able to achieve normalcy if it was subsequently subjected to a normal mechanical environment. Bertram and Biewener (1988) propose that the high incidence of long bone curvature observed in mammals is cause to believe that there must be a strong benefit to curvature, given that curvature decreases strength. They suggest that this benefit is increased predictability in bending patterns, an important consideration for animals that experience a highly variable loading environment during their normal range of activity. This hypothesis, along with tests of robusticity, are tested and the results are presented and discussed in Chapter V: FEA of Human and Neanderthal Femora, but first we must firmly establish the relationship between skeletal variables and mobility.

CHAPTER III

INTRA-GENERIC PRIMATE COMPARATIVE STUDY

Introduction: Ranging hypotheses

The first phase of the project is to establish the comparative basis relating mobility to skeletal variables. Important work in this regard has already been performed in humans, as noted above, but this study supplements that work by taking advantage of decades of work on primate ecology. A key behavioral variable recorded in ecological studies is average day range. Day range is the distance an animal or focal group typically travels in the pursuit of resources in the course of one day. Ranging behavior is linked to subsistence strategy in that an animal must forage (and, thus, travel) in order to meet its daily caloric requirements. Mobility is defined here as linear movement across the landscape (Carlson et al. 2007; Kelly 1995), and is often quantified as the ecological variable day range. Accordingly, day range is a useful surrogate for mobility, and mobility patterns elucidate aspects of culture in prehistoric societies such as subsistence strategies, hunting techniques, seasonal activity levels, home range size, resource availability, and other behavioral variables (Larsen 1987) which are of interest to paleoanthropologists. This study examines femoral and humeral morphology in groups of closely related primate species that employ similar modes of locomotion, but that have different day ranges.

The first *null hypothesis tested here is that no relationship exists between ranging distance and skeletal variables that measure robusticity*. The prediction is that if a relationship exists between ranging behavior and skeletal morphology, primates who range farther will have more robust humeri/femora than primates with limited ranges.

Animal limb bones are theorized to be designed in such a way as to be as strong as necessary for most situations encountered by the animal, but with a minimum amount of physiological investment with regards to the material involved in the initial formation of bone and the energetic cost of moving the limb during locomotion (Currey, 2002). Additionally, bones possess a mechanism for detecting patterns of stress, thereby controlling strain distribution through remodeling (Bertram and Biewener, 1988), meaning that changes to a bone's biomechanical environment result in architectural modifications (through bone remodeling) that eventually return stress magnitudes back to the baseline value (Woo, 1981). Finally, recall that the main determinants of bone remodeling are rate, frequency, and magnitude of dynamically applied loads. Increasing the magnitude of a load, in combination with increasing rate and frequency of loading, yields increasing remodeling. Statically applied loads do not produce high levels of remodeling (O'Connor and Lanyon, 1982; Turner et al., 1995; Skerry, 2000).

The second *null hypothesis being tested is that no relationship exists between ranging distance and longitudinal curvature*. The prediction is that if a relationship exists between ranging behavior and skeletal morphology, primates who range farther will have more curved humeri/femora than primates with limited ranges. Curved bones are weaker when subjected to bending moments than straight bones, yet all animal limb bones exhibit some degree of curvature. In fact, contra the statement above, animal limb bones are more robust than would be necessary if they were straight rather than curved. Bone curvature, therefore, may serve an adaptive purpose (Biewener, 1983; Bertram and Biewener, 1988). Curvature weakens bones when axial compressive forces are applied; however, when unpredictable loading environments dominate, such as those experienced

by mammals during locomotion, the limitation of load will be determined by a bone's strength during bending, rather than its strength during purely axial compression. Since curvature pre-determines a structure's bending direction, increases in load on a curved bone only change the magnitude of stress, instead of the magnitude *and* type or distribution of stress, as would occur in a straight bone. Curvature thus increases the predictability of the direction of force transmission through the bone's axis, enabling the bone to reinforce itself along the weaker axis through remodeling if excessive bending moments are regularly detected. Structures of pre-determined curvature are hypothesized to be less likely to catastrophically fail than straight structures when either is subjected to loads from variable directions. The amount of curvature expressed in a bone then, will be determined by the best compromise between loading variability, rate/frequency of loading, and body size.

Limb Bone Curvature in Primates as it Relates to Locomotion

The influence of various forms of locomotion on long bone curvature has been studied in several species of primates. Long bone curvature of brachiators, terrestrial quadrupeds, and arboreal quadrupeds will be discussed. Additionally, strength properties of prosimian long bones as they relate to mode of locomotion will be reviewed.

A study by Yamanaka and colleagues (2005) using humeral and femoral specimens from captive and wild olive baboons, crab eating macaques, southern pig-tail macaques, howler monkeys, spider monkeys, wooly monkeys, and gibbons demonstrated that anthropoid femora curve laterally moving from proximal to distal positions and at mid-shaft are anteriorly convex. Among the species selected for this study, the Old

World monkeys (OWMs) are primarily terrestrial quadrupeds whereas the New World monkeys (NWMs) are primarily arboreal quadrupeds. The ratio of femoral antero-posterior curvature to length is twice as large in OWMs as in NWMs, with the largest difference at the mid-shaft level. Gibbons, who brachiate, exhibit the least amount of antero-posterior curvature relative to length. Conversely, NWMs and gibbons possess larger values for medio-lateral femoral curvature relative to length than OWMs, but the difference between the two groups for this property is smaller. The anthropoid humerus shows the same patterns as the femur (Yamanaka et al. 2005).

Calculation of theoretical bending strength of individual bones led Yamanaka and colleagues (2005) to suggest that arboreal quadrupeds and brachiators have significantly stronger bones when loaded in axial compression than their terrestrial counterparts, probably as a result of decreased bone curvature. The compliant nature of limb branches relative to the immobile ground means that arboreal quadrupeds experience decreased substrate reaction forces during locomotion. This, as well as different limb movements resulting from positioning limbs to walk on tree limbs, could affect boney characteristics in a number of ways, thereby resulting in the differences between arboreal and terrestrial quadrupeds observed in this study.

Swartz (1990) quantified curvature of thirteen species of anthropoid primates with the primary goal of exploring forelimb curvature of two brachiating species, Old World gibbons and New World spider monkeys, relative to quadrupeds. Brachiators' upper limbs are subjected to different forces than the limbs of quadrupeds. Because brachiators suspend their bodies from their upper limbs, their bones experience more tensile forces due to gravity than the limbs of quadrupeds, which act mainly as support columns loaded

primarily in compression. However, muscle forces generated within the brachiator's limb function to mediate tensile forces by exerting compressive forces, thereby balancing extrinsic tensile loads with intrinsic compressive loads and generating bending stress. Swartz (1990) notes that bones subjected to increased axial loads should show a decrease in curvature in order to limit the magnitude of bending stress induced by curvature. Additionally, torsional forces may play a more important role in constraining bone shape in brachiators than in quadrupedal primates since brachiation results in significant rotation of the body around the long axis of the forelimb as well as rotation of the forelimb around its long axis. Shear stresses are the most significant result of torsion and "will increase in direct proportion to increasing orthogonal distance from the axis about which the torque is applied" (Swartz 1990, pp 480). This means that shear stresses will be largest at the areas of greatest curvature and it would be advantageous for suspensory primates to have reduced long bone curvature. And in fact, gibbons and spider monkeys do have significantly straighter humeri than nonsuspensory primates, a modification which likely reduces shear stresses generated during brachiation. The gibbon radius, however, is significantly more curved than that of nonsuspensory primates, which may be necessary to support relatively larger supinator musculature in brachiators, although Swartz (1990) does not find that muscle mass development is the primary determinant of limb bone curvature. Regarding the hindlimb, gibbons have significantly more curved femora and fibulae than nonsuspensory primates. Spider monkeys have more curved fibulae, but exhibit no difference in femoral curvature. Thus, locomotor specialization, in this case, brachiation, can result in distinctive long bone morphology.

Swartz (1990) also shows that among all primate species used in this study, curvature increases with increasing body size, contra the trend demonstrated across mammals (Biewener 1983). In general, though, primates have less curved limb bones than other mammals, perhaps because primates have relatively longer limb bones than other mammals, thereby increasing the need to reduce risk of failure by the bending stress associated with curvature.

Although data specifically concerning long bone curvature of prosimians is lacking, cross-sectional properties indicate that species who specialize in leaping have stronger midshaft femoral sections than quadrupedal primates of comparable body size, especially in the antero-posterior dimension (Demes and Jungers 1993). Quadrupedal species, in general, exhibit less differentiation in femoral and humeral strength, and there is less difference in strength between medio-lateral and antero-posterior planes. Slow climbers typically have less bone strength than other locomotor types, but there are exceptions to this generalization. Interestingly, cortical bone distribution, torsional and bending rigidity per unit area, and cortical wall thickness do not closely correlate with type of locomotion among prosimians (Demes and Jungers 1993).

Based on these data, it seems that among primates, locomotor specialization can produce limb bones of distinct morphology. Specialized locomotion (brachiation, vertical leaping, etc.) produces more distinct morphology than quadrupedalism. There are also differences in bone properties between arboreal and terrestrial quadrupedal primates, perhaps due to differences in compliance of the surfaces on which they travel. These results are consistent with Ruff's (2002) study, in which it is demonstrated that mode of locomotion correlates with limb strength and articular surface/diaphyseal cross-

sectional properties. This section pertains to large locomotor differences among a diverse array of taxa. The aim of the following section is not to document differences in bone morphology associated with different modes of locomotion, but rather to determine if species' day range predicts strength of humeri and femora within particular genera.

Materials: The extant primate sample

In order to test the null hypotheses listed above, a literature review was undertaken in which day range (DR) data were obtained for ten primate genera, totaling 40 species. However, due to collection availability in museums and budgetary constraints, only five genera (21 species) are included in this study. Ecological studies of the relevant genera are summarized below. Every effort was made to incorporate information such as method of day range calculation, length of study, season of study, number in group, etc. The following information is also listed in Table 3.1 and number of males and females per species are listed in Table 3.2.

Saguinus. This study samples four species within the genus *Saguinus*, commonly known as tamarins. Tamarins are small, New World arboreal quadrupeds that walk, run, and leap. They have relatively long trunks, legs, and tails.

Saguinus fuscicollis, the saddle-back tamarin, incorporates a high frequency of leaping between vertical supports and from branches to trunks (Fleagle 1999). Terborgh (1983) studied one group of five *Saguinus fuscicollis*, in Peru, during both wet and dry seasons. The ranging behavior of this group was calculated by pacing and mapping the entire distance traveled by the group on 19 days. The average day range of *S. fuscicollis* was determined to be 1.2 kilometers. Garber (1993) cites a number of studies that

represent a total of 10 years of observation of *S. fuscicollis*, and states that the combined average day range for this group is 1.4 kilometers. Thus, the combined average DR for *S. fuscicollis* used in this study is 1.3 kilometers.

Saguinus mystax, the moustached tamarin, typically travels quadrupedally on thin, flexible supports (Fleagle 1999). One group of two to six *S. mystax* was followed and mapped for two days by Castro and Soini (1977). The average DR is stated to be 1.2 kilometers. This number is slightly lower than the number cited by Garber (1993), who combines 42 months of observation from various sources and gives an average DR of 1.9 kilometers. The combined average DR for *S. mystax* is therefore 1.55 kilometers.

Saguinus oedipus, the cotton-top tamarin, was observed by Newman (1978) in Colombia during a 2-year study. During this time, 2500 contact hours were made with three groups of cotton-top tamarins; however, only the complete DR data for one group were reported. Day range was calculated by following the focal group, marking the path with a machete, and mapping the path on a gridded map. In this way, one group, averaging nine individuals, was observed to travel between 1.5 and 1.9 kilometers daily, with the midpoint DR being 1.7 kilometers.

Saguinus geoffroyi is stated to have an average DR of 2.1 kilometers based on a total of 27 months of observation (Garber 1993). Dawson (1979) observed *S. geoffroyi* in Panama during both wet and dry seasons. Two groups were tracked with radio-collars over the course of 60 days.

In summary, *S. fuscicollis*, has a relatively short day range (~1.3 km), while *S. mystax* (1.55 km) and *S. oedipus* (1.7 km) have intermediate day ranges, and *S. geoffroyi* (2.1 km) ranges farthest.

Cercopithecus. Guenons, members of the genus *Cercopithecus*, are Old World monkeys found in the forests of sub-Saharan Africa. Although all guenons are arboreal quadrupeds, they vary slightly in the amount of leaping incorporated into their locomotor repertoires (Fleagle 1999). Seven species of *Cercopithecus* monkeys are included in this study. Some species of *Cercopithecus* commonly form interspecific associations and those associations affect DR values.

Cercopithecus nictitans, the greater spot-nosed monkey, and *C. pogonias*, the crowned monkey, are the two species that typically travel the farthest in a given day. Gautier-Hion and Gautier (1974) and Gautier-Hion et al. (1983) observed groups of *C. nictitans* and *C. pogonias* for a total of 12 months during both wet and dry seasons in Gabon, Africa. Day ranges were calculated based primarily on radio-collar tracking data. When *C. nictitans* traveled in a group (of 13 individuals) without associating with other *Cercopithecus* species, the group was observed to travel on average 1.6 kilometers per day. When a group of 20 *C. nictitans* was observed in association with a group of 18 *C. pogonias*, the average DR increased to 1.8 kilometers per day for each species. When the same group of *C. nictitans* formed associations with the same group of *C. pogonias* and *C. cephus* (15 individuals), the average DR increased further to two kilometers per day for each species. Thus, the combined average DR of *C. nictitans* and *C. pogonias* is 1.8 kilometers.

Interestingly, when *C. cephus*, the moustached monkey, was observed in non-mixed groups, they tended to have some of the shortest day ranges within the genus *Cercopithecus*. During a three month study in Gabon, Gautier-Hion and Gautier (1974) observed a group of *C. cephus*, averaging between five and six individuals. The DR of

this group was 0.8 kilometers. During a separate four-month study, also in Gabon, Gautier-Hion et al. (1983) observed a group of 15 *C. cephus*. They found that when *C. cephus* travelled alone, the DR was only 1.3 kilometers on average, but when *C. cephus* formed associations with *C. nictitans* and *C. pogonias*, the DR increased to two kilometers, indicating that DR is highly variable even within the same group of animals. The combined average DR of *C. cephus* is 1.4 kilometers.

Cercopithecus diana also varies in the amount of time spent in interspecific associations. Whitesides (1989) studied two groups of Diana monkeys and gathered DR information on 96 days during a 14-month study (including both wet and dry seasons) in Sierra Leone. The group of 20 did not form interspecific associations, and typically ranged one kilometer per day. However, a separate group of 27, observed for 39 days during an 11- month study in Sierra Leone was found to have an average DR of 1.5 kilometers (Whitesides 1989). The combined average DR is used in this study, making the DR of *C. diana* approximately 1.3 kilometers.

Cercopithecus ascanius, the red-tailed monkey, is similar in DR to *C. cephus*. Based on 65 days of DR observation over the course of a 13-month study, which included both wet and dry seasons, Struhsaker (1980) cites an average DR of 1.4 kilometers. This is based on observations of one group in Uganda, averaging 33 in number, and was calculated by plotting individuals on a gridded map.

Cercopithecus neglectus is one of the most sexually dimorphic guenon species, and mainly live in the understory of flooded forests, frequently traveling to the ground where they are slow quadrupeds (Fleagle 1999). The DR of *C. neglectus* is the shortest

of all *Cercopithecus* species at 0.5 kilometers. This is based on a radio-collar tracking study by Gautier-Hion and Gautier (1978).

Day ranges of *Cercopithecus mitis*, the blue monkey, vary from 1.1 kilometers at the low end of the range to 1.4 kilometers at the upper end. Day range observations were made of *C. mitis* on over 300 days over the course of 10+ years of study. In all cases, DR length was calculated by mapping a group's location on a gridded map. Butynski (1990) studied groups averaging 20 individuals in Uganda, and Kaplin (2001) studied one group in Rwanda. The combined average DR of *C. mitis* is approximately in the middle of *Cercopithecus* DR values at 1.3 kilometers.

In summary, *C. nictitans* and *C. pogonias* occupy the high end of the *Cercopithecus* DR spectrum at 1.8 kilometers per day; *C. cephus, C. diana, C. ascanius* and *C. mitis* have DRs in the middle of the spectrum at 1.3-1.4 kilometers; and *C. neglectus* has the shortest DR at approximately 0.5 kilometers.

<u>*Macaca*</u>. The genus *Macaca* is characterized by several variable species, five of which are included in this study.

Macaca arctoides has a day range of between 400 meters and three kilometers, according to a three-month study documenting ranging behavior of nine troops, none of which contained more than 20 individuals, in both monsoon and dry forests in Southern Thailand (Bertrand 1969). If the food source (fruit) was concentrated, the day range was small (closer to 400 meters), if the food source was sparse, scattered, or located farther from the troops' sleeping locations, travel would commonly increase to over one kilometer. None of the troops studied ranged farther than three kilometers, and the mean was one km.

Aldrich-Blake (1980) conducted an 11-month study in wet and dry seasons, during which time a group of *Macaca fascicularis* was followed and mapped on 38 days. The average DR was found to be 0.8 kilometers. Payne and Francis (1985) observed a group of 25 *M. fascicularis* and cite an average DR of 0.9 kilometers. Both of these studies give similar DRs that are less than the following two studies. MacKinnon and MacKinnon (1980) conducted a 7-month study in Malaysia during which a group of 17 *M. fascicularis* was followed from dawn until dusk on ten days and cite an average DR of 1.4 kilometers. Wheatley (1980) conducted a study in Sumatra over the course of 14 months. During this time, four groups of *M. fascicularis* were observed on 35 days and the cited average DR is 1.9 kilometers. While it is beneficial to know the exact number of days actual and complete DRs were tallied, that is not always possible as some authors are more precise in their reports than others. However, it is clear that on at least 39 days *M. fascicularis* exhibited short DRs. On at least 45 days, *M. fascicularis* exhibited long DRs. Thus, the combined average DR is 1.3 kilometers.

Lindburg (1971) calculated DRs for three groups of *Macaca mulatta,* averaging 41 individuals, in India on 38 days. The average DR was found to be 1.4 kilometers.

MacKinnon and MacKinnon (1980) followed one group of *M. nemestrina,* averaging 35 individuals, from dawn to dusk on 10 separate days and calculated an average DR of two kilometers.

Macaca nigra was observed by O'Brien and Kinnaird (1997) in Indonesia over the course of 18 months. Three groups, averaging 70 individuals, were mapped every half hour and the DR was observed to be 2.4 kilometers.

Macaca radiata were observed to have variable day ranges. Sugiyama (1971) conducted a 2-year study in India in both wet and dry seasons, during which time the DR of one group of *M. radiata* was observed on 57 days. The average DR was 0.8 kilometers. This number is in contrast to the figure calculated by Kuruvilla (1980), whose 12-month study in India led to the calculation of an average DR of 1.8 kilometers based on group follows. The specific number of days the group was followed was not specified, making it difficult to assess which DR value is more accurate. Thus, the combined average DR of 1.3 kilometers will be used in this study.

Kurup and Kumar (1993) followed two Indian groups of *Macaca silenus,* averaging 26 individuals, from dawn until dusk on four days during both hot and cold seasons. The average DR was calculated to be 1.7 kilometers.

In summary, *M. arctoides* is the macaque species with the shortest DR at one kilometer. *M. radiata*, *M. mulatta* and *M. fascicularis* have mid-level DRs at 1.3 to 1.4 kilometers. *Macaca nemestrina* and *M. nigra* have the longest DRs at two to 2.4 kilometers, respectively. Finally, *M. silenus* is intermediate between the mid-level DRs and the long DRs at 1.7 kilometers.

<u>*Papio* and *Theropithecus*</u>. Baboons, members of the genera *Papio* and *Theropithecus,* are excellent for this study as they are large, primarily terrestrial quadrupeds with day ranges that differ markedly between species. *Theropithecus gelada* has the shortest DR of the baboons according to Dunbar and Dunbar (1974). Over the course of a 6-month study in Ethiopia, which included both wet and dry seasons, Dunbar and Dunbar (1974) followed and plotted on a gridded map the movements of five groups

of *T. gelada*, averaging 50 in number. Their complete movements were recorded on eight days and an average DR of 0.6 kilometers is given.

Papio anubis, the olive baboon, and *P. cynocephalus*, the yellow baboon, have similar day ranges depending on the most accurate DR value for *P. anubis*. Dunbar and Dunbar (1974) tracked seven groups of *P. anubis*, averaging 20 in number, and plotted their travels on a gridded map for 13 days in Ethiopia. According to this study, which took place during both the wet and dry seasons, the average DR of *P. anubis* is 1.2 kilometers. Rowell (1966) cites a DR for *P. anubis* of 2.4 kilometers, but the two groups he surveyed in Uganda were never continuously mapped from dawn to dusk, which makes this measure subject to question. Two other ecological studies of *P. anubis* were conducted in Kenya and Ethiopia and yield higher DR values. Harding (1976) studied one group, averaging 50 in number, over the course of 12 months in Kenya and gives an average DR of five kilometers. However, the specific number of days' travel this figure is based on was not reported. Aldrich-Blake et al. (1971) studied one group of *P. anubis*, averaging 87 in number, in Ethiopia over the course of two months. Entire travel periods were recorded on 12 days and the average DR of this group of olive baboons was 5.8 kilometers. Thus, some authors have recorded DR values that are much lower than others. The combined average DR value for *P. anubis* is 3.6 kilometers.

Altmann and Altmann (1970) cite a DR of 5.9 km for *P. cynocephalus*, based on an 11-month study of one group in Kenya, averaging 41 individuals.

Papio ursinus, the chacma baboon, has been observed to travel farther than either *P. anubis* or *P. cynocephalus*. DeVore and Hall (1965) studied three groups of chacma baboons averaging 45 individuals over the course of a 12-month study in South Africa.

On 32 days, DR values were recorded with the average DR being 4.7 kilometers. Stoltz and Saayman (1970) conducted a 16-month study in South Africa and observed six groups of chacma baboons averaging 47 individuals each. Two average DR values are cited from this study. The first, 6.4 kilometers, is based on 31 days of observation. The second, 10.5 kilometers, is based on 23 days of observation. The combined average DR for *P. ursinus* is 7.2 kilometers.

Papio hamadryas has the longest day range of any baboon species. On the low end of observed DRs for this species, Sigg and Stolba (1981) give a mean DR of 8.6 kilometers based on 57 days of dawn to dusk observation of one group of hamadryas baboons, averaging 66 in number. A separate group of hamadryas baboons was followed from dawn until dusk on 13 days. This group averaged 10.4 kilometers of travel per day. Both of these figures are based on an 18-month study in Ethiopia that included all seasons. Finally, Kummer (1968) mapped the movements of one group of approximately 120 hamadryas baboons in Ethiopia on nine days and gives an average DR of 13.2 kilometers. Thus, the combined average DR for *P. hamadryas* is 10.7 kilometers.

Therefore, *T. gelada* has the shortest DR at 0.6 kilometers. The combined average DR for *Papio anubis* (3.6 km) is distinct from *Papio cynocephalus* (5.9 km). *Papio ursinus* typically ranges farther than the previous three species at 7.2 kilometers, and the hamadryas baboon, *Papio hamadryas*, has the longest DR at 10.7 kilometers.

Methods: Data collection

Only free-ranging adult animals were used in this study, i.e., not animals living in zoos, to the best of my knowledge. Adult status was determined by eruption of the third

molar when possible, or by degree of epiphyseal fusion in the absence of a cranium. Left sided bones were preferably chosen, but if the left side was broken, missing, or otherwise unusable (e.g. presented visible pathology), the right bone was used instead. Data were collected on humeri and femora by two methods. Maximum length of each bone was measured to the nearest millimeter using an osteometric board. Maximum femoral and humeral head diameters were measured to the nearest tenth of a millimeter using calipers. Any available information on sex, age, health condition, circumstances of capture/acquisition, etc. was also noted prior to scanning.

External morphology was obtained with a NextEngine 3D Scanner (NextEngine, Inc.), which captures color and texture information for external surfaces. Scanner settings are adjustable such that scans can be made at quicker or slower speeds. For this project, scans were made using wide precision (0.15 inches) on quick speed (40 seconds per scan). The triangle size, which is a measure of scan resolution, was set at 0.0225 inches, and smoothing was set at level two. Both of these parameters are defined at levels that capture the most information. Scanning proceeded in two steps. First, each bone was placed with its longitudinal axis presented to the scanner. Typically, eight scans of each bone were made in this position, so that a single scan captured approximately 45 degrees. After longitudinal scanning was complete, the bone was positioned such that first the proximal end and then the distal end faced the scanner. In these positions, three scans were made of each surface. Once these raw data were obtained, the scans were aligned, fused, and exported using the software ScanStudioHD v.1.3.2 (NextEngine, Inc., ShapeTools LLC, and INUS Technology Inc.). Alignment was achieved through a combination of automatic and manual methods. Typically,

ScanStudio HD was able to successfully align the longitudinal images automatically, but scans of the proximal and distal ends of each bone had to be aligned manually by placing "pins" on the same point in separate scans, the purpose of which was to inform the software how each family of scans fit together (Figure 3.1). After alignment, the model was fused. Every model was fused with a 0.0025 inch tolerance level, but the resolution ratio varied between 0.6 and 0.9 depending on the quality of the initial scans. (A number of variables affect scan quality, including size and shape, but one of the most important is lighting, which was uncontrolled in museum settings.) Fusing the individual aligned scans together creates a water-tight 360 degree surface model (Figure 3.2). Each bone model was exported from ScanStudioHD to the 3D modeling software *amira 5.2.0* (ResolveRT – FEI Edition) as an STL file.

In *amira*, the model was manipulated so as to obtain images of transverse cross-sections. In this study, surface models were "cut" along the transverse plane at 30, 50, and 70 percent of the model's length, beginning proximally and moving distally (Figure 3.3). Because scanning only captures the external morphology, the interior of the model is a solid surface, an acceptable limitation of the method as bone near the perimeter of a cross-section is more important in calculating robusticity than bone closer to the center (Stock and Shaw 2007). Each "cut" was marked with a scale bar so that resolution (pixels/mm) could be calculated, and the images were exported as 8-bit grayscale TIF files (Figure 3.3) to the image editing software program, ImageJ (Rasband 1997-2014). MomentMacroJ v1.4 is a publicly accessible free macro (available at http://www.hopkinsmedicine.org/FAE/mmacro.htm) that interfaces with ImageJ and

calculates moments of area and other related variables given a particular set of user input conditions such as scale, density threshold, and perimeter.

Curvature

In addition to obtaining data from model cross-sections, the entire model was manipulated so as to measure maximum curvature moment arm. Curvature moment arm, measured here as subtense, was only measured in the antero-posterior (AP) dimension on femora, but medio-lateral (ML) curvature was measured in addition to AP curvature on humeri. Data from humeri and femora were obtained using the same protocol but orientation varied between the two bones. In *amira*, each femur was aligned with the anterior surface projecting downwards on the screen and the posterior surface projecting upwards. A scale bar was created for use in ImageJ, where measurements were made. Once the models were thus aligned and the scale bar was present, they were exported as TIF images. These images were loaded into ImageJ, where the scale was set. A chord was drawn across the length of the bone, from the distal-most point on the condyles to the proximal-most point on the head for each femur (Figure 3.4). For each humerus, the initial alignment was the same; the posterior surface projected upwards on the screen and the anterior surface projected downwards. A chord was drawn from the proximal-most point on the humeral head, to the distal-most point of the bone (Figure 3.5). Medio-lateral subtense measurement protocol was similar, but the humerus was aligned vertically along its longitudinal axis with the posterior surface facing the viewer. A chord was drawn from the proximal-most point on the humeral head, to the proximal-most point of the trochlea (Figure 3.6). These alignments and landmarks were chosen in

order to maximize reproducibility and consistency, in addition to accounting for joint morphology, an important component of a biomechanical analysis (Swartz 1990).

Once the chord was drawn, another series of lines was added to each image. First, the point of maximum curvature *in reference to the chord* was found. Then, an angle of 90 ± 1 degrees was drawn at the same location in order to ensure that subtense measurements were made orthogonal to the chord. The diameter of the bone at the point of maximum curvature was then marked and measured. The neutral axis was assumed to exist in the center of the bone. Subtense, then, was measured from the center of the bone (half of the diameter) to the chord.

Robusticity

The term "robusticity" refers to the strength of a bone as reflected by its size and shape (Stock and Shaw 2007). Five properties used to estimate robusticity in this study are total area (TA), second moments of area about the maximum (I_{max}) and minimum (I_{min}) bending axes, polar moment of area (J), and section modulus (Z_p). According to the theory of beam biomechanics, a bone's strength is a function of the amount of cortical bone present, and the distribution of the cortical bone around the neutral axis. Since bone located farther from the neutral axis is more important in resisting bending and torsional loading than bone close to the centroid, the periosteal surface is more relevant to determining the bone's ability to resist stress than is the endosteal surface (Bertram and Swartz 1991). This indicates that accurate quantification of the periosteal contour is of primary importance in estimating diaphyseal strength, which means that internal dimensions need not necessarily be obtained via computed tomography (CT) scanning (which captures external and internal data). Therefore, humeral and femoral robusticity

and curvature were measured using external geometry provided by the complete bone surface models described above.

Total area (TA) (mm^2) is the entire area of a cross-section. Second moments of area (I) (mm^4) are calculated about the x- and y-axes of a cross-section and are used to measure the maximum/minimum bending strength, or ability of a bone to resist bending. It has been hypothesized that shape ratios created from I_{max}/I_{min} can yield information about the preferred plane of bending in a bone, but experimental work has led to rejection of that hypothesis (Lieberman et al. 2004). Polar moment of area (J) (mm^4) is calculated as the sum of any perpendicular second moments of area and measures torsional strength. Polar section modulus (Z_p) (mm^3) is a measure of average bending and torsional strength, and equals polar moment of area divided by average overall radius (Ruff 2005). Methodological research has shown that TA, I, and J calculated from solid surfaces with an accurate measurement of periosteal contours have very low prediction errors (Stock and Shaw 2007), although Lieberman et al. (2004) caution that absolute values of cross-sectional geometric properties calculated around centroidal axes do not equal values calculated around experimentally determined neutral axes, as documented through *in vivo* strain gauge data collected from midshafts of sheep tibiae and metatarsals. Differences between second moments of area calculated from centroidal axes compared to those calculated from neutral axes can be substantial (percent differences: I = 23-28%; Z = 50-55%; and J = 11-26%); however, patterns are highly correlated ($r^2 \geq 0.87$) (Lieberman et al. 2004). Due to these error estimates, J is the most accurate estimator of resistance to torsion (in circular cross-sections) because errors in determination of the position of the neutral axis are offset by errors in the orthogonal second moment of area; conversely, Z_p

is likely the worst parameter to use in the absence of an experimentally determined neutral axis.

Measures of skeletal robusticity must be standardized to body size and/or body mass because these have a significant influence on mechanical loading, and therefore a bone's dimensions. Bone length was used as a proxy for stature since it correlates well with stature, but body mass is the better determinant of mechanical loading, and a measure of body size was used to standardize cross-sectional areas. Most primates do not have regression formulae for body mass published in the literature so the cubed geometric mean of maximum femoral head diameter, maximum humeral head diameter, maximum femoral length, and maximum humeral length was used as a proxy for body mass (abbreviated BS). Moments of area (I and J) were standardized by the product of body size and bone length (Stock and Shaw 2007). Polar section modulus and total area were standardized by body mass. Because absolute subtense is the biomechanically relevant measure of curvature, this variable was not normalized by body size or body mass proxies.

Statistical Analyses

The purpose of this study is to determine whether species of primates within a single genus exhibit significantly more robust and/or more curved humeri and femora as average day range (DR) increases. Multiple analyses were performed in order to test for relationships between the five robusticity variables previously discussed (J, I_{max}, I_{min}, TA, and Z_p) and DR and between curvature (C) and DR. The null hypotheses tested in this study are that there are no relationships between DR and robusticity and DR and curvature of humeri and femora. To this end, multiple regression analyses were used to

explore the explanatory effect of the dependent variable (DR) on the independent variables (J, I_{max}, I_{min}, TA, and $Z_{p,}$ and C) while implementing a statistical control of body size (BS), as this variable is known to influence these particular dependent variables (Vogt 1993). The level of statistical significance is $\alpha = 0.05$.

Important results generated by the multiple regression include the coefficient of determination (r^2), which indicates the amount of variation in the dependent variable that is accounted for by variation in the independent variables. Thus, it equals explained variation divided by total variation and is useful for interpreting how well the model fits the data. A similar statistic, R^2, is known as the multiple coefficient of determination; it is used instead of r^2 in the case of a multiple regression equation rather than a single equation. Adjusted R^2 is the multiple coefficient of determination revised, or adjusted, to take into account the number of variables and sample size used in a model. Therefore, adjusted R^2 is the statistic that best indicates how well a multiple regression model fits the data (Triola and Triola 2006), and is used in in the present paper. The explanatory power of the model is improved as the coefficient of determination approaches one.

The estimated coefficient gives the value of the slope that was calculated by the regression. Standard error (of the coefficient estimate) is a measure of the coefficient's variability. The p-value gives the probability that a particular variable is not a meaningful predictor in the model. The F-statistic is given for the entire model. It is derived by comparing a particular model to a model that has fewer parameters. Theoretically, more parameters should increase the explanatory power of the model, resulting in a higher F-statistic and a lower p-value. Note that the F-statistic and its associated p-value give information for the entire model, rather than single variables.

Interaction effects between bone length (as a measure of size) and sex in models with femoral head diameter (FHD) or humeral head diameter (HHD) as the dependent variable were explored with ordinary least squares regressions and analyses of covariance. There were no significant interaction effects between size and sex in any genus, indicating that male and female slopes are not significantly different: *Saguinus* (p_{FHD} = 0.832 based on femoral head diameter (FHD); p_{HHD} = 0.549 based on humeral head diameter (HHD)), *Cercopithecus* (p_{FHD} = 0.767; p_{HHD} = 0.912), *Macaca*, (p_{FHD} = 0.892; p_{HHD} = 0.475), or *Papio/Theropithecus* (p_{FHD} = 0.389; p_{HHD} = 0.737). Multiple regressions were performed on separate male-female groups due to sexual size dimorphism as indicated by different intercepts of the male-female regressions in all genera except *Saguinus*: *Saguinus* (p_F = 0.484; p_H = 0.782), *Cercopithecus* (p_F < 0.001; p_H < 0.001), *Macaca*, (p_F = 0.935; p_H < 0.009), and *Papio/Theropithecus* (p_F = 0.058; p_H < 0.001).

Results

Saguinus. There were no statistically significant results for the robusticity variables of TA, I_{max}, I_{min}, J, or Z_p on distal and midshaft femoral cross-sections for either male or female samples (Tables 3.2 and 3.3 and Figures 3.7 and 3.8, respectively). However, proximal femoral cross-section results do indicate significant findings in the male sample. TA (p = 0.001), I_{max} (p = 0.004), I_{min} (p = 0.000), J (p = 0.001) and Z_p (p = 0.002) all indicate that there is a significant relationship with DR (Table 3.4). When these results are graphed, it is apparent that *S. fuscicollis* and *S. mystax* overlap one another and have higher values for robusticity, while *S. oedipus* is separate from either

group (Figure 3.9). However, *S. oedipus* has the longest DR (1.7 km), whereas *S. fuscicollis* (1.3 km) and *S. mystax* (1.6 km) have shorter DRs.

There are no significant results to report for robusticity variables of humeral cross-sections in either male or female samples at any of the three locations analyzed, but body size is significant for I_{max}, J, and Z_p on the distal humerus, for I_{max} on the proximal humerus as well as for all five variables on the humerus at midshaft (Tables 3.5-3.7 and Figures 3.10-3.12) for females. Maximum femoral curvature does not appear to be related to DR in either male or female samples (Table 3.8 and Figure 3.13). Humeral curvature was not measured due to poor scan quality of proximal and distal ends as a result of the very small size of tamarin bones.

The explanatory power of many of these models is low, with only one model resulting in an adj. R^2 value above 0.7 (male proximal femur I_{min} adj. $R^2 = 0.725$). Regardless, there is no significant relationship between DR and robusticity when body size is held constant. Thus, results from robusticity variables and curvature of the *Saguinus* species investigated in this study prevent the rejection of the null hypotheses that there is no relationship between DR, robusticity, and curvature.

<u>*Cercopithecus*</u>. Of all femoral cross-sections, across each robusticity variable analyzed in this study (Tables 3.9-3.11 and Figures 3.14-3.16), only two indicate a significant relationship with DR: female midshaft femoral total area ($p = 0.039$) and female midshaft Z_p as shown in Table 3.10 and Figure 3.15. Looking at the DR of each of these species, it is not true that the more robust individuals are the species that range farther: *C. ascanius* and *C. cephus* have identical DRs (1.4 km); *C. mitis* (1.3 km) is very similar to *C. ascanius* and *C. cephus; C nictitans* and *C. pogonias* are identical at 1.8 km;

and *C. neglectus* has the shortest DR (0.5 km), yet *C. neglectus* consistently presents higher average values than *C. mitis* and overlaps with *C. pogonias* and *C. nictitans*. It appears then, that although midshaft femoral TA and Z_p exhibit significant variation between different DRs, the pattern does not match the predicted pattern since the species with the shortest DR is more robust than one species with a higher DR, while the other species are broadly indistinguishable. Additionally, results indicate that body size is a powerful explanatory factor of variation in all femoral cross-sections in female groups.

Results for the humerus of cercopithecines, show that in females, on all cross-sections, body size is statistically significant, and on the distal humerus each robusticity variable is also significant: TA p = 0009; I_{max} p = 0.008; I_{min} p = 0.039; J p = 0.011; Z_p p = 0.007). Graphical representation of the data show that for the humerus (Figs. 3.17-3.19), unlike the femur, there is a trend of increasing robusticity with longer DR, and the adjusted R^2 values for female samples are quite high (ranging 0.788 to 0.850), although very low for the male samples. Although dependent variables are only statistically significant in the female groups on the distal humerus, the trend of increasing robusticity with longer DR is generally consistent across both sexes and all cross-sections. However, note that it would be expected that even if no pattern was actually present, some tests will produce significant results by random chance.

Femoral curvature is not a significant predictor of DR in male or females groups (Table 3.15). Humeral antero-posterior curvature is significant in males (p = 0.005) and humeral medio-lateral curvature is significant in females (p = 0.031). Adjusted R^2 values are low in both models (adj. R^2 = 0.092 and 0.087, respectively). When graphed, there is no clear association with DR (Figure 3.20). In the male group, humeral antero-posterior

curvature is very similar across each group with the exception of *C. neglectus*. *C. neglectus* exhibits more AP curvature than any other species, contra the prediction, as it is the species with the shortest DR. Female humeral medio-lateral curvature is fairly consistent across all species with the exception of *C. pogonias,* which is less curved than the other species. Although species averages do not overlap, there is some overlap between *C. pogonias*, *C. ascanius,* and *C. mitis*. *C. mitis* exhibits a large range of variation and *C. ascanius* is represented by only one individual. As with male humeral AP curvature, female humeral ML curvature does not match the prediction since the species with the longest DR has the least curved bones.

Results from robusticity variables and curvature of the *Cercopithecus* species investigated in this study lead to failure to reject the null hypotheses that there is no relationship between DR, robusticity, and curvature with regards to the femur, but partial rejection of the null hypothesis with regards to the humerus. The predicted pattern that species that range farther have more robust bones than species with shorter day ranges is found for the humerus, although only on the distal humerus is the relationship statistically significant.

<u>*Macaca*</u>. There are no statistically significant results at any cross-section for any robusticity variable on either the humerus or femur. All results are listed in Tables 3.16-3.21. Scatterplots indicate that *M. fascicularis*, the species that is best represented in the female macaque sample, and has a low-level DR, is the least robust except with regards to total area. *M. mulatta, M. nemestrina*, and *M. nigra* are only represented by one female individual per species. *M. mulatta* generally overlaps with *M. fascicularis* (except for TA, where it is less strong), while *M. nigra*, the species with the longest DR, is the most

robust. Regarding females, these results mean that the species with longest DR (*M. nigra* at 2.4 km) is the most robust, but the other species show considerable overlap (Figures 3.21-3.26). With such low sample sizes, it is difficult to predict what the trend actually is. Male samples' robusticity differences are less distinct, and the current data show significant overlap with no apparent trend.

Humeral curvature is not correlated with DR, but antero-posterior femoral curvature in the female sample is statistically significant ($p = 0.014$) (Table 3.22). Additionally, the adjusted R^2 value is moderately high in this model (adj. $R^2 = 0.715$). Despite the significant result, the predicted pattern of longer DR leading to more curvature is not evident given that *M. mulatta* females show more curvature than *M. nemestrina* and *M. nigra* females despite the species' shorter DR (Figure 3.27). As with the robusticity variables, *M. fascicularis* has the least curvature. It is difficult to discuss species averages within this genus given the poor representation of many species, and these results, therefore, have limited power.

Results from robusticity variables and curvature of the *Macaca* species investigated in this study result in failure to reject the null hypotheses that there is no relationship between DR, robusticity, and curvature. Species that range farther do not have more robust and more curved bones than species with shorter day ranges, although given the female data, with larger sample sizes, these results could change with representation of additional individuals.

Papio and Theropithecus. Variation in baboon femoral robusticity is not well explained by DR. Overall, adjusted R^2 values in the female samples are relatively high, but male adjusted R^2 values remain low. Body size significantly accounts for variation in

all robusticity variables in the female samples on all femoral cross-sections except TA (Table 3.23-25); however, no dependent variable is significant. In the male sample, no femoral robusticity variables are statistically significant. At the femoral midshaft (Table 3.24), in the female sample, both body size and robusticity variables are statistically significant or approach significance. Results are as follows for female femoral midshaft: TA ($p = 0.039$), I_{max} ($p = 0.087$), I_{min} ($p = 0.066$), J ($p = 0.074$), and Z_p ($p = 0.054$). Neither dependent variables nor the covariate are significant in the male samples. Results for the proximal femur are similar to those of the distal femur (Table 3.25).

At the distal humerus, in the female sample, both body size and robusticity variables are statistically significant (Table 3.26). Results are as follows for the female distal humerus: TA ($p = 0.009$), I_{max} ($p = 0.008$), I_{min} ($p = 0.039$), J ($p = 0.011$), and Z_p ($p = 0.007$). Adjusted R^2 values range from 0.827 to 0.850. Neither dependent variables nor the covariate are significant in the male samples and adjusted R^2 values remain low. Body size accounts for variation in robusticity variables at the humeral midshaft (Table 3.27) and proximal humerus (Table 3.28) in the female samples (but not male samples), but no dependent variables are statistically significant.

Despite the significant results for the female groups reported above, it seems that longer DR does not lead to more robust bones. Female individuals represent three species within the genus *Papio* (*P. anubis*, DR = 3.6 km; *P. cynocephalus*, DR = 5.9 km; and *P. hamadryas*, DR = 10.7 km). Results at each location on the humerus show that variation within *P. anubis* mostly encompasses variation within the other two species (Figures 3.32-3.33), although female *P. hamadryas* exhibit fairly high femoral TA values.

In addition to the three species represented by females, two more species are represented by the male samples (*P. ursinus*, DR = 7.2 km and *Theropithecus gelada*, DR = 0.6 km). Unfortunately only one male *P. cynocephalus* and two *T. gelada* individuals are represented. At each location on the humerus, ranges of variation generally overlap with no apparent trend (Figures 3.31-3.33). It is evident, then, that longer DRs do not result in more robust humeri in males. Results for male femora are slightly different, but point towards the same conclusion (Figures 3.28-3.30). *P. anubis* males have more robust femora than any other species (except with regards to TA); the species averages do overlap, though. (However, note that *P. cynocephalus* and *T. gelada* are only represented by one individual each.) *P. cynocephalus* is always least robust with regards to males, although that is not true for female *P. cynocephalus*.

Results for curvature are similar to robusticity results. In the female samples, body size significantly predicts femoral and humeral curvature ($p < 0.00$). The only significant result from the males samples comes from medio-lateral humeral curvature ($p = 0.042$), but the adjusted R^2 value is very low (0.116) (Table 3.29).

Trends in curvature are less apparent (Figure 3.34). In females, average femoral and medio-lateral humeral curvature is very similar for *P. anubis* and *P. cynocephalus* with *P. hamadryas* exhibiting much less curvature, on average. Antero-posterior humeral curvature exhibits a different trend. Species averages for *P. anubis* and *P. hamadryas* are very similar, and higher, than is *P. cynocephalus*, although the range of *P. anubis* completely encompasses both other species. In males, femoral curvature is highest in *P. anubis*. Humeral antero-posterior curvature is approximately equal between all species except *P. cynocephalus*, which is less curved. The range of variation in *P. anubis*

encompasses all other species' ranges. Humeral medio-lateral curvature is approximately equal between all species except *T. gelada*, which exhibits the least curvature; its range of variation does not overlap with any other species aside from one outlier of *P. hamadryas*.

Results from robusticity variables and curvature of the *Papio/Theropithecus* species investigated in this study lead to failure to reject the null hypotheses that no relationship exists between DR, robusticity, and curvature. Species that range farther do not have more robust and more curved bones than species with shorter day ranges.

Discussion and Conclusion

The predictions are that primate species with longer day ranges will have more robust and more curved bones. Results did not match the predictions, and neither null hypothesis was rejected within any genus. While some models did yield statistically significant results, further analysis reveals that the species with longer DRs do not exhibit stronger bones, as measured by maximum bending strength, minimum bending strength, strength in torsion, or average bending and torsional strength measured at three locations on humeral and femoral shafts. Additionally, species with longer DRs do not exhibit more longitudinally curved humeri or femora. In many analyses, body size accounted for much variation in robusticity variables and also curvature.

Baboons are the largest and most terrestrial primates used in this study; therefore, they are the group with the least compliant substrate. Compliant substrates, such as tree branches that are able to sway with the weight of an animal, lessen reaction forces, so it might be expected that, in general, arboreal animals would have less robust limb bones than terrestrial animals, and that DR would have less impact on the skeletal variables

analyzed in this study. Indeed, more models were significant in the *Papio/Theropithecus* genera than in the others. Despite this, the nature of the relationship between DR and robusticity/curvature is not clearly defined via this study. In the face of statistically insignificant results and low R^2 values, it may be that controlling for phylogenetic relationships and then grouping together species (within a genus) that have very similar DRs for the purpose of statistical analysis would be beneficial. Sample sizes can always be increased, and some species in this study are seriously underrepresented. Undoubtedly increasing sample size would increase the range of variation. How the species average will shift with the addition of more specimens is unpredictable.

Differences in locomotion may also be a confounding factor. Although broadly similar within the species analyzed here, differences do exist in the amount of time spent in terrestrial versus arboreal environments, and also in the amount of leaping versus strict quadrupedalism incorporated in an animal's locomotor repertoire.

A different route to explore is in adjustment of the placement of the neutral axis of bending. Robusticity calculations for each variable are dependent on assumptions about the location of the neutral axis running through the bone. It has been experimentally shown that section moduli calculated from a centroidal axis (as was done in the current study), rather than the actual neutral axis exhibit large errors in absolute values, although patterns of differences show high correspondence (Lieberman et al. 2004). Location of the true neutral axis varies under different loading conditions and throughout the gait cycle; it tends to shift toward the cortex of bone that experiences tension (Lieberman et al. 2004). Perhaps simple calculations of robusticity based on an assumed centrally located neutral axis are not refined enough to fully or accurately

capture robusticity of cross-sections within a shaft for these primate species. Moreover, regardless of if an accurate neutral axis can be defined, it may be that determining robusticity at a few specific locations is not comprehensive enough to assess strength of an entire bone, which is why the design and implications of experiments in Chapter V: FEA OF HUMAN AND NEANDERTHAL FEMORA are particularly important. Although the methods employed in this study are more sophisticated than many that have been used in the past due to advancements in technology, bones remain integrated structures and their analyses benefit from comprehensive, nuanced techniques that are not achievable through measurements of discrete variables. Future investigations will continue to explore this relationship.

Finally, it may be that relatively small increases in day range simply are not positively correlated with robusticity or curvature, and no matter how refined the analyses become, no significant relationship will be found due to the very complex interaction of bones, their loading histories, and terrain differences.

Table 3.1	DR (km)	Avg. DR (km)	Combined Avg. DR	Time observed	Reference
Saguinus					
S. fuscicollis			**1.3**		
	0.9-1.6	1.2		19 days	(Terborgh 1983)
		1.4			(Garber 1993)
S. geoffroyi	1.7-2.5	2.1		60 days	(Dawson 1979)
S. mystax			**1.6**		
	1.1-1.2	1.2		2 days	(Castro and Soini 1977)
		1.9			(Garber 1993)
S. nigricollis		1			Iwaza (1978)
S. oedipus	1.5-1.9	1.7		2500 hours	(Neyman 1977)
Cercopithecus					
C. ascanius	1.1-2	1.4		65 days	(Struhsaker 1980)
C. cephus			**1.4**		
		0.8		50 hours	(Gautier-Hion and Gautier 1974)
		1.3			(Gautier-Hion et al. 1983)
		2			(Gautier-Hion et al. 1983)
C. diana			**1.3**		
		1		96 days	(Whitesides 1989)
		1.5		39 days	(Whitesides 1989)
C. mitis			**1.3**		
	0.8-1.5	1.1		12 days	(Butynski 1990)
	0.8-1.9	1.2		13 days	(Butynski 1990)
	0.7-1.7	1.2		19 days	(Butynski 1990)
	1-1.6	1.3		80-160 days	(Kaplin 2001)
	0.7-2.2	1.3		61 days	(Butynski 1990)
	0.7-2.4	1.4		71 days	(Butynski 1990)
C. neglectus	0.3-1	0.5			(Gautier-Hion and Gautier 1978)
C. nictitans			**1.8**		
		1.6			(Gautier-Hion and Gautier 1974)
		1.8			(Gautier-Hion et al. 1983)
		2			(Gautier-Hion et al. 1983
C. pogonias			**1.8**		
		1.6			(Gautier-Hion and Gautier 1974)
		1.8			(Gautier-Hion et al. 1983)
		1.2			(Gautier-Hion et al. 1983
Macaca					
M. arctoides	0.4-3	1			(Bertrand 1969)
M. fascicularis			**1.3**		
	0.2-1.5	0.9		38 days	(Aldrich-Blake 1980)
	0.2-1.5	0.9			(Payne and Francis 1985)
		1.4		10 days	(MacKinnon and MacKinnon 1980)
		1.9		35 days	(Wheatley 1980)
M. mulatta	0.4-2.8	1.4		38 days	(Lindburg 1977)
M. nemestrina		2		10 days	(MacKinnon and MacKinnon 1980)
M. nigra	0.5-6	2.4			(O'Brien and Kinnaird 1997)
M. radiata			**1.3**		
	0-2	0.8		57 days	(Sugiyama 1971)
	1-2.5	1.8			(Kuruvilla 1980)

Table 3.1	DR (km)	Avg. DR (km)	Combined Avg. DR	Time observed	Reference
M. silenus	0.8-2.5	1.7		4 days	(Kurup and Kumar 1993)
Papio and Theropithecus					
P. anubis			**3.6**		
	0.3-2	1.2		13 days	(Dunbar and Dunbar 1974)
	1.6-6.5	2.4			(Rowell 1966)
		5			(Harding 1976)
		5.8		12 days	(Aldrich-Blake et al. 1971)
P. cynocephalus		5.9			(Altmann and Altmann 1970)
P. hamadryas			**10.7**		
	7-10.2	8.6		57 days	(Sigg and Stolba 1981)
	8.1-12.7	10.4		13 days	(Sigg and Stolba 1981)
	4.1-19.2	13.2		9 days	(Kummer 1990)
P. ursinus			**7.2**		
	1.6-8	8.6		32 days	(DeVore and Hall 1965)
	3.2-9.7	10.4		31 days	(Stoltz and Saayman 1970)
	2.4-14.5	13.2		23 days	(Stoltz and Saayman 1970)
T. gelada	0.5-1	0.6		8 days	(Dunbar and Dunbar 1974)
Leontopithecus					
L. chrysomelas	1.4-2.2	1.8			Rylands (1993)
L. chrysopygus	2.1-2.6	2.3		7 days	Keuroghlian (1990)
L. rosalia	1.3-1.5	1.4		55 days	Peres (1989)
Trachypithecus					
T. cristatus			**0.4**		
	0.4-0.7	0.4			Kool (1989)
	0.2-0.5	0.4			Bernstein (1968)
	0.4-0.7	0.5			Kool (1989)
T. obscurus			**0.8**		
		0.6		29 days	Curtin (1980)
		1		10 days	MacKinnon and MacKinnon (1980)
T. phayrei		1			Stanford (1988)
T. pileatus	0.05-0.5	0.2			Stanford (1988)
Gorilla gorilla					
G. g. beringei			**0.7**		
	0.1-1.8	0.3			Schaller (1963)
	0.1-2.5	0.4		91 days	Fossey and Harcourt (1977)
	0.1-0.8	0.4		8 months	Caro (1976)
G. g. beringei					
	0.1-2.5	0.5		41 days	Elliott (1976)
	0.1-1.1	0.5		35 days	Caro (1976)
	0.1-1	0.5			Schaller (1963)
	0.1-1.8	0.7			Schaller (1963)
	0.5-1.2	0.8		3 days	Goodall (1977)
	0.1-3.4	0.9		~7 months	Schaller (1963)
	1.3-1.9	1.6		6 days	
G. g. gorilla			**1**		
	0.7-1.1	0.9			Jones and Sabater Pi (1971)
	0.7-1.6	1.1		5 days	Jones and Sabater Pi (1971)
	0.3-1.8	1.2		2 days	Williamson (1988)
G. g. graueri	0.6-3	0.9		36 days	Casimir and Butenandt (1973)
Pongo					
P. abelii			**0.7**		

Table 3.1	DR (km)	Avg. DR (km)	Combined Avg. DR	Time observed	Reference
	0.2-1.8	0.5			Rijksen (1978)
	0.2-1.3	0.6			Rijksen (1978)
	0.3-2	0.9			Rijksen (1978)
P. pygmaeus			**0.5**		
		0.3			Rodman (1977)
		0.5			MacKinnon (1974)
		0.8			Galdikas (1978)

Table 3.2 Number of specimens present per species

	Femur		Humerus	
Species	**Female**	**Male**	**Female**	**Male**
Saguinus fuscicollis	2	2	3	0
S. mystax	4	4	4	5
S. oedipus	4	9	4	8
Cercopithecus ascanius	1	5	1	6
C. cephus	4	18	5	18
C. diana	1	0	1	0
C. mitis	2	2	4	5
C. neglectus	2	5	2	5
C. nictitans	5	15	4	14
C. pogonias	5	12	6	13
Macaca fascicularis	4	0	4	1
M. mulatta	2	1	1	1
M. nemestrina	1	7	1	7
M. nigra	1	0	1	0
M. silenus	0	1	0	1
Theropithecus gelada	0	1	0	2
Papio anubis	7	9	7	10
P. cynocephalus	2	1	3	1
P. ursinus	0	3	0	3
P. hamadryas	2	4	2	5

Note that in Tables 3.3 through 3.30, BS (body size, which is calculated as the cubed geometric mean of femoral head diameter, humeral head diameter, maximum femoral length, and maximum humeral length) is an independent variable, the effect of which was controlled for, with robusticity variables (TA, I, J, and Z_p) as independent variables. The effect of the dependent variable day range (DR) on independent variables was tested.

Table 3.3

Saguinus: Distal Femur	**Females**			**Males**		
	Distal Femoral Total Area					
	Coefficient	Std. Error	p-value	Coefficient	Std. Error	p-value
Intercept	-0.828	0.491	0.136	-0.109	0.475	0.822
log10(BS)	0.259	0.142	0.111	0.049	0.130	0.712
log10(F.dist.TA)	-0.118	0.286	0.693	-0.302	0.237	0.227
n	10			15		
multiple R^2	0.431			0.159		
adj. R^2	0.268			0.019		
F-statistic	2.651			1.136		
p-value	0.139			0.353		
	Distal Femoral I_{max}					
	Coefficient	Std. Error	p-value	Coefficient	Std. Error	p-value
Intercept	-1.318	0.594	0.062	-0.933	0.648	0.176
log10(BS)	0.231	0.127	0.113	0.050	0.123	0.690
log10(F.dist.I_{max})	-0.148	0.133	0.304	-0.217	0.132	0.127
n	10			15		
multiple R^2	0.504			0.221		
adj. R^2	0.363			0.091		
F-statistic	3.561			1.701		
p-value	0.086			0.224		
	Distal Femoral I_{min}					
	Coefficient	Std. Error	p-value	Coefficient	Std. Error	p-value
Intercept	-0.592	0.967	0.560	-0.994	0.807	0.242
log10(BS)	0.286	0.126	0.058	0.087	0.125	0.500
log10(F.dist.I_{min})	0.065	0.190	0.743	-0.192	0.153	0.234
n	10			15		
multiple R^2	0.427			0.156		
adj. R^2	0.263			0.016		
F-statistic	2.605			1.112		
p-value	0.143			0.360		
	Distal Femoral J					
	Coefficient	Std. Error	p-value	Coefficient	Std. Error	p-value
Intercept	-1.220	0.714	0.131	-0.974	0.687	0.182
log10(BS)	0.261	0.130	0.085	0.063	0.123	0.617
log10(F.dist.J)	-0.106	0.167	0.548	-0.227	0.145	0.144
n	10			15		
multiple R^2	0.449			0.207		
adj. R^2	0.291			0.075		
F-statistic	2.848			1.567		
p-value	0.125			0.249		
	Distal Femoral Z_p					
	Coefficient	Std. Error	p-value	Coefficient	Std. Error	p-value
(Intercept)	-1.051	0.602	0.124	-0.700	0.617	0.279
log10(BS)	0.261	0.136	0.097	0.058	0.128	0.656
log10(F.dist.Z_p)	-0.100	0.216	0.658	-0.257	0.195	0.212
n	10			15		
multiple R^2	0.434			0.167		
adj. R^2	0.273			0.028		
F-statistic	2.688			1.199		
p-value	0.136			0.335		

Table 3.4

Saguinus: Midshaft Femur	**Females**			**Males**		
	Midshaft Femoral Total Area					
	Coefficient	Std. Error	p-value	Coefficient	Std. Error	p-value
Intercept	-0.888	0.495	0.115	-0.474	0.510	0.371
log10(BS)	0.273	0.203	0.221	-0.053	0.163	0.749
log10(F.mid.TA)	-0.021	0.266	0.939	-0.327	0.228	0.178
n	10			15		
multiple R^2	0.418			0.185		
adj. R^2	0.251			0.049		
F-statistic	2.511			1.360		
p-value	0.151			0.294		
	Midshaft Femoral I_{max}					
	Coefficient	Std. Error	p-value	Coefficient	Std. Error	p-value
Intercept	-1.093	0.625	0.124	-0.741	0.616	0.252
log10(BS)	0.246	0.146	0.135	0.059	0.126	0.646
log10(F.mid.I_{max})	-0.081	0.156	0.618	-0.161	0.114	0.184
n	10			15		
multiple R^2	0.439			0.181		
adj. R^2	0.279			0.045		
F-statistic	2.738			1.330		
p-value	0.132			0.301		
	Midshaft Femoral I_{min}					
	Coefficient	Std. Error	p-value	Coefficient	Std. Error	p-value
Intercept	-0.804	0.610	0.229	-0.831	0.604	0.194
log10(BS)	0.297	0.141	0.073	0.052	0.123	0.681
log10(F.mid.I_{min})	0.027	0.134	0.848	-0.185	0.112	0.125
n	10			15		
multiple R^2	0.421			0.222		
adj. R^2	0.255			0.092		
F-statistic	2.539			1.713		
p-value	0.148			0.222		
	Midshaft Femoral J					
	Coefficient	Std. Error	p-value	Coefficient	Std. Error	p-value
Intercept	-0.938	0.599	0.161	-0.750	0.591	0.229
log10(BS)	0.274	0.145	0.101	0.055	0.124	0.668
log10(F.mid.J)	-0.024	0.149	0.874	-0.178	0.115	0.148
n	10			15		
multiple R^2	0.419			0.205		
adj. R^2	0.254			0.072		
F-statistic	2.528			1.543		
p-value	0.149			0.253		
	Midshaft Femoral Z_p					
	Coefficient	Std. Error	p-value	Coefficient	Std. Error	p-value
(Intercept)	-0.881	0.537	0.145	-0.587	0.544	0.302
log10(BS)	0.285	0.144	0.088	0.049	0.127	0.706
log10(F.mid.Z_p)	-0.002	0.181	0.993	-0.223	0.154	0.172
n	10			15		
multiple R^2	0.417			0.188		
adj. R^2	0.251			0.053		
F-statistic	2.505			1.393		
p-value	0.151			0.286		

Table 3.5

Saguinus: Proximal Femur	**Females**			**Males**		
	Proximal Femoral Total Area					
	Coefficient	Std. Error	p-value	Coefficient	Std. Error	p-value
Intercept	-0.887	0.483	0.109	-0.466	0.268	0.110
log10(BS)	0.260	0.208	0.252	-0.157	0.082	0.083
log10(F.prox.TA)	-0.039	0.248	0.880	-0.469	0.109	0.001**
n	10			14		
multiple R^2	0.419			0.640		
adj. R^2	0.253			0.574		
F-statistic	2.527			9.768		
p-value	0.149			0.004		
	Proximal Femoral I_{max}					
	Coefficient	Std. Error	p-value	Coefficient	Std. Error	p-value
Intercept	-0.843	0.591	0.197	-0.772	0.345	0.047
log10(BS)	0.295	0.154	0.098	0.030	0.073	0.684
log10(F.prox.I_{max})	0.016	0.151	0.918	-0.195	0.054	0.004**
n	10			14		
multiple R^2	0.418			0.555		
adj. R^2	0.252			0.474		
F-statistic	2.515			6.848		
p-value	0.150			0.012		
	Proximal Femoral I_{min}					
	Coefficient	Std. Error	p-value	Coefficient	Std. Error	p-value
Intercept	-0.990	0.535	0.107	-0.918	0.251	0.004
log10(BS)	0.253	0.146	0.126	-0.032	0.055	0.573
log10(F.prox.I_{min})	-0.051	0.114	0.670	-0.272	0.046	0.000**
n	10			14		
multiple R^2	0.433			0.767		
adj. R^2	0.271			0.725		
F-statistic	2.675			18.090		
p-value	0.137			0.000		
	Proximal Femoral J					
	Coefficient	Std. Error	p-value	Coefficient	Std. Error	p-value
Intercept	-0.924	0.548	0.136	-0.796	0.294	0.020
log10(BS)	0.272	0.151	0.116	0.005	0.064	0.937
log10(F.prox.J)	-0.023	0.136	0.871	-0.234	0.051	0.001**
n	10			14		
multiple R^2	0.420			0.663		
adj. R^2	0.254			0.602		
F-statistic	2.530			10.830		
p-value	0.149			0.003		
	Proximal Femoral Z_p					
	Coefficient	Std. Error	p-value	Coefficient	Std. Error	p-value
(Intercept)	-0.898	0.512	0.122	-0.661	0.302	0.051
log10(BS)	0.277	0.151	0.109	0.011	0.069	0.875
log10(F.prox.Z_p)	-0.019	0.176	0.917	-0.305	0.075	0.002**
n	10			14		
multiple R^2	0.418			0.611		
adj. R^2	0.252			0.540		
F-statistic	2.515			8.642		
p-value	0.150			0.006		

Table 3.6

Saguinus: Distal Humerus	**Females**			**Males**		
	Distal Humeral Total Area					
	Coefficient	Std. Error	p-value	Coefficient	Std. Error	p-value
Intercept	-0.715	0.415	0.128	0.150	0.211	0.495
log10(BS)	0.250	0.146	0.130	0.007	0.059	0.909
log10(H.dist.TA)	0.017	0.212	0.937	-0.016	0.109	0.887
n	11			13		
multiple R^2	0.470			0.012		
adj. R^2	0.318			-0.185		
F-statistic	3.100			0.063		
p-value	0.109			0.940		
	Distal Humeral I_{max}					
	Coefficient	Std. Error	p-value	Coefficient	Std. Error	p-value
Intercept	-0.479	0.626	0.469	0.201	0.304	0.523
log10(BS)	0.246	0.096	0.037*	0.012	0.042	0.778
log10(H.dist.I_{max})	0.059	0.119	0.636	0.006	0.051	0.909
n	11			13		
multiple R^2	0.487			0.012		
adj. R^2	0.341			-0.186		
F-statistic	3.324			0.059		
p-value	0.097			0.943		
	Distal Humeral I_{min}					
	Coefficient	Std. Error	p-value	Coefficient	Std. Error	p-value
Intercept	-0.809	0.467	0.127	0.170	0.251	0.514
log10(BS)	0.230	0.106	0.067	0.013	0.045	0.775
log10(H.dist.I_{min})	-0.026	0.095	0.790	0.000	0.056	0.998
n	11			13		
multiple R^2	0.475			0.010		
adj. R^2	0.325			-0.188		
F-statistic	3.166			0.052		
p-value	0.105			0.950		
	Distal Humeral J					
	Coefficient	Std. Error	p-value	Coefficient	Std. Error	p-value
Intercept	-0.664	0.540	0.258	0.185	0.288	0.534
log10(BS)	0.246	0.100	0.044*	0.013	0.041	0.753
log10(H.dist.J)	0.019	0.114	0.872	0.004	0.057	0.952
n	11			13		
multiple R^2	0.471			0.011		
adj. R^2	0.320			-0.187		
F-statistic	3.120			0.054		
p-value	0.108			0.948		
	Distal Humeral Z_p					
	Coefficient	Std. Error	p-value	Coefficient	Std. Error	p-value
(Intercept)	-0.604	0.441	0.213	0.102	0.227	0.662
log10(BS)	0.256	0.099	0.037*	0.011	0.041	0.802
log10(H.dist.Z_p)	0.063	0.123	0.624	-0.027	0.066	0.691
n	11			12		
multiple R^2	0.488			0.027		
adj. R^2	0.342			-0.168		
F-statistic	3.341			0.137		
p-value	0.096			0.874		

Table 3.7

Saguinus: Midshaft Humerus	**Females**			**Males**		
	Midshaft Humeral Total Area					
	Coefficient	Std. Error	p-value	Coefficient	Std. Error	p-value
Intercept	-0.515	0.423	0.264	0.047	0.233	0.844
log10(BS)	0.325	0.129	0.040*	-0.002	0.046	0.959
log10(H.mid.TA)	0.191	0.208	0.390	-0.065	0.093	0.501
n	11			13		
multiple R^2	0.526			0.056		
adj. R^2	0.391			-0.132		
F-statistic	3.884			0.298		
p-value	0.073			0.748		
	Midshaft Humeral I_{max}					
	Coefficient	Std. Error	p-value	Coefficient	Std. Error	p-value
Intercept	-0.271	0.595	0.663	0.015	0.259	0.954
log10(BS)	0.252	0.092	0.029*	0.016	0.040	0.704
log10(H.mid.I_{max})	0.110	0.115	0.372	-0.032	0.044	0.478
n	11			13		
multiple R^2	0.530			0.061		
adj. R^2	0.396			-0.127		
F-statistic	3.950			0.326		
p-value	0.071			0.729		
	Midshaft Humeral I_{min}					
	Coefficient	Std. Error	p-value	Coefficient	Std. Error	p-value
Intercept	-0.383	0.549	0.508	0.010	0.349	0.977
log10(BS)	0.256	0.094	0.030*	0.022	0.044	0.626
log10(H.mid.I_{min})	0.087	0.105	0.433	-0.027	0.053	0.621
n	11			13		
multiple R^2	0.517			0.035		
adj. R^2	0.379			-0.158		
F-statistic	3.745			0.183		
p-value	0.078			0.835		
	Midshaft Humeral J					
	Coefficient	Std. Error	p-value	Coefficient	Std. Error	p-value
Intercept	-0.350	0.549	0.544	0.002	0.291	0.994
log10(BS)	0.254	0.093	0.029*	0.019	0.041	0.645
log10(H.mid.J)	0.100	0.111	0.396	-0.034	0.050	0.514
n	11			13		
multiple R^2	0.525			0.054		
adj. R^2	0.389			-0.136		
F-statistic	3.863			0.284		
p-value	0.074			0.759		
	Midshaft Humeral Z_p					
	Coefficient	Std. Error	p-value	Coefficient	Std. Error	p-value
(Intercept)	-0.449	0.473	0.374	-0.020	0.256	0.940
log10(BS)	0.260	0.094	0.028*	0.022	0.040	0.602
log10(H.mid.Z_p)	0.123	0.138	0.401	-0.055	0.060	0.383
n	11			12		
multiple R^2	0.524			0.086		
adj. R^2	0.388			-0.096		
F-statistic	3.847			0.472		
p-value	0.075			0.637		

Table 3.8

Saguinus: Proximal Humerus	**Females**			**Males**		
	Proximal Humeral Total Area					
	Coefficient	Std. Error	p-value	Coefficient	Std. Error	p-value
Intercept	-0.765	0.410	0.104	0.165	0.216	0.463
log10(BS)	0.212	0.175	0.263	0.013	0.044	0.780
log10(H.prox.TA)	-0.055	0.273	0.846	-0.003	0.078	0.969
n	11			13		
multiple R^2	0.472			0.010		
adj. R^2	0.321			-0.188		
F-statistic	3.132			0.053		
p-value	0.107			0.949		
	Proximal Humeral I_{max}					
	Coefficient	Std. Error	p-value	Coefficient	Std. Error	p-value
Intercept	-0.788	0.617	0.242	0.054	0.234	0.820
log10(BS)	0.240	0.098	0.045*	0.020	0.041	0.645
log10(H.prox.I_{max})	-0.016	0.131	0.909	-0.022	0.033	0.529
n	11			13		
multiple R^2	0.470			0.051		
adj. R^2	0.319			-0.139		
F-statistic	3.107			0.267		
p-value	0.108			0.771		
	Proximal Humeral I_{min}					
	Coefficient	Std. Error	p-value	Coefficient	Std. Error	p-value
Intercept	-0.944	0.505	0.104	0.351	0.294	0.260
log10(BS)	0.198	0.118	0.138	0.003	0.042	0.943
log10(H.prox.I_{min})	-0.086	0.142	0.562	0.032	0.045	0.490
n	11			13		
multiple R^2	0.496			0.059		
adj. R^2	0.352			-0.130		
F-statistic	3.443			0.312		
p-value	0.091			0.739		
	Proximal Humeral J					
	Coefficient	Std. Error	p-value	Coefficient	Std. Error	p-value
Intercept	-0.860	0.550	0.162	0.119	0.254	0.649
log10(BS)	0.229	0.104	0.062	0.016	0.042	0.711
log10(H.prox.J)	-0.044	0.138	0.759	-0.010	0.039	0.804
n	11			13		
multiple R^2	0.477			0.017		
adj. R^2	0.327			-0.180		
F-statistic	3.190			0.085		
p-value	0.104			0.920		
	Proximal Humeral Z_p					
	Coefficient	Std. Error	p-value	Coefficient	Std. Error	p-value
(Intercept)	-0.963	0.480	0.085	0.224	0.152	0.172
log10(BS)	0.195	0.113	0.129	0.025	0.039	0.543
log10(H.prox.Z_p)	-0.154	0.211	0.488	0.036	0.030	0.266
n	11			13		
multiple R^2	0.507			0.131		
adj. R^2	0.366			-0.043		
F-statistic	3.597			0.754		
p-value	0.084			0.495		

Table 3.9

Saguinus: Femoral Curvature	**Females**			**Males**		
	Femoral Curvature					
	Coefficient	Std. Error	p-value	Coefficient	Std. Error	p-value
Intercept	0.009	0.144	0.950	-0.022	0.235	0.928
log10(BS)	0.178	0.199	0.389	0.297	0.304	0.344
log10(F.C.AP)	0.200	0.164	0.247	-0.007	0.105	0.947
n	14			17		
multiple R2	0.266			0.064		
adj. R2	0.133			-0.069		
F-statistic	1.997			0.483		
p-value	0.182			0.627		

Table 3.10

Cercopithecus: Distal Femur	**Females**			**Males**		
	Distal Femoral Total Area					
	Coefficient	Std. Error	p-value	Coefficient	Std. Error	p-value
Intercept	10.263	2.659	0.005	-1.272	4.313	0.772
log10(BS)	-0.863	0.432	0.081	-1.242	0.686	0.090
log10(F.dist.TA)	1.503	1.127	0.219	-2.730	1.454	0.080
n	20			57		
multiple R^2	0.689			0.230		
adj. R^2	0.611			0.127		
F-statistic	8.862			2.240		
p-value	0.009			0.141		
	Distal Femoral I_{max}					
	Coefficient	Std. Error	p-value	Coefficient	Std. Error	p-value
Intercept	10.754	3.119	0.009	-4.240	5.267	0.433
log10(BS)	-1.323	0.323	0.003**	-0.269	0.600	0.660
log10(F.dist.I_{max})	0.644	0.522	0.252	-1.471	0.743	0.067
n	20			57		
multiple R^2	0.681			0.246		
adj. R^2	0.601			0.145		
F-statistic	8.529			2.444		
p-value	0.010			0.121		
	Distal Femoral I_{min}					
	Coefficient	Std. Error	p-value	Coefficient	Std. Error	p-value
Intercept	10.673	3.998	0.028	-4.519	5.246	0.403
log10(BS)	-1.415	0.379	0.006**	-0.169	0.608	0.785
log10(F.dist.I_{min})	0.501	0.573	0.408	-1.381	0.674	0.058
n	20			57		
multiple R^2	0.653			0.257		
adj. R^2	0.566			0.158		
F-statistic	7.527			2.594		
p-value	0.015			0.108		
	Distal Femoral J					
	Coefficient	Std. Error	p-value	Coefficient	Std. Error	p-value
Intercept	10.841	3.418	0.013	-4.380	5.141	0.408
log10(BS)	-1.382	0.342	0.004**	-0.203	0.601	0.740
log10(F.dist.J)	0.628	0.560	0.295	-1.509	0.726	0.055
n	20			57		
multiple R^2	0.672			0.262		
adj. R^2	0.589			0.163		
F-statistic	8.177			2.660		
p-value	0.012			0.103		
	Distal Femoral Z_p					
	Coefficient	Std. Error	p-value	Coefficient	Std. Error	p-value
(Intercept)	11.033	2.863	0.005	-2.009	4.696	0.675
log10(BS)	-1.363	0.315	0.003**	-0.353	0.603	0.567
log10(F.dist.Z_p)	1.082	0.723	0.173	-1.761	0.981	0.093
n	20			57		
multiple R^2	0.703			0.217		
adj. R^2	0.629			0.113		
F-statistic	9.476			2.080		
p-value	0.008			0.160		

Table 3.11

Cercopithecus: Midshaft Femur	**Females**			**Males**		
	Midshaft Femoral Total Area					
	Coefficient	Std. Error	p-value	Coefficient	Std. Error	p-value
Intercept	10.766	1.937	0.001	0.928	4.120	0.825
log10(BS)	-0.424	0.428	0.351	-1.330	0.833	0.131
log10(F.mid.TA)	2.379	0.966	0.039*	-2.190	1.622	0.197
n	19			59		
multiple R^2	0.784			0.152		
adj. R^2	0.730			0.039		
F-statistic	14.510			1.345		
p-value	0.002			0.290		
	Midshaft Femoral I_{max}					
	Coefficient	Std. Error	p-value	Coefficient	Std. Error	p-value
Intercept	11.438	2.532	0.002	-1.621	5.220	0.760
log10(BS)	-1.244	0.286	0.002	-0.485	0.615	0.443
log10(F.mid.I_{max})	0.884	0.453	0.087	-1.132	0.800	0.177
n	19			59		
multiple R^2	0.742			0.161		
adj. R^2	0.678			0.049		
F-statistic	11.520			1.440		
p-value	0.004			0.268		
	Midshaft Femoral I_{min}					
	Coefficient	Std. Error	p-value	Coefficient	Std. Error	p-value
Intercept	13.646	3.233	0.003	-1.913	5.016	0.708
log10(BS)	-1.364	0.282	0.001**	-0.549	0.603	0.377
log10(F.mid.I_{min})	1.216	0.570	0.066	-1.260	0.796	0.134
n	19			59		
multiple R^2	0.758			0.185		
adj. R^2	0.697			0.076		
F-statistic	12.500			1.704		
p-value	0.003			0.215		
	Midshaft Femoral J					
	Coefficient	Std. Error	p-value	Coefficient	Std. Error	p-value
Intercept	Coefficient	Std. Error	p-value	-1.546	4.977	0.760
log10(BS)	12.087	2.684	0.002	-0.511	0.608	0.414
log10(F.mid.J)	-1.291	0.282	0.002**	-1.222	0.808	0.151
n	1.036	0.503	0.074	59		
multiple R^2	19			0.175		
adj. R^2	0.752			0.065		
F-statistic	0.689			1.591		
p-value	12.100			0.236		
	Midshaft Femoral Z_p					
	Coefficient	Std. Error	p-value	Coefficient	Std. Error	p-value
(Intercept)	11.423	2.272	0.001	-0.019	4.463	0.997
log10(BS)	-1.210	0.273	0.002**	-0.600	0.613	0.343
log10(F.mid.Z_p)	1.515	0.673	0.054*	-1.507	1.079	0.183
n	19			59		
multiple R^2	0.767			0.158		
adj. R^2	0.709			0.046		
F-statistic	13.190			1.412		
p-value	0.003			0.274		

Table 3.12

Cercopithecus: Proximal Femur	**Females**			**Males**		
	Proximal Femoral Total Area					
	Coefficient	Std. Error	p-value	Coefficient	Std. Error	p-value
Intercept	9.396	1.577	0.000	-1.289	4.695	0.787
log10(BS)	-0.858	0.378	0.047*	-1.285	0.747	0.106
log10(F.prox.TA)	1.221	0.740	0.130	-2.774	1.726	0.129
n	22			64		
multiple R^2	0.766			0.189		
adj. R^2	0.719			0.080		
F-statistic	16.340			1.744		
p-value	0.001			0.209		
	Proximal Femoral I_{max}					
	Coefficient	Std. Error	p-value	Coefficient	Std. Error	p-value
Intercept	10.569	1.972	0.000	-4.103	6.091	0.511
log10(BS)	-1.247	0.246	0.000**	-0.194	0.648	0.768
log10(F.prox.I_{max})	0.682	0.390	0.111	-1.329	0.837	0.133
n	22			64		
multiple R^2	0.772			0.186		
adj. R^2	0.726			0.077		
F-statistic	16.890			1.712		
p-value	0.001			0.214		
	Proximal Femoral I_{min}					
	Coefficient	Std. Error	p-value	Coefficient	Std. Error	p-value
Intercept	10.713	2.378	0.001	-4.315	5.568	0.451
log10(BS)	-1.366	0.253	0.000**	-0.323	0.604	0.601
log10(F.prox.I_{min})	0.554	0.397	0.193	-1.490	0.809	0.085
n	22			64		
multiple R^2	0.751			0.224		
adj. R^2	0.701			0.121		
F-statistic	15.040			2.170		
p-value	0.001			0.149		
	Proximal Femoral J					
	Coefficient	Std. Error	p-value	Coefficient	Std. Error	p-value
Intercept	10.510	2.057	0.000	-4.444	5.784	0.454
log10(BS)	-1.303	0.246	0.000**	-0.214	0.626	0.737
log10(F.prox.J)	0.636	0.396	0.139	-1.511	0.853	0.097
n	22			64		
multiple R^2	0.763			0.214		
adj. R^2	0.716			0.109		
F-statistic	16.100			2.037		
p-value	0.001			0.165		
	Proximal Femoral Z_p					
	Coefficient	Std. Error	p-value	Coefficient	Std. Error	p-value
(Intercept)	10.013	1.758	0.000	-2.464	5.050	0.633
log10(BS)	-1.263	0.245	0.000**	-0.338	0.612	0.589
log10(F.prox.Z_p)	0.879	0.508	0.114	-1.860	1.096	0.110
n	22			64		
multiple R^2	0.770			0.202		
adj. R^2	0.725			0.096		
F-statistic	16.780			1.900		
p-value	0.001			0.184		

Table 3.13

Cercopithecus: Distal Humerus	**Females**			**Males**		
	Distal Humeral Total Area					
	Coefficient	Std. Error	p-value	Coefficient	Std. Error	p-value
Intercept	11.393	1.547	0.000	0.872	4.791	0.858
log10(BS)	-0.453	0.282	0.143	0.165	0.951	0.864
log10(H.dist.TA)	2.434	0.730	0.009**	0.338	1.951	0.864
n	23			61		
multiple R^2	0.872			0.002		
adj. R^2	0.844			-0.109		
F-statistic	30.730			0.018		
p-value	0.000			0.983		
	Distal Humeral I_{max}					
	Coefficient	Std. Error	p-value	Coefficient	Std. Error	p-value
Intercept	15.727	2.665	0.000	-1.112	6.218	0.860
log10(BS)	-1.660	0.216	0.000**	0.093	0.691	0.895
log10(H.dist.I_{max})	1.304	0.385	0.008**	-0.273	0.904	0.766
n	23			61		
multiple R^2	0.874			0.005		
adj. R^2	0.846			-0.105		
F-statistic	31.310			0.048		
p-value	0.000			0.953		
	Distal Humeral I_{min}					
	Coefficient	Std. Error	p-value	Coefficient	Std. Error	p-value
Intercept	12.838	2.547	0.001	3.096	6.759	0.652
log10(BS)	-1.280	0.200	0.000**	-0.041	0.699	0.954
log10(H.dist.I_{min})	1.080	0.447	0.039*	0.471	0.967	0.632
n	23			61		
multiple R^2	0.827			0.013		
adj. R^2	0.788			-0.096		
F-statistic	21.480			0.122		
p-value	0.000			0.886		
	Distal Humeral J					
	Coefficient	Std. Error	p-value	Coefficient	Std. Error	p-value
Intercept	14.643	2.498	0.000	0.324	6.385	0.960
log10(BS)	-1.516	0.199	0.000**	0.051	0.698	0.943
log10(H.dist.J)	1.301	0.407	0.011*	-0.009	0.970	0.993
n	23			61		
multiple R^2	0.866			0.000		
adj. R^2	0.836			-0.111		
F-statistic	29.110			0.003		
p-value	0.000			0.997		
	Distal Humeral Z_p					
	Coefficient	Std. Error	p-value	Coefficient	Std. Error	p-value
(Intercept)	12.292	1.712	0.000	0.092	5.186	0.986
log10(BS)	-1.158	0.167	0.000**	0.046	0.679	0.946
log10(H.dist.Z_p)	1.816	0.524	0.007**	-0.103	1.294	0.938
n	23			61		
multiple R^2	0.878			0.001		
adj. R^2	0.850			-0.110		
F-statistic	32.260			0.006		
p-value	0.000			0.994		

Table 3.14

Cercopithecus: Midshaft Humerus	**Females**			**Males**		
	Midshaft Humeral Total Area					
	Coefficient	Std. Error	p-value	Coefficient	Std. Error	p-value
Intercept	8.772	2.228	0.003	0.802	4.484	0.860
log10(BS)	-1.032	0.317	0.010*	0.156	0.891	0.863
log10(H.mid.TA)	0.728	0.862	0.420	0.305	1.659	0.856
n	22			60		
multiple R^2	0.735			0.002		
adj. R^2	0.677			-0.109		
F-statistic	12.510			0.020		
p-value	0.003			0.981		
	Midshaft Humeral I_{max}					
	Coefficient	Std. Error	p-value	Coefficient	Std. Error	p-value
Intercept	8.809	3.077	0.019	1.385	5.969	0.819
log10(BS)	-1.296	0.299	0.002**	0.012	0.698	0.987
log10(H.mid.I_{max})	0.230	0.410	0.589	0.180	0.815	0.828
n	22			60		
multiple R^2	0.724			0.003		
adj. R^2	0.663			-0.108		
F-statistic	11.810			0.027		
p-value	0.003			0.973		
	Midshaft Humeral I_{min}					
	Coefficient	Std. Error	p-value	Coefficient	Std. Error	p-value
Intercept	8.911	3.118	0.019	0.595	5.679	0.918
log10(BS)	-1.278	0.280	0.001**	0.045	0.682	0.948
log10(H.mid.I_{min})	0.261	0.445	0.572	0.043	0.804	0.958
n				60		
multiple R^2	0.725			0.000		
adj. R^2	0.664			-0.111		
F-statistic	11.860			0.004		
p-value	0.003			0.996		
	Midshaft Humeral J					
	Coefficient	Std. Error	p-value	Coefficient	Std. Error	p-value
Intercept	8.897	3.084	0.018	1.031	5.734	0.859
log10(BS)	-1.297	0.295	0.002**	0.028	0.691	0.968
log10(H.mid.J)	0.260	0.441	0.570	0.127	0.825	0.879
n	22			60		
multiple R^2	0.725			0.002		
adj. R^2	0.664			-0.109		
F-statistic	11.870			0.015		
p-value	0.003			0.986		
	Midshaft Humeral Z_p					
	Coefficient	Std. Error	p-value	Coefficient	Std. Error	p-value
(Intercept)	8.998	2.457	0.005	1.158	4.618	0.805
log10(BS)	-1.276	0.259	0.001**	0.071	0.680	0.918
log10(H.mid.Z_p)	0.470	0.559	0.422	0.325	1.074	0.766
n	22			60		
multiple R^2	0.735			0.005		
adj. R^2	0.676			-0.105		
F-statistic	12.490			0.048		
p-value	0.003			0.953		

Table 3.15

Cercopithecus: Proximal Humerus	**Females**			**Males**		
	Proximal Humeral Total Area					
	Coefficient	Std. Error	p-value	Coefficient	Std. Error	p-value
Intercept	8.230	1.880	0.002	3.976	5.271	0.460
log10(BS)	-1.069	0.306	0.007**	0.407	0.757	0.598
log10(H.prox.TA)	0.515	0.700	0.481	1.690	1.746	0.346
n	23			60		
multiple R^2	0.731			0.050		
adj. R^2	0.671			-0.056		
F-statistic	12.200			0.471		
p-value	0.003			0.632		
	Proximal Humeral I_{max}					
	Coefficient	Std. Error	p-value	Coefficient	Std. Error	p-value
Intercept	9.611	2.753	0.007	4.594	6.785	0.507
log10(BS)	-1.341	0.280	0.001**	-0.217	0.756	0.778
log10(H.prox.I_{max})	0.362	0.372	0.357	0.628	0.839	0.464
n	23			61		
multiple R^2	0.742			0.030		
adj. R^2	0.684			-0.077		
F-statistic	12.910			0.283		
p-value	0.002			0.757		
	Proximal Humeral I_{min}					
	Coefficient	Std. Error	p-value	Coefficient	Std. Error	p-value
Intercept	7.234	2.227	0.010	6.891	6.807	0.325
log10(BS)	-1.202	0.262	0.001**	-0.357	0.745	0.638
log10(H.prox.I_{min})	-0.005	0.302	0.987	0.932	0.818	0.269
n	23			61		
multiple R^2	0.714			0.068		
adj. R^2	0.651			-0.036		
F-statistic	11.260			0.653		
p-value	0.004			0.533		
	Proximal Humeral J					
	Coefficient	Std. Error	p-value	Coefficient	Std. Error	p-value
Intercept	8.399	2.522	0.009	5.672	6.748	0.412
log10(BS)	-1.264	0.275	0.001**	-0.298	0.758	0.698
log10(H.prox.J)	0.191	0.357	0.605	0.810	0.859	0.358
n	23			61		
multiple R^2	0.723			0.047		
adj. R^2	0.662			-0.058		
F-statistic	11.760			0.447		
p-value	0.003			0.646		
	Proximal Humeral Z_p					
	Coefficient	Std. Error	p-value	Coefficient	Std. Error	p-value
(Intercept)	9.040	2.176	0.002	4.549	5.429	0.413
log10(BS)	-1.296	0.257	0.001**	-0.103	0.674	0.880
log10(H.prox.Z_p)	0.453	0.443	0.333	1.204	1.142	0.306
n	23			61		
multiple R^2	0.744			0.058		
adj. R^2	0.687			-0.046		
F-statistic	13.090			0.559		
p-value	0.002			0.582		

Table 3.16

Cercopithecus: Curvature	**Females**			**Males**		
	Femoral Curvature					
	Coefficient	Std. Error	p-value	Coefficient	Std. Error	p-value
Intercept	0.310	0.772	0.691	0.733	0.534	0.174
log10(BS)	-0.034	0.860	0.969	-0.330	0.511	0.521
log10(F.C.AP)	-0.183	0.521	0.727	-0.242	0.276	0.382
n	34			71		
multiple R2	0.007			0.030		
adj. R2	-0.057			0.001		
F-statistic	0.116			1.043		
p-value	0.891			0.358		
	Humeral AP Curvature					
	Coefficient	Std. Error	p-value	Coefficient	Std. Error	p-value
Intercept	0.314	0.715	0.664	0.707	0.487	0.151
log10(BS)	0.079	0.698	0.910	-0.086	0.420	0.839
log10(H.C.AP)	-0.382	0.351	0.285	-0.572	0.195	0.005**
n	35			70		
multiple R2	0.039			0.119		
adj. R2	-0.021			0.092		
F-statistic	0.650			4.508		
p-value	0.529			0.015		
	Humeral ML Curvature					
	Coefficient	Std. Error	p-value	Coefficient	Std. Error	p-value
Intercept	0.326	0.674	0.632	0.327	0.516	0.528
log10(BS)	0.196	0.633	0.759	0.036	0.497	0.943
log10(H.C.ML)	-0.558	0.247	0.031	-0.269	0.206	0.195
n	35			70		
multiple R2	0.141			0.031		
adj. R2	0.087			0.002		
F-statistic	2.628			1.062		
p-value	0.088			0.352		

Table 3.17

Macaca: Distal Femur	**Females**			**Males**		
	Distal Femoral Total Area					
	Coefficient	Std. Error	p-value	Coefficient	Std. Error	p-value
Intercept	0.749	1.830	0.699	-0.028	0.812	0.973
log10(BS)	0.368	0.203	0.130	-0.023	0.183	0.905
log10(F.dist.TA)	0.764	0.675	0.309	-0.133	0.226	0.579
n	7			8		
multiple R^2	0.401			0.064		
adj. R^2	0.162			-0.247		
F-statistic	1.675			0.207		
p-value	0.277			0.819		
	Distal Femoral I_{max}					
	Coefficient	Std. Error	p-value	Coefficient	Std. Error	p-value
Intercept	0.885	2.268	0.712	-0.037	0.825	0.966
log10(BS)	0.130	0.225	0.588	0.017	0.156	0.917
log10(F.dist.I_{max})	0.298	0.316	0.390	-0.050	0.096	0.621
n	7			8		
multiple R^2	0.361			0.054		
adj. R^2	0.105			-0.262		
F-statistic	1.412			0.170		
p-value	0.327			0.848		
	Distal Femoral I_{min}					
	Coefficient	Std. Error	p-value	Coefficient	Std. Error	p-value
Intercept	2.280	2.335	0.374	-0.028	0.846	0.975
log10(BS)	0.051	0.210	0.819	0.026	0.156	0.872
log10(F.dist.I_{min})	0.509	0.333	0.186	-0.037	0.096	0.716
n	7			8		
multiple R^2	0.488			0.034		
adj. R^2	0.283			-0.288		
F-statistic	2.380			0.106		
p-value	0.188			0.901		
	Distal Femoral J					
	Coefficient	Std. Error	p-value	Coefficient	Std. Error	p-value
Intercept	1.424	2.261	0.557	-0.022	0.828	0.980
log10(BS)	0.092	0.221	0.693	0.021	0.156	0.895
log10(F.dist.J)	0.398	0.333	0.286	-0.044	0.096	0.664
n	7			8		
multiple R^2	0.415			0.044		
adj. R^2	0.181			-0.275		
F-statistic	1.772			0.138		
p-value	0.262			0.874		
	Distal Femoral Z_p					
	Coefficient	Std. Error	p-value	Coefficient	Std. Error	p-value
(Intercept)	0.972	2.156	0.671	-0.075	0.847	0.932
log10(BS)	0.121	0.220	0.607	0.026	0.153	0.872
log10(F.dist.Z_p)	0.500	0.481	0.346	-0.079	0.153	0.625
n	7			8		
multiple R^2	0.382			0.053		
adj. R^2	0.134			-0.263		
F-statistic	1.543			0.167		
p-value	0.301			0.850		

Table 3.18

Macaca: Midshaft Femur	**Females**			**Males**		
	Midshaft Femoral Total Area					
	Coefficient	Std. Error	p-value	Coefficient	Std. Error	p-value
Intercept	-0.386	1.887	0.846	-0.115	0.831	0.894
log10(BS)	0.308	0.233	0.243	-0.030	0.179	0.874
log10(F.mid.TA)	0.305	0.719	0.689	-0.170	0.246	0.516
n	7			8		
multiple R^2	0.274			0.083		
adj. R^2	-0.017			-0.222		
F-statistic	0.942			0.273		
p-value	0.450			0.770		
	Midshaft Femoral I_{max}					
	Coefficient	Std. Error	p-value	Coefficient	Std. Error	p-value
Intercept	-0.233	2.383	0.926	-0.058	0.864	0.949
log10(BS)	0.212	0.223	0.386	0.027	0.155	0.867
log10(F.mid.I_{max})	0.139	0.360	0.715	-0.042	0.104	0.699
n	7			8		
multiple R^2	0.269			0.037		
adj. R^2	-0.023			-0.284		
F-statistic	0.922			0.116		
p-value	0.456			0.893		
	Midshaft Femoral I_{min}					
	Coefficient	Std. Error	p-value	Coefficient	Std. Error	p-value
Intercept	0.400	2.608	0.884	-0.132	0.857	0.883
log10(BS)	0.164	0.242	0.527	0.023	0.151	0.882
log10(F.mid.I_{min})	0.223	0.367	0.571	-0.062	0.101	0.561
n	7			8		
multiple R^2	0.299			0.070		
adj. R^2	0.019			-0.241		
F-statistic	1.067			0.224		
p-value	0.411			0.806		
	Midshaft Femoral J					
	Coefficient	Std. Error	p-value	Coefficient	Std. Error	p-value
Intercept	-0.008	2.394	0.998	-0.077	0.851	0.931
log10(BS)	0.192	0.231	0.445	0.025	0.153	0.876
log10(F.mid.J)	0.177	0.365	0.648	-0.052	0.103	0.632
n	7			8		
multiple R^2	0.282			0.051		
adj. R^2	-0.006			-0.265		
F-statistic	0.980			0.161		
p-value	0.438			0.855		
	Midshaft Femoral Z_p					
	Coefficient	Std. Error	p-value	Coefficient	Std. Error	p-value
(Intercept)	-0.313	2.236	0.894	-0.163	0.864	0.857
log10(BS)	0.208	0.230	0.406	0.026	0.150	0.867
log10(F.mid.Z_p)	0.192	0.509	0.721	-0.109	0.165	0.534
n	7			8		
multiple R^2	0.269			0.077		
adj. R^2	-0.024			-0.230		
F-statistic	0.917			0.252		
p-value	0.458			0.785		

Table 3.19

Macaca: Proximal Femur	**Females**			**Males**		
Proximal Femoral Total Area						
	Coefficient	Std. Error	p-value	Coefficient	Std. Error	p-value
Intercept	-0.711	2.062	0.744	-0.047	0.806	0.955
log10(BS)	0.281	0.238	0.291	-0.045	0.194	0.823
log10(F.prox.TA)	0.156	0.782	0.849	-0.174	0.257	0.523
n	7			8		
multiple R^2	0.254			0.081		
adj. R^2	-0.045			-0.225		
F-statistic	0.849			0.265		
p-value	0.481			0.776		
Proximal Femoral I_{max}						
	Coefficient	Std. Error	p-value	Coefficient	Std. Error	p-value
Intercept	-0.705	2.763	0.809	-0.020	0.855	0.982
log10(BS)	0.233	0.244	0.383	0.026	0.158	0.874
log10(F.prox.I_{max})	0.058	0.408	0.892	-0.035	0.109	0.758
n	7			8		
multiple R^2	0.251			0.028		
adj. R^2	-0.049			-0.297		
F-statistic	0.836			0.085		
p-value	0.486			0.919		
Proximal Femoral I_{min}						
	Coefficient	Std. Error	p-value	Coefficient	Std. Error	p-value
Intercept	-0.025	2.698	0.993	-0.056	0.817	0.948
log10(BS)	0.193	0.243	0.463	0.008	0.157	0.960
log10(F.prox.I_{min})	0.159	0.383	0.695	-0.063	0.101	0.556
n	7			8		
multiple R^2	0.273			0.071		
adj. R^2	-0.018			-0.239		
F-statistic	0.938			0.229		
p-value	0.451			0.802		
Proximal Femoral J						
	Coefficient	Std. Error	p-value	Coefficient	Std. Error	p-value
Intercept	-0.416	2.643	0.881	-0.029	0.831	0.973
log10(BS)	0.215	0.245	0.420	0.019	0.158	0.910
log10(F.prox.J)	0.107	0.400	0.800	-0.049	0.106	0.662
n	7			8		
multiple R^2	0.258			0.044		
adj. R^2	-0.038			-0.274		
F-statistic	0.870			0.140		
p-value	0.474			0.873		
Proximal Femoral Z_p						
	Coefficient	Std. Error	p-value	Coefficient	Std. Error	p-value
(Intercept)	-0.837	2.423	0.744	-0.081	0.829	0.925
log10(BS)	0.239	0.242	0.368	0.012	0.155	0.939
log10(F.prox.Z_p)	0.058	0.539	0.919	-0.105	0.171	0.560
n	7			8		
multiple R^2	0.249			0.070		
adj. R^2	-0.051			-0.240		
F-statistic	0.830			0.225		
p-value	0.488			0.805		

Table 3.20

Macaca: Distal Humerus	**Females**			**Males**		
	Distal Humeral Total Area					
	Coefficient	Std. Error	p-value	Coefficient	Std. Error	p-value
Intercept	-0.450	4.091	0.918	-0.416	0.772	0.607
log10(BS)	0.461	0.368	0.279	0.250	0.121	0.077
log10(H.dist.TA)	0.500	1.660	0.778	0.196	0.235	0.432
n	6			9		
multiple R^2	0.427			0.381		
adj. R^2	0.141			0.204		
F-statistic	1.490			2.152		
p-value	0.328			0.187		
	Distal Humeral I_{max}					
	Coefficient	Std. Error	p-value	Coefficient	Std. Error	p-value
Intercept	-0.511	6.222	0.939	-0.520	0.846	0.558
log10(BS)	0.301	0.445	0.536	0.197	0.115	0.132
log10(H.dist.I_{max})	0.165	0.897	0.863	0.057	0.107	0.608
n	6			9		
multiple R^2	0.419			0.346		
adj. R^2	0.128			0.159		
F-statistic	1.442			1.853		
p-value	0.338			0.226		
	Distal Humeral I_{min}					
	Coefficient	Std. Error	p-value	Coefficient	Std. Error	p-value
Intercept	-1.298	5.522	0.826	0.190	1.036	0.860
log10(BS)	0.354	0.353	0.373	0.165	0.112	0.182
log10(H.dist.I_{min})	0.053	0.835	0.953	0.170	0.144	0.277
n	6			9		
multiple R^2	0.415			0.432		
adj. R^2	0.122			0.270		
F-statistic	1.416			2.664		
p-value	0.343			0.138		
	Distal Humeral J					
	Coefficient	Std. Error	p-value	Coefficient	Std. Error	p-value
Intercept	-0.812	6.013	0.899	-0.362	0.886	0.695
log10(BS)	0.322	0.421	0.488	0.189	0.115	0.144
log10(H.dist.J)	0.129	0.927	0.896	0.087	0.120	0.493
n	6			9		
multiple R^2	0.417			0.367		
adj. R^2	0.125			0.186		
F-statistic	1.430			2.025		
p-value	0.340			0.202		
	Distal Humeral Z_p					
	Coefficient	Std. Error	p-value	Coefficient	Std. Error	p-value
(Intercept)	-2.371	3.536	0.539	-0.354	0.819	0.679
log10(BS)	0.415	0.298	0.236	0.185	0.114	0.148
log10(H.dist.Z_p)	-0.173	0.795	0.838	0.126	0.149	0.427
n	6			9		
multiple R^2	0.421			0.382		
adj. R^2	0.131			0.206		
F-statistic	1.453			2.164		
p-value	0.335			0.186		

Table 3.21

Macaca: Midshaft Humerus	**Females**			**Males**		
	Midshaft Humeral Total Area					
	Coefficient	Std. Error	p-value	Coefficient	Std. Error	p-value
Intercept	-1.810	3.492	0.632	-0.322	0.790	0.696
log10(BS)	0.362	0.285	0.273	0.231	0.111	0.076
log10(H.mid.TA)	-0.068	1.307	0.961	0.196	0.205	0.371
n	6			9		
multiple R^2	0.414			0.398		
adj. R^2	0.122			0.226		
F-statistic	1.415			2.312		
p-value	0.343			0.170		
	Midshaft Humeral I_{max}					
	Coefficient	Std. Error	p-value	Coefficient	Std. Error	p-value
Intercept	-2.218	3.794	0.590	-0.305	0.890	0.742
log10(BS)	0.410	0.326	0.277	0.182	0.116	0.160
log10(H.mid.I_{max})	-0.085	0.535	0.881	0.087	0.110	0.451
n	6			9		
multiple R^2	0.418			0.376		
adj. R^2	0.127			0.198		
F-statistic	1.435			2.109		
p-value	0.339			0.192		
	Midshaft Humeral I_{min}					
	Coefficient	Std. Error	p-value	Coefficient	Std. Error	p-value
Intercept	-1.948	3.977	0.650	-0.031	0.978	0.975
log10(BS)	0.391	0.328	0.299	0.149	0.123	0.262
log10(H.mid.I_{min})	-0.044	0.542	0.939	0.107	0.105	0.343
n	6			9		
multiple R^2	0.415			0.407		
adj. R^2	0.123			0.238		
F-statistic	1.419			2.401		
p-value	0.342			0.161		
	Midshaft Humeral J					
	Coefficient	Std. Error	p-value	Coefficient	Std. Error	p-value
Intercept	-2.207	3.984	0.609	-0.215	0.907	0.819
log10(BS)	0.410	0.340	0.295	0.169	0.118	0.196
log10(H.mid.J)	-0.086	0.582	0.889	0.097	0.109	0.401
n	6			9		
multiple R^2	0.417			0.389		
adj. R^2	0.126			0.215		
F-statistic	1.432			2.230		
p-value	0.340			0.178		
	Midshaft Humeral Z_p					
	Coefficient	Std. Error	p-value	Coefficient	Std. Error	p-value
(Intercept)	-1.582	4.260	0.729	-0.204	0.909	0.829
log10(BS)	0.371	0.222	0.169	0.213	0.109	0.092
log10(H.mid.Z_p)	0.011	0.805	0.990	0.131	0.145	0.395
n	6			9		
multiple R^2	0.414			0.391		
adj. R^2	0.121			0.217		
F-statistic	1.413			2.245		
p-value	0.343			0.177		

Table 3.22

Macaca: Proximal Humerus	**Females**			**Males**		
	Proximal Humeral Total Area					
	Coefficient	Std. Error	p-value	Coefficient	Std. Error	p-value
Intercept	-4.561	3.260	0.234	-0.659	0.809	0.443
log10(BS)	0.253	0.237	0.346	0.216	0.116	0.106
log10(H.prox.TA)	-1.115	1.186	0.400	0.070	0.206	0.745
n	6			9		
multiple R^2	0.520			0.330		
adj. R^2	0.280			0.139		
F-statistic	2.167			1.726		
p-value	0.230			0.246		
	Proximal Humeral I_{max}					
	Coefficient	Std. Error	p-value	Coefficient	Std. Error	p-value
Intercept	-7.340	4.061	0.145	-0.726	0.937	0.464
log10(BS)	0.791	0.343	0.082	0.201	0.125	0.152
log10(H.prox.I_{max})	-0.815	0.567	0.224	0.017	0.107	0.876
n	6			9		
multiple R^2	0.614			0.322		
adj. R^2	0.421			0.128		
F-statistic	3.178			1.661		
p-value	0.149			0.257		
	Proximal Humeral I_{min}					
	Coefficient	Std. Error	p-value	Coefficient	Std. Error	p-value
Intercept	-3.695	3.188	0.311	-0.602	0.921	0.534
log10(BS)	0.526	0.309	0.163	0.194	0.122	0.155
log10(H.prox.I_{min})	-0.279	0.410	0.533	0.037	0.107	0.741
n	6			9		
multiple R^2	0.475			0.331		
adj. R^2	0.212			0.139		
F-statistic	1.809			1.729		
p-value	0.276			0.245		
	Proximal Humeral J					
	Coefficient	Std. Error	p-value	Coefficient	Std. Error	p-value
Intercept	-5.321	3.634	0.217	-0.679	0.910	0.480
log10(BS)	0.656	0.334	0.121	0.198	0.124	0.154
log10(H.prox.J)	-0.539	0.513	0.353	0.026	0.108	0.817
n	6			9		
multiple R^2	0.541			0.325		
adj. R^2	0.311			0.132		
F-statistic	2.355			1.684		
p-value	0.211			0.253		
	Proximal Humeral Z_p					
	Coefficient	Std. Error	p-value	Coefficient	Std. Error	p-value
(Intercept)	-5.275	4.938	0.346	-0.659	0.875	0.476
log10(BS)	0.636	0.407	0.194	0.195	0.125	0.163
log10(H.prox.Z_p)	-0.825	1.096	0.494	0.040	0.139	0.781
n	6			9		
multiple R^2	0.487			0.327		
adj. R^2	0.230			0.135		
F-statistic	1.896			1.703		
p-value	0.264			0.250		

Table 3.23

Macaca: Curvature	**Females**			**Males**		
	Femoral Curvature					
	Coefficient	Std. Error	p-value	Coefficient	Std. Error	p-value
Intercept	-0.928	0.321	0.034	-0.548	0.451	0.263
log10(BS)	1.776	0.405	0.007**	0.612	0.342	0.116
log10(F.C.AP)	-1.194	0.323	0.014**	0.035	0.223	0.880
n	7			9		
multiple R2	0.797			0.326		
adj. R2	0.715			0.133		
F-statistic	9.794			1.690		
p-value	0.019			0.252		
	Humeral AP Curvature					
	Coefficient	Std. Error	p-value	Coefficient	Std. Error	p-value
Intercept	-0.792	0.605	0.247	-0.690	0.405	0.149
log10(BS)	1.473	1.039	0.216	0.505	0.375	0.236
log10(H.C.AP)	-0.871	0.972	0.411	0.295	0.209	0.217
n	7			7		
multiple R2	0.346			0.623		
adj. R2	0.084			0.473		
F-statistic	1.323			4.138		
p-value	0.346			0.087		
	Humeral ML Curvature					
	Coefficient	Std. Error	p-value	Coefficient	Std. Error	p-value
Intercept	-1.272	0.800	0.172	-0.498	0.414	0.267
log10(BS)	1.506	0.864	0.142	0.409	0.417	0.359
log10(H.C.ML)	-0.471	0.402	0.294	0.302	0.376	0.448
n	7			9		
multiple R2	0.404			0.380		
adj. R2	0.166			0.203		
F-statistic	1.697			2.149		
p-value	0.274			0.187		

Table 3.24

Papio/Theropithecus: Distal Femur	**Females**			**Males**		
	Distal Femoral Total Area					
	Coefficient	Std. Error	p-value	Coefficient	Std. Error	p-value
Intercept	10.263	2.659	0.005	-1.272	4.313	0.772
log10(BS)	-0.863	0.432	0.081	-1.242	0.686	0.090
log10(F.dist.TA)	1.503	1.127	0.219	-2.730	1.454	0.080
n	11			18		
multiple R^2	0.689			0.230		
adj. R^2	0.611			0.127		
F-statistic	8.862			2.240		
p-value	0.009			0.141		
	Distal Femoral I_{max}					
	Coefficient	Std. Error	p-value	Coefficient	Std. Error	p-value
Intercept	10.754	3.119	0.009	-4.240	5.267	0.433
log10(BS)	-1.323	0.323	0.003**	-0.269	0.600	0.660
log10(F.dist.I_{max})	0.644	0.522	0.252	-1.471	0.743	0.067
n	11			18		
multiple R^2	0.681			0.246		
adj. R^2	0.601			0.145		
F-statistic	8.529			2.444		
p-value	0.010			0.121		
	Distal Femoral I_{min}					
	Coefficient	Std. Error	p-value	Coefficient	Std. Error	p-value
Intercept	10.673	3.998	0.028	-4.519	5.246	0.403
log10(BS)	-1.415	0.379	0.006**	-0.169	0.608	0.785
log10(F.dist.I_{min})	0.501	0.573	0.408	-1.381	0.674	0.058*
n	11			18		
multiple R^2	0.653			0.257		
adj. R^2	0.566			0.158		
F-statistic	7.527			2.594		
p-value	0.015			0.108		
	Distal Femoral J					
	Coefficient	Std. Error	p-value	Coefficient	Std. Error	p-value
Intercept	10.841	3.418	0.013	-4.380	5.141	0.408
log10(BS)	-1.382	0.342	0.004**	-0.203	0.601	0.740
log10(F.dist.J)	0.628	0.560	0.295	-1.509	0.726	0.055*
n	11			18		
multiple R^2	0.672			0.262		
adj. R^2	0.589			0.163		
F-statistic	8.177			2.660		
p-value	0.012			0.103		
	Distal Femoral Z_p					
	Coefficient	Std. Error	p-value	Coefficient	Std. Error	p-value
(Intercept)	11.033	2.863	0.005	-2.009	4.696	0.675
log10(BS)	-1.363	0.315	0.003**	-0.353	0.603	0.567
log10(F.dist.Z_p)	1.082	0.723	0.173	-1.761	0.981	0.093
n	11			17		
multiple R^2	0.703			0.217		
adj. R^2	0.629			0.113		
F-statistic	9.476			2.080		
p-value	0.008			0.160		

Table 3.25

Papio/Theropithecus: Midshaft Femur	**Females**			**Males**		
	Midshaft Femoral Total Area					
	Coefficient	Std. Error	p-value	Coefficient	Std. Error	p-value
Intercept	10.766	1.937	0.001	0.928	4.120	0.825
log10(BS)	-0.424	0.428	0.351	-1.330	0.833	0.131
log10(F.mid.TA)	2.379	0.966	0.039*	-2.190	1.622	0.197
n	11			18		
multiple R^2	0.784			0.152		
adj. R^2	0.730			0.039		
F-statistic	14.510			1.345		
p-value	0.002			0.290		
	Midshaft Femoral I_{max}					
	Coefficient	Std. Error	p-value	Coefficient	Std. Error	p-value
Intercept	11.438	2.532	0.002	-1.621	5.220	0.760
log10(BS)	-1.244	0.286	0.002**	-0.485	0.615	0.443
log10(F.mid.I_{max})	0.884	0.453	0.087	-1.132	0.800	0.177
n	11			18		
multiple R^2	0.742			0.161		
adj. R^2	0.678			0.049		
F-statistic	11.520			1.440		
p-value	0.004			0.268		
	Midshaft Femoral I_{min}					
	Coefficient	Std. Error	p-value	Coefficient	Std. Error	p-value
Intercept	13.646	3.233	0.003	-1.913	5.016	0.708
log10(BS)	-1.364	0.282	0.001**	-0.549	0.603	0.377
log10(F.mid.I_{min})	1.216	0.570	0.066	-1.260	0.796	0.134
n	11			18		
multiple R^2	0.758			0.185		
adj. R^2	0.697			0.076		
F-statistic	12.500			1.704		
p-value	0.003			0.215		
	Midshaft Femoral J					
	Coefficient	Std. Error	p-value	Coefficient	Std. Error	p-value
Intercept	12.087	2.684	0.002	-1.546	4.977	0.760
log10(BS)	-1.291	0.282	0.002**	-0.511	0.608	0.414
log10(F.mid.J)	1.036	0.503	0.074	-1.222	0.808	0.151
n	11			18		
multiple R^2	0.752			0.175		
adj. R^2	0.689			0.065		
F-statistic	12.100			1.591		
p-value	0.004			0.236		
	Midshaft Femoral Z_p					
	Coefficient	Std. Error	p-value	Coefficient	Std. Error	p-value
(Intercept)	11.423	2.272	0.001	-0.019	4.463	0.997
log10(BS)	-1.210	0.273	0.002**	-0.600	0.613	0.343
log10(F.mid.Z_p)	1.515	0.673	0.054	-1.507	1.079	0.183
n	11			18		
multiple R^2	0.767			0.158		
adj. R^2	0.709			0.046		
F-statistic	13.190			1.412		
p-value	0.003			0.274		

Table 3.26

Papio/Theropithecus: Proximal Femur	**Females**			**Males**		
	Proximal Femoral Total Area					
	Coefficient	Std. Error	p-value	Coefficient	Std. Error	p-value
Intercept	9.396	1.577	0.000	-1.289	4.695	0.787
log10(BS)	-0.858	0.378	0.047*	-1.285	0.747	0.106
log10(F.prox.TA)	1.221	0.740	0.130	-2.774	1.726	0.129
n	13			18		
multiple R^2	0.766			0.189		
adj. R^2	0.719			0.080		
F-statistic	16.340			1.744		
p-value	0.001			0.209		
	Proximal Femoral I_{max}					
	Coefficient	Std. Error	p-value	Coefficient	Std. Error	p-value
Intercept	10.569	1.972	0.000	-4.103	6.091	0.511
log10(BS)	-1.247	0.246	0.000**	-0.194	0.648	0.768
log10(F.prox.I_{max})	0.682	0.390	0.111	-1.329	0.837	0.133
n	13			18		
multiple R^2	0.772			0.186		
adj. R^2	0.726			0.077		
F-statistic	16.890			1.712		
p-value	0.001			0.214		
	Proximal Femoral I_{min}					
	Coefficient	Std. Error	p-value	Coefficient	Std. Error	p-value
Intercept	10.713	2.378	0.001	-4.315	5.568	0.451
log10(BS)	-1.366	0.253	0.000**	-0.323	0.604	0.601
log10(F.prox.I_{min})	0.554	0.397	0.193	-1.490	0.809	0.085
n	13			18		
multiple R^2	0.751			0.224		
adj. R^2	0.701			0.121		
F-statistic	15.040			2.170		
p-value	0.001			0.149		
	Proximal Femoral J					
	Coefficient	Std. Error	p-value	Coefficient	Std. Error	p-value
Intercept	10.510	2.057	0.000	-4.444	5.784	0.454
log10(BS)	-1.303	0.246	0.000**	-0.214	0.626	0.737
log10(F.prox.J)	0.636	0.396	0.139	-1.511	0.853	0.097
n	13			18		
multiple R^2	0.763			0.214		
adj. R^2	0.716			0.109		
F-statistic	16.100			2.037		
p-value	0.001			0.165		
	Proximal Femoral Z_p					
	Coefficient	Std. Error	p-value	Coefficient	Std. Error	p-value
(Intercept)	10.013	1.758	0.000	-2.464	5.050	0.633
log10(BS)	-1.263	0.245	0.000**	-0.338	0.612	0.589
log10(F.prox.Z_p)	0.879	0.508	0.114	-1.860	1.096	0.110
n	13			18		
multiple R^2	0.770			0.202		
adj. R^2	0.725			0.096		
F-statistic	16.780			1.900		
p-value	0.001			0.184		

Table 3.27

Papio/Theropithecus: Distal Humerus	**Females**			**Males**		
	Distal Humeral Total Area					
	Coefficient	Std. Error	p-value	Coefficient	Std. Error	p-value
Intercept	11.393	1.547	0.000	0.872	4.791	0.858
log10(BS)	-0.453	0.282	0.143	0.165	0.951	0.864
log10(H.dist.TA)	2.434	0.730	0.009**	0.338	1.951	0.864
n	12			21		
multiple R^2	0.872			0.002		
adj. R^2	0.844			-0.109		
F-statistic	30.730			0.018		
p-value	0.000			0.983		
	Distal Humeral I_{max}					
	Coefficient	Std. Error	p-value	Coefficient	Std. Error	p-value
Intercept	15.727	2.665	0.000	-1.112	6.218	0.860
log10(BS)	-1.660	0.216	0.000**	0.093	0.691	0.895
log10(H.dist.I_{max})	1.304	0.385	0.008**	-0.273	0.904	0.766
n	12			21		
multiple R^2	0.874			0.005		
adj. R^2	0.846			-0.105		
F-statistic	31.310			0.048		
p-value	0.000			0.953		
	Distal Humeral I_{min}					
	Coefficient	Std. Error	p-value	Coefficient	Std. Error	p-value
Intercept	12.838	2.547	0.001	3.096	6.759	0.652
log10(BS)	-1.280	0.200	0.000**	-0.041	0.699	0.954
log10(H.dist.I_{min})	1.080	0.447	0.039*	0.471	0.967	0.632
n	12			21		
multiple R^2	0.827			0.013		
adj. R^2	0.788			-0.096		
F-statistic	21.480			0.122		
p-value	0.000			0.886		
	Distal Humeral J					
	Coefficient	Std. Error	p-value	Coefficient	Std. Error	p-value
Intercept	14.643	2.498	0.000	0.324	6.385	0.960
log10(BS)	-1.516	0.199	0.000**	0.051	0.698	0.943
log10(H.dist.J)	1.301	0.407	0.011*	-0.009	0.970	0.993
n	12			21		
multiple R^2	0.866			0.000		
adj. R^2	0.836			-0.111		
F-statistic	29.110			0.003		
p-value	0.000			0.997		
	Distal Humeral Z_p					
	Coefficient	Std. Error	p-value	Coefficient	Std. Error	p-value
(Intercept)	12.292	1.712	0.000	0.092	5.186	0.986
log10(BS)	-1.158	0.167	0.000**	0.046	0.679	0.946
log10(H.dist.Z_p)	1.816	0.524	0.007**	-0.103	1.294	0.938
n	12			21		
multiple R^2	0.878			0.001		
adj. R^2	0.850			-0.110		
F-statistic	32.260			0.006		
p-value	0.000			0.994		

Table 3.28

Papio/Theropithecus: Midshaft Humerus	**Females**			**Males**		
	Midshaft Humeral Total Area					
	Coefficient	Std. Error	p-value	Coefficient	Std. Error	p-value
Intercept	8.772	2.228	0.003	0.802	4.484	0.860
log10(BS)	-1.032	0.317	0.010*	0.156	0.891	0.863
log10(H.mid.TA)	0.728	0.862	0.420	0.305	1.659	0.856
n	12			21		
multiple R^2	0.735			0.002		
adj. R^2	0.677			-0.109		
F-statistic	12.510			0.020		
p-value	0.003			0.981		
	Midshaft Humeral I_{max}					
	Coefficient	Std. Error	p-value	Coefficient	Std. Error	p-value
Intercept	8.809	3.077	0.019	1.385	5.969	0.819
log10(BS)	-1.296	0.299	0.002**	0.012	0.698	0.987
log10(H.mid.I_{max})	0.230	0.410	0.589	0.180	0.815	0.828
n	12			21		
multiple R^2	0.724			0.003		
adj. R^2	0.663			-0.108		
F-statistic	11.810			0.027		
p-value	0.003			0.973		
	Midshaft Humeral I_{min}					
	Coefficient	Std. Error	p-value	Coefficient	Std. Error	p-value
Intercept	8.911	3.118	0.019	0.595	5.679	0.918
log10(BS)	-1.278	0.280	0.001	0.045	0.682	0.948
log10(H.mid.I_{min})	0.261	0.445	0.572	0.043	0.804	0.958
n	12			21		
multiple R^2	0.725			0.000		
adj. R^2	0.664			-0.111		
F-statistic	11.860			0.004		
p-value	0.003			0.996		
	Midshaft Humeral J					
	Coefficient	Std. Error	p-value	Coefficient	Std. Error	p-value
Intercept	8.897	3.084	0.018	1.031	5.734	0.859
log10(BS)	-1.297	0.295	0.002	0.028	0.691	0.968
log10(H.mid.J)	0.260	0.441	0.570	0.127	0.825	0.879
n	12			21		
multiple R^2	0.725			0.002		
adj. R^2	0.664			-0.109		
F-statistic	11.870			0.015		
p-value	0.003			0.986		
	Midshaft Humeral Z_p					
	Coefficient	Std. Error	p-value	Coefficient	Std. Error	p-value
(Intercept)	8.998	2.457	0.005	1.158	4.618	0.805
log10(BS)	-1.276	0.259	0.001**	0.071	0.680	0.918
log10(H.mid.Z_p)	0.470	0.559	0.422	0.325	1.074	0.766
n	12			21		
multiple R^2	0.735			0.005		
adj. R^2	0.676			-0.105		
F-statistic	12.490			0.048		
p-value	0.003			0.953		

Table 3.29

Papio/Theropithecus: Proximal Humerus	**Females**			**Males**		
	Proximal Humeral Total Area					
	Coefficient	Std. Error	p-value	Coefficient	Std. Error	p-value
Intercept	8.230	1.880	0.002	3.976	5.271	0.460
log10(BS)	-1.069	0.306	0.007**	0.407	0.757	0.598
log10(H.prox.TA)	0.515	0.700	0.481	1.690	1.746	0.346
n	12			21		
multiple R^2	0.731			0.050		
adj. R^2	0.671			-0.056		
F-statistic	12.200			0.471		
p-value	0.003			0.632		
	Proximal Humeral I_{max}					
	Coefficient	Std. Error	p-value	Coefficient	Std. Error	p-value
Intercept	9.611	2.753	0.007	4.594	6.785	0.507
log10(BS)	-1.341	0.280	0.001**	-0.217	0.756	0.778
log10(H.prox.I_{max})	0.362	0.372	0.357	0.628	0.839	0.464
n	12			21		
multiple R^2	0.742			0.030		
adj. R^2	0.684			-0.077		
F-statistic	12.910			0.283		
p-value	0.002			0.757		
	Proximal Humeral I_{min}					
	Coefficient	Std. Error	p-value	Coefficient	Std. Error	p-value
Intercept	7.234	2.227	0.010	6.891	6.807	0.325
log10(BS)	-1.202	0.262	0.001**	-0.357	0.745	0.638
log10(H.prox.I_{min})	-0.005	0.302	0.987	0.932	0.818	0.269
n	12			21		
multiple R^2	0.714			0.068		
adj. R^2	0.651			-0.036		
F-statistic	11.260			0.653		
p-value	0.004			0.533		
	Proximal Humeral J					
	Coefficient	Std. Error	p-value	Coefficient	Std. Error	p-value
Intercept	8.399	2.522	0.009	5.672	6.748	0.412
log10(BS)	-1.264	0.275	0.001**	-0.298	0.758	0.698
log10(H.prox.J)	0.191	0.357	0.605	0.810	0.859	0.358
n	12			21		
multiple R^2	0.723			0.047		
adj. R^2	0.662			-0.058		
F-statistic	11.760			0.447		
p-value	0.003			0.646		
	Proximal Humeral Z_p					
	Coefficient	Std. Error	p-value	Coefficient	Std. Error	p-value
(Intercept)	9.040	2.176	0.002	4.549	5.429	0.413
log10(BS)	-1.296	0.257	0.001**	-0.103	0.674	0.880
log10(H.prox.Z_p)	0.453	0.443	0.333	1.204	1.142	0.306
n	12			21		
multiple R^2	0.744			0.058		
adj. R^2	0.687			-0.046		
F-statistic	13.090			0.559		
p-value	0.002			0.582		

Table 3.30

Baboons: Curvature	**Females**			**Males**		
	Femoral Curvature					
	Coefficient	Std. Error	p-value	Coefficient	Std. Error	p-value
Intercept	4.775	0.580	0.000	0.846	1.988	0.676
log10(BS)	-2.620	0.499	0.000**	0.207	1.605	0.899
log10(F.C.AP)	-0.622	0.383	0.133	-0.485	1.153	0.679
n	14			21		
multiple R2	0.820			0.010		
adj. R2	0.787			-0.100		
F-statistic	24.970			0.091		
p-value	0.000			0.913		
	Humeral AP Curvature					
	Coefficient	Std. Error	p-value	Coefficient	Std. Error	p-value
Intercept	5.199	0.777	0.000	0.614	2.143	0.778
log10(BS)	-2.997	0.476	0.000**	-0.164	1.383	0.907
log10(H.C.AP)	-0.529	0.552	0.361	0.239	0.954	0.805
n	13			22		
multiple R2	0.810			0.004		
adj. R2	0.771			-0.101		
F-statistic	21.240			0.037		
p-value	0.000			0.964		
	Humeral ML Curvature					
	Coefficient	Std. Error	p-value	Coefficient	Std. Error	p-value
Intercept	4.628	0.676	0.000	3.425	2.087	0.117
log10(BS)	-2.825	0.615	0.001**	-2.892	1.766	0.118
log10(H.C.ML)	-0.218	0.365	0.563	1.540	0.707	0.042
n	13			22		
multiple R2	0.799			0.200		
adj. R2	0.759			0.116		
F-statistic	19.890			2.379		
p-value	0.000			0.120		

Figure. 3.1 Alignment procedure in ScanStudio. 3.1a shows scans of the humeral shaft aligned, but without proximal and distal ends attached. 3.1b indicates placement of "pins" used to attach the single scan of the superior surface of the humerus to the previously aligned shaft scans. The same procedure was used to attach the distal end scan.

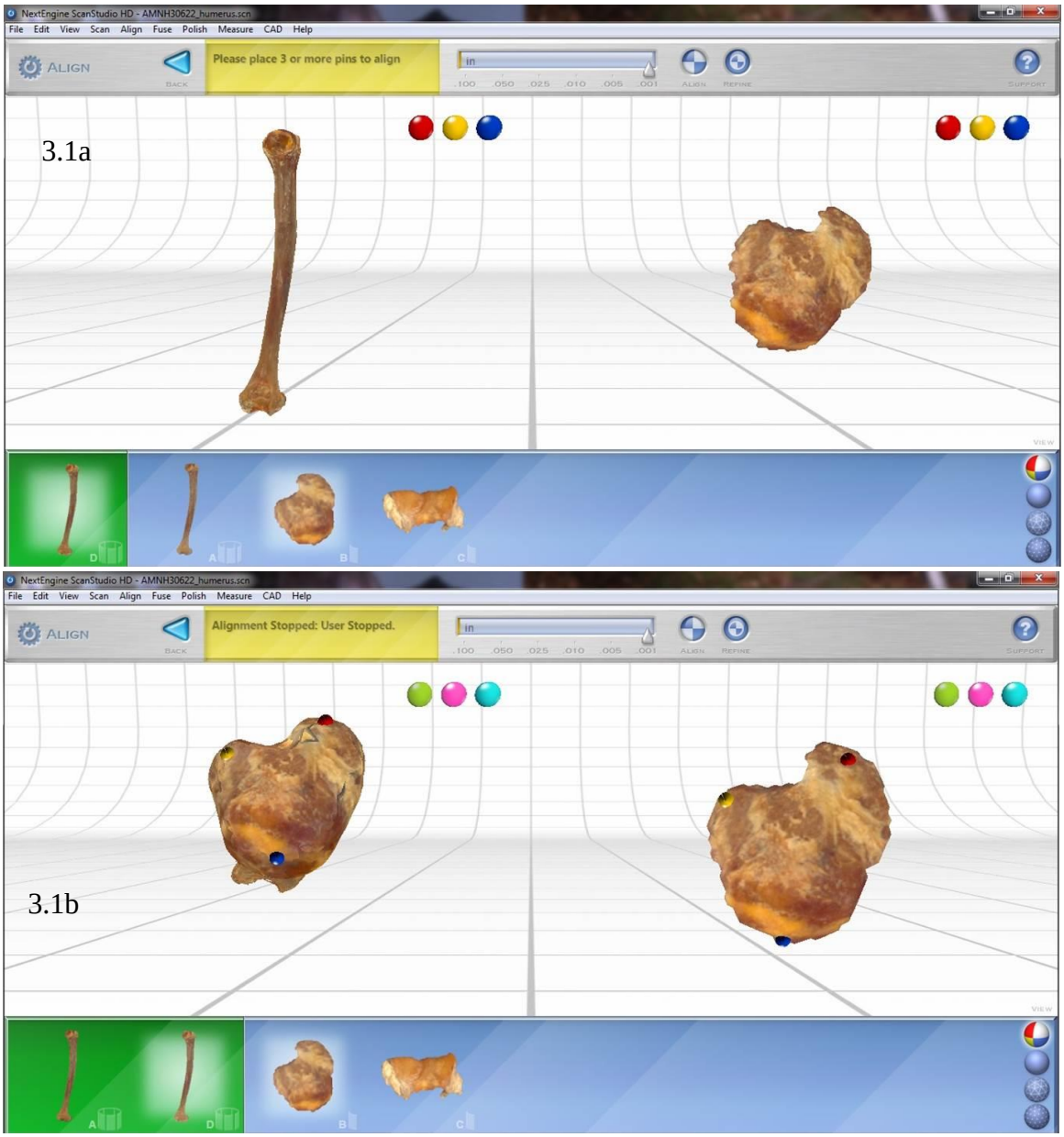

Figure. 3.2 Fused model in ScanStudio. This figure shows a model without texture. Once the model is exported as an STL file it loses any texture data. Models could be saved with texture if desired.

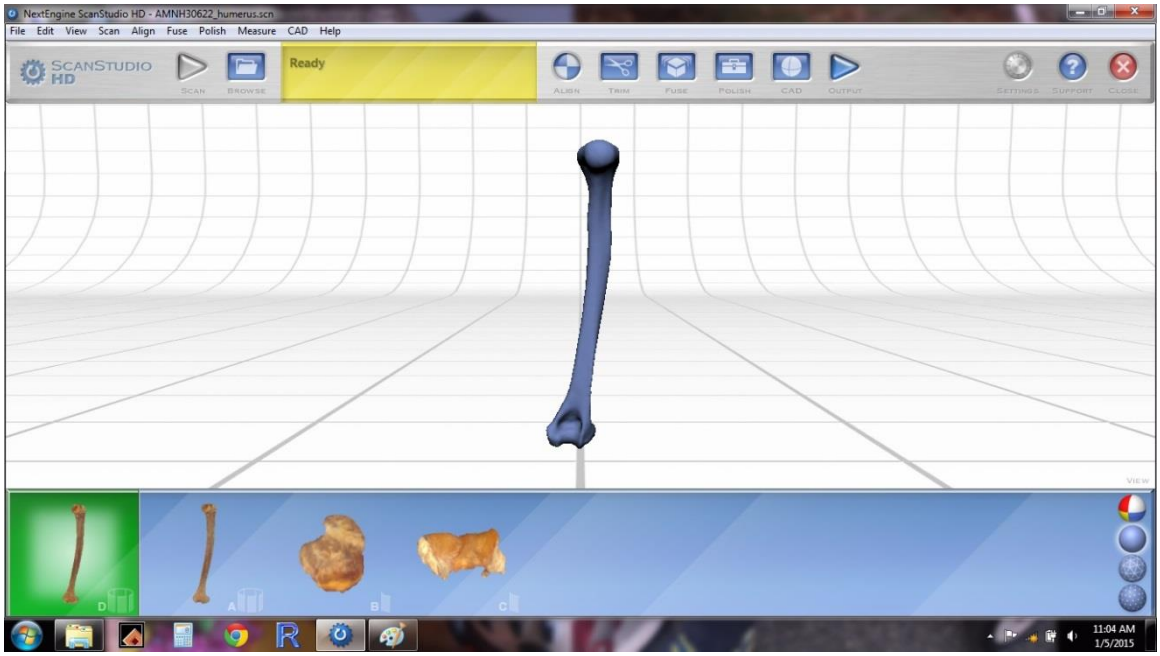

Figure. 3.3 Cross-section creation in amira. 3.3a indicates 70% of the length of the bone and the location of distal cross-section. 3.3b indicates 50% of bone length and the location of midshaft cross-sections. 3.3c indicates 30% of bone length and locations of proximal cross-sections. 3.3d, e, f show a superior view of proximal, midshaft, and distal cross-sections (with millimeter scale bars), respectively.

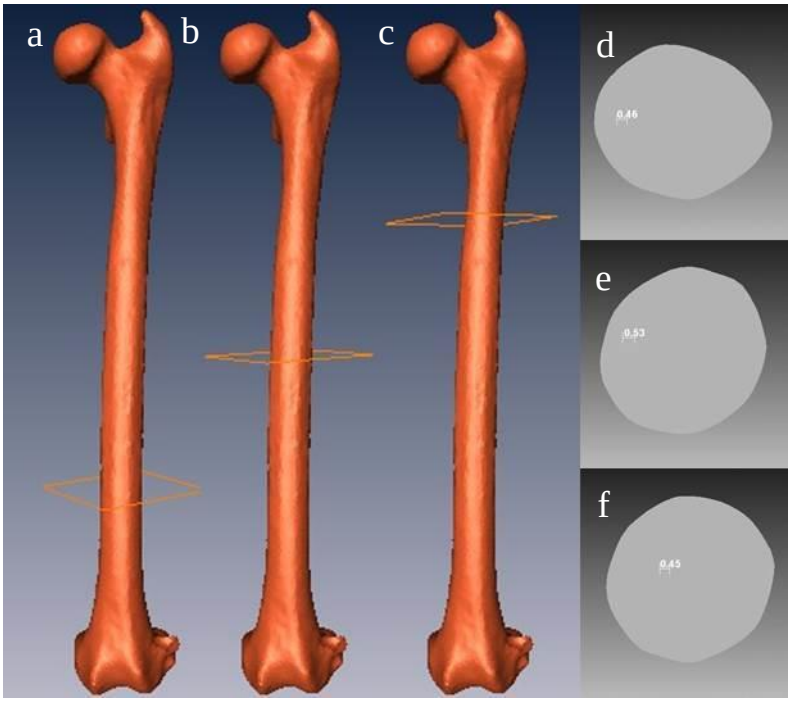

Figure 3.4 Protocol for measuring femoral curvature.

Figure 3.6 Protocol for measuring medio-lateral humeral curvature.

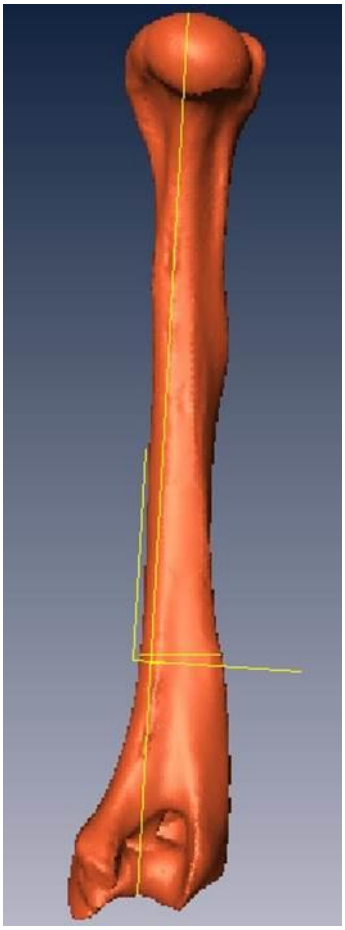

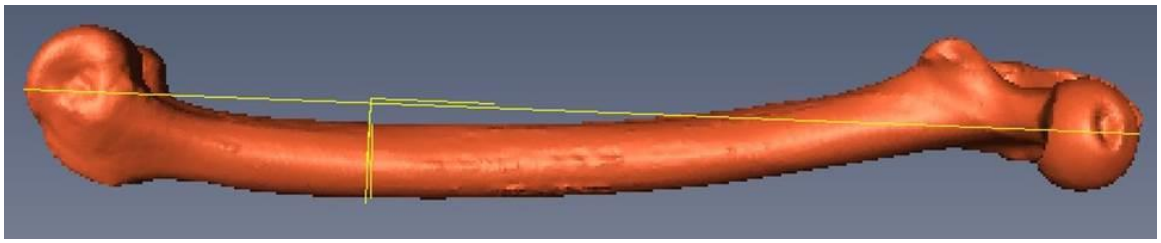

Figure 3.5 Protocol for measuring antero-posterior humeral curvature.

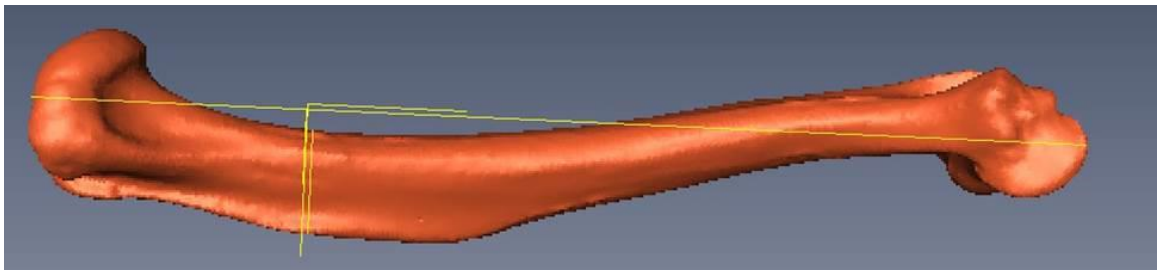

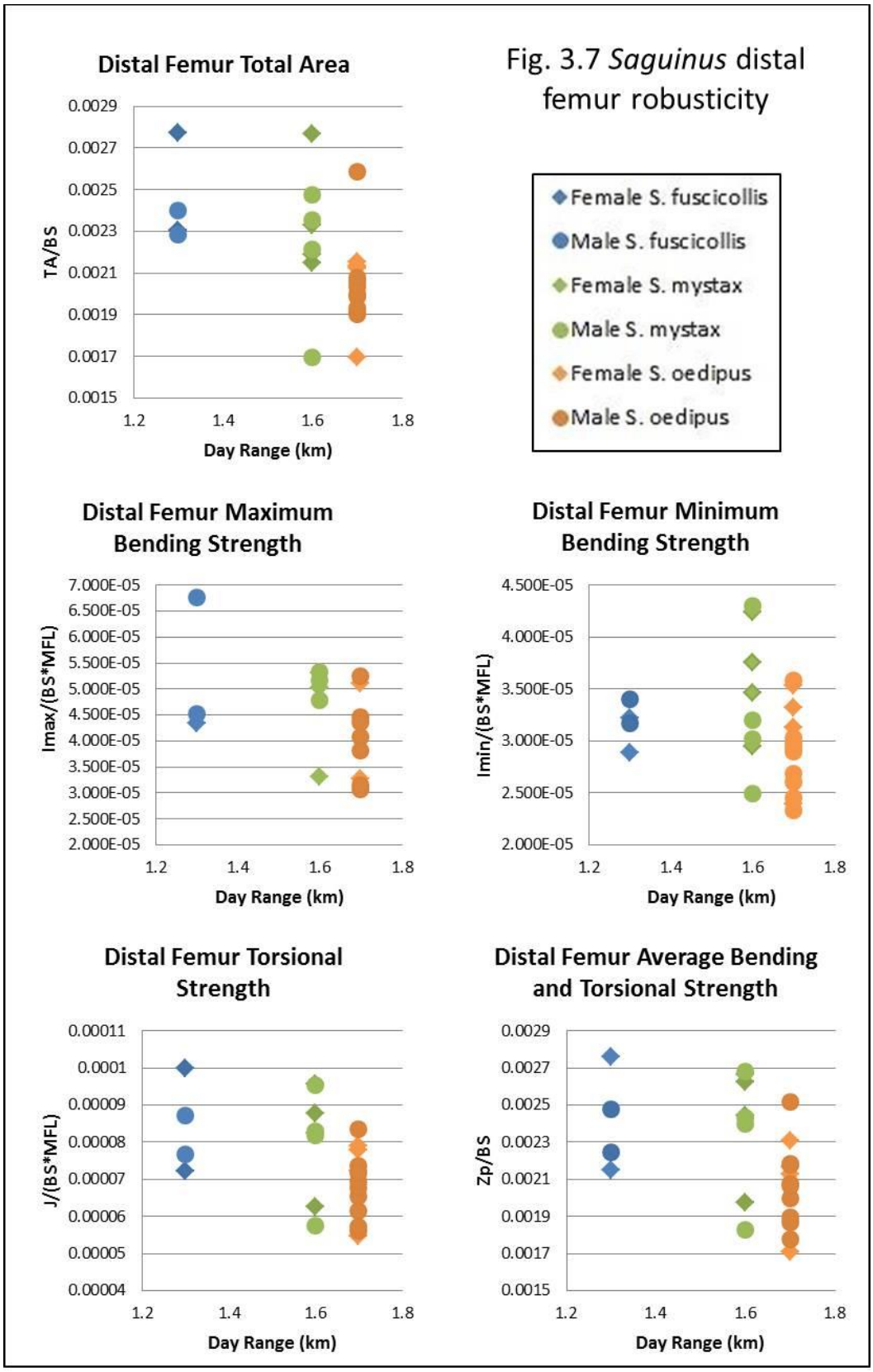
Distal Femur Total Area
TA/BS
0.0029
0.0027
0.0025
0.0023
0.0021
0.0019
0.0017
0.0015
1.2
1.4
1.6
1.8
Day Range (km)
Fig. 3.7 *Saguinus* distal femur robusticity
Female S. fuscicollis
Male S. fuscicollis
Female S. mystax
Male S. mystax
Female S. oedipus
Male S. oedipus
Distal Femur Maximum Bending Strength
Imax/(BS*MFL)
7.000E-05
6.500E-05
6.000E-05
5.500E-05
5.000E-05
4.500E-05
4.000E-05
3.500E-05
3.000E-05
2.500E-05
2.000E-05
Day Range (km)
Distal Femur Minimum Bending Strength
Imin/(BS*MFL)
4.500E-05
4.000E-05
3.500E-05
3.000E-05
2.500E-05
2.000E-05
Day Range (km)
Distal Femur Torsional Strength
J/(BS*MFL)
0.00011
0.0001
0.00009
0.00008
0.00007
0.00006
0.00005
0.00004
Day Range (km)
Distal Femur Average Bending and Torsional Strength
Zp/BS
0.0029
0.0027
0.0025
0.0023
0.0021
0.0019
0.0017
0.0015
Day Range (km)

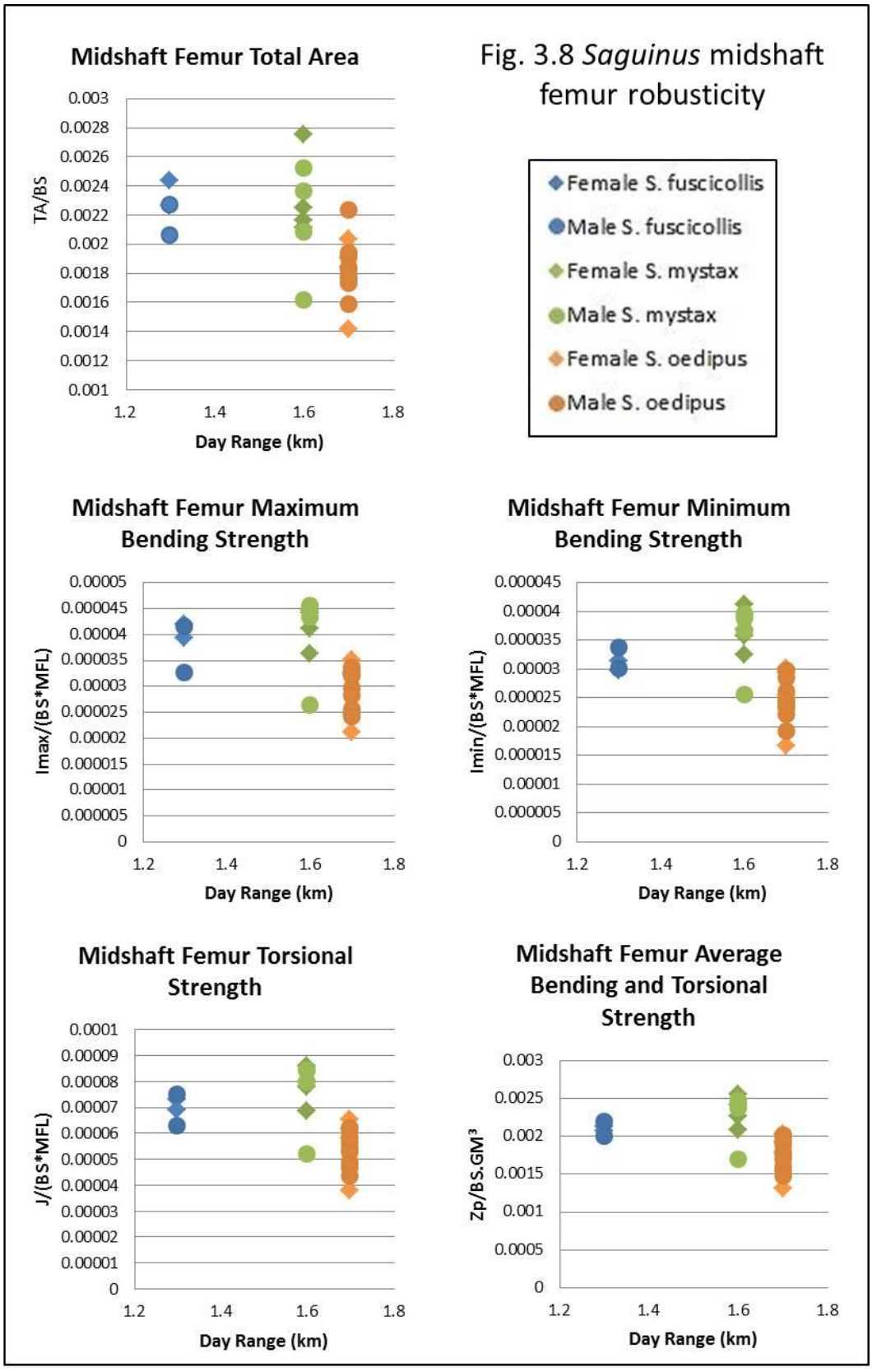
Midshaft Femur Total Area
TA/BS
0.003
0.0028
0.0026
0.0024
0.0022
0.002
0.0018
0.0016
0.0014
0.0012
0.001
1.2
1.4
1.6
1.8
Day Range (km)
Fig. 3.8 Saguinus midshaft femur robusticity
Female S. fuscicollis
Male S. fuscicollis
Female S. mystax
Male S. mystax
Female S. oedipus
Male S. oedipus
Midshaft Femur Maximum Bending Strength
Imax/(BS*MFL)
0.00005
0.000045
0.00004
0.000035
0.00003
0.000025
0.00002
0.000015
0.00001
0.000005
0
Day Range (km)
Midshaft Femur Minimum Bending Strength
Imin/(BS*MFL)
0.000045
0.00004
0.000035
0.00003
0.000025
0.00002
0.000015
0.00001
0.000005
0
Day Range (km)
Midshaft Femur Torsional Strength
J/(BS*MFL)
0.0001
0.00009
0.00008
0.00007
0.00006
0.00005
0.00004
0.00003
0.00002
0.00001
0
Day Range (km)
Midshaft Femur Average Bending and Torsional Strength
Zp/BS.GM³
0.003
0.0025
0.002
0.0015
0.001
0.0005
0
Day Range (km)

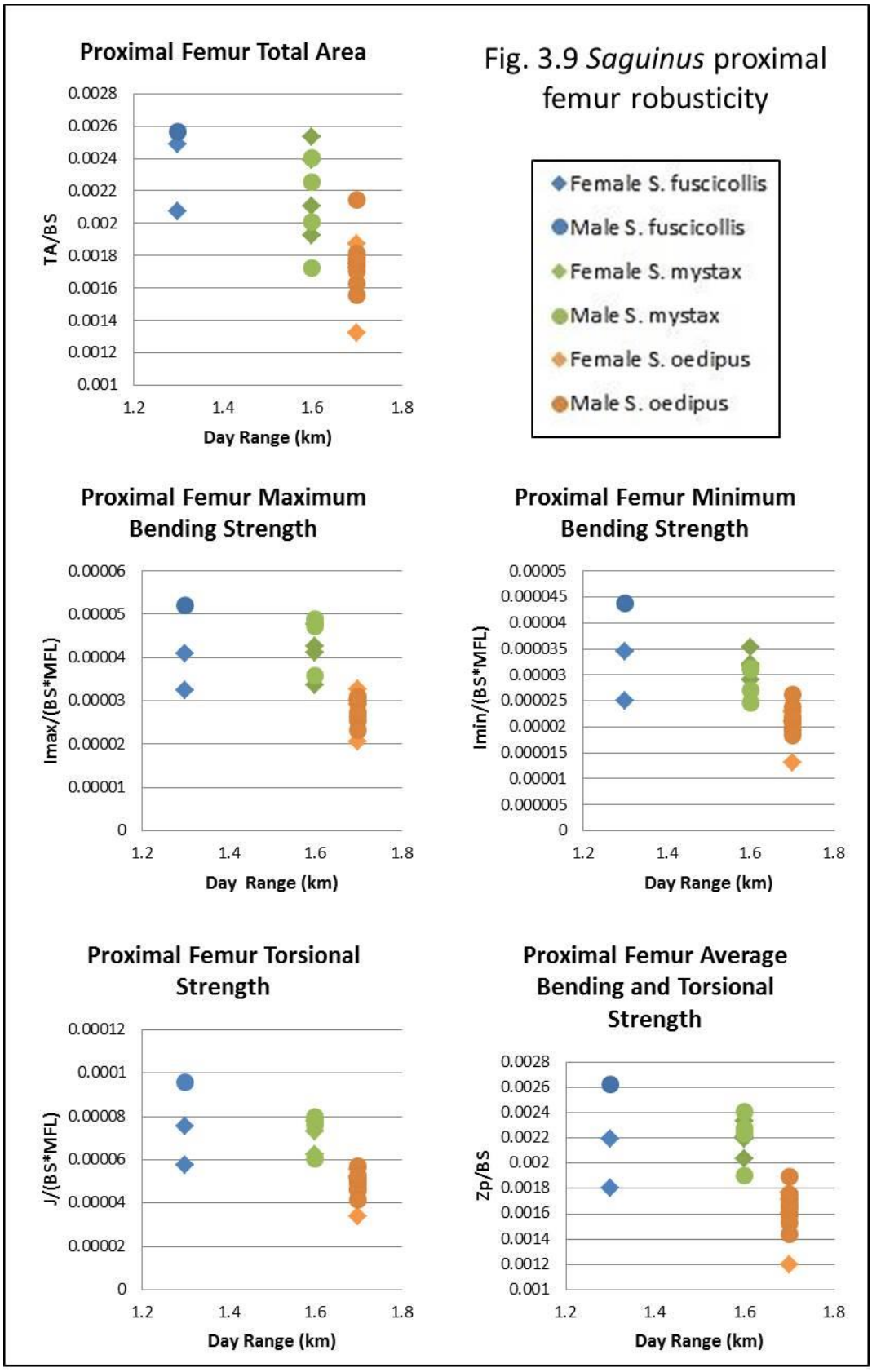
Proximal Femur Total Area
TA/BS
0.0028
0.0026
0.0024
0.0022
0.002
0.0018
0.0016
0.0014
0.0012
0.001
1.2
1.4
1.6
1.8
Day Range (km)
Fig. 3.9 Saguinus proximal femur robusticity
Female S. fuscicollis
Male S. fuscicollis
Female S. mystax
Male S. mystax
Female S. oedipus
Male S. oedipus
Proximal Femur Maximum Bending Strength
Imax/(BS*MFL)
0.00006
0.00005
0.00004
0.00003
0.00002
0.00001
0
1.2
1.4
1.6
1.8
Day Range (km)
Proximal Femur Minimum Bending Strength
Imin/(BS*MFL)
0.00005
0.000045
0.00004
0.000035
0.00003
0.000025
0.00002
0.000015
0.00001
0.000005
0
1.2
1.4
1.6
1.8
Day Range (km)
Proximal Femur Torsional Strength
J/(BS*MFL)
0.00012
0.0001
0.00008
0.00006
0.00004
0.00002
0
1.2
1.4
1.6
1.8
Day Range (km)
Proximal Femur Average Bending and Torsional Strength
Zp/BS
0.0028
0.0026
0.0024
0.0022
0.002
0.0018
0.0016
0.0014
0.0012
0.001
1.2
1.4
1.6
1.8
Day Range (km)

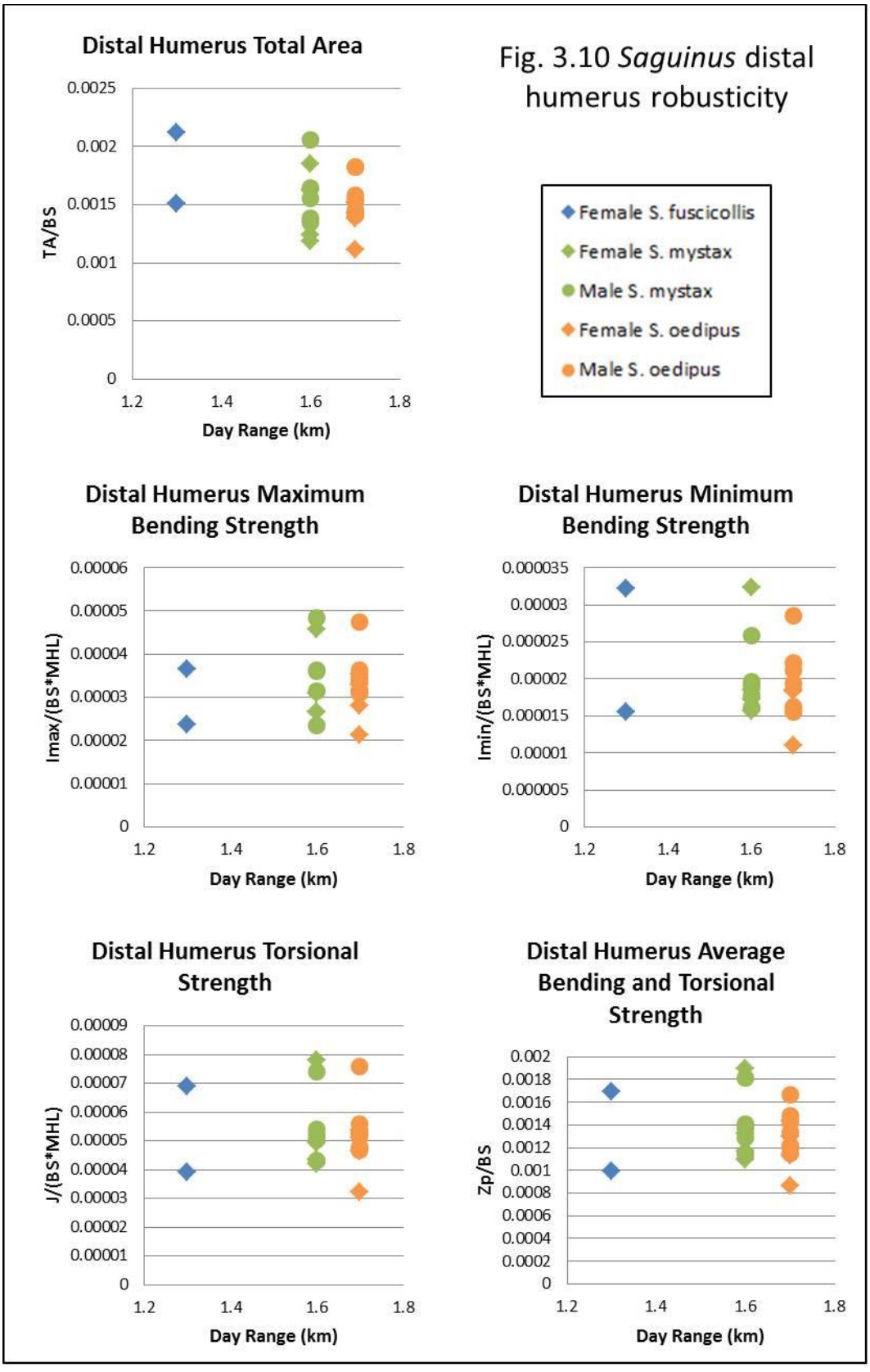

Fig. 3.10 *Saguinus* distal humerus robusticity

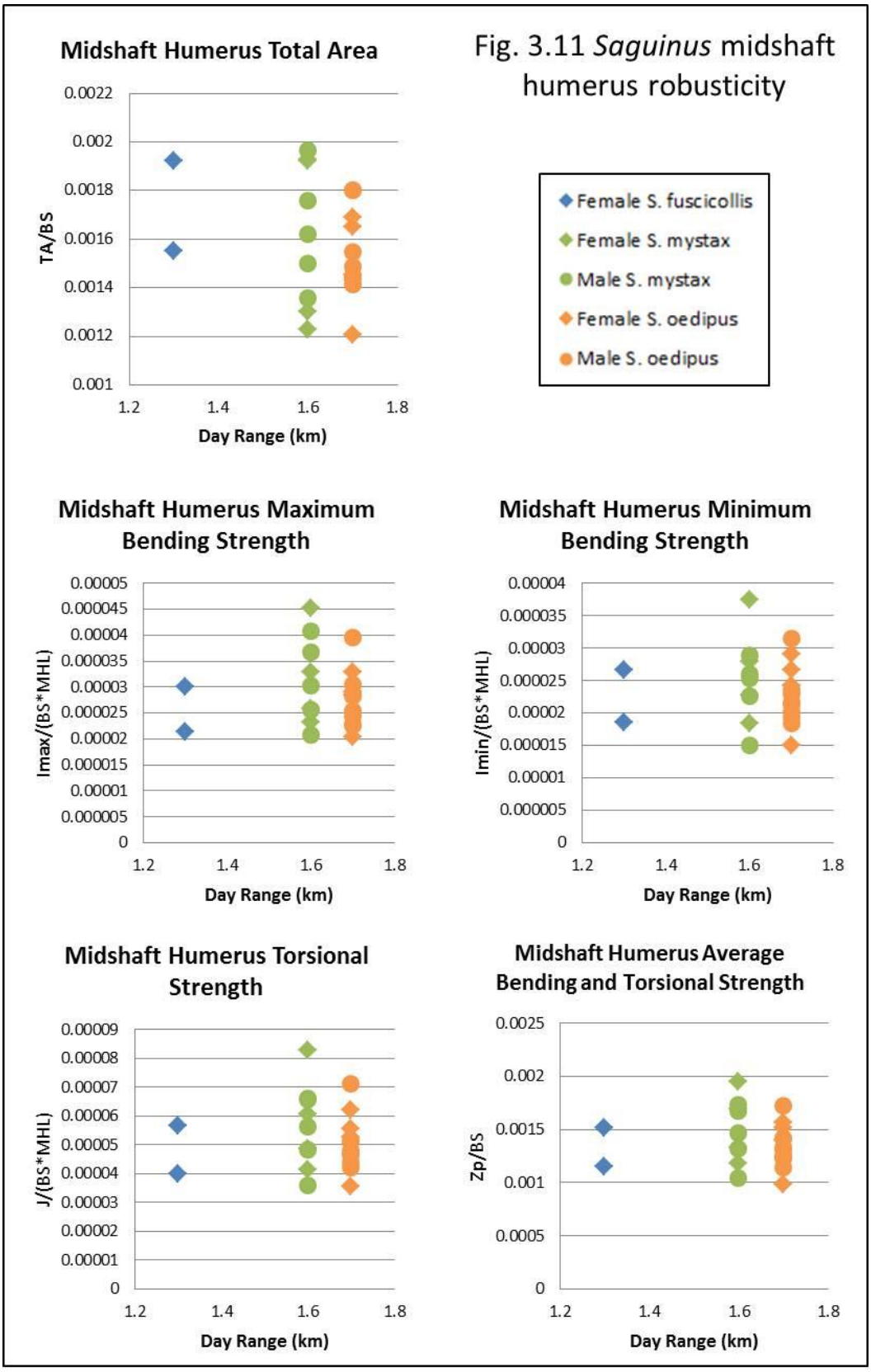

Fig. 3.11 *Saguinus* midshaft humerus robusticity

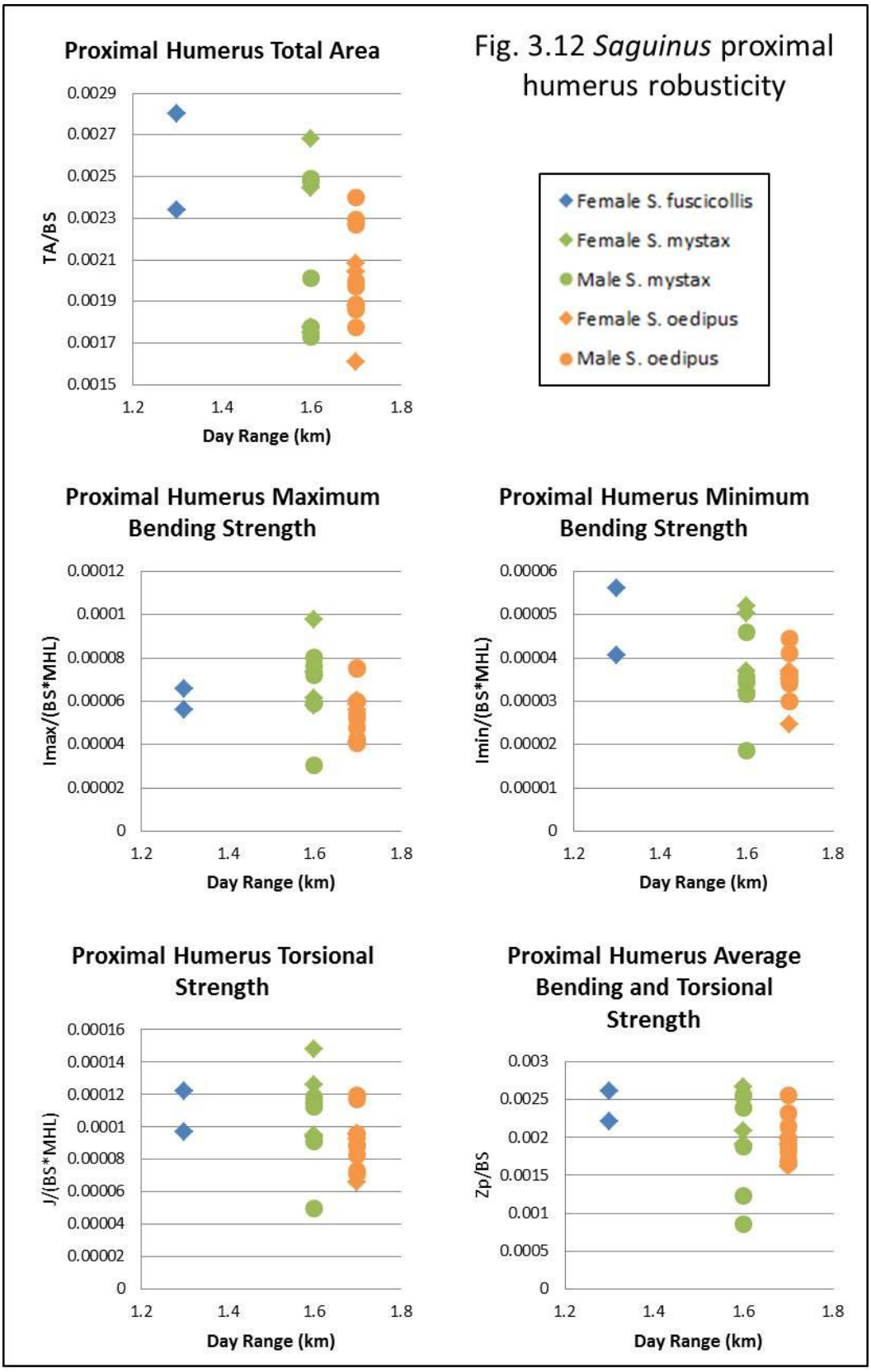

Fig. 3.12 *Saguinus* proximal humerus robusticity

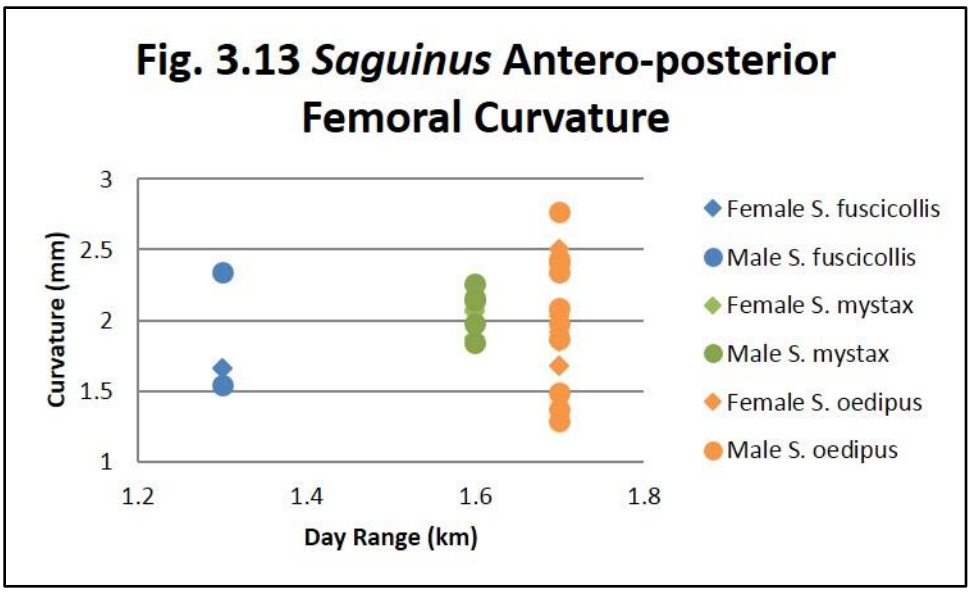
Fig. 3.13 *Saguinus* Antero-posterior Femoral Curvature
Curvature (mm)
3
2.5
2
1.5
1
1.2
1.4
1.6
1.8
Day Range (km)
Female S. fuscicollis
Male S. fuscicollis
Female S. mystax
Male S. mystax
Female S. oedipus
Male S. oedipus

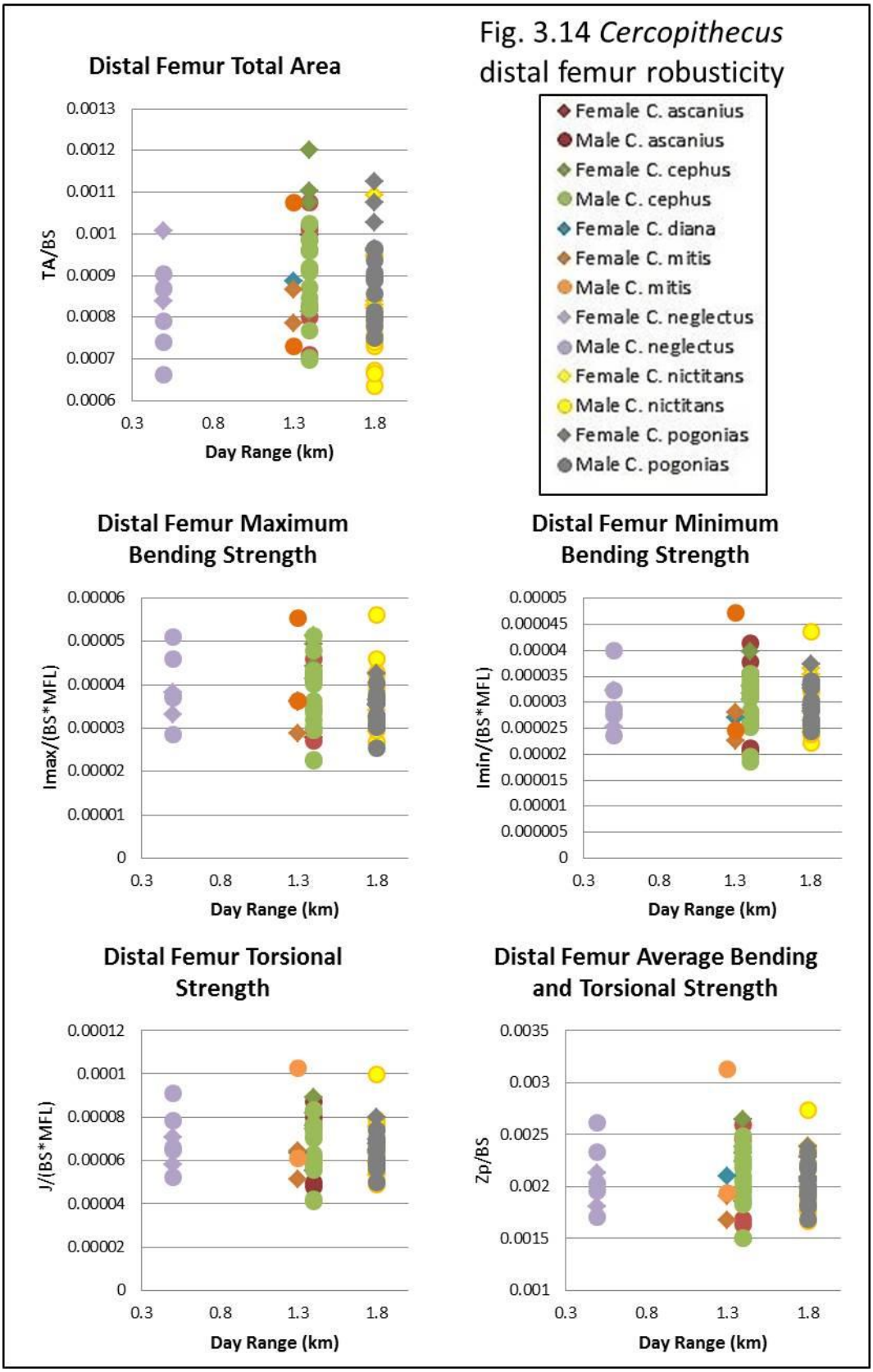

Fig. 3.14 *Cercopithecus* distal femur robusticity

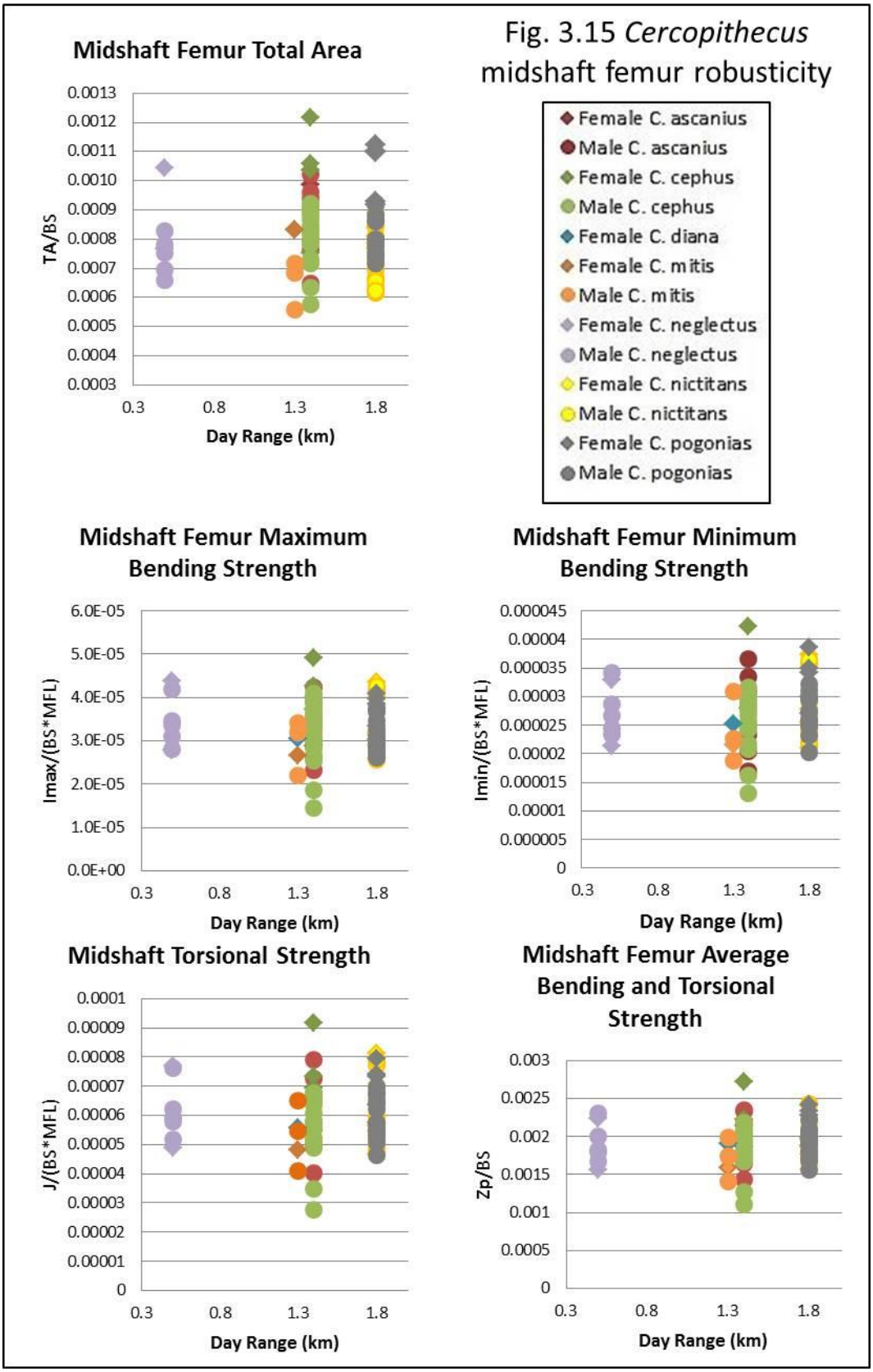

Fig. 3.15 *Cercopithecus* midshaft femur robusticity

Fig. 3.16 *Cercopithecus* proximal femur robusticity

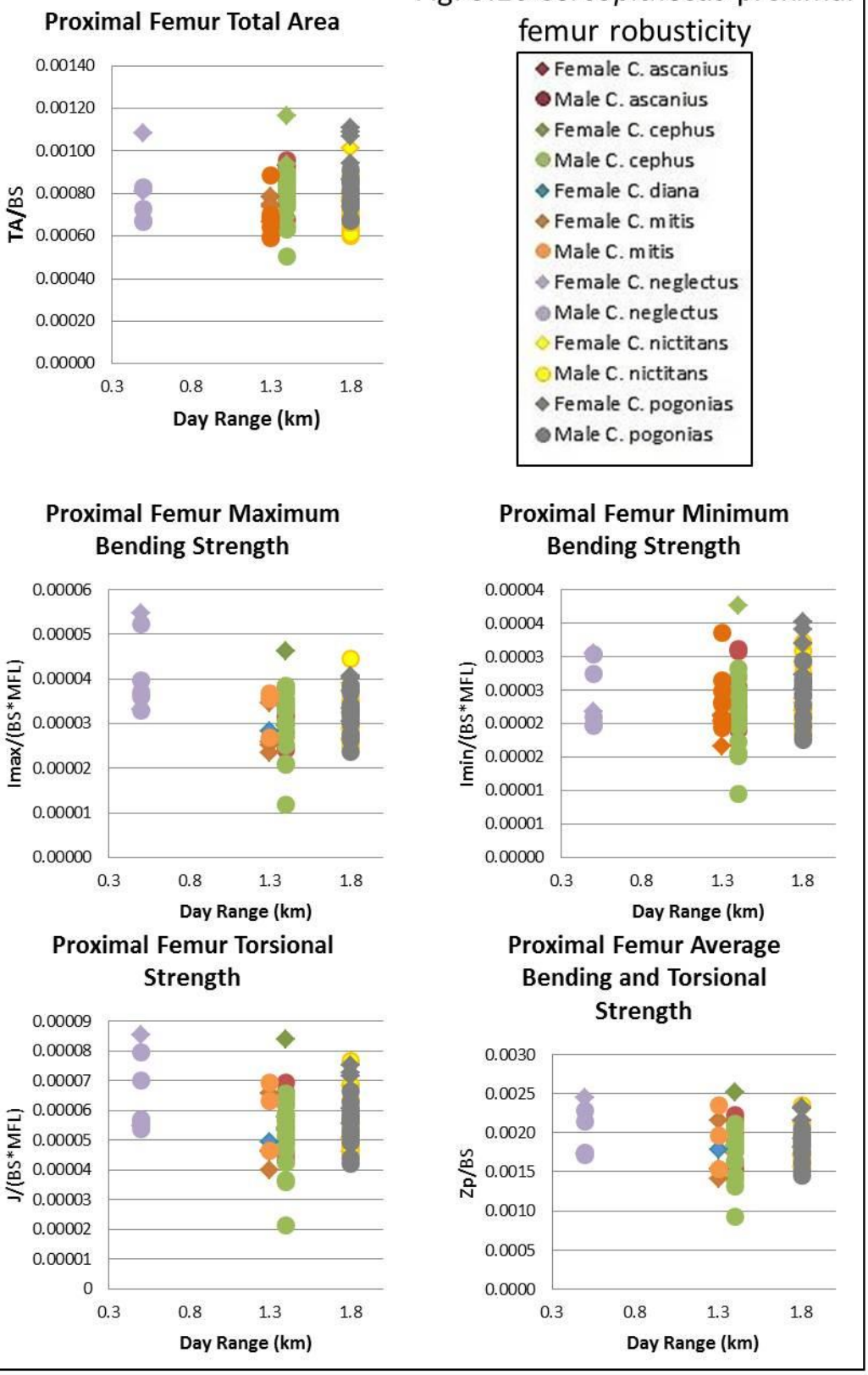

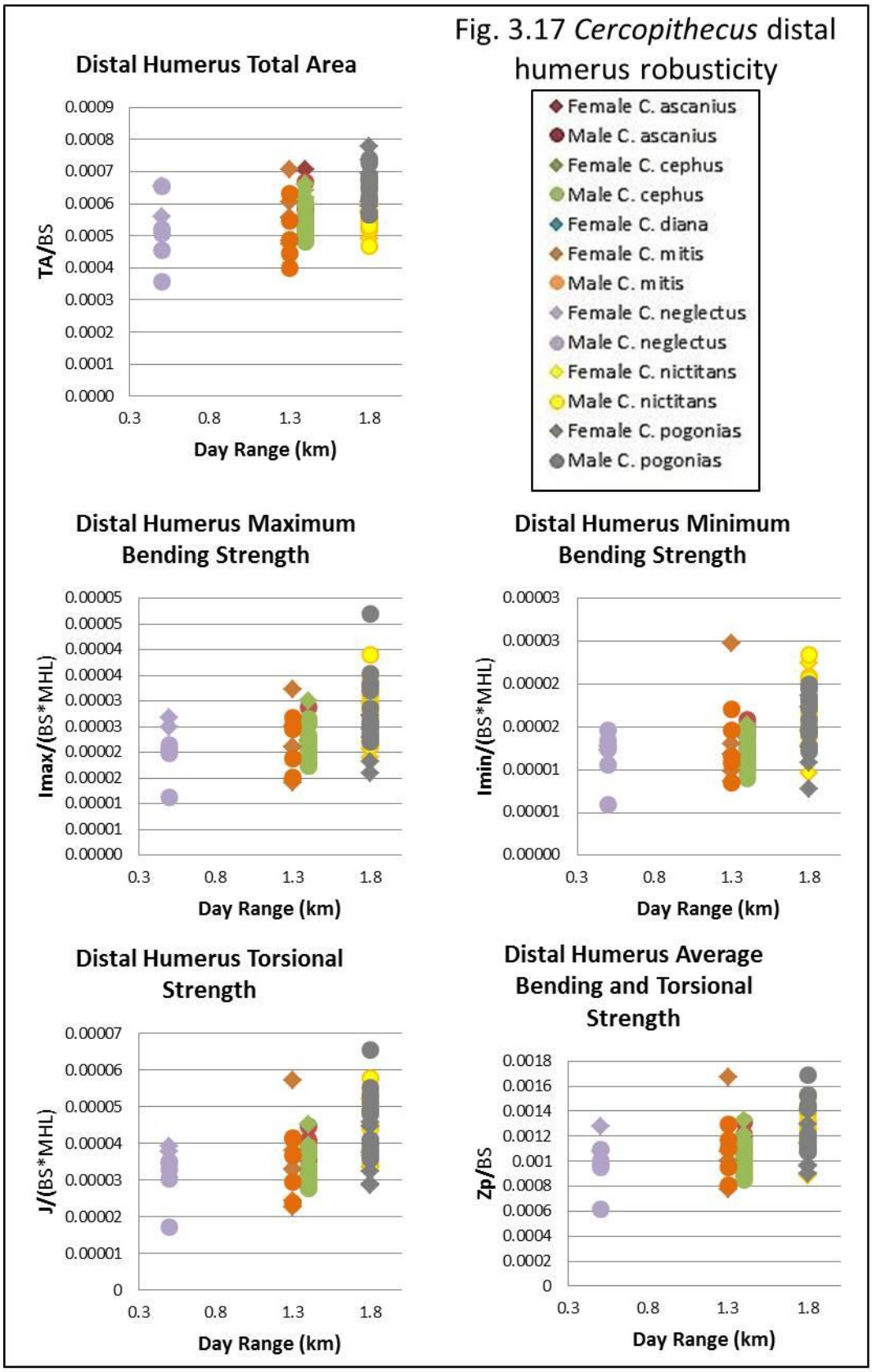

Fig. 3.17 *Cercopithecus* distal humerus robusticity

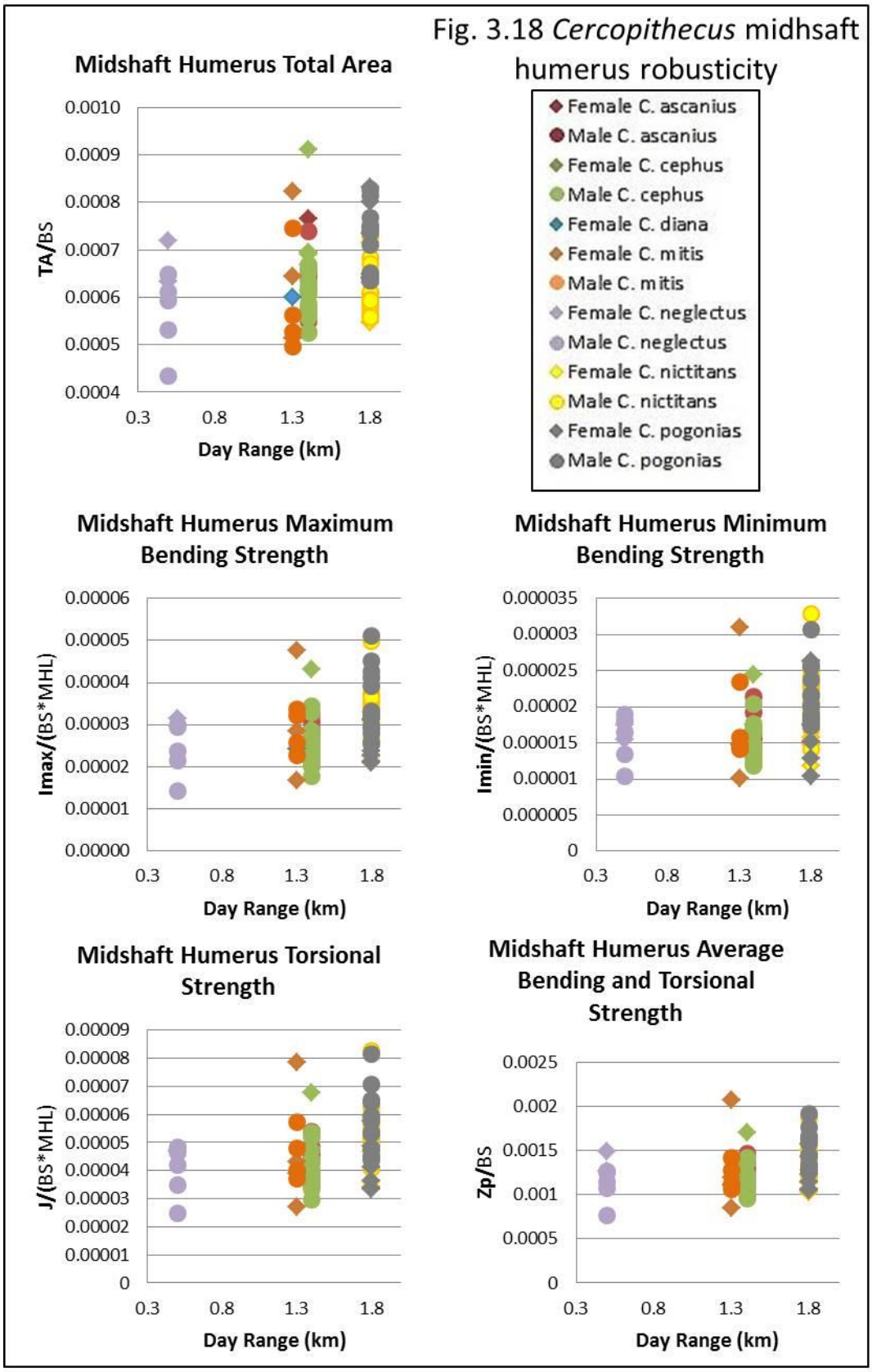

Fig. 3.18 *Cercopithecus* midhsaft humerus robusticity

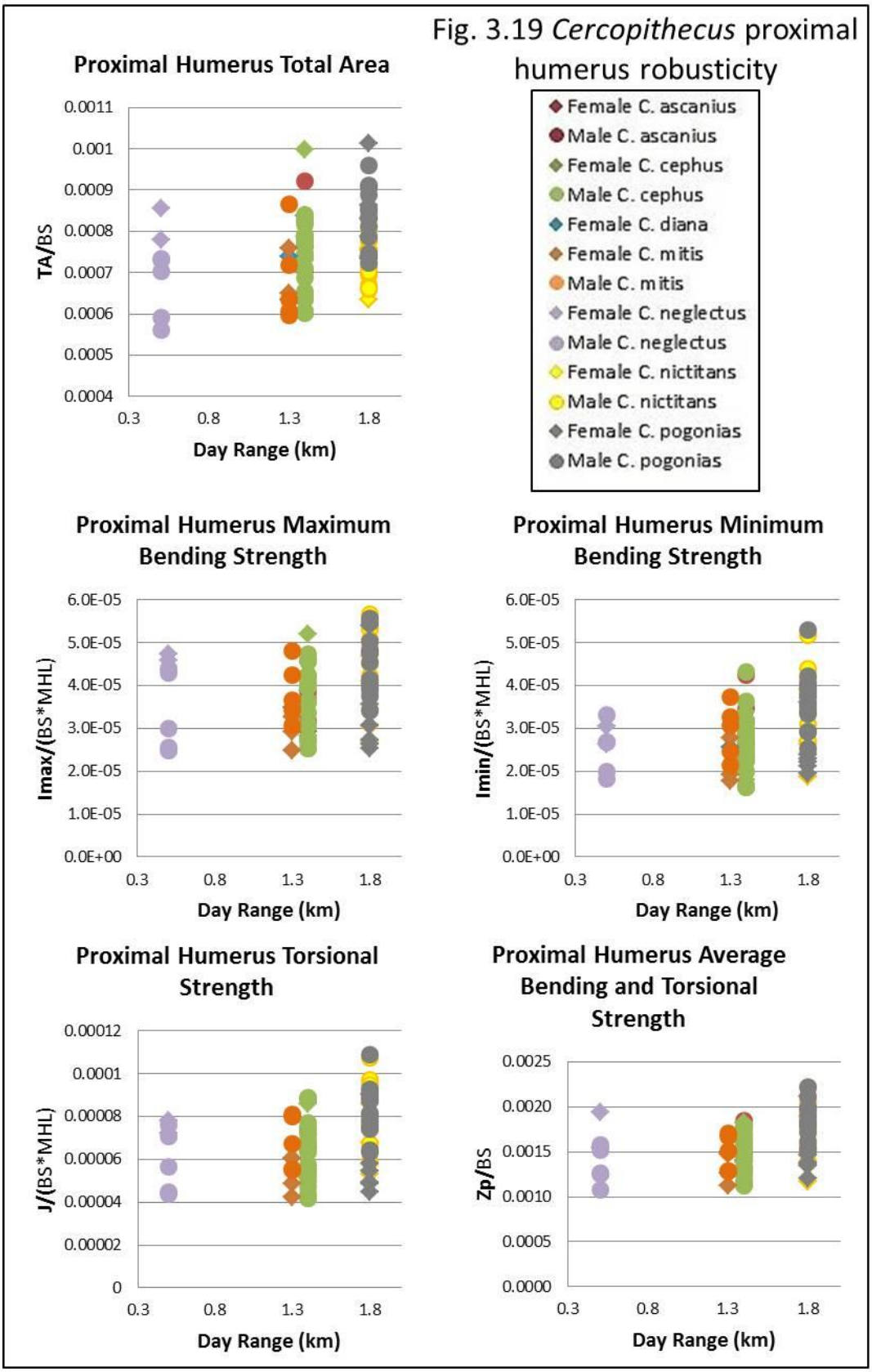

Fig. 3.19 *Cercopithecus* proximal humerus robusticity

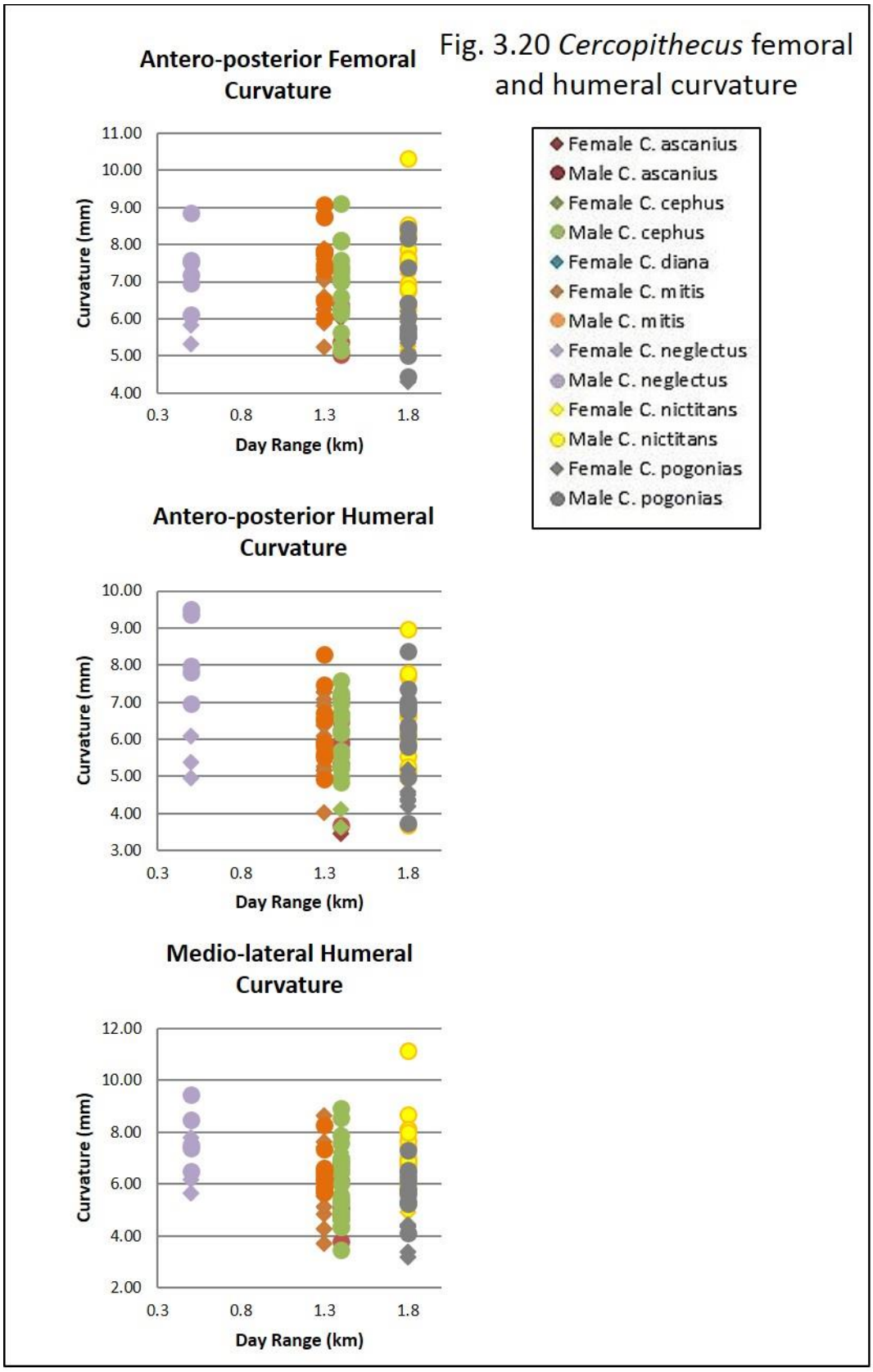

Fig. 3.20 *Cercopithecus* femoral and humeral curvature

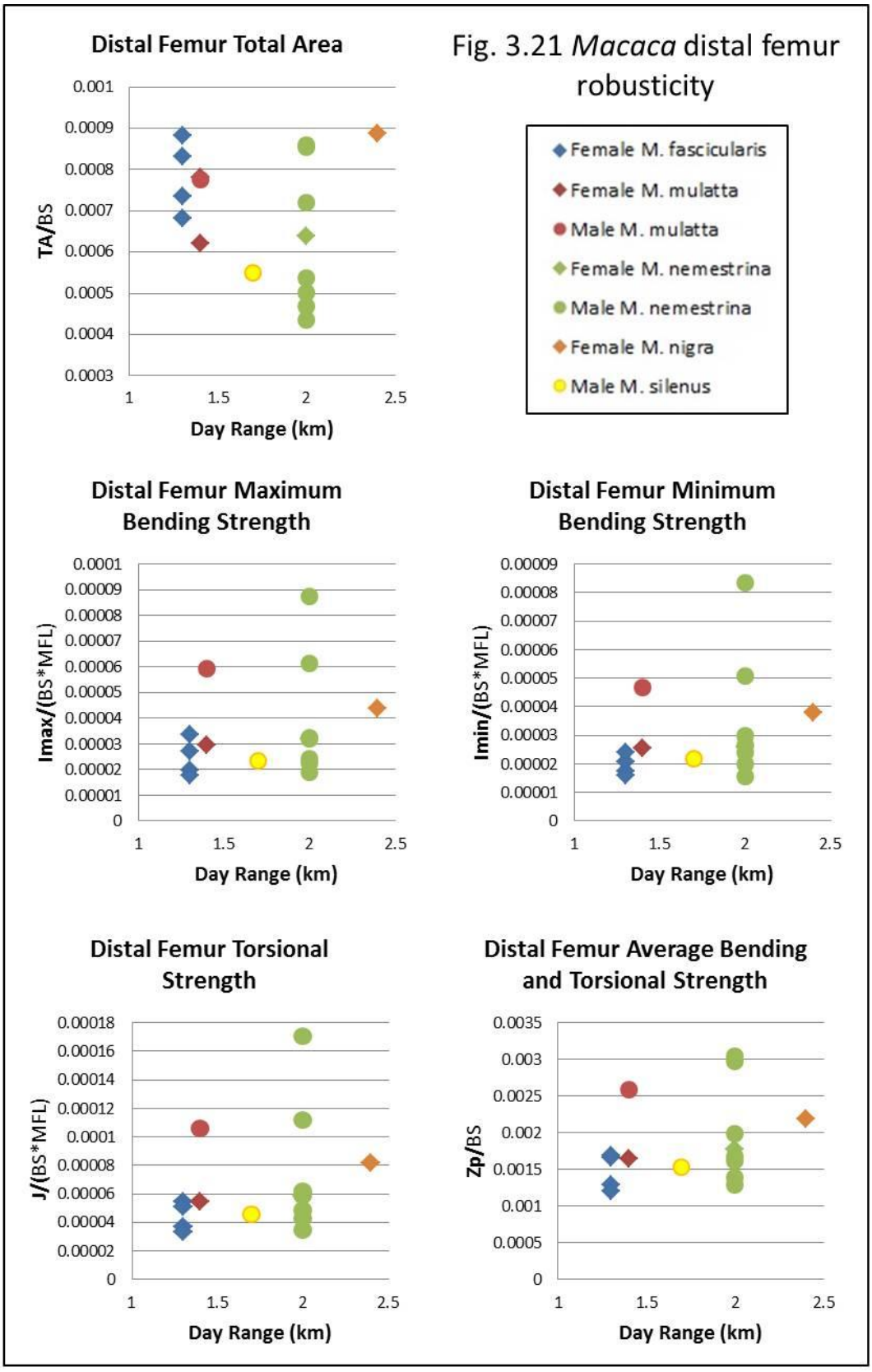
Distal Femur Total Area
TA/BS
0.001
0.0009
0.0008
0.0007
0.0006
0.0005
0.0004
0.0003
1
1.5
2
2.5
Day Range (km)
Fig. 3.21 *Macaca* distal femur robusticity
Female M. fascicularis
Female M. mulatta
Male M. mulatta
Female M. nemestrina
Male M. nemestrina
Female M. nigra
Male M. silenus
Distal Femur Maximum Bending Strength
Imax/(BS*MFL)
0.0001
0.00009
0.00008
0.00007
0.00006
0.00005
0.00004
0.00003
0.00002
0.00001
0
Day Range (km)
Distal Femur Minimum Bending Strength
Imin/(BS*MFL)
0.00009
0.00008
0.00007
0.00006
0.00005
0.00004
0.00003
0.00002
0.00001
0
Day Range (km)
Distal Femur Torsional Strength
J/(BS*MFL)
0.00018
0.00016
0.00014
0.00012
0.0001
0.00008
0.00006
0.00004
0.00002
0
Day Range (km)
Distal Femur Average Bending and Torsional Strength
Zp/BS
0.0035
0.003
0.0025
0.002
0.0015
0.001
0.0005
0
Day Range (km)

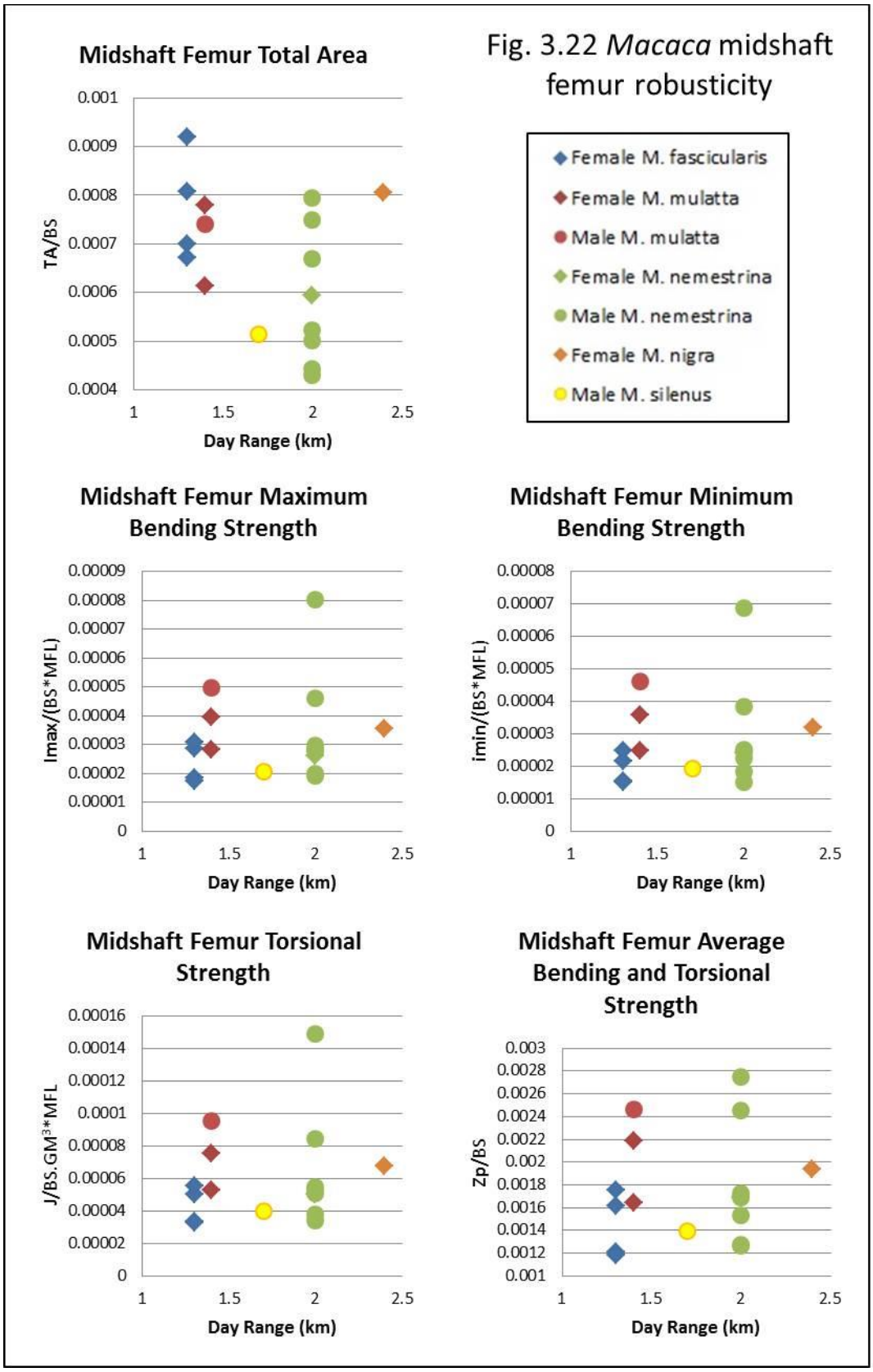
Midshaft Femur Total Area
TA/BS
Day Range (km)
Fig. 3.22 *Macaca* midshaft femur robusticity
Female M. fascicularis
Female M. mulatta
Male M. mulatta
Female M. nemestrina
Male M. nemestrina
Female M. nigra
Male M. silenus
Midshaft Femur Maximum Bending Strength
Imax/(BS*MFL)
Day Range (km)
Midshaft Femur Minimum Bending Strength
imin/(BS*MFL)
Day Range (km)
Midshaft Femur Torsional Strength
J/BS.GM³*MFL
Day Range (km)
Midshaft Femur Average Bending and Torsional Strength
Zp/BS
Day Range (km)

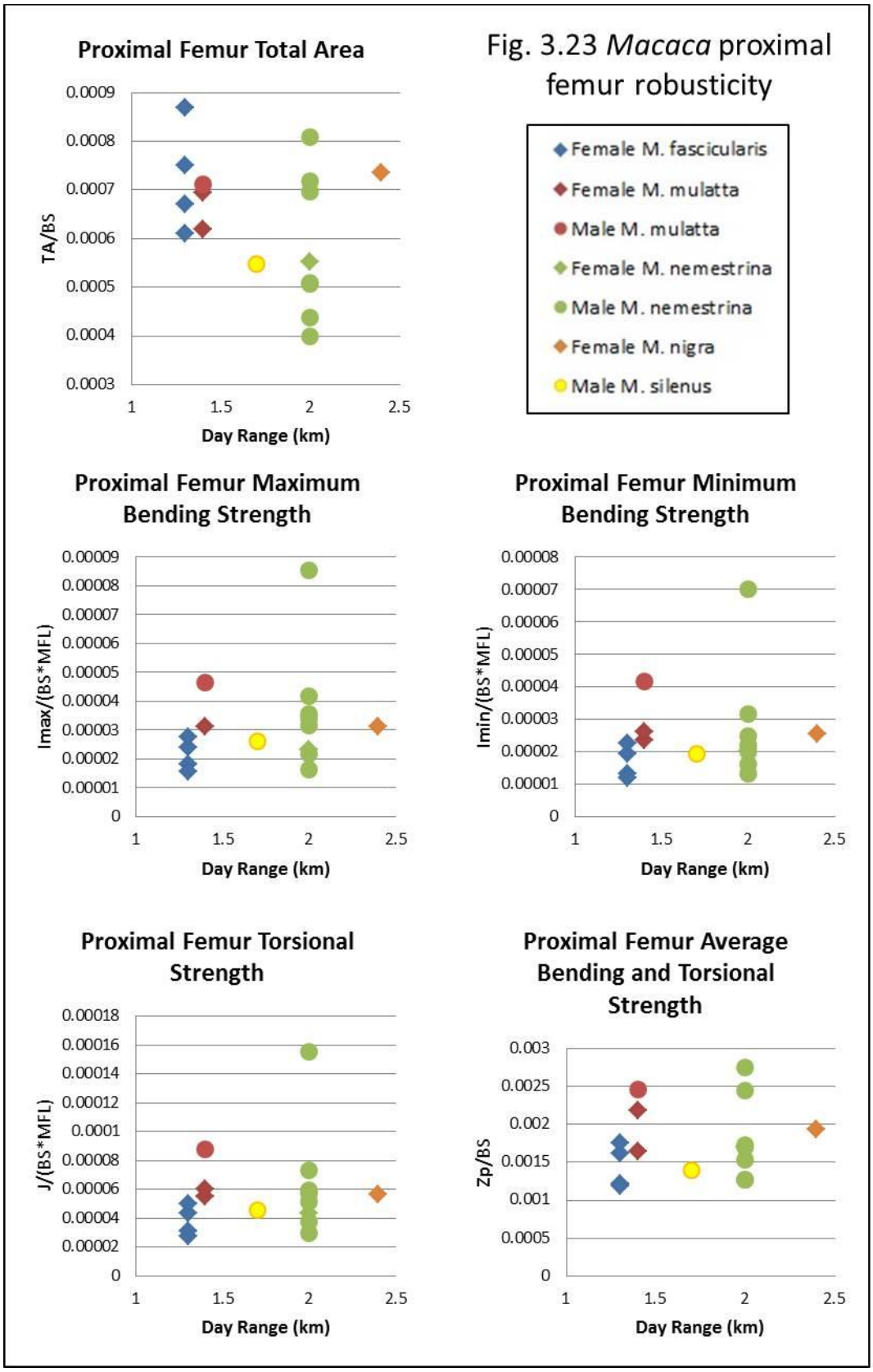
Proximal Femur Total Area
TA/BS
0.0009
0.0008
0.0007
0.0006
0.0005
0.0004
0.0003
1
1.5
2
2.5
Day Range (km)
Fig. 3.23 *Macaca* proximal femur robusticity
Female M. fascicularis
Female M. mulatta
Male M. mulatta
Female M. nemestrina
Male M. nemestrina
Female M. nigra
Male M. silenus
Proximal Femur Maximum Bending Strength
Imax/(BS*MFL)
0.00009
0.00008
0.00007
0.00006
0.00005
0.00004
0.00003
0.00002
0.00001
0
Day Range (km)
Proximal Femur Minimum Bending Strength
Imin/(BS*MFL)
0.00008
0.00007
0.00006
0.00005
0.00004
0.00003
0.00002
0.00001
0
Day Range (km)
Proximal Femur Torsional Strength
J/(BS*MFL)
0.00018
0.00016
0.00014
0.00012
0.0001
0.00008
0.00006
0.00004
0.00002
0
Day Range (km)
Proximal Femur Average Bending and Torsional Strength
Zp/BS
0.003
0.0025
0.002
0.0015
0.001
0.0005
0
Day Range (km)

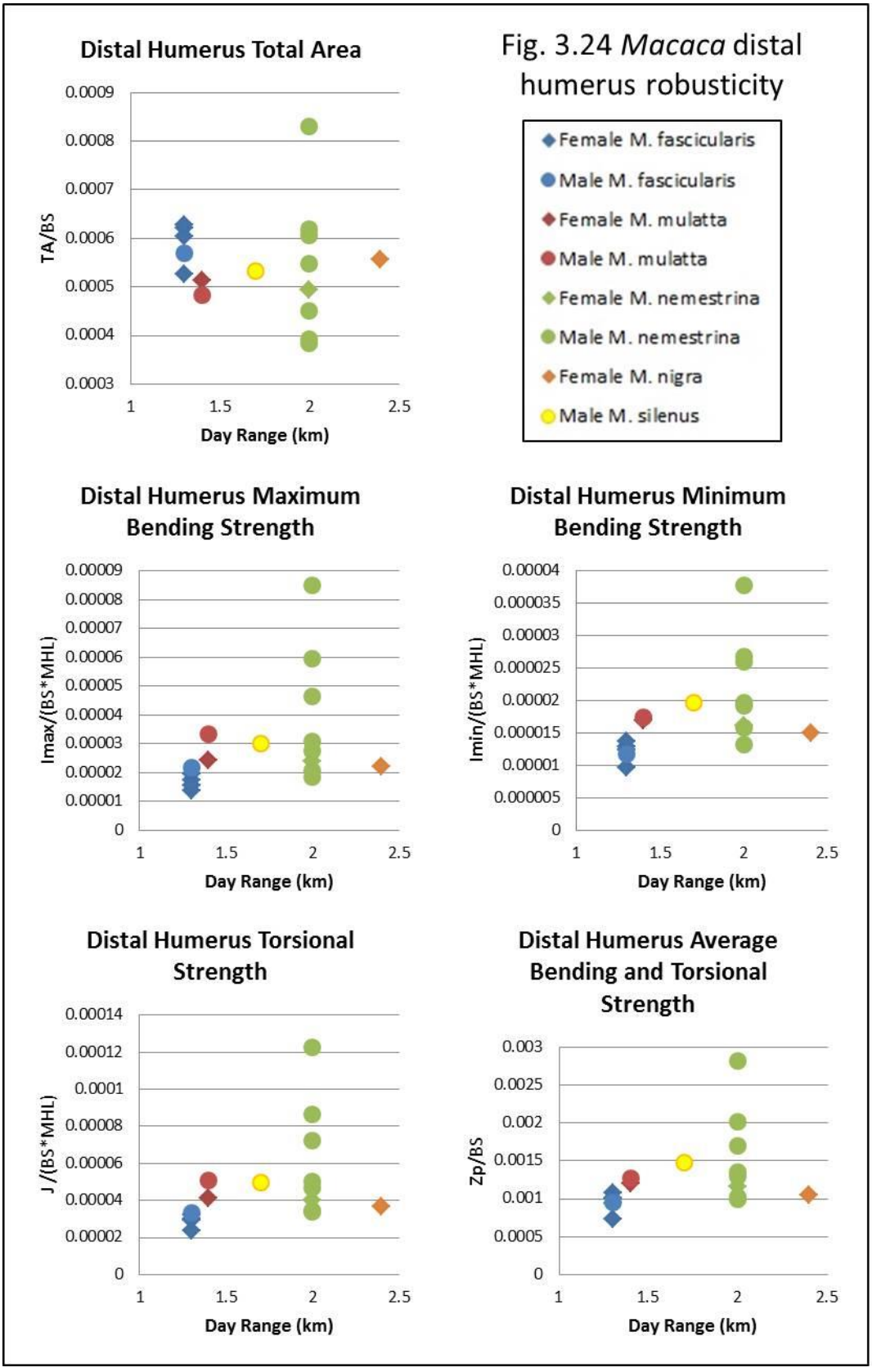
Distal Humerus Total Area
TA/BS
0.0009
0.0008
0.0007
0.0006
0.0005
0.0004
0.0003
1
1.5
2
2.5
Day Range (km)
Fig. 3.24 *Macaca* distal humerus robusticity
Female M. fascicularis
Male M. fascicularis
Female M. mulatta
Male M. mulatta
Female M. nemestrina
Male M. nemestrina
Female M. nigra
Male M. silenus
Distal Humerus Maximum Bending Strength
Imax/(BS*MHL)
0.00009
0.00008
0.00007
0.00006
0.00005
0.00004
0.00003
0.00002
0.00001
0
1
1.5
2
2.5
Day Range (km)
Distal Humerus Minimum Bending Strength
Imin/(BS*MHL)
0.00004
0.000035
0.00003
0.000025
0.00002
0.000015
0.00001
0.000005
0
1
1.5
2
2.5
Day Range (km)
Distal Humerus Torsional Strength
J /(BS*MHL)
0.00014
0.00012
0.0001
0.00008
0.00006
0.00004
0.00002
0
1
1.5
2
2.5
Day Range (km)
Distal Humerus Average Bending and Torsional Strength
Zp/BS
0.003
0.0025
0.002
0.0015
0.001
0.0005
0
1
1.5
2
2.5
Day Range (km)

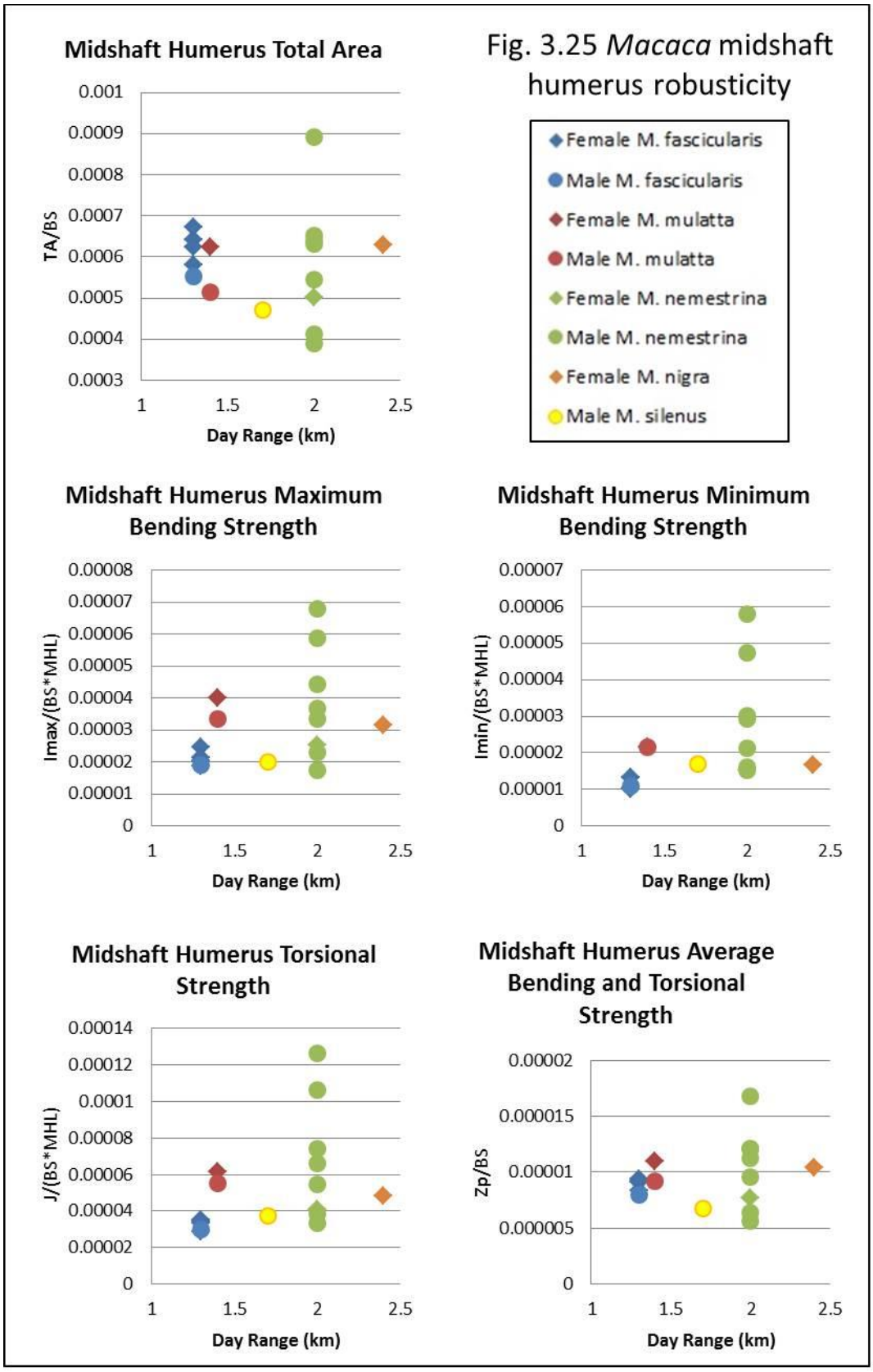
Midshaft Humerus Total Area
TA/BS
0.001
0.0009
0.0008
0.0007
0.0006
0.0005
0.0004
0.0003
1
1.5
2
2.5
Day Range (km)
Fig. 3.25 *Macaca* midshaft humerus robusticity
Female M. fascicularis
Male M. fascicularis
Female M. mulatta
Male M. mulatta
Female M. nemestrina
Male M. nemestrina
Female M. nigra
Male M. silenus
Midshaft Humerus Maximum Bending Strength
Imax/(BS*MHL)
0.00008
0.00007
0.00006
0.00005
0.00004
0.00003
0.00002
0.00001
0
Day Range (km)
Midshaft Humerus Minimum Bending Strength
Imin/(BS*MHL)
0.00007
0.00006
0.00005
0.00004
0.00003
0.00002
0.00001
0
Day Range (km)
Midshaft Humerus Torsional Strength
J/(BS*MHL)
0.00014
0.00012
0.0001
0.00008
0.00006
0.00004
0.00002
0
Day Range (km)
Midshaft Humerus Average Bending and Torsional Strength
Zp/BS
0.00002
0.000015
0.00001
0.000005
0
Day Range (km)

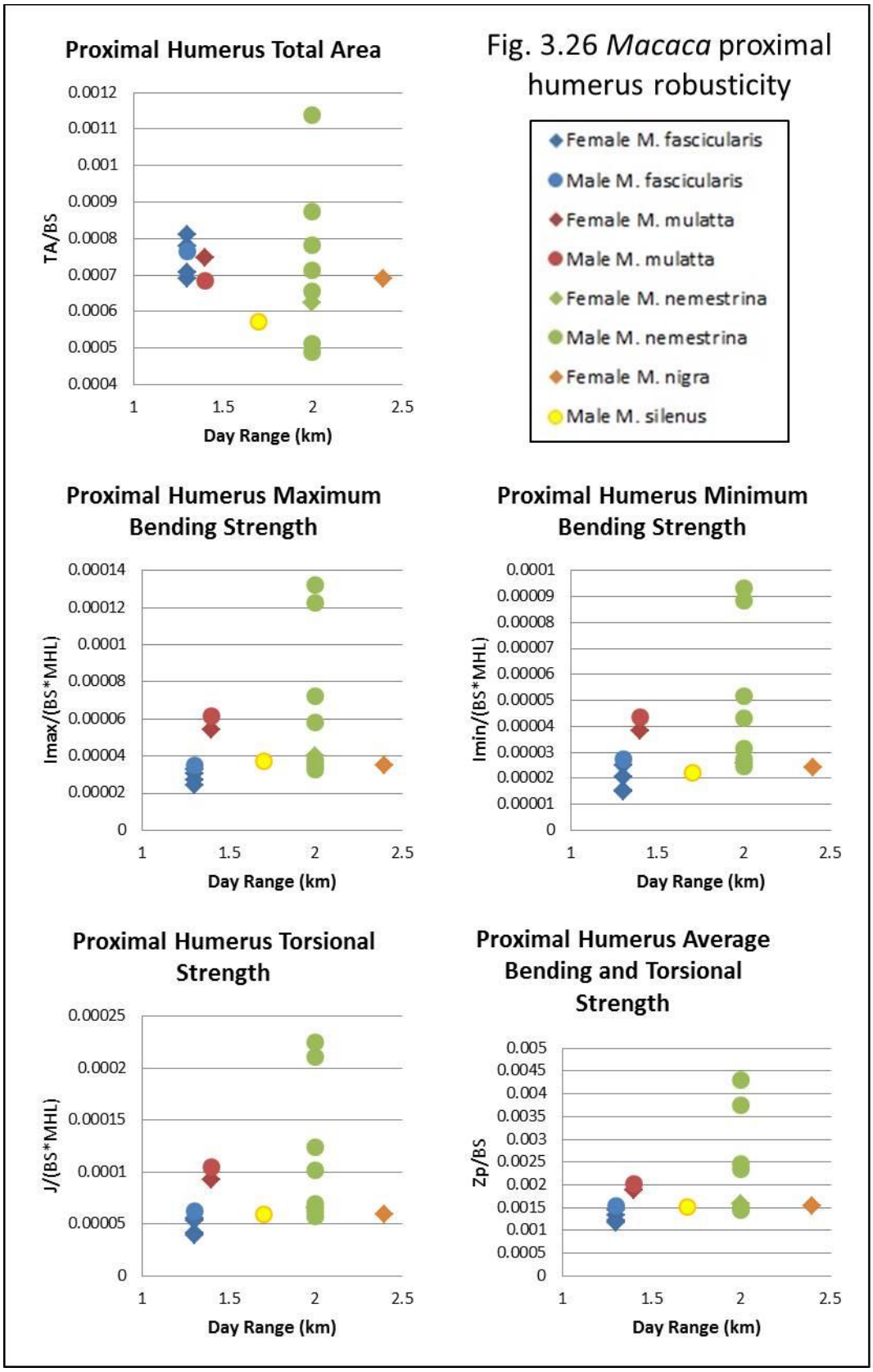
Proximal Humerus Total Area
TA/BS
Day Range (km)
Fig. 3.26 *Macaca* proximal humerus robusticity
Female M. fascicularis
Male M. fascicularis
Female M. mulatta
Male M. mulatta
Female M. nemestrina
Male M. nemestrina
Female M. nigra
Male M. silenus
Proximal Humerus Maximum Bending Strength
Imax/(BS*MHL)
Day Range (km)
Proximal Humerus Minimum Bending Strength
Imin/(BS*MHL)
Day Range (km)
Proximal Humerus Torsional Strength
J/(BS*MHL)
Day Range (km)
Proximal Humerus Average Bending and Torsional Strength
Zp/BS
Day Range (km)

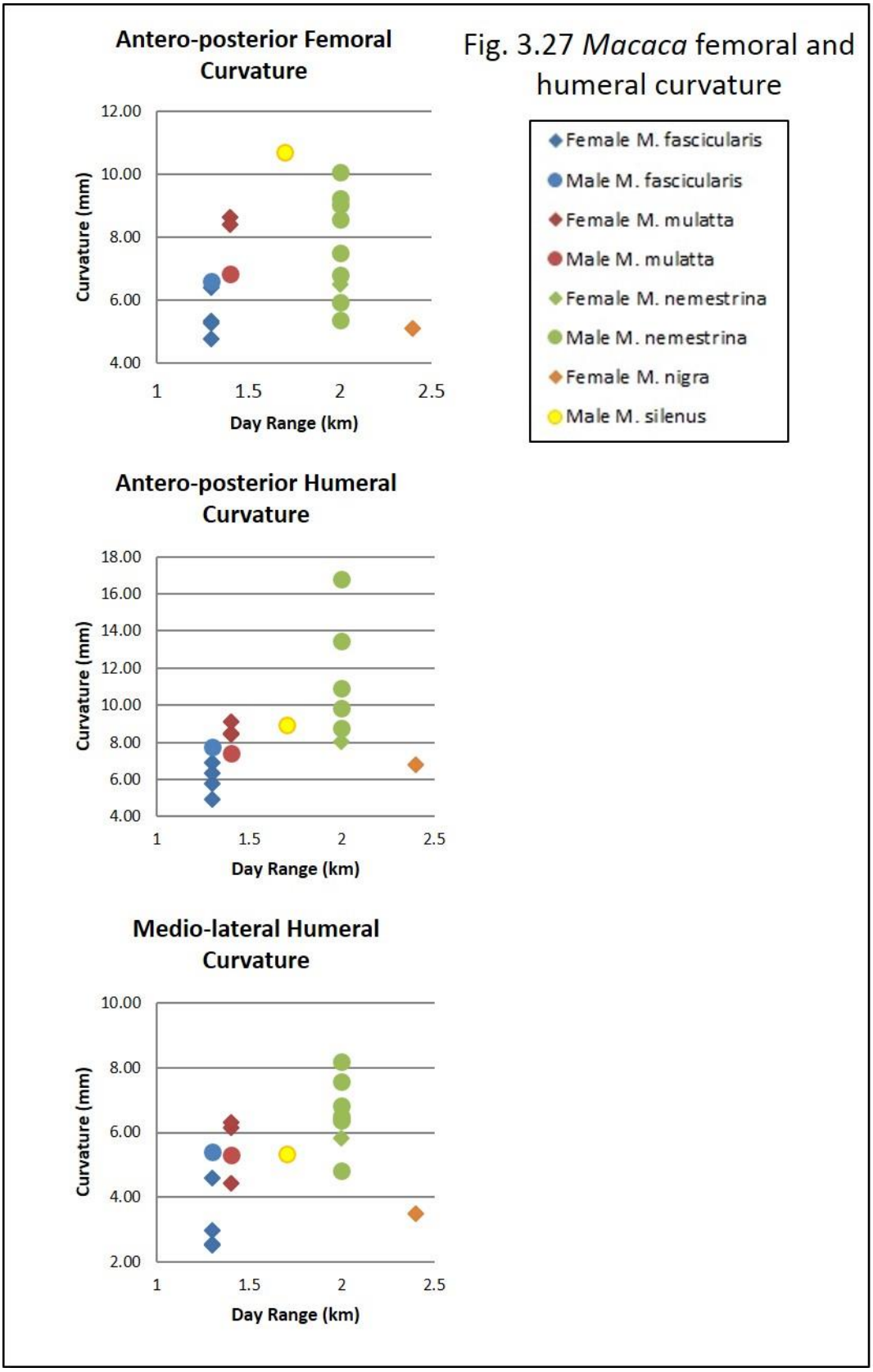

Fig. 3.27 *Macaca* femoral and humeral curvature

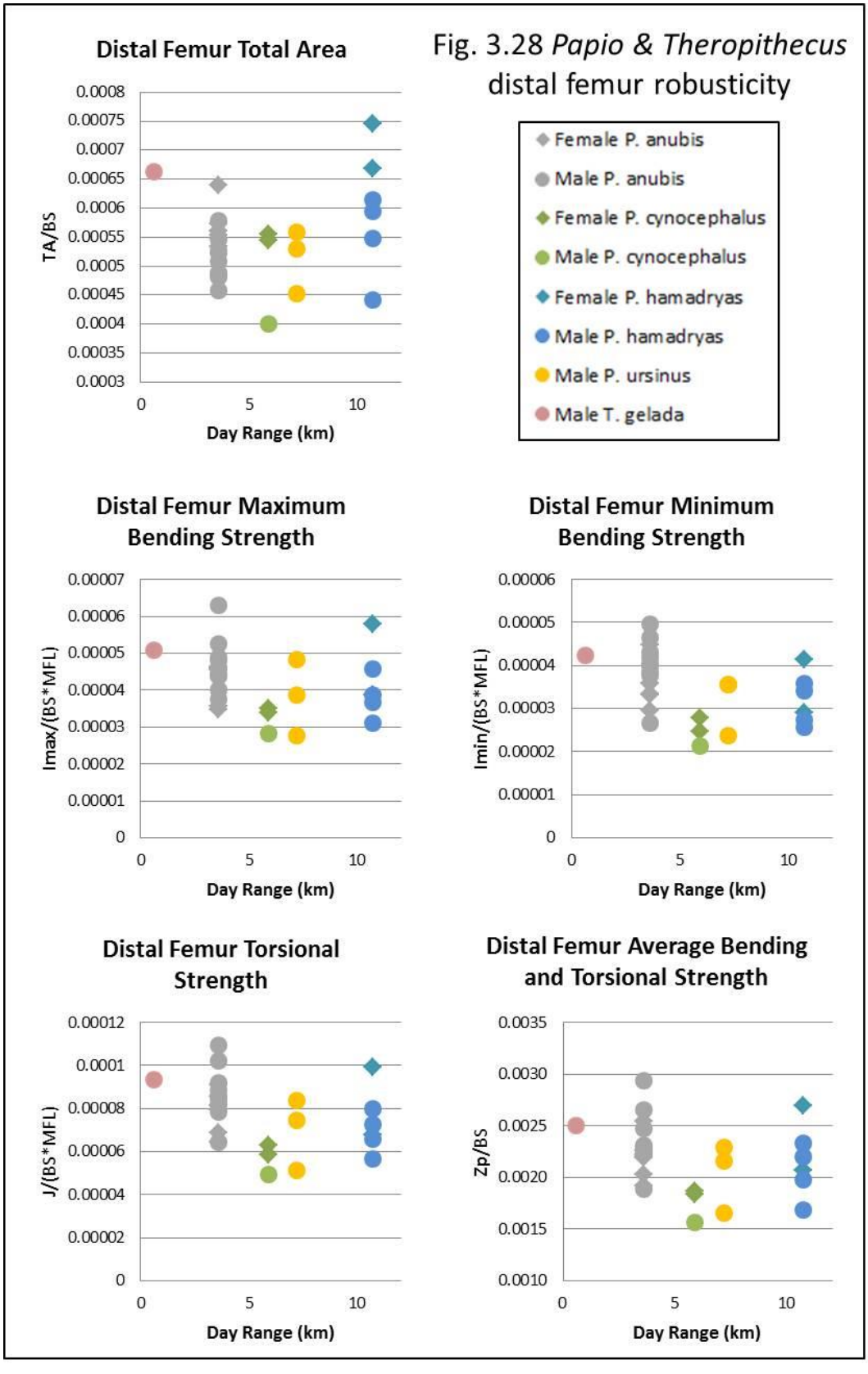
Distal Femur Total Area
TA/BS
0.0008
0.00075
0.0007
0.00065
0.0006
0.00055
0.0005
0.00045
0.0004
0.00035
0.0003
0
5
10
Day Range (km)
Fig. 3.28 Papio & Theropithecus distal femur robusticity
Female P. anubis
Male P. anubis
Female P. cynocephalus
Male P. cynocephalus
Female P. hamadryas
Male P. hamadryas
Male P. ursinus
Male T. gelada
Distal Femur Maximum Bending Strength
Imax/(BS*MFL)
0.00007
0.00006
0.00005
0.00004
0.00003
0.00002
0.00001
0
0
5
10
Day Range (km)
Distal Femur Minimum Bending Strength
Imin/(BS*MFL)
0.00006
0.00005
0.00004
0.00003
0.00002
0.00001
0
0
5
10
Day Range (km)
Distal Femur Torsional Strength
J/(BS*MFL)
0.00012
0.0001
0.00008
0.00006
0.00004
0.00002
0
0
5
10
Day Range (km)
Distal Femur Average Bending and Torsional Strength
Zp/BS
0.0035
0.0030
0.0025
0.0020
0.0015
0.0010
0
5
10
Day Range (km)

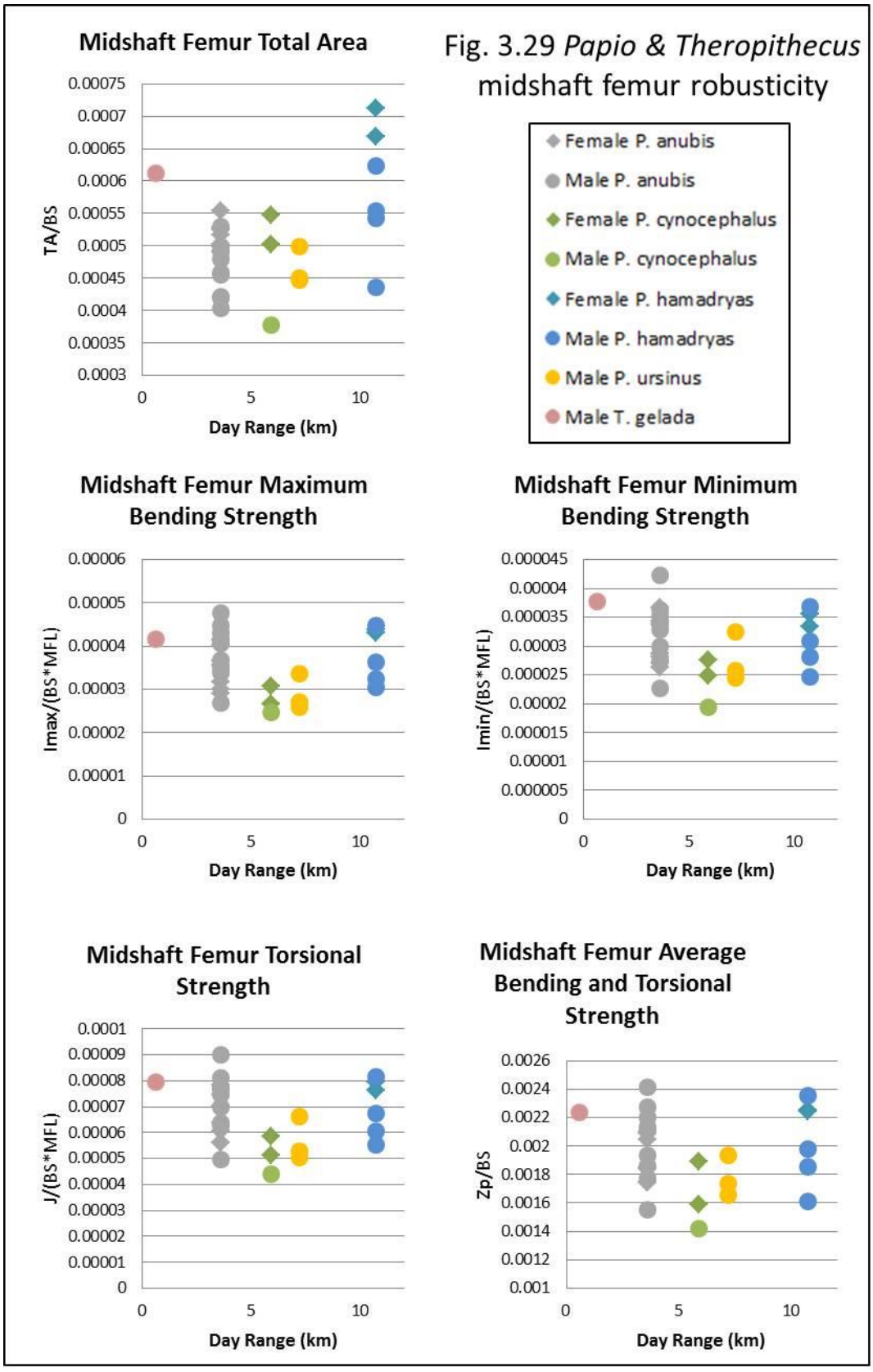
Midshaft Femur Total Area
TA/BS
0.00075
0.0007
0.00065
0.0006
0.00055
0.0005
0.00045
0.0004
0.00035
0.0003
0
5
10
Day Range (km)
Fig. 3.29 Papio & Theropithecus midshaft femur robusticity
Female P. anubis
Male P. anubis
Female P. cynocephalus
Male P. cynocephalus
Female P. hamadryas
Male P. hamadryas
Male P. ursinus
Male T. gelada
Midshaft Femur Maximum Bending Strength
Imax/(BS*MFL)
0.00006
0.00005
0.00004
0.00003
0.00002
0.00001
0
0
5
10
Day Range (km)
Midshaft Femur Minimum Bending Strength
Imin/(BS*MFL)
0.000045
0.00004
0.000035
0.00003
0.000025
0.00002
0.000015
0.00001
0.000005
0
0
5
10
Day Range (km)
Midshaft Femur Torsional Strength
J/(BS*MFL)
0.0001
0.00009
0.00008
0.00007
0.00006
0.00005
0.00004
0.00003
0.00002
0.00001
0
0
5
10
Day Range (km)
Midshaft Femur Average Bending and Torsional Strength
Zp/BS
0.0026
0.0024
0.0022
0.002
0.0018
0.0016
0.0014
0.0012
0.001
0
5
10
Day Range (km)

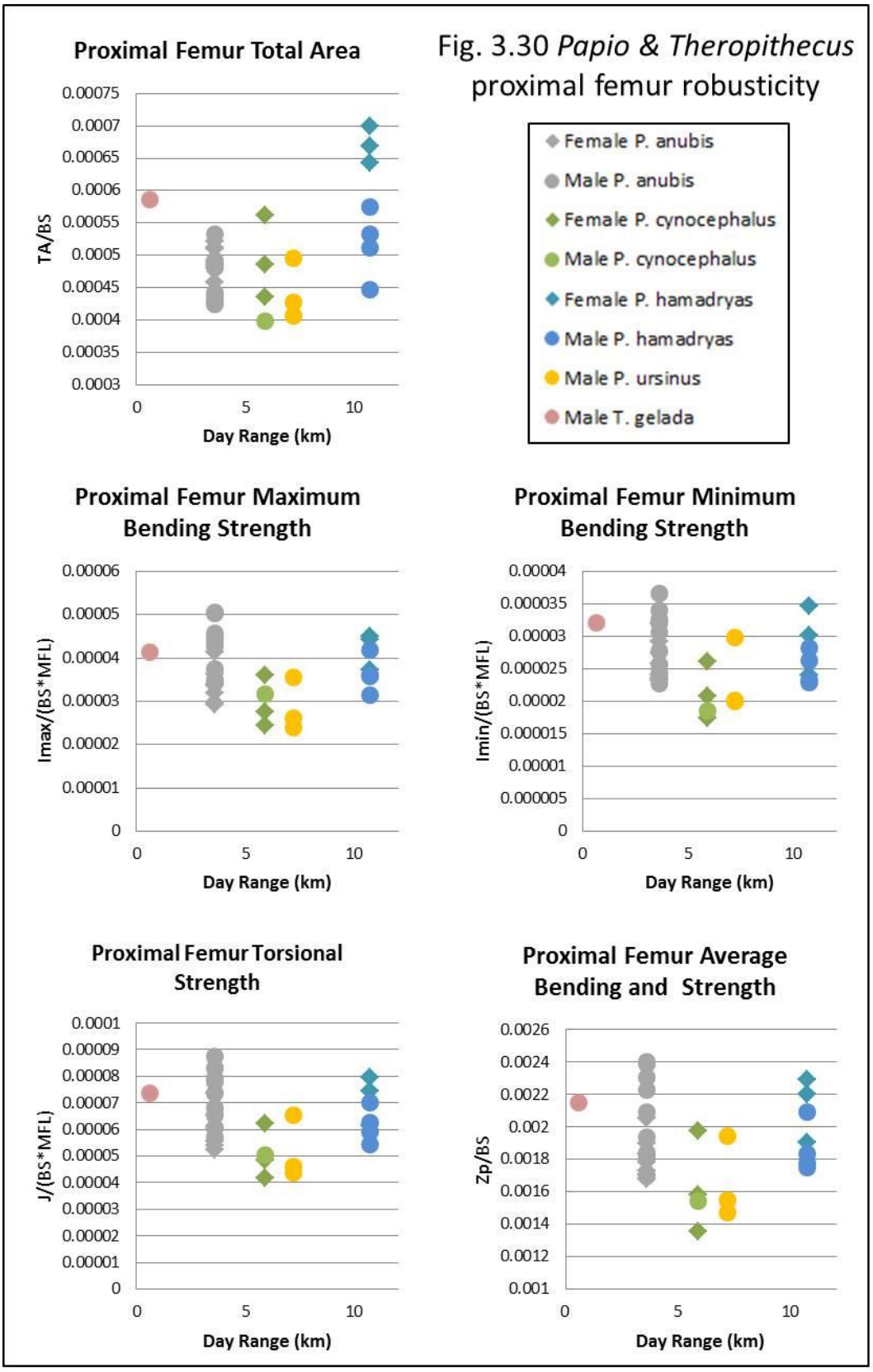
Proximal Femur Total Area
TA/BS
0.00075
0.0007
0.00065
0.0006
0.00055
0.0005
0.00045
0.0004
0.00035
0.0003
0
5
10
Day Range (km)
Fig. 3.30 *Papio & Theropithecus* proximal femur robusticity
Female P. anubis
Male P. anubis
Female P. cynocephalus
Male P. cynocephalus
Female P. hamadryas
Male P. hamadryas
Male P. ursinus
Male T. gelada
Proximal Femur Maximum Bending Strength
Imax/(BS*MFL)
0.00006
0.00005
0.00004
0.00003
0.00002
0.00001
0
0
5
10
Day Range (km)
Proximal Femur Minimum Bending Strength
Imin/(BS*MFL)
0.00004
0.000035
0.00003
0.000025
0.00002
0.000015
0.00001
0.000005
0
0
5
10
Day Range (km)
Proximal Femur Torsional Strength
J/(BS*MFL)
0.0001
0.00009
0.00008
0.00007
0.00006
0.00005
0.00004
0.00003
0.00002
0.00001
0
0
5
10
Day Range (km)
Proximal Femur Average Bending and Strength
Zp/BS
0.0026
0.0024
0.0022
0.002
0.0018
0.0016
0.0014
0.0012
0.001
0
5
10
Day Range (km)

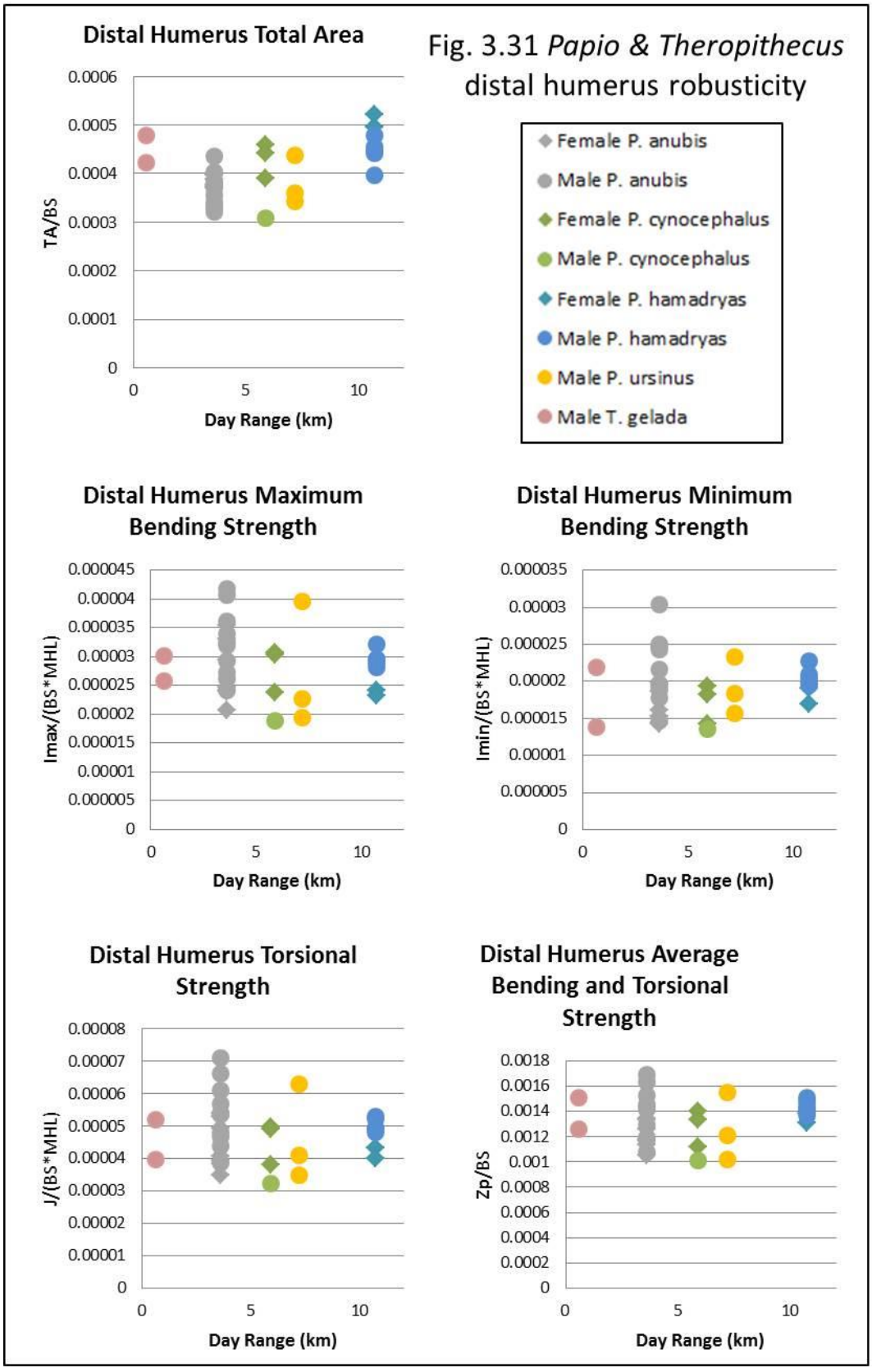
Distal Humerus Total Area
TA/BS
0.0006
0.0005
0.0004
0.0003
0.0002
0.0001
0
0
5
10
Day Range (km)
Fig. 3.31 *Papio & Theropithecus* distal humerus robusticity
Female P. anubis
Male P. anubis
Female P. cynocephalus
Male P. cynocephalus
Female P. hamadryas
Male P. hamadryas
Male P. ursinus
Male T. gelada
Distal Humerus Maximum Bending Strength
Imax/(BS*MHL)
0.000045
0.00004
0.000035
0.00003
0.000025
0.00002
0.000015
0.00001
0.000005
0
0
5
10
Day Range (km)
Distal Humerus Minimum Bending Strength
Imin/(BS*MHL)
0.000035
0.00003
0.000025
0.00002
0.000015
0.00001
0.000005
0
0
5
10
Day Range (km)
Distal Humerus Torsional Strength
J/(BS*MHL)
0.00008
0.00007
0.00006
0.00005
0.00004
0.00003
0.00002
0.00001
0
0
5
10
Day Range (km)
Distal Humerus Average Bending and Torsional Strength
Zp/BS
0.0018
0.0016
0.0014
0.0012
0.001
0.0008
0.0006
0.0004
0.0002
0
0
5
10
Day Range (km)

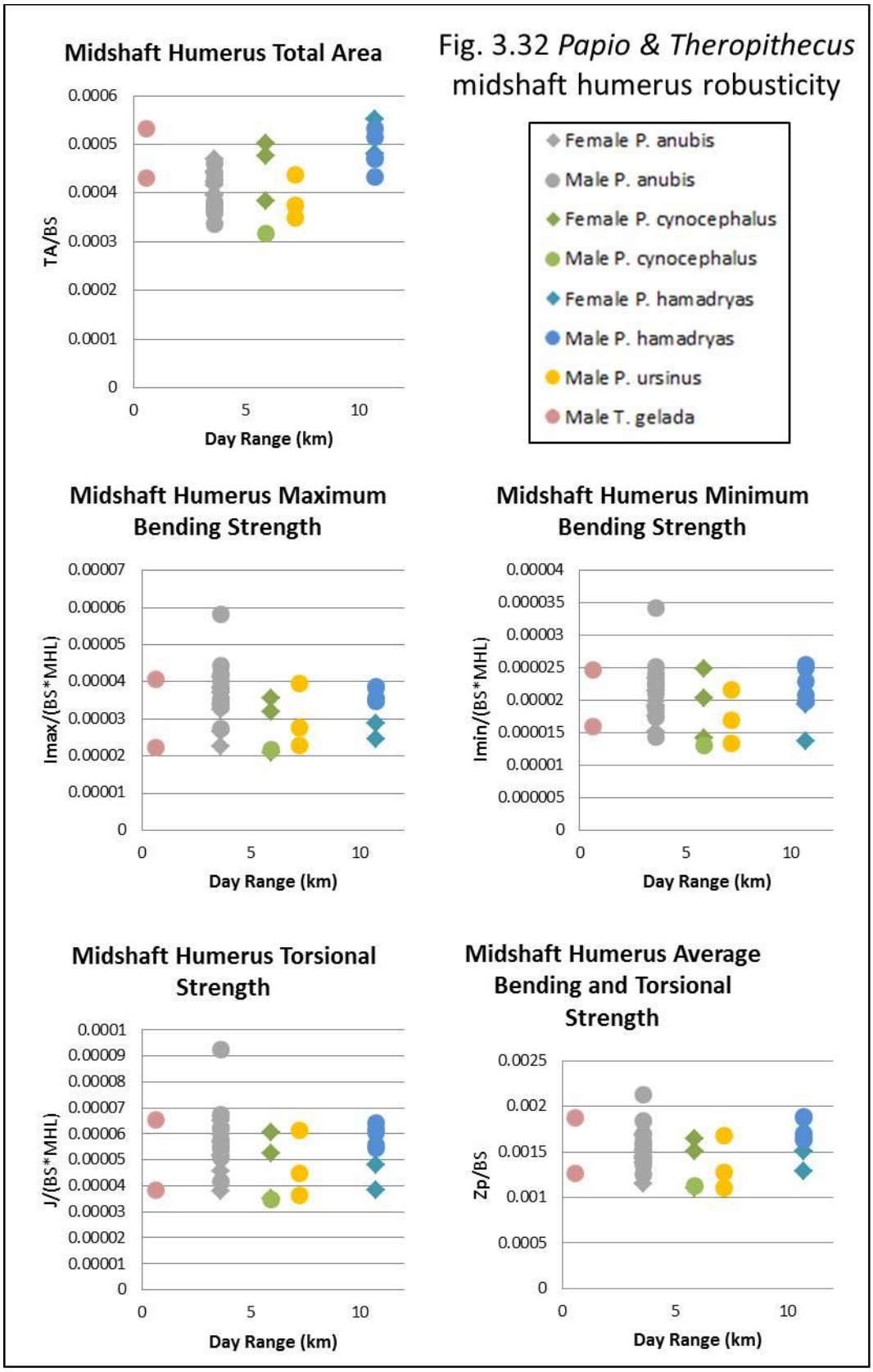
Midshaft Humerus Total Area
TA/BS
0.0006
0.0005
0.0004
0.0003
0.0002
0.0001
0
0
5
10
Day Range (km)
Fig. 3.32 Papio & Theropithecus midshaft humerus robusticity
Female P. anubis
Male P. anubis
Female P. cynocephalus
Male P. cynocephalus
Female P. hamadryas
Male P. hamadryas
Male P. ursinus
Male T. gelada
Midshaft Humerus Maximum Bending Strength
Imax/(BS*MHL)
0.00007
0.00006
0.00005
0.00004
0.00003
0.00002
0.00001
0
0
5
10
Day Range (km)
Midshaft Humerus Minimum Bending Strength
Imin/(BS*MHL)
0.00004
0.000035
0.00003
0.000025
0.00002
0.000015
0.00001
0.000005
0
0
5
10
Day Range (km)
Midshaft Humerus Torsional Strength
J/(BS*MHL)
0.0001
0.00009
0.00008
0.00007
0.00006
0.00005
0.00004
0.00003
0.00002
0.00001
0
0
5
10
Day Range (km)
Midshaft Humerus Average Bending and Torsional Strength
Zp/BS
0.0025
0.002
0.0015
0.001
0.0005
0
0
5
10
Day Range (km)

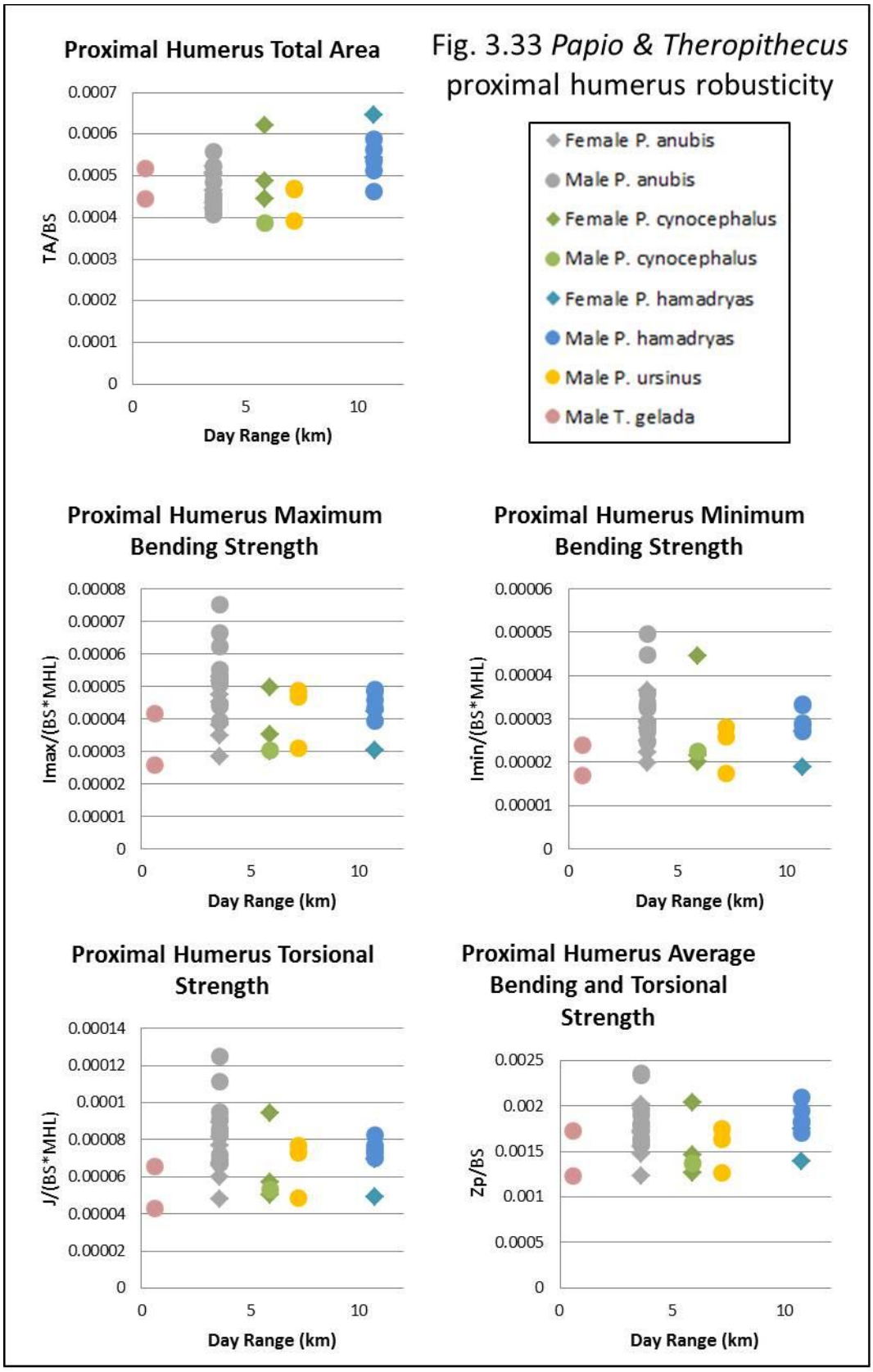

Fig. 3.33 *Papio & Theropithecus* proximal humerus robusticity

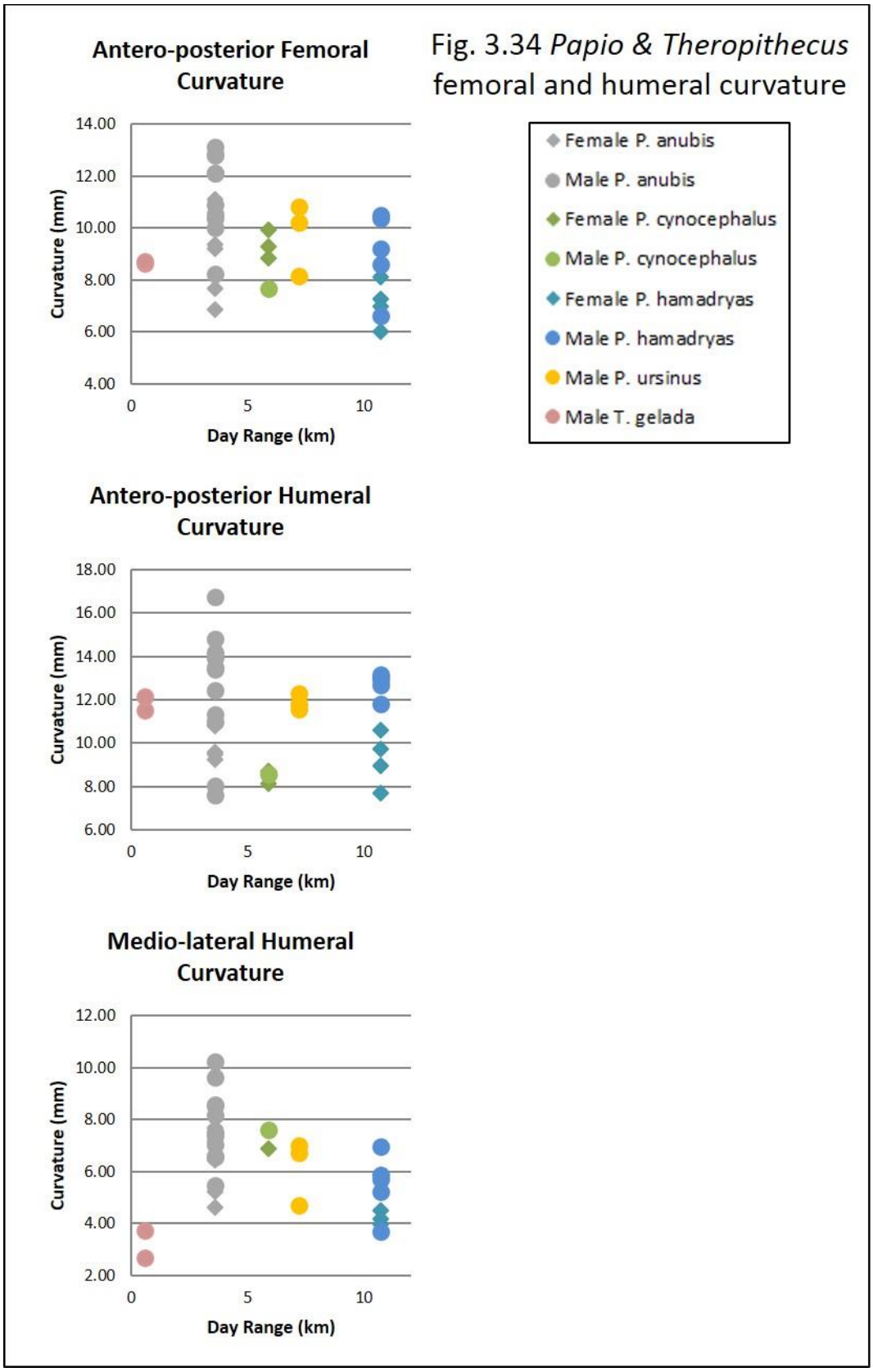

Fig. 3.34 *Papio & Theropithecus* femoral and humeral curvature

CHAPTER IV

FINITE ELEMENT ANALYSIS: VALIDATION STUDY

Finite element models (FEMs) provide an advantage relative to two-dimensional analyses (such as applying beam analysis to variously imaged cross-sections of bone (Ruff, 1989)) in that they can potentially provide a more complete understanding of bone behavior under various, specified loading environments. For this reason, finite element analysis (FEA) has a promising role to play in mobility studies aimed at deciphering the effect of long bone morphology on bone behavior.

This method is particularly powerful in that, once a model is created and validated, an array of modeling experiments can be performed to test various questions regarding the modeled structure. In principle, such experiments are limited only by the accuracy of input data, such as geometry, material properties, or muscle force magnitudes and directions. Note, however, that FEA does not provide direct information about mobility patterns or ranging behavior. Rather, FEA provides a means of testing how well structures "perform" mechanically under specific loading conditions that may simulate those experienced by an organism during particular behaviors. If these hypothesized conditions reflect those experimentally determined to be adaptive in organisms that, for example, range over long distances, then it is possible to test whether or not expressed morphologies of organisms confer a biomechanical advantage compared to alternative morphologies (e.g. structures of different shapes). For example, if it is hypothesized that a given bone is routinely loaded with high forces, or that it is loaded especially frequently, then one might hypothesize that the bone should exhibit a morphology that makes it structurally strong. Alternatively, it might possess a shape that increases the

predictability of its strain environment. In either case, these predictions are mechanical in nature, and can be tested with FEA.

Finite Element Analysis: Overview

One purpose of FEA is to elucidate the manner or degree to which a structure responds to external loads. Key outputs of FEA include information about stress (force per unit area) and strain (change in length divided by original length) (Richmond et al. 2005) experienced by a loaded object. Two applications of FEA are of particular interest in this study. In the first application, biologically realistic models are created for use in experiments aimed at better understanding how the bone (or structure of interest) behaves under specific loading conditions. For this application, a well-validated model (discussed below) is of the utmost importance. The second application involves comparisons between similar structures, as may occur when comparing different fossil taxa. In other words, how do different skeletal designs compare mechanically to one another? For example, how do differences in femoral shape and size between the Neanderthal and modern human lower limb affect each system's ability to withstand loads associated with walking? Since muscle force data, and to some degree, body mass data, are unknowable for extinct taxa, this application is better employed when investigating the structures' relative abilities to resist loads.

There are three main steps involved in FEA: model creation, model solving, and validation and interpretation. The first step, model creation, is often the most time consuming process. During model creation, the investigator makes decisions regarding the geometric design of the structure of interest, boundary conditions, material properties,

and the loads that will be applied to the model. Once a model is created, it is solved by computer software capable of performing a vast number of mathematical equations that result in stress, strain and displacement calculations for the entire structure. Finally, the really interesting questions can be asked. Are the results realistic, and what do they mean in a biological context?

Finite element models of skeletal structures are typically created from serial computed tomography (CT) scans so that both external and internal geometry can be modeled. Tessellated surface models, composed of hundreds of thousands of geometrically simple surfaces (such as triangles) arranged in a mosaic pattern, enclosing volumes representing bone are generated using medical imaging software in a multi-step process. These software programs typically require the use of a combination of manual and automatic thresholding techniques to separate trabecular bone from cortical bone, and bone from air. This procedure can be quite time consuming, but long bones, particularly the diaphysis, that are key structures of mobility studies, have relatively simple geometries and thus are less difficult to model than skeletal structures like crania. Once the separate volumes of bone are created, they are divided into a large, but finite number of elements of a simple shape, joined together at vertices called nodes. These simple shapes create the mesh that comprises the model. Depending on the software being used, the shapes may represent tetrahedra or "bricks" with a varying number of nodes and sides. As the number of nodes and/or elements increases the accuracy of the model should increase, although more computational power is needed to solve the model (Richmond et al. 2005).

Following creation of a FEM, it must be assigned material properties. In the case of a femur, the relevant material is bone. Key properties include the elastic modulus and Poisson's ratio. The elastic modulus (*E*) describes how much strain a structure will experience in response to a given stress when the object is loaded axially. More specifically, it represents the slope of the linear (elastic) portion of the stress-strain curve for a given material. This describes the stiffness of the object during tension or compression. Poisson's ratio (v = lateral strain/axial strain) describes how much the sides of an object will contract or expand laterally during tensile or compressive axial loads, respectively. If a material is isotropic, then its material properties are the same in all directions at any given point, and thus the elastic modulus and Poisson's ratio are the only two properties that need to be specified. Most FEA studies assume that cortical bone is isotropic, but this is not typically the case in life. Rather, bone tends to range between being roughly transversely isotropic (i.e. material properties in the axial direction of a long bone may differ from those in the cross-section of the bone) to being orthotropic (material properties vary in each of three orthogonal directions). Moreover, most FEA studies assume that the material properties of cortical bone are spatially homogenous (i.e., they are the same in all regions of the bone), when in fact those properties may be heterogeneously distributed (i.e., they may vary from region to region) (Peterson and Dechow 2003; Wang and Dechow 2006). Finally, cortical and trabecular bone have different elastic moduli; cortical bone is much stiffer than trabecular bone (Currey 2002).

Constraints and applied forces are referred to as boundary conditions. For a loaded object to experience stress and deformation, it is necessary to constrain the model

from moving in at least some fashion, although it is also important not to overly constrain it as that may result in unrealistic stresses and/or strains throughout the model (Richmond et al. 2005). The application of constraints ensures that models resist translational or rotational movement; it anchors them in 3-dimensional space and ensures that the applied forces will cause deformations in the model. Constraints are typically chosen in locations imitating biological constraints, such as ligaments, or contact between bones. For instance, when modeling a femur, one might choose to apply constraints at the fovea capitis on the femoral head and on the distal-most surface of the epiphyses to simulate contact with the tibial plateau. Because the selected nodes are not allowed to move, strain will be concentrated at and around those locations, possibly producing unrealistic local strains. Therefore, if possible, it is best to analyze strain at locations away from the constraints so as not to bias the results of the experiment.

Muscle forces can be applied to the model as vectors running from the muscle's origin towards its insertion. Muscles with multiple compartments that may not all act simultaneously are best modeled with multiple origins or as separate muscles. Ideally, surface scans of the bones articulating with the bone of interest will be positioned such that they can serve as origin and insertion points for the muscles. For instance, surface scans of the pelvis, tibia, and fibula may be necessary to apply muscle forces to a femur FEM during simulation of bipedal walking insofar as many muscles active during walking either arise from or insert on one of these surrounding bones.

Once a model has been created, the volumes have been assigned material properties, and boundary conditions have been applied, it is possible to solve the model and interpret the results. Computer software solves the model by calculating nodal

displacements due to applied forces, and the stresses and strains corresponding to the nodal displacements (Zienkiewicz et al. 2005).

Once a model has been solved, there is not yet reason to be confident that the model accurately depicts what happens in a real biological system. In order to know this, the investigator must validate the model. Preferably, this would mean comparing strain data obtained from the FEM of a bone to strain data obtained from *in vivo* measurements by strain gages affixed to the same bones during the same loading scenario as was applied to the bone's model. However, this is not always possible due to both practical and ethical reasons (in the case of humans and animals, respectively) as the procedure is more than minimally surgically intrusive. In fact, *in vivo* measurements for this purpose are not even the norm, especially for experiments whose focus is humans. In cases where *in vivo* strain gage measurements are impossible to obtain, *in vitro* cadaveric experiments are a reasonable alternative. However, *in vivo* and *in vitro* validation experiments measure different things. Generally speaking, *in vitro* bone strain experiments entail the application of forces that only coarsely approximate those used in actual behaviors. However, an advantage of such studies is that it is generally relatively straightforward to simulate those loads (as well as constraints) in FEA. Thus, *in vitro* validation is most useful in assessing the validity of the geometry and material properties of a bony structure. In contrast, *in vivo* validation experiments examine the degree to which all of the assumptions incorporated into the simulation of a behavior (e.g. geometry, loads, constraints, material properties) are collectively valid. In a perfect scenario, FEMs would be validated using both *in vivo* and *in vitro* techniques, although this is not typically done. Regardless, a well-validated model is essential if the investigator's purpose is to

realistically depict the structure's performance in a biological context. Once it is reasonably certain that the FEM behaves in a biologically realistic manner, the loads or other input variables can be changed to reflect those obtained from *in vivo* experiments, and interpretation of the results may proceed with a level of confidence equal to the rigor of the validation test.

Examination of the patterns of stress or strain due to specific loads allow an investigator to identify weak points in the structure, the overall pattern of deformation, or how each set of loading conditions affects the model's behavior. Applying the same loads to different models shows how size *and* shape differences in the structures affect each structure's ability to resist loads. However, when comparing bones of different morphology, an investigator may want to know what effect shape alone has on stress and strain. By scaling the magnitudes of the forces applied to a FEM by the model's volume raised to the 2/3 power, one can remove size as a factor in FEA experiments and simply compare the effects of scale-free shape differences (Dumont et al. 2009).

Finite element analysis of a human femur: Materials

Model Creation. Serial computed tomography (CT) scans of a modern (young adult male) human femur from the University at Albany teaching collection were made courtesy of Dr. Gary Siskin at ImageCare Medical Imaging (Latham, NY). The serial CT scans were first imported as .TIF files and processed in the computer software program Mimics v. 13 (Materialise, Ann Arbor, MI, USA), in which surface meshes composed of triangles were created. An automatic thresholding algorithm was used to separate bone from empty space. Then, through manual slice-by-slice segmentation,

three separate surfaces were generated representing the outer layer of cortical bone, and two volumes of trabecular bone, one each in the proximal and distal ends of the bone. The medullary cavity was modeled as an empty space.

These surfaces were exported to the surface editing program Geomagic Studio v. 12 (Research Triangle Park, NC, USA) as binary .STL files. In Geomagic Studio, the surfaces were rid of imperfections such as holes, overlapping triangles or triangles with poor aspect ratios, spikes, and other abnormalities or distortions created during the manual segmentation process. Once the geometry was "clean", the surfaces were re-imported into Mimics where the surfaces were once again meshed to check for triangle integrity. If no intersections were found, the surfaces were volume meshed to create watertight solid volumes composed of thousands of tiny tetrahedral elements connected by nodes, rather than simple surfaces. The end result of this process was four mutually exclusive volumes: outer cortical bone, inner medullary cavity, proximal and distal trabecular bone (Figure 4.1).

Each volume was imported into the Strand7 Finite Element Analysis Software System (Strand7 Pty Ltd, Sydney, NSW) as a NASTRAN (.NAS) file. Strand7 allows the application of various material properties, constraints, and force loads. In this model, the medullary cavity volume was deleted, leaving an empty space within the volume of cortical bone between each trabecular bone volume. Volumes were assigned isotropic material properties. Cortical bone was given an elastic modulus (E) of 20 gigapascals (GPa), and a Poisson's ratio (v) of 0.3 (Currey et al. 1975). Trabecular bone was modeled as a solid rather than as individual trabeculae due to the prohibitively time-

consuming nature of modeling individual trabeculae. Trabecular bone was assigned E = 749 megapascals (MPa) and v = 0.3 (Kaneko et al. 2004).

Validation

Because this validation study did not measure strain on the femur from which the FE model was created, it is not verifying that measured strains on the actual femur correspond to strains measured on the FE model. Instead, it validates the pattern and magnitude of strain on the FE model when it is subjected to a similar load as an actual human femur in order to confirm that the FEM behaves like a real human femur. This FEM was validated by replicating a cadaveric experiment conducted by Huiskes (1982). In that experiment, an embalmed human femur, dissected free of all soft tissue, was secured in a laboratory setting, and loaded with strain gages at seven horizontal levels along the diaphysis (Figure 4.2). At each of these horizontal levels, seven strain gages were applied to the circumference of the diaphysis to calculate maximum and minimum principal stress. Ten thousand Newton millimeters (Nmm) of torque were applied to the femoral head; the resulting principal stresses were calculated at 49 locations on the diaphysis of the femur. In order to recreate the loading regime of the cadaveric femur for the femur FEM, it was determined that the force couple producing 10,000 Nmm torque in the human cadaveric femur was 454.54 N for a femoral head with a radius of 22 mm, as in the FEM. In order to create a torque, two forces (one each directed posteriorly and anteriorly) were applied to the femoral head. So (10,000 Nmm/(22 mm))/2 = 227.27 N. Therefore a 227.27 N force directed posteriorly was applied to the superior portion of the

femoral head, and a 227.27 N force directed anteriorly was applied to the inferior surface of the femoral head (Figure 4.3).

Constraints

Constraints were applied at seven locations on the femur (Figure 4.4). One node on the inferior most surface of each femoral condyle was constrained from moving in the vertical direction. This simulates contact between the femur and the tibia. One node on the inner surface of each condyle within the intercondylar groove was constrained from moving in the antero-posterior direction, simulating the effect of the cruciate ligaments. One node was constrained from moving in the medio-lateral direction on the lateral surfaces of each epicondyle, corresponding to the collateral ligaments. Finally, one node within the fovea capitis was constrained from antero-posterior and medio-lateral movement to simulate ligamentum teres. It is important not to over-constrain the FEM, as would be the case if a region of nodes corresponding to the cross-sectional area of each ligament was constrained, since this can have an adverse effect on results (e.g. (Haut Donahue et al. 2002)).

Results

Once the model was solved in Strand7, maximum and minimum principal stresses were measured at approximately the same seven horizontal locations as on the cadaveric femur. Huiskes (1982) did not report strain gage data recorded at each of these locations, but using the graphs provided in the original paper, the relationship between the cadaver study and FEA were compared. Values measured on the femur FEM were superimposed

on a virtual representation of Huiskes (1982) graphs, which allowed an evaluation of differences in both magnitude and pattern of stress (Figure 4.5).

Magnitude of stress

The most distal level, "a", shows the greatest disparity between point measurements. This difference occurs along the distal postero-lateral region of the diaphysis and could be caused by differences in constraints between the cadaveric femur experiment and femur FEM. Error could also be generated from disparities between the location of the strain gage and the point of measurement on the FEM. Locations of strain gages in Huiskes' (1982) experiment were not strictly reported and small differences between measurement locations could result in large discrepancies. Additionally, the difference in stress magnitude may not be a data collection artifact, but a real difference in behavior between the cadaveric femur and the femur FEM. Stress data collected from level "b", the next most distal horizontal level, support the idea that differences in constraints caused the disparity in stress magnitude at these two locations. At the same location along level "b", there is a small discrepancy between the cadaveric femur and the femur FEM. All other levels along the diaphysis show a very close correspondence in stress magnitude at each of the seven locations along each horizontal level. Stress magnitude data of the FE study are reported in Table 4.1. It is uncertain exactly how the cadaveric femur was constrained, Huiskes (1982, 65) only writes that it was "fixed into a laboratory setting" at its distal end. It is likely that this setting provided a more rigid constraint than that of the FEM, and in fact, it is the cadaveric femur that experiences higher stress, not the femur FEM, as would be predicted in such a case.

Pattern of stress

In addition to stress magnitude, pattern of stress is also relevant in a validation study. Figure 4.5 clearly shows that the pattern of stress experienced by the cadaveric and femur FEM are very similar. Under the specified loading environment, both femora experience tension (maximum principal stress) along the anterior diaphysis that changes to compression (minimum principal stress) along the posterior diaphysis. As with comparisons of magnitude, it is the most distal level, "a", that shows the greatest differences between femora. The pattern is mostly similar, even at level "a", but the femur FEM shifts from tensile stress to compressive stress along the postero-lateral aspect of the diaphysis whereas the cadaveric femur experiences this shift slightly more posteriorly, resulting in a small change of pattern.

Conclusion

In conclusion, these data show a close correspondence in both pattern and magnitude. When subjected to a posterior bending moment, the femur experiences tension along the anterior portion of the diaphysis, and compression posteriorly, as does the femur FEM. These results indicate that the femur FEM responds the same way as a real human femur; its geometry and material properties are valid and can be used with confidence to address questions of biomechanical consequence.

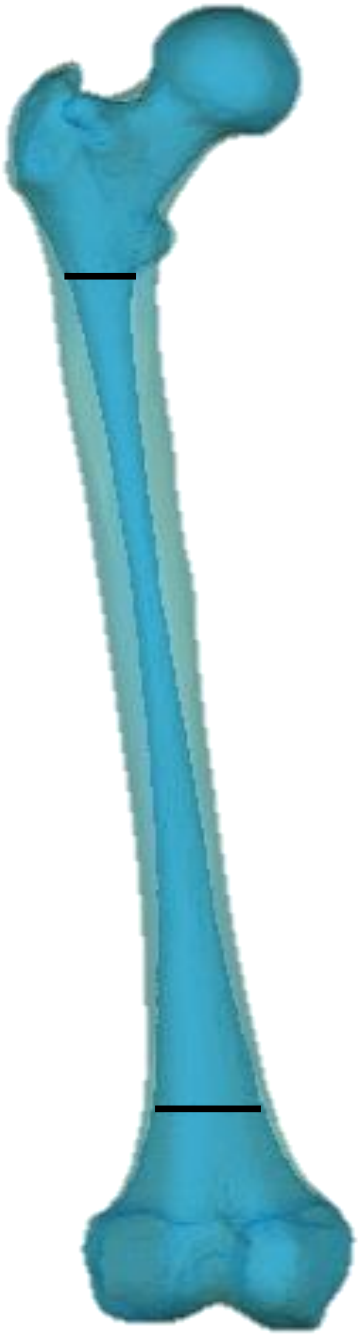

Figure 4.1. Human FE model with transparent cortical bone. Solid black lines indicate divisions between proximal and distal volumes modeled as trabecular bone and the “empty” medullary cavity.

Figure 4.2. Locations of horizontal levels of strain gage placement from Huiskes (1982).

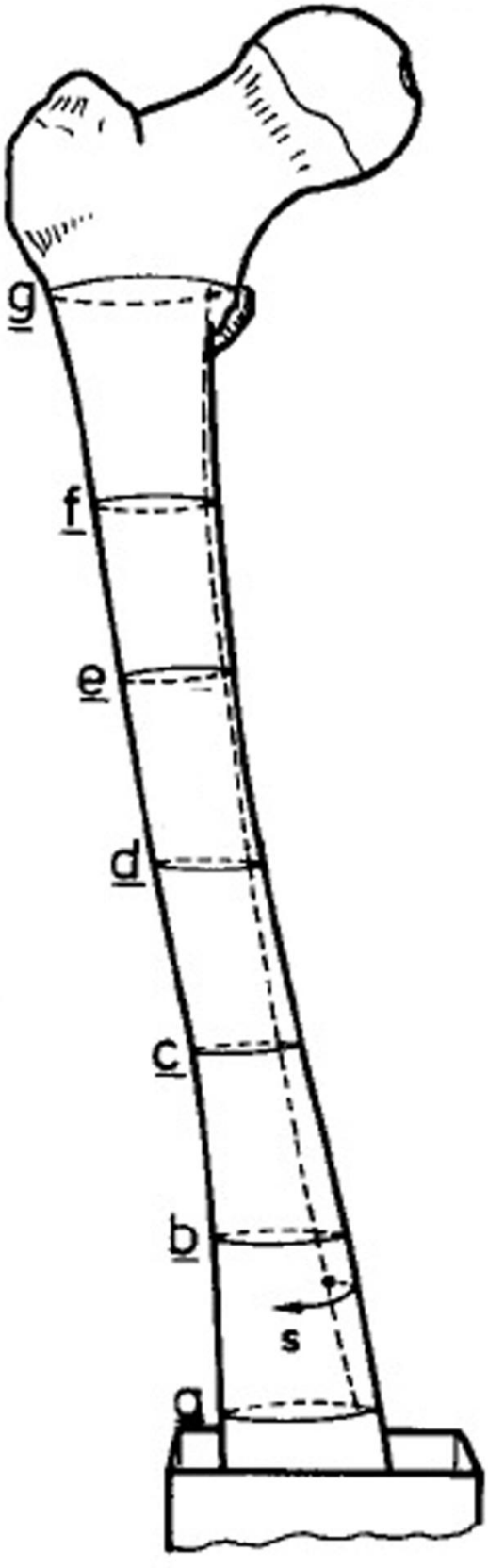

Figure 4.3. Arrows indicate direction of forces (227.27 N each) applied to the superior and inferior femoral head to create a torque in order to replicate Huiskes' (1982) cadaveric femur's loading conditions.

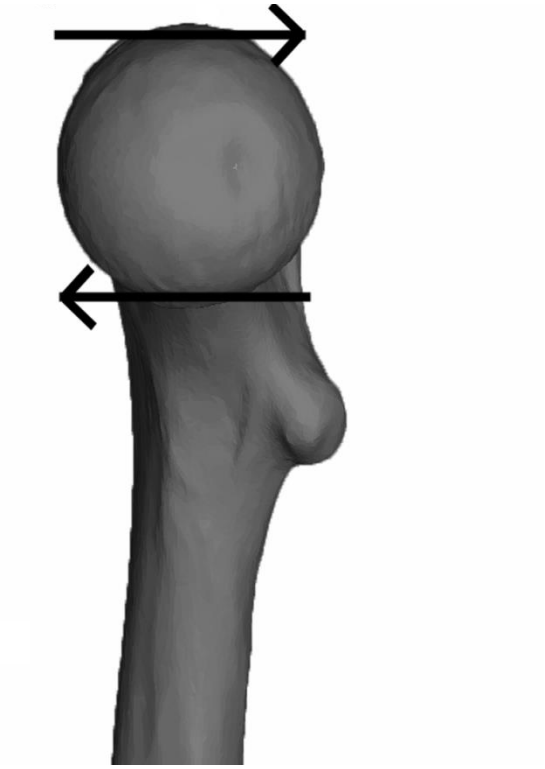

Figure 4.4. Locations of constraints

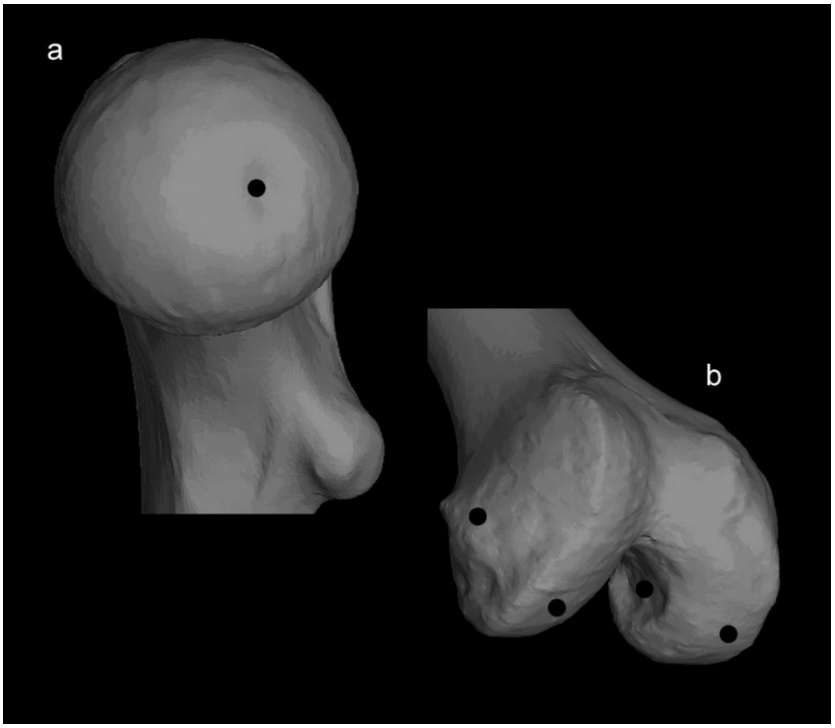

Solid black circles represent locations of the seven constraints on the proximal (a) and distal (b) femur FE model. Constraints indicated on the lateral epicondyle and medial aspect of the intercondylar notch are mirrored on the medial epicondyle and lateral aspect of the intercondylar notch.

Table 4.1. Validation: Stress (MPa) measured on the human femur FE model

Level "a"		Level "e"	
1	-2.26	**1**	-3.20
2	1.80	**2**	1.48
3	2.46	**3**	3.57
4	2.23	**4**	4.39
5	-1.97	**5**	-0.94
6	-2.57	**6**	-3.85
7	-2.44	**7**	-4.35
8	-2.26	**8**	-3.20
Level "b"		**Level "f"**	
1	-2.36	**1**	-4.27
2	2.46	**2**	3.80
3	2.90	**3**	4.67
4	2.39	**4**	4.17
5	-1.95	**5**	-1.68
6	-3.19	**6**	-4.88
7	-2.93	**7**	-4.84
8	-2.36	**8**	-4.27
Level "c"		**Level "g"**	
1	-3.01	**1**	-4.06
2	2.59	**2**	1.63
3	3.63	**3**	4.64
4	2.68	**4**	4.22
5	-2.67	**5**	-1.51
6	-3.61	**6**	-3.31
7	-3.41	**7**	-4.06
8	-3.01		
Level "d"			
1	-1.98		
2	2.43		
3	3.08		
4	3.45		
5	-1.28		
6	-3.97		
7	-3.29		
8	-1.98		

Levels correspond to horizontal levels depicted on Figure 4.2

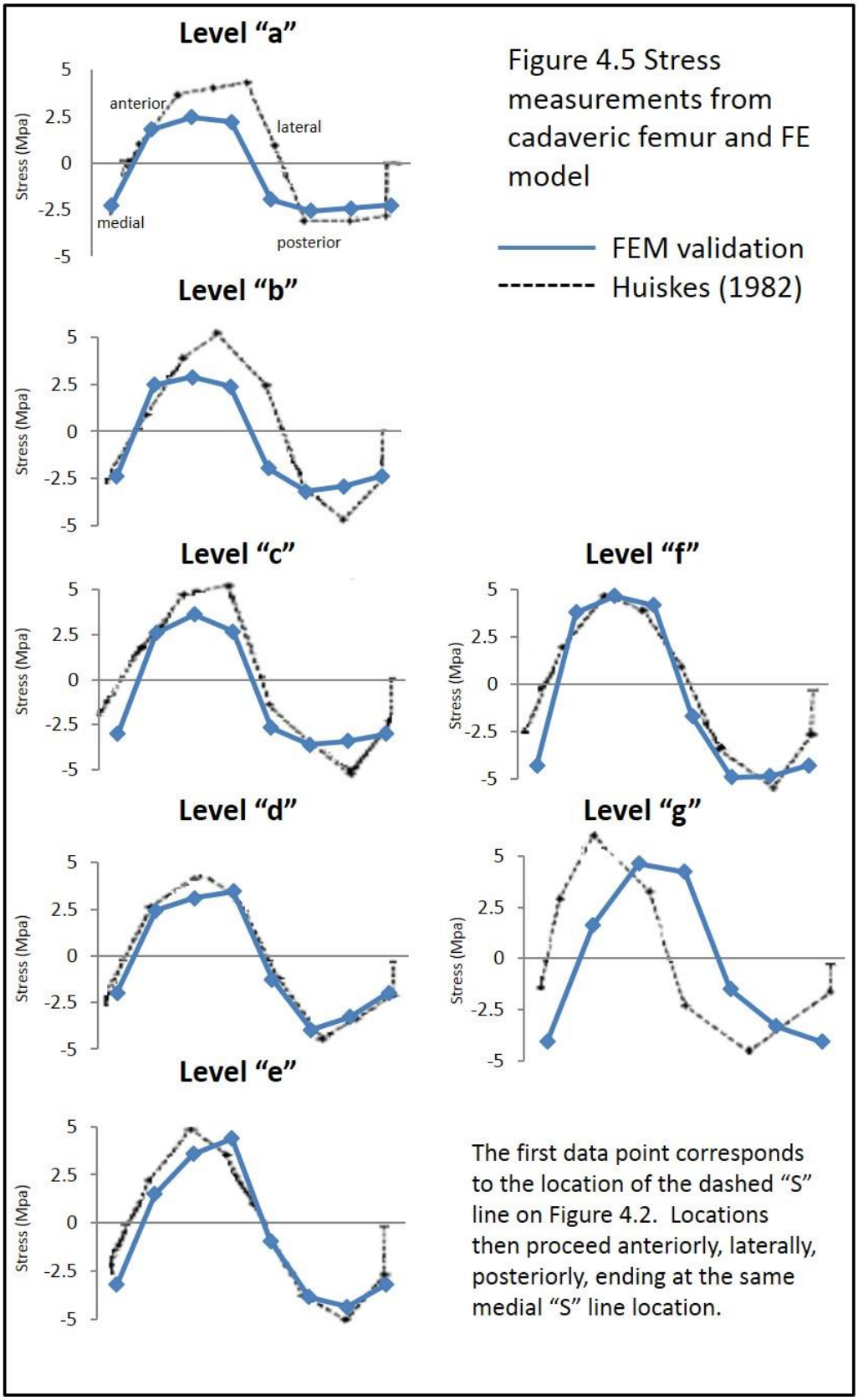

Figure 4.5 Stress measurements from cadaveric femur and FE model

The first data point corresponds to the location of the dashed "S" line on Figure 4.2. Locations then proceed anteriorly, laterally, posteriorly, ending at the same medial "S" line location.

CHAPTER V

COMPARISONS OF NEANDERTHAL AND HUMAN FEMORA USING FEA

The final stage of the project uses finite element analysis (FEA) to perform an assessment of the biomechanical strengths of the complete femora of Neanderthals and recent modern humans. This is necessary for several reasons. First, although the skeletal variables described above (neck-shaft angle, cross-sectional geometry, curvature, and size) each pertain to aspects of femoral strength, none of them describe the strength of the femur as a whole. This is relevant, because skeletal modifications that increase the structural stiffness in one part of a bone can have the effect of transferring load to other, unmodified parts, thereby elevating stresses in that location. For example, strengthening the midshaft of the femur will not be advantageous if, by doing so, the neck is put at increased risk of failure. The modification of particular skeletal traits can have complex and unpredictable effects on stress distributions (e.g. Strait et al., 2007), so the individual variables that are the focus of this study do not, by themselves, provide a full picture of total bone strength. FEA, however, is an engineering technique used to examine how complex objects respond to load, and is ideally suited to examining how variation in skeletal form relates to structural integrity. One might potentially find that the femora of Neanderthals and modern humans exhibit similar levels of stress despite their differences in morphology because their different configurations minimize stress in different ways. Alternatively, one might find that a particular femoral form does not act to minimize stress but rather maximizes the predictability of the stresses experienced by the femur under a variety of loading conditions. Measurements of shaft curvature and cross-sectional shape allow predictions regarding strength and predictability, but FEA allows a

simulation of loading that provides a far more detailed picture of how, precisely, morphology affects strength and predictability. Indeed, Lieberman et al. (2004) found that cross-sectional properties estimate bone strength by relying on assumptions about bending that are not physiologically realistic. This finding provides further reason for using FEA to look at stress and strain distribution within long bones. Finally, Neanderthal and modern human femora may not have been loaded in precisely the same way owing to differences in the configurations of the hip and knee joints in these two species. Specifically, the orientations of the muscle forces being applied to the femora may have differed subtly, and these may have an effect on femoral stresses. FEA allows an assessment of the importance of muscle orientation on stress patterns.

Hypotheses

Do Neanderthal and anatomically modern human femora differ with respect to strength and predictability? Two null hypotheses are tested here. The first is that *Neanderthal and anatomically modern human femora are equally strong within the anatomical/biomechanical contexts in which they are habitually loaded.* The second hypothesis is that *Neanderthal and anatomically modern human femora experience equally predictable strains in response to habitual and irregular loads.* These null hypotheses provide a framework for analysis, but there is reason to suspect that they are false.

Differences in femoral geometry between Neanderthals and modern humans may exist because each shape is better suited to its respective anatomical and biomechanical environment to ensure strength and/or predictability. For example, Neanderthals have

broad pelves with flaring ilia and medio-laterally long pubic bones (Rak 1991; Trinkaus 1983; Trinkaus 1984), whereas modern humans have narrower pelves with ilia exhibiting less flare, and medio-laterally short pubic bones (Vandermeersch 1981). Additionally, the shape of the Neanderthal pelvis is such that the ilio-tibial tract (fibrous reinforcement of the fascia lata originating at the crest of the ilium and running down the femur to insert on the lateral condyle of the tibia) is in a more lateral position relative to that of modern humans, which could more effectively reduce medio-lateral bending in the femur.

Neanderthals have a smaller neck-shaft angle than modern humans. The large femoral neck-shaft angles of modern humans could reduce medio-lateral bending relative to that experienced by Neanderthals, meaning the two groups had differing means of compensating for medio-lateral bending, which would influence femoral diaphyseal morphology.

Also, a bone's cross-sectional geometry serves to reinforce its structural integrity (Bertram and Biewener, 1988), and differences in cross-sectional shape have been shown to be significantly related to differences in mobility (Holt, 2003). If a bone is wider in one cross-sectional dimension (for example, the antero-posterior direction) than another, this will influence the predictability of bending direction. Although the narrow dimension will be less stable than the wide dimension, if predictability of bending is the primary target, the result will be the same as that of curvature (Bertram and Biewener 1988). Thus, reduction of curvature may be associated with increases in cross-sectional asymmetry. And in fact, Neanderthals and modern humans display this association.

Variation in curvature is not strongly influenced by body size, diaphyseal length, or the manner in which the femur articulates with the lower leg (tibia + fibula)

(Shackelford and Trinkaus, 2002), meaning that other variables must be more important in determining femoral curvature. Bending of the femur is an inescapable consequence of bipedal locomotion, and, in fact, curvature increases bending stress rather than alleviating it. However, the orientation of muscles attaching to the femur may exert forces on the femoral shaft such that curvature is lessened during some parts of the gait cycle, thereby retaining the predictive benefit of stress transmission while at the same time reducing the detrimental effects of bending. The complex interplay of the skeletal variable listed above make it essential to consider the femur as a whole structure in order to evaluate the validity of the hypotheses being tested.

Gait

A brief overview of bipedal locomotion is relevant to the third approach. Bipedalism is the form of locomotion used by modern humans, Neanderthals, and in fact, all hominins. It has been determined to be a particularly efficient form of locomotion, with only seven percent more oxygen being consumed by the body during standing than when lying supine (Aiello and Dean 1990). Since joint surfaces and bone cross-sections in all mammals must be proportional in size to the amount of force transmitted through them, a biomechanical approach to differences in bone morphology is particularly relevant.

Gait is defined as the walking cycle and is composed of consecutive strides. One stride is typically defined from heel strike of one foot through a second heel strike of that same foot. Gait is composed of two major phases, the stance phase and the swing phase. Stance phase makes up approximately 40 percent of a stride and is defined as the portion

of time when one leg is supporting the body. Swing phase begins after toe-off, which propels the body forward, and is defined as the time when the leg is moving forward in order to begin the next stride (Suzuki 1985).

At the beginning of each stride, the hip is flexed, the knee is extended, the leg is laterally rotated, and the ankle is dorsiflexed. At heel strike, the thigh adductor muscles pull the weight of the body over the supporting limb, thereby beginning the stance phase. Mid-stance is defined as the point when the full weight of the body is centered over the supporting foot. Both hip and knee joints are extended at mid-stance. As the stance phase progresses, the ankle dorsiflexes and the hip and knee joints pass anteriorly to the supporting foot. The terminal portion of the stance phase begins with toe-off, which transmits the weight of the body through the hallux, extending the hip, extending the knee, and dorsiflexing the ankle. The swing phase begins after toe-off. The hip and knee flex, lifting the leg off the ground and bringing it forward. As the knee passes the opposite, supporting leg (which is now in stance phase), it begins to extend. At the end of the swing phase, the leg is again laterally rotated and the hip begins to flex, thereby preparing for heel strike and the gait cycle repeats (Aiello and Dean 1990; Suzuki 1985).

During bipedal locomotion, the leg acts like a compound pendulum, making use of kinetic energy. For this reason, there is little muscle activity during slow walking, especially during the swing phase (Suzuki 1985; Tuttle et al. 1979a; Tuttle et al. 1979b). Animals naturally choose the most energetically efficient gait. Humans typically transition from walking to running at speed of approximately 2.5 meters per second. It is at this speed that walking becomes more energetically costly than running due to the forces exerted on the ground by the feet during mid-stance when the hip and knee are

fully extended and muscles must work to elevate the body's mass off the ground. As speed increases, force patterns through the foot onto the ground fluctuate, peak forces are higher in magnitude, and the rate of stepping increases (Aiello and Dean 1990; Alexander 1984a; Alexander 1984b).

Running patterns are somewhat different than walking patterns. The time the foot is on the ground is shorter during running, force patterns fluctuate less, peak forces for each step are higher, and both feet are never on the ground at the same time (Aiello and Dean 1990; Alexander 1980).

Muscles

Muscles performing five actions are of principal importance in understanding bipedal locomotion. These muscles, their origins, and their attachments will be important to realistically loading femoral finite element models. The primary hip flexors include iliopsoas, rectus femoris, tensor fascia latae, and sartorius (Figure 1). Iliopsoas is composed of two muscles, psoas major and iliacus. Psoas major originates on thoracic vertebra 12 through lumbar vertebra five, and inserts onto the lesser trochanter. Iliacus arises from the internal surface of the iliac fossa and the lateral portion of the sacrum and inserts onto the tendon of psoas major, thereby inserting onto the lesser trochanter. Rectus femoris, a muscle within quadriceps femoris, not only flexes the thigh, but also extends the knee. It originates on the anterior inferior iliac spine and the adjacent portion of the acetabulum, and inserts onto the patella via a tendon. Tensor fascia latae, an important hip flexor (and knee extender), originates on the anterior aspect of the iliac crest and anterior superior iliac spine, and inserts onto a tough band of tissue called the iliotibial tract. The iliotibial tract inserts onto the lateral aspect of the tibia near the head

of the fibula. Tensor fascia latae acts to pull the iliotibial tract superiorly and anteriorly. In addition to flexing the hip and extending the knee, tensor fascia latae also abducts and medially rotates the thigh at the hip. Significantly, tensor fascia latae and the iliotibial tract counteract medio-lateral bending stresses experienced by the femur and stabilize the knee joint when it is extended. Finally, sartorius flexes the knee, medially and laterally rotates the thigh, flexes and adducts the thigh. It originates on the anterior superior iliac spine, runs anteriorly along the thigh, and inserts onto the upper part of the anterior tibia.

Thigh extensors include the hamstrings and gluteus maximus. Biceps femoris (long head), semimembranosus, and semitendinosus (the hamstring muscle group) all originate on the ischial tuberosity. Biceps femoris (short head) arises from the linea aspera of the femur and supracondylar line. Both heads of biceps femoris insert onto the fibular head. Semimembranosus and semitendinosus insert onto the medial, superior portion of the tibia. Gluteus maximus, a thigh extensor and lateral rotator, originates on the posterior aspect of the iliac crest, the sacrum, coccyx, and sacrotuberous ligament. It inserts onto the femoral gluteal ridge and the iliotibial tract. Not an active muscle during normal walking, gluteus maximus is primarily active during power activities like running, climbing, and rising from a sitting posture, but it is also active during upper limb activities such as carrying, digging, and throwing, during which it acts to stabilize the trunk.

Because the pelvis must remain stable during bipedal locomotion, thigh abductors are important in human musculature, where they play a different role than in the chimpanzee. Gluteus medius and gluteus minimus are the most important thigh abductors. Gluteus medius is superficial to g. minimus; it arises from the lateral portion

of the ilium and inserts onto the greater trochanter. Its anterior fibers rotate the thigh medially while the posterior fibers laterally rotate the thigh. Gluteus minimus arises from the lateral portion of the ilium and also inserts onto the greater trochanter.

Thigh adductors include adductor magnus, adductor longus, adductor brevis, pectineus, and gracilis. Adductor magnus is the largest of the thigh adductors. It arises from the ischial tuberosity and ischiopubic ramus and inserts below the greater trochanter onto the linea aspera running along the posterior aspect of the femur, terminating on the adductor tubercle of the medial epicondyle. Due to this positioning, it not only adducts the thigh, but can also extend the thigh when the thigh is already flexed. Adductor longus originates on the pubis, inserts onto the linea aspera along the middle third of the femoral shaft, and performs the same action as adductor magnus. Adductor brevis arises from the lower portion of the pubis, inserts proximal to the linea aspera on the upper third of the femoral shaft, and performs similar actions to adductor magnus and a. longus. Pectineus originates on the pubis, inserts onto the upper half of the pectineal line, and adducts the thigh. Gracilis originates on the body and inferior ramus of the pubis. It inserts onto the proximal portion of the anterior tibia, and adducts the thigh. It can also flex and medially rotate the leg.

Lateral rotators of the thigh are the last group of muscles discussed here. They include piriformis, obturator externus, obturator internus, superior and inferior gemellus, and quadratus femoris. Obturator externus arises from the outer surface of the obturator membrane and bone surrounding the obturator foramen, runs outwardly below the hip, wraps around the neck of the femur, and inserts onto the trochanteric fossa. Obturator internus arises from the inner surface of the obturator membrane and inserts onto the

inner surface of the greater trochanter. Superior gemellus originates on the ischial spine and upper portion of the greater sciatic notch and inserts on the greater trochanter. Inferior gemellus arises just below superior gemellus, on the inferior portion of the sciatic notch, and inserts onto the greater trochanter. Lastly, quadratus femoris arises laterally on the ischial tuberosity and inserts onto the quadrate tubercle on the intertrochanteric crest.

From bipedal walking to running to sprinting, step length, cadence, velocity, and range of motion in the lower limb increase as speed increases. The center of gravity within the body becomes lower due to increased flexion of the hip, knee, and ankle joints (Mann and Hagy 1980). The quadriceps femoris retains the same function during walking, running, and sprinting, but rectus femoris, one muscle within the quadriceps group, becomes acting in the early swing phase during running and sprinting, but not during walking. This observation shows variability that must be considered when modeling muscle activity at different speeds and different moments within a stride. Mann and Hagy (1980) found that sprinters do not absorb as much shock at the knee joint as do runners, but instead primarily at the ankle joint. This is probably because graphs of hip, knee, and ankle motion during sprinting show that primarily the ankle (and secondarily the knee) are flexed at the time of ground strike, whereas the hip is extended, meaning that shock absorption will occur in the ankle rather than the hip or knee. This could potentially have implications for ground reaction forces transmitted through the femur, perhaps lessening forces during sprinting relative to running.

Paul (1971b), Pedersen et al. (1997), Lengsfeld et al. (1996), Taylor et al. (1996), and Bergmann et al. (1993) measured muscle forces and joint reaction forces for several

adults at different gaits. These muscle forces will be referred to during the appropriate stage of the finite element analysis of the femur, but it should be noted that Duda et al. (1997), Brand et al. (1982) and Duda et al. (1996) warn of high inter-individual variability in muscle sizes (and therefore forces generated) and attachment sites. Brand et al. (1982) state that measurement error of muscle insertions is negligible compared to the high level of inter-individual variability, and that the use of average datasets may result in very large errors. Additionally, Duda et al. (1996) found that some muscle moment arms are more sensitive to their "anatomical situation" than are others, meaning that a small error in modeling one muscle maybe not yield erroneous results, but that same magnitude of error in modeling a different muscle could give unrealistic results.

The femur, without the influence of muscles, is more or less antero-posteriorly curved. Therefore, a question that has been investigated is whether the femur is primarily loaded in compression or bending. This is important to understand since predicted bending moments for various loading regimes may be physiologically unsound (Taylor et al. 1996). Pauwels (1980) theoretical framework predicted that the application of muscle forces to the femur will deform it in such a way as to pull the bone straighter, meaning that it will be loaded in compression rather than bending, thereby significantly decreasing overall strain. In experimental modeling of the femur, Taylor et al. (1996) found that with the application of the abductors, the iliotibial tract (tensor fascia latae and gluteus maximus), and iliopsoas, bending was decreased, but not entirely eliminated. However, in a comparative x-ray analysis of the femoral head position in which the femur was loaded during mid-stance and when it was unloaded, the femoral head experienced insignificant deflection. They therefore assert that the femur is actually loaded in

compression since if it was loaded in bending, either the head or the diaphysis should have deflected much more than what was actually observed. Upon further investigation, they found that when the angle of the joint reaction force (at the acetabulum) was increased from 13 degrees (proposed by Lengsfeld et al. (1996)) to 20 degrees, the distribution of stress and strain became more uniform. Davy et al. (1988) and Bergmann et al. (1993) report *in vivo* joint reaction force angles ranging from 17 to 25 degrees, so the increase to 20 degrees was deemed more physiologically appropriate. Therefore, with the addition of muscle moments and an appropriate joint reaction force, the femur appears to be primarily loaded in compression (Taylor et al. 1996).

Finally, it should be noted that the human lower limb is a dynamic and complex system. In order to most accurately investigate the loading environment of the femur, as many muscle forces as possible should be incorporated into the model. While one muscle group may increase bending, another group may counteract that bending. If both are not modeled, results may not be physiologically accurate (Duda et al. 1997).

Ivanenko et al. (2004) investigated the neural control patterns of gait. They state that due to the high variability in electromyography (EMG) activity reported by several authors within one individual (between consecutive steps), the overall activity pattern should be investigated over a step *cycle*. In a complex study examining waveform shapes that need not be detailed here, Ivanenko et al. (2004) found that five statistically defined factors are consistently observed during each step cycle. The timing of the factor patterns, representing bursts of EMG activity occurring at certain points, differs according to speed, but the basic underlying patterns remain consistent across speeds. With increasing speed, the patterns are shifted to earlier phases of the step cycle, which

makes intuitive sense. It was found that some muscles (rectus femoris, vastus lateralis, the adductors, sartorius, and tensor fascia latae) have systematic trends in activity, whereas others (gluteus maximus) appear to load evenly regardless of speed. Also, the muscles exhibiting a trend have more variable activity at low speeds than at high speeds. Another interesting finding is that the separate patterns appear to be timed according to toe-off, not heel strike, implying that toe-off might be a more physiologically appropriate division between strides.

Materials

Two femur FEMs were used in this study. The first is a human femur FEM (HFM), the creation of which was described in Chapter IV. The second is a Neanderthal femur FEM (NFM) built from a CT scan of the femur historically associated with the individual Spy 2 (specimen Spy 8) obtained from NESPOS (Database 2012). Spy 8 is a mostly complete right femur from a young adult male Neanderthal; it is missing only the superior greater trochanter (Trinkaus and Ruff 1989). The NFM was created using the same protocol as the HFM; however, because the greater trochanter is a significant muscle attachment site necessary for the proper transmission of muscle forces in the following experiments, the trochanter region of the HFM was copied and transferred to the NFM. In Geomagic Studio, the human trochanter region was attached to the NFM unchanged with the exception of slight scaling (it needed to be larger to fit the larger Neanderthal femur). Although trochanter regions likely differ slightly between Neanderthals and humans, this region is not of particular interest in the current study, except as a site of muscle attachment and thus force transmission. No data were collected

from this region, so it is unlikely that this alteration of the Neanderthal morphology will greatly influence the results; however during this remodeling process, the NFM was mirrored and thus transformed from a right femur into a left femur. This mirroring process will in no way affect the results of the experiments.

Methods

Given what we know about beam theory, size and shape differences between Neanderthal and human femora, and gait, several modeling experiments were performed in order to evaluate the strength and predictability hypotheses listed above. Note that these experiments were not designed to precisely reconstruct the stress regime of the Neanderthal femur. Rather, they were designed to facilitate comparison between the femora.

Material properties. Each FEM was given the same isotropic material properties. Volumes representing cortical bone were assigned an elastic modulus (E) of 20 GPa, and a Poisson's ratio (v) of 0.3 (Currey et al. 1975). Trabecular bone was modeled as a solid volume and was assigned E = 749 megapascals (MPa) and v = 0.3 (Kaneko et al. 2004).

Boundary conditions. Boundary conditions include constraints and applied forces. Constraints remain the same between models through all experiments, but applied forces vary. Each model was constrained at seven locations on the femur. One node on the inferior most surface of each femoral condyle was constrained from moving in the vertical direction. This simulates contact between the femur and the tibia. One node on the inner surface of each condyle within the intercondylar groove was constrained from moving in the antero-posterior direction, simulating the effect of the cruciate ligaments.

One node was constrained from moving in the medio-lateral direction on the lateral surfaces of each epicondyle, corresponding to the collateral ligaments. Finally, one node within the fovea capitis was constrained from antero-posterior and medio-lateral movement to simulate ligamentum teres. This is the same constraint scenario used in the validation study (Chapter IV, Figure 4.4) and was experimentally determined to yield the most accurate results of the five constraint scenarios that were tested as part of the in vitro validation study.

Muscle forces were estimated by Pedersen et al. (1997) at 32 instances of the gait cycle using a healthy 72-year old male subject who underwent surgery for a total hip replacement and received a specially instrumented hip prosthesis that enabled the calculation of information on location, direction, and magnitude of acetabular contact forces and muscle forces, the methods of which are well documented (Bell et al. 1990; Brand et al. 1982; Brand et al. 1994; Crowninshield et al. 1978). The model used by Pedersen et al. (1997) was based on optimization techniques and a modified straight-line muscle model that was improved over earlier models as it included modifications such that muscles were figured to pass outside the femoral head and joint capsule, allowed layering of superficial muscles over deep muscles, and allowed superficial muscles to exert a force on deeper muscles in addition to their independent force. Cross-sectional areas of muscles (necessary for the optimization techniques) were estimated from Friederich and Brand (1990). These muscle forces were applied to each FEM using the origin and attachment sites described in the preceding section of this chapter. Using a NextEngine 3D surface scanner (NextEngine, Inc.), surface models of a pelvis and tibia belonging to the same individual as the human femur from which the model was built

were used to specify muscle attachment sites on the HFM. Casts of a reconstructed Neanderthal pelvis (composite from Kebara 2, Feldhofer, and La Ferrassie 1) and tibia/fibula (composite with material from La Ferrassie 1 and Spy 1) (Sawyer and Maley 2005) were scanned to create surface models that were used to specify Neanderthal muscles force pathways.

On each model, a roughly rectangular region of bricks on the superior femoral head was selected to receive acetabular contact forces (ACFs) (estimated by Pedersen et al. (1997)), which were distributed evenly over the entire selection of brick faces (i.e. the force was divided by the number of bricks in the selection so that each brick only received a small portion of force rather than each brick receiving the entire force). Acetabular contact force was divided into three dimensions corresponding to the proximo-distal (X), medio-lateral (Y), and antero-posterior planes (Z). These planes are associated with the femoral reference plane of Pedersen et al. (1997) and were defined on each model by creating a new coordinate system using a node on the superior surface of the femoral head and one node on the inferior-most surface in the middle of each condyle. Because muscle and body weight forces differ between experiments, these boundary conditions will be further detailed in the relevant experiments.

Experiments. In each experiment, the HFM is compared to the NFM using 1) the same acetabular and muscle forces and 2) the NFM loaded with acetabular and muscle force magnitudes that were isometrically scaled (Dumont et al. 2009) by a factor of 1.26, due to measured differences in volume$^{2/3}$ between the HFM and NFM. Comparing the HFM to the unscaled NFM does not incorporate likely differences between human and Neanderthal muscle force magnitudes, but these values are unknowable for Neanderthals.

This procedure allows an assessment of strength that incorporates information about both the size and the shape of the femur. Comparing the HFM to the scaled NFM allows an assessment of strength that is strictly a consequence of differences in femoral shape; size has been excluded as a factor. Moreover, the scaling factor is very close to the estimated size differences between Neanderthals and modern humans, meaning that the acetabular contact force in the scaled Neanderthal may be approximately accurate. Thus, in general, a comparison between the HFM and the scaled NFM is most useful. Muscle force orientations varied according to the anatomical differences between the two species in their lower limb configurations (e.g. differences in pelvic and femoral shape affect the relative positions of the attachments of the hip muscles, thereby affecting force orientations).

Pedersen et al. (1997) determined that acetabular contact forces are highest at two instances of the gait cycle: heel-strike and toe-off. Accordingly, the first (heel-strike) and second (toe-off) experiments compare the strengths of the Neanderthal and human femora under loading conditions corresponding to these two gait events. Acetabular contact forces (ACFs) and muscles forces can be found in Table 5.1, and are as follows. In the first experiment, heel-strike, on both the HFM and the unscaled NFM, a force of 1427 N was directed distally (X), 561 N were directed laterally (Y), 273 N were directed anteriorly (Z). The scaled NFM received the following forces X = 1798.02 N, Y = 706.86 N, Z = 343.98 N. In addition to ACFs, muscle forces were also applied to each model using the tangential-plus-normal loading procedure of Boneload v.6 (Grosse et al. 2007), a software package that interfaces with Strand7 and allows the modeling of complex muscle vectors that wrap around the surface of a model. Muscle forces were

applied as the femur was in a slightly flexed position relative to the pelvis, as would occur during heel-strike (Figure 5.1a). Only muscles that were active at the instant of heel-strike, as determined by Pedersen et al. (1997), were modeled and are as follows: adductor magnus (unscaled: 73 N; scaled: 91.98 N), gluteus maximus (unscaled: 316 N; scaled: 398.16 N), g. medius (unscaled: 298 N; scaled: 375.48 N), and g. minimus (unscaled: 89 N; scaled: 112.14 N), inferior gemelli (unscaled: 3 N; scaled: 3.78 N), obturator internus (unscaled: 25 N; scaled: 31.5 N), piriformis (unscaled: 26 N; scaled: 32.76 N), quadratus femoris (unscaled: 35 N; scaled: 44.1 N), superior gemelli (unscaled: 2 N; scaled: 2.52 N), biceps femoris (unscaled: 201 N; scaled: 253.26 N), and rectus femoris (unscaled: 55 N; scaled: 69.3 N). Note that adductor magnus and the gluteal muscle forces were divided into three components due to their linearly large attachment areas; tensor fascia latae was not modeled because it neither originates nor inserts directly on the femur.

In the second experiment, toe-off, on both the HFM and the unscaled NFM, a force of 1859 N was directed distally (X), 555 N were directed laterally (Y), and 214 N were directed anteriorly (Z). The scaled NFM received the following forces X = 2342.34 N, Y = 699.3 N, Z = 269.64 N. In addition to ACFs, muscle forces were also applied to each model with the femur in a slightly extended position relative to the pelvis, as would occur during toe-off (Figure 5.1b). Only muscles that were active at the instant of toe-off, as determined by Pedersen et al. (1997), were modeled and are as follows: gluteus maximus (unscaled: 210 N; scaled: 264.6 N), g. medius (unscaled: 286 N; scaled: 360.36 N), and g. minimus (unscaled: 124 N; scaled: 156.24 N), inferior gemelli (unscaled: 7 N; scaled: 8.82 N), obturator internus (unscaled: 40 N; scaled: 50.4 N), piriformis (unscaled:

98 N; scaled: 123.48 N), iliacus (unscaled: 91 N; scaled: 114.66 N), superior gemelli (unscaled: 3 N; scaled: 3.78 N), biceps femoris (unscaled: 256 N; scaled: 322.56 N), and rectus femoris (unscaled: 338 N; scaled: 425.88 N). As in the first experiment, the gluteal muscle forces were divided into three components due to the large attachment area of these muscles.

The next series of experiments assessed strength and predictability in the two femora under loading conditions simulating irregular steps. Bergmann et al. (1993) have documented that stumbling is associated with only minor changes in acetabular force orientation, but a substantial change in force magnitude (up to three times greater). Accordingly, in these experiments, resultant hip force magnitude is tripled relative to that employed in the first experiment (heel-strike) which serves as a comparative baseline. Muscle forces were unaffected. Moreover, within each of these experiments, the orientation of the hip joint force was varied in each experiment such that the force was rotated 5° anteriorly, 5° posteriorly, 5° medially, and 5° laterally, respectively, under the assumption that the limb is being held in an irregular position.

Finally, a third series of experiments assessed strength and predictability in response to simulated traumatic loads. In these experiments, a horizontal force of 500 N was applied to the midshaft of the HFM and the unscaled NFM in addition to the muscle and ACFs employed in the first experiment (heel-strike). The scaled NFM received a horizontal force of 630 N. In each experiment, roughly rectangular regions of bricks were selected on the diaphysis surface to receive this force; the horizontal force was directed posteriorly, medially, and postero-medially, respectively. Accordingly, a region of bricks on the anterior surface of the femur received the posteriorly directed force;

bricks on the antero-lateral surface received the postero-medially directed force; and bricks on the lateral diaphysis received the medially directed force (Figure 5.2).

Results

Assessing strength

As a ductile material, bone failure is correlated with von Mises (VM) stress (Keyak and Rossi, 2000), a measure of distortional stress. Accordingly, although maximum and minimum principal stresses were recorded in each model as an aid to understanding deformation patterns (e.g. torsion, bending, etc.) and risk fracture, peak von Mises stress is the key metric for understanding femoral strength. Peak von Mises stress was recorded on the proximal, middle, and distal surfaces of the diaphysis of each FEM; the surface of the femoral neck; on cross-sections through the midshaft and at 30% and 70% of bone length; and on a cross section through the middle of the neck perpendicular to its long axis.

The first two experiments are designed to detect differences in stress pattern and magnitude during two instances of the gait cycle when acetabular contact forces are highest. The experiment simulating heel-strike indicates that VM stress is highest in the femoral neck (surface and cross-section) and lowest in the middle diaphysis (surface and cross-section) in the HFM (Table 5.2 and Figures 5.3a, 5.9a). The HFM shows a marked decline in VM stress from the neck surface to the proximal diaphysis relative to the NFMs, and it continues to decline through the midshaft, with a slight increase at the distal diaphysis. Both NFMs experience peak VM stress at the distal diaphysis, but have lower stress at all other locations with the exception of the proximal diaphysis where the scaled

NFM and HFM are approximately equally stressed. The lateral metaphysis on both NFMs experiences high VM stress that the HFM does not. Recall that scaling the forces applied to the NFM allows a comparison between the HFM and NFM that only incorporates shape information. Comparing the HFM to the scaled NFM shows that based solely on shape differences, the human femur experiences about twice as much stress on the most highly stressed region of the neck surface than the NFM, about equal stress on the proximal diaphysis surface, but slightly higher stress at midshaft (HFM = 19.83 MPa; scaled NFM = 12.73 MPa). The distal diaphysis surface is more highly stressed in both NFMs (20.93 and 26.37 MPa, unscaled and scaled , respectively) than is the HFM (17.83 MPa). These results indicate that, under loading conditions simulating heel-strike, as a consequence of both size and shape, the midshaft diaphysis is stronger in Neanderthals than humans, while the distal diaphysis is weaker in Neanderthals. The largest difference is seen on the neck surface and the HFM is more highly stressed. The proximal diaphysis shows less difference in VM stress magnitude between models. The scaled NFM is as strong as or stronger than the HFM at all locations except the distal diaphysis.

The experiment simulating toe-off shows a slightly different pattern and slightly larger magnitudes of stress than recorded during heel-strike with two significant differences. During this gait event, the HFM experiences less VM stress than either NFM on the neck and distal diaphysis, and the overall level of VM stress experienced by the HFM is fairly low and flat without significant relief (Table 5.3 and Figures 5.3b, 5.9b) The stress pattern is more variable in the NFMs. Importantly, the magnitude of VM stress on the HFM neck is about 13 MPa lower during toe-off than heel-strike, *and* is less

than either NFM. The NFMs experience more stress at the distal diaphysis than they do during heel-strike, and the magnitude of difference between them and the HMF is higher than during heel-strike (HFM = 27.65 MPa; NFM = 35.89 MPa; scaled NFM = 45.11 MPa). Thus, during toe-off, the human femur experiences less stress on the distal diaphysis than the NFMs, while it experiences more stress than during heel-strike. The NFMs were most highly stressed at the distal diaphysis during heel-strike, and while they are still most highly stressed at the distal diaphysis during toe-off, the magnitude of stress is15 MPa higher in the NFM and 20 MPa higher in the scaled NFM. However, as during heel-strike, the HFM is again weaker than the NFM at the proximal diaphysis and midshaft when differences in size are not accounted for, but the HFM and scaled NFM experience almost identical VM stress at midshaft (surface and cross-section) and the proximal cross-section. These results indicate that overall stress is slightly higher during toe-off in all three models, but the HFM is better at withstanding forces transmitted through the neck when the femur is in an extended position relative to itself during heel-strike than the NFMs. These results also suggest that strictly as a consequence of shape, the human femur and Neanderthal femur are equally well equipped to dissipate stress through the proximal and middle section of the diaphysis. Overall, the scaled NFM is weaker than or equally as strong as the HFM at all locations. This is a different pattern than what is observed during heel-strike.

Stumbling experiments were designed to explore the differences in stress patterns and magnitudes during the event of an irregular step. Because irregular steps are mostly different from regular steps in the magnitude of acetabular contact forces, these

magnitudes were tripled in each of these experiments relative to heel-strike, which is probably when a stumble is more likely to happen, as opposed to toe-off.

In the first stumbling experiment, the resultant ACF was tripled relative to heel-strike and was rotated five degrees anteriorly; the same muscle forces were applied as were applied during heel-strike (Table 5.1). Results are given in Table 5.4 and Figures 5.4a, 5.10a. In the HFM, the neck is the most highly stressed region (112 MPa), whereas on both NFMs, the distal diaphysis is the most highly stressed region (85 MPa and 108 MPa in the unscaled and scaled models, respectively). The HFM experiences VM stress within a 16 MPa range along the proximal diaphysis through the distal diaphysis, but the neck experiences 26 MPa more stress than the most highly stressed location on the diaphysis. Moreover, the risk factor of failure (RF) is less than two. (Risk factor of failure is calculated by comparing the VM stress to the principal stress at the region of interest. If the region of interest principally experiences compression, as is the case at the femoral neck, risk factor is calculated by comparing VM stress relative to ultimate compressive strength of bone. If the region of interest is most highly stressed due to tension, VM stress would be compared to the ultimate strength of bone in tension. Ultimate longitudinal compressive strength of bone is ~205 MPa; ultimate longitudinal tensile strength of bone is ~135 MPa. As this ratio approaches one, the bone is closer to reaching its yield limit and is at risk of fracture.) The HFM experiences more stress than either NFM at all locations except on the neck cross-section, where it is slightly less stressed than the scaled NFM, and at the proximal diaphysis, where stress is about equal with the scaled NFM, and the distal diaphysis, where it is less stressed than the scaled NFM and approximately equal to the unscaled NFM. These results indicate that the

Neanderthal femur is better at dissipating high ACFs due to its size and shape, and based strictly on its shape, it is better than or equal to the HFM at dissipating stress except at the distal diaphysis.

In the second stumbling experiment, the resultant ACF was tripled relative to heel-strike and was rotated five degrees posteriorly; the same muscle forces were applied as were applied during heel-strike (Table 5.1). Results are listed in Table 5.5 and Figures 5.4b, 5.10b. The pattern of peak VM stress is broadly similar as was observed during an anterior stumble. The HFM experiences highest stress along the neck (115 MPa) and the NFMs experience their highest stress at the distal diaphysis (85 MPa and 107 MPa in the unscaled and scaled models, respectively). The NFMs are slightly less stressed along the neck during a posterior stumble compared to during an anterior stumble (a differences of 8-10 MPa), whereas the HFM is slightly more stressed at this location (about 3 MPa more). At the proximal diaphysis each model is less stressed than during an anterior stumble, and the HFM is the most stressed by 4 MPa relative to the scaled NFM. The midshaft diaphysis is more stressed than during an anterior stumble and the HFM is the most highly stressed by a magnitude of 6 MPa. The distal diaphysis is approximately equally stressed during a posterior stumble as an anterior stumble, but the HFM is 4 MPa less stressed than the NFM and 26 MPa less than the scaled NFM.

In the third stumbling experiment, the resultant ACF was tripled relative to heel-strike and was rotated five degrees medially; the same muscle forces were applied as were applied during heel-strike (Table 5.1). Results are listed in Table 5.6 and Figures 5.4c, 5.11a. The patterns and magnitudes are similar to the previous two stumbling experiments. The HFM is most highly stressed along neck locations and the NFMs are

most highly stressed along the distal diaphysis. The HFM is more highly stressed than either NFM at all locations except the proximal diaphysis, where it is about equal to the scaled NFM and the distal diaphysis where it is about equal to the unscaled NFM. Both NFMs are slightly more stressed during a medial stumble than during a posterior stumble. The HFM is more stressed during a medial stumble (119.5 MPA) at the neck than during anterior (112 MPa) or posterior stumbles (115 MPa), and the same is true of the NFMs at the distal diaphysis. The neck risk factor of fracture for the HFM is 1.7 whereas the distal diaphysis RF for the NFM is 2.3; this indicates that the HFM is closer to its yield limit at its most highly stressed region than the NFM is at its most highly stressed region. Another interesting result of the medial stumble is that the difference in peak VM stress between the scaled and unscaled NFMs is higher than in any other experiment (23 MPa, compared to 16 MPa in the anterior stumble, 14 MPa in the posterior stumble, and 11 MPa in the lateral stumble) at the proximal diaphysis. This suggests that the shape of the Neanderthal femur at this region is worse at dissipating stress during this loading scenario than in other loading scenarios. Together, these results indicate that the Neanderthal femur is better than the HFM at dissipating forces associated with a medial stumble due to both size and shape differences except at the distal diaphysis, where due to size and shape it is equally able to dissipate stress, and due strictly to shape, it is less able to dissipate stress than is the human femur.

In the fourth stumbling experiment, the resultant ACF was tripled relative to heel-strike and was rotated five degrees laterally; the same muscle forces were applied as were applied during heel-strike (Table 5.1). Results are listed in Table 5.7 and Figures 5.4d, 5.11b. The pattern of peak VM stress is very similar in this experiment compared to each

of the others, particularly the posterior stumble. The HFM is most highly stressed at all locations except the distal diaphysis, where it experiences 2 MPa less than the unscaled NFM and 21 MPa less than the scaled NFM. The neck is again the most highly stressed location on the HFM (119.7 MPa), and is, in fact, the most highly stressed as a consequence of a lateral stumble than any of the other three stumbles, although the difference is negligible relative to the medial stumble. As in the other stumbling experiments, the distal diaphysis is the most highly stressed location on both NFMs. The scaled NFM, though, is 11 MPa less stressed at the distal diaphysis than it was relative to the medial stumble, which means that while the HFM experiences *the most* stress at its most highly stressed location, the NFM experiences *the least* stress at its most highly stressed location in this loading scenario.

It is clear from the results of all four stumbling experiments that the HFM is more highly stressed (and, thus, weaker) than either NFM model in all experiments at all locations, with exceptions only at the distal diaphysis, where it is approximately as equally stressed as the unscaled NFM; it is never less stressed than the unscaled NFM. Additionally, in no loading scenario does either NFM experience higher peak stress than the HFM, even in their respective locations of highest peak stress. The human femoral neck is not able to dissipate stresses due to stumbling as well as the Neanderthal femur, due to either size and shape differences or only shape differences. The Neanderthal femur's shape is not as good at dissipating forces as the human femur's shape at the distal diaphysis, and size differences are the only reason that it is less stressed at this location.

The traumatic load experiments are designed to explore differences in stress patterns and magnitudes when the femur is subjected to a hit from various directions,

specifically, a blow to the anterior diaphysis, the lateral diaphysis and the antero-lateral diaphysis, as might occur in the life of an individual. Traumatic blows are expected to occur in some activities, perhaps particularly during hunting activities or random accidents. Neanderthal activities may have put them at high risk of trauma (Berger and Trinkaus 1995). In modern contexts, this could also happen, of course, particularly but not exclusively during sporting events. In the first traumatic load (TL) experiment, a horizontal force was directed posteriorly on each model in addition to the acetabular contact and muscles forces used heel-strike (Table 5.1). In each model, the pattern is very similar at locations on the midshaft and proximally, but the patterns diverge at the distal diaphysis. Most significantly, these results show that the scaled NFM experiences higher VM stress at all locations than the HFM, although some of the differences are not very large (Table 5.8 and Figures 5.5a, 5.12a). This indicates that the Neanderthal femur, based strictly on its shape, is weaker when struck with a traumatic load from a frontal direction, particularly along the distal diaphysis, a result that would not be predicted given its strong anterior curvature. Relative to experiments at heel-strike during normal gait, a new pattern emerges in which the diaphysis experiences more VM stress, such that there is no longer a rapid decrease moving distally down the shaft to a final uptick in stress on the distal diaphysis, but instead the magnitude of VM stress gradually decreases in the proximal diaphysis, then levels off in the middle and distal diaphysis. The HFM experiences more stress than the unscaled NFM on the proximal diaphysis (surface and cross section) and middle diaphysis (surface and cross-section); stress increases slightly at the distal diaphysis in both NFMs but not the HFM. The HFM is least stressed at the

distal diaphysis. This distal diaphysis pattern is completely different than in either of the other TL experiments.

In the experiment simulating a medially directed horizontal blow, the same boundary conditions were applied as during heel-strike, in addition to a medially directed horizontal force (Table 5.1). The overall pattern is much different than the pattern seen in the posteriorly directed traumatic load experiment, particularly along the femoral neck (Table 5.9 and Figures 5.5b, 5.12b). The HFM experiences much higher VM stress on the femoral neck surface (42.9 MPa) compared to either the scaled or unscaled NFM (a difference of 17 MPa and 22.5 MPa, respectively), but lower VM stress in the proximal diaphysis surface relative to the scaled NFM (a difference of less than 3 MPa). The HFM is slightly more stressed at the middle diaphysis than either NFM (a difference of 8MPA relative to the NFM and only about 5 MPa relative to the scaled NFM). The HFM and NFM have approximately equal VM stress on the distal diaphysis surface (18.1 and 16.7 MPa, respectively) whereas the unscaled NFM is higher than either (21.2 MPa). On the distal cross-section, the unscaled NFM experiences the lowest VM stress (14.15 MPa), the HFM is intermediate (15.34 MPa), and the scaled NFM has the highest VM stress (17.83), but these differences are quite small. Overall, the HFM appears to be notably weaker along the neck loading environment, and the NFMs are particularly strong at the middle diaphysis. VM stress is very low in the Neanderthal femur at midshaft, and the most notable finding is that even when the applied horizontal force is scaled by a factor of 1.26, the NFM still exhibits very low stress at this location. In the case of the posteriorly directed blow, the NFMs evidence a relatively large increase in VM stress between the scaled and unscaled loads. These results suggests that the Neanderthal

morphology at midshaft is well equipped to dissipate forces associated with medially directed traumatic blows, and is particularly interesting given the results from the posteriorly directed traumatic load in which the NFMs are not particularly strong at midshaft. Lastly, while the HFM shows a sharp decline in VM stress at the distal diaphysis in the posteriorly directed TL experiment, stress magnitude in the medially directed TL experiment is largely similar between all three models.

In the next experiment, the FEMs were applied with the same boundary conditions as during heel-strike and were then loaded with a horizontal force directed postero-medially (Table 5.1). The pattern of VM in this load case is different from either of the previous two experiments (Table 5.10 and Figures 5.5c, 5.12c). Stress is highest in the neck in all three models. It is lowest in the midshaft cross-section on both NFMs, but is lowest on the distal cross-section in the HFM. Interestingly, the HFM experiences the least VM stress at all locations except the neck surface, where VM stress is ~10 MPa higher in this model than the unscaled NFM and ~4 MPa higher than in the scaled NFM. In this particular loading scenario, the HFM experiences the least VM stress of any model at proximal, middle and distal locations. Given the results from the other TL scenarios, in which the HFM experiences higher VM stress at all locations except the distal diaphysis, it is surprising that when the horizontal force is a combination of the previous two forces (postero-medially directed), the HFM is noticeably less stressed. Thus, while the HFM better dissipates forces associated with a postero-medially directed blow, the NFMs do not respond as well as they do to a medially directed blow, with a range of 25-16 MPa (NFM) and 32-20 MPa (unscaled NFM) in this experiment compared to 9-20 MPa (NFM) and 11-25 MPa (unscaled NFM) after a medially directed blow. Taken

together, these results suggest that the Neanderthal femur is not well-suited to coping with posteriorly directed forces and the human femur is not particularly well-equipped to cope with medially directed forces. The human femur is least stressed in this TL scenario with the exception of the neck locations, at which is it intermediate between the posteriorly directed TL (lowest) and the medially directed TLs (highest).

Overall, when considering all of the traumatic load experiments, one cannot conclude that the Neanderthal femur is demonstrably stronger than the modern human femur, because in two of the three experiments the scaled NFM is weaker at nearly all locations, and in the third experiment, it is weaker at some locations. Despite its shaft robusticity, the Neanderthal femur is not especially well suited to withstand traumatic loads.

Assessing predictability

Stress patterns are predictable when stress concentrations are found in roughly the same location despite changes in the loading environment. Thus, predictability can be assessed by measuring the distance between the locations of peak von Mises stress as recorded in the planes and on the surfaces as described above. Distances were calculated using 3-D coordinate information preserved in the FEMs according to the formula $[\sqrt{((X_2 - X_1)^2 + (Y_2 - Y_1)^2 + (Z_2 - Z_1)^2)}]$, and were scaled by femoral length. Small distances between the positions of homologous regions of peak stresses (i.e. on the femoral neck and proximal, middle, and distal diaphysis) on a given model in the different experiments indicate high predictability. Heel-strike was always used as the baseline to which other experiments were compared.

The first predictability comparison was made between the HFM and NFM at heel-strike and toe-off (Table 5.11 and Figure 5.6a). Overall, the NFM and HFM exhibit approximately the same degree of predictability, but the HFM is slightly more predictable than the NFM, as evidenced by the total distance between areas of peak von Mises stress. On both models, the locations of peak von Mises stress are very predictable between heel-strike and toe-off on the middle and distal diaphysis. The largest difference between the models occurs on the femoral neck, where the HFM shows more predictability than the NFM even though it is almost uniformly more highly stressed than the NFM. The proximal diaphysis is also a location of some difference with the HFM showing less predictability than the NFM.

During an anterior stumble compared to heel-strike, the Neanderthal is overall less predictable (Figure 5.6b). The only location that is less predictable on the HFM than the NFM is the distal diaphysis and that result will be discussed in more detail below. The same pattern is apparent during a posterior stumble (Figure 5.6c), but predictability increases during this load case compared to the anterior stumble. Again, the pattern and magnitude are the same during medial and lateral stumbles as during the anterior and posterior stumbles (Figures 5.6d and 5.6e, respectively), with one small exception. During the medial stumble, the HFM is slightly less predictable at midshaft than the NFM, a result that will be discussed in more detail below. These results are also documented in Table 5.11.

When the locations of peak von Mises stress are compared between heel-strike and the posteriorly directed traumatic load (Table 5.11 and Figure 5.6f), the HFM is again more predictable than then NFM, but the locations experiencing the least

predictability being the proximal diaphysis and neck cross-section. Both models are similarly predictable at the middle diaphysis and neck surface, but the NFM is less predictable at the proximal diaphysis. Indeed, both models exhibit a very high correspondence in locations of peak von Mises stress between heel-strike and the posteriorly directed TL, with the slight exception of the proximal diaphysis.

Comparing heel-strike and the medially directed force, the NFM and HFM are overall similarly predictable, but relative to the posteriorly directed TL, they show less predictability in the middle diaphysis, and the human femur is less predictabl along the distal diaphysis (Table 5.11 and Figure 5.6g).

Finally, when comparing heel-strike and the postero-medially directed TL (Table 5.11 and Figure5.6h), the pattern is more similar to the comparison of heel-strike and the posteriorly directed TL than heel-strike and the medially directed TL, primarily due to the decreased predictability at the middle and distal diaphysis as a result of the medially directed force. Overall, predictability increases compared to the medially and posteriorly directed forces.

Figures 5.7 and 5.8 were created as an aid to understanding exactly what is occurring during different loading environments at each location. Figure 5.7a shows that the neck surface is a region of high predictability during normal walking, although the NFM behaves less predictably during normal walking than the HFM. Only the NFM shows a relatively high level of unpredictability during any loading scenario along the neck surface, and that occurs during an anterior stumble. The neck-cross section of the NFM is less predictable than the HFM during stumbling, but both behave very predictably during normal walking and in the case of traumatic loads (Figure 5.8a).

In the HFM, the proximal diaphysis is approximately equally predictable in all traumatic load experiments and during normal walking, but the NFM is less predictable than the HFM during a posteriorly directed TL (Figure 5.7b). Predictability decreases during all stumbling experiments, with the largest decrease occurring during a medial stumble, particularly in regards to the HFM. On the proximal cross-section of each FEM, predictability is fairly equal and high between both models across each comparison, but the HFM is less predictable than the NFM (Figure 5.8b).

At the middle diaphysis, the HFM experiences the lowest level of predictability when subjected to an anterior and medial stumble (Figure 5.7c), but is more predictable than the NFM in all load cases except the medial stumble. So while the NFM was less stressed during the stumbling experiments, it is less predictable. On the middle diaphysis cross-section (Figure 5.8c), the two models show high predictability in all comparisons, but the NFM is less predictable than the HFM, particularly during the stumbling experiments.

On the distal diaphysis surface, predictability is very high in the NFM, and by comparison the HFM is much less predictable (Figure 5.7d). This is because it is always the lateral metaphysis that is most highly stressed in the NFMs. The NFM is also very predictable, on the distal cross-section (Figure 5.8d), with the least predictability during a posteriorly directed TL occurring during heel-strike. Predictability is rather high in both models and across all comparisons relative to the other cross-section regions.

Note that Figure 5.7e, a comparison of total distances, shows that in each stumbling experiment, the NFM exhibits less predictability. Midshaft is least predictable in both HFM and NFM, particularly in regards to stumbling, as indicated by the

difference in degree of predictability at this location compared to the neck, proximal diaphysis and distal diaphysis locations.

Discussion and Conclusion

Overall, the Neanderthal femur is not stronger than the human femur during normal gait. This results in failure to reject the null hypothesis. At heel strike, the scaled NFM is stronger or equally as strong at most location except the distal diaphysis. At toe-off, the scaled NFM is weaker than or equally as strong as the HFM at all locations. In every gait cycle, each femur experiences both heel-strike and toe-off, so it is impossible to conclude that one femur is, overall, stronger than the other during normal bipedal walking.

During stumbling, the NFM is consistently stronger, or as strong as, the HFM at all locations except the distal diaphysis. Therefore, the null hypothesis is rejected during stumbling. This finding is consistent with, although not necessarily evidence of, a scenario in which Neanderthals are adapted to traveling over uneven terrain, where irregular steps may be more frequent. The modern human femoral neck is especially vulnerable during stumbling, highlighting the danger of fracturing this region in individuals with osteoporosis.

The Neanderthal femur is not especially well configured to withstand traumatic loads. The scaled NFM is weaker than the HFM at nearly all locations during two of the three traumatic load experiments, and at some locations in the third experiment. These results indicate rejection of the null hypothesis, although not in the way that was

predicted. Neanderthals may or may not have had a lifestyle that exposed them to a high risk of trauma, but regardless, their femora appear not to have adapted to those risks.

The predictability data are equally intriguing. On average, predictability is less in the Neanderthal femur than the modern human femur. Yet this pattern is not consistent across all regions. The Neanderthal is less predictable at the femoral neck and midshaft, whereas the human femur is less predictable at the proximal and distal diaphysis. Interestingly, in both models, the regions of highest stress exhibit high predictability. The neck in the human femur is highly stressed and has more predictability than the Neanderthal femoral neck. The distal diaphysis in Neanderthal femora is highly stressed and has more predictability than the human. This is the pattern one would expect if increasing predictability is a strategy to avoid fracture. Thus, although the overall pattern of predictability is complicated, in each model, predictability is greatest where it is needed most. This result is easy to understand for the Neanderthal pattern: the high level of curvature that reaches its maximum distally results in high stress along the distal diaphysis and predictability is also highest at the distal diaphysis. The cause of the results for the human femur is harder to interpret.

Patterns of maximum and minimum principal stresses indicate that the femoral shaft experiences both antero-posterior and medio-lateral bending during the gait cycle. Trinkaus and Ruff (1999) compared second moment of area at mid-shaft to body mass times length and found that the Neanderthals are slightly more gracile relative to *early* anatomically modern humans in the antero-posterior dimension, but not significantly more so. However, along the medio-lateral dimension, the Neanderthals are more robust than humans. This is probably due to the circular shape of Neanderthal femora making it

more resistant to bending in the medio-lateral direction than the elliptical shape of the human femur, where the minor axis is located along the medio-lateral plane. These results are supported by results obtained in this study, and confirm that the relationship between Neanderthals and recent modern humans is the same. Medio-lateral bending is dominant along the proximal diaphysis, is transitional through midshaft, and antero-posterior bending predominates at the distal diaphysis. Thus, the femur needs to behave predictably under both bending orientations. It is possible that Neanderthals and modern humans achieve predictability in different ways. Neanderthal and human femora both exhibit shaft curvature which pre-determines the antero-posterior bending direction and thus increases predictability. Because the human femoral neck-shaft angle is higher, the femur is more columnar. This means that if circular in cross-section, it would behave unpredictably. The elliptical cross-section of humans, then, increases the predictability of medio-lateral bending by creating a shaft that is thinner medio-laterally. In the Neanderthal femur, the shaft is relatively more offset from the acetabulum (where body weight is transmitted to the femur) due to the lower femoral neck-shaft angle, and thus the medio-lateral bending path is pre-determined, thus creating medio-lateral bending predictability.

The aim of this chapter was to understand the biomechanical significance of different femoral morphologies. Results of this study add to our understanding of human variation by illuminating biomechanical consequences of variation between recent human and Neanderthal femora. Differences in morphology have been associated with mobility level (determined through degree of robusticity), environmental factors such as terrain relief, and genetics (i.e. body proportions). Each of these factors alters the mechanical

environment in which a femur exists and can therefore affect its morphology. Robusticity, as measured through amount of cortical bone is slightly different between Neanderthals and EAMHs, and is least robust in recent modern humans, such as the one used to create the HFM of this study. Ruff (1994) determines that although Neanderthal femora are absolutely stronger, the difference between Neanderthals and EAMHs is the result of differences in body mass, rather than locomotion. This study shows that when differences in size are accounted for (by isometrically scaling the muscle and ACFs by a factor that closely approximates estimated differences in body mass), the Neanderthal is not summarily more robust relative to *recent* modern humans.

Shackelford and Trinkaus found that "variation in curvature…is not strongly influenced by body size or lower-limb articular positioning" (2002, pp 367). This study did not test the effect of curvature on strength per se, but rather used whole femora to investigate the combined effects of size and shape with regards to strength and predictability. It seems logical that the increased bending moment created by increased curvature would result in higher stress in the Neanderthal femur under conditions in which force transmission through the femoral head was particularly high, as occurs during a stumble, but locations of peak stress should also be more predictable. It is therefore reasonable that the NFM performed more poorly during toe-off than during heel-strike since ACFs would create a greater bending moment with the limb in a slightly flexed rather than extended position. Yet, despite the greater curvature, the NFM was less predictable. Additionally, only in the stumbling experiment in which the ACFs were rotated anteriorly (further increasing the bending moment), does the scaled NFM exceed VM stress magnitude measured on the HFM at a location other than the distal diaphysis.

Neanderthal (and EAMH) femora show more distal points of maximum curvature compared to later humans. This could be the reason for the higher stress in the lateral metaphysis (distal diaphyseal surface) of Neanderthals which was a clear and consistent finding in this study.

Many studies (Biewener and Taylor 1986; Biewener et al. 1983; Rubin and Lanyon 1982) provide strong evidence that most stress generated in long bones during locomotion is the result of bending, yet long bones of animals consistently develop curvature when exposed to normal mechanical environments. This observation indicates that curvature plays a vital role in optimum design for function. Bertram and Biewener (1988) propose that the best compromise between loading variability and body size determine the final degree of curvature. Neanderthals have higher body mass than modern humans, and yet they have more curved bones, contra the pattern in most other mammals. Due to their increased curvature, it was predicted that the NFM would show more predictability than the HFM. Results indicate that this is not true.

As stated previously, cross-sectional geometry also influences predictability and may be associated with reduction of curvature. Since most stress is generated due to bending, logic dictates that it would be a better design to increase strength and predictability by changes in cortical thickness and cross-sectional shape than curvature, if that is an option. Results in this study indicate that human femora are overall more predictable than Neanderthal femora, despite being less curved.

It stands to reason that EAMHs who were more robust and had the characteristic elliptical cross-sectional shape were particularly well adapted for dissipating stresses. Adding a femur model representing morphology of EAMHs would allow this hypothesis

to be tested. If low risk of fracture is a characteristic that increases fitness then EAMH morphology would be more advantageous than Neanderthal morphology. It is possible then, that modern human femoral morphology is more fit and has merely continued a trend towards increased gracility (as measured by cortical bone area) because such strength was not as necessary for survival as subsistence strategies became more sophisticated and a sedentary lifestyle was adopted. With a more technologically sophisticated means of subsistence, modern human femora were freed from evolutionary constraints to maintain a high level of robusticity and curvature was also allowed to decrease because their cross-sectional geometry was adequately able endure typical stresses.

Regarding cross-sectional shape, Neanderthals vary more than modern humans in the orientation of the major axis (the long axis of an ellipse) (Trinkaus and Ruff 1999). FEA experiments often suffer from lack of variability in their sample. Creating a FE model is a time consuming and laborious process, and complete fossil hominin specimens are difficult to obtain, but it would be worthwhile to consider additional Neanderthal femoral specimens and also early anatomically modern human femora, which are morphologically different from both Neanderthals and recent modern humans.

I suggest that the trend in reduction of curvature from early humans to recent humans is not necessarily the result of decreased mobility (because curvature does not increase predictability *more* than cross-sectional geometry does), but is because the elliptical versus circular cross-sectional shape is safer (insofar as curvature increases bending moments and most stress in femora is due to bending) *and* better at increasing predictability. Perhaps a reduction in robusticity through time is attributable to decreased

mobility, but a reduction in curvature is due to an increase in diaphyseal asymmetry. The HFM is weaker medio-laterally, but it is possible that human behavior was not such that the bone needed medio-lateral reinforcement. Circular cross-sectional shape is the primitive condition as femora of *Homo erectus* are also platymeric (Anton 2003), elliptical cross-sectional shape is derived in modern humans and could confer an adaptive advantage by maintaining a predictable stress environment without the need for physiologically costly robusticity, while also performing better than curvature. Habitual *types* of movement may also play a role in the development of an elliptical shape. Perhaps modern humans participated in more linear movement across an open landscape whereas Neanderthals more often navigated terrain that was mountainous, wooded, or necessitated obstacle avoidance that resulted in more medio-lateral movements.

The femoral neck is consistently the location of highest von Mises stress in the HFM. It is only on the human femoral neck that the risk factor of failure drops below two, indicating that there is more than half of the stress necessary to create a fracture. Voo et al. (2004) demonstrate that neck length and neck-shaft angle are the two primary variables of interest in femoral neck fracture. Longer femoral necks and higher neck-shaft angles result in increased risk of fracture, particularly the more unpredictable tension-type fractures rather than predictable compressive fractures on the inferior neck surface. Higher femoral neck-shaft angles may reduce medio-lateral bending as a consequence of the manner in which ACFs are transmitted from the femoral head through the shaft; however, the consequence of increasing neck-shaft angle is that it significantly increases fracture risk, which is not at all advantageous. In fact, Voo et al. (2004) found that increasing neck-shaft angle by just 12 degrees increases the probability of fracture by

85%. Given the high magnitude of VM stress measured on the HFM neck, it seems that fracture risk is a rather large trade-off for medio-lateral stress reduction. High neck-shaft angle and long femoral neck length, then, are likely a by-product of the linear body form that is characteristic of modern humans. Even so, reduction in medio-lateral bending through increased neck-shaft angle would be a positive trait and may be another reason that an elliptical cross-sectional shape developed. Humans did not engage in activities that typically result in high medio-lateral stress, whereas Neanderthals did, and the long femoral neck/high neck-shaft angle of human femora provided a means of reducing medio-lateral bending stress whereas the Neanderthal's short femoral neck and small neck-shaft angle did not.

Table 5.1 Forces Applied in Each FEA Experiment

ACFs and Muscles	Heel-strike forces (N)		Toe-off forces (N)		Stumbling forces (N)*				Traumatic load forces (N)	
	HFM & NFM	Scaled NFM	HFM & NFM	Scaled NFM	HFM & NFM		Scaled NFM		HFM & NFM	Scaled NFM
Distally directed (X)	1427	1798	1859	2342.34	(A) 4336.1 (M) 4411	(P) 4193.33 (L) 4118.29	(A) 5463.45 (M) 5557.9	(P) 5283.6 (L) 5189	1427	1798
Laterally directed (Y)	561	706.86	555	699.3	(A) 1683 (M) 1303.02	(P) 1683 (L) 2049.3	(A) 2120.6 (M) 1642	(P) 2120.6 (L) 2582.1	561	706.86
Anteriorly directed (Z)	273	343.98	214	269.64	(A) 442 (M) 819	(P) 1189 (L) 819	(A) 556.92 (M) 1031.9	(P) 1533.8 (L) 1031.9	273	343.98
Adductor magnus	73	91.98	0	0	73		91.98		73	91.98
Gluteus maximus	316	398	210	264	316		398		316	398
Gluteus medius	289	375	286	360.36	289		375		289	375
Gluteus minimus	89	112	124	156.24	89		112		89	112
Inferior gemelli	3	3.78	7	8.82	3		3.78		3	3.78
Obturator internus	25	31.5	40	50.4	25		31.5		25	31.5
Piriformis	26	32.76	98	123.48	26		32.76		26	32.76
Quadratus femoris	35	44.1	-	-	35		44.1		35	44.1
Superior gemelli	2	2.52	3	3.78	2		2.52		2	2.52
Biceps femoris	201	253.26	256	322.56	201		253.26		201	253.26
Rectus femoris	55	69.3	338	425.88	55		69.3		55	69.3
Iliacus	-	-	91	114.66	-		-		-	-
TL*	-	-	-	-	-		-		500	630

*Acetabular contact forces during stumbling vary according to orientation of the stumble. (A) = anterior (P) = posterior (M) = medial (L) = lateral. TL = traumatic load

Table 5.2 Heel-strike Stress Magnitudes				
Location	**Model**	**Maximum Principal Stress (Mpa)**	**Minimum Principal Stress (MPa)**	**von Mises Stress (MPa)**
Diaphysis surface_proximal	Human	-0.82	-22.76	21.80
	Neanderthal	-0.59	-19.32	17.90
	Neanderthal scaled	-0.75	-24.35	22.55
Diaphysis surface_middle	Human	-0.45	-18.14	17.59
	Neanderthal	0.40	-9.91	10.11
	Neanderthal scaled	0.51	-12.49	12.73
Diaphysis surface_distal	Human	0.01	-18.55	17.83
	Neanderthal	-1.36	-23.21	20.93
	Neanderthal scaled	-1.72	-29.25	26.37
Neck surface	Human	9.11	-36.25	40.91
	Neanderthal	-0.72	-22.54	20.14
	Neanderthal scaled	-0.90	-28.40	25.37
Midshaft cross-section	Human	0.57	-13.29	13.64
	Neanderthal	0.38	-7.57	7.71
	Neanderthal scaled	0.48	-9.54	9.71
Proximal cross-section	Human	0.69	-19.59	19.95
	Neanderthal	0.37	-13.18	13.29
	Neanderthal scaled	0.47	-16.60	16.75
Distal cross-section	Human	0.11	-15.01	14.81
	Neanderthal	0.29	-14.09	13.89
	Neanderthal scaled	0.36	-17.76	17.50
Neck cross-section	Human	3.77	-30.59	31.00
	Neanderthal	-1.15	-21.87	20.04
	Neanderthal scaled	-1.45	-27.56	25.26

Table 5.3 Toe-off Stress Magnitudes				
Location	**Model**	**Maximum Principal Stress (Mpa)**	**Minimum Principal Stress (MPa)**	**von Mises Stress (MPa)**
Diaphysis surface_proximal	Human	-0.99	-32.26	29.97
	Neanderthal	-0.90	-30.29	27.66
	Neanderthal scaled	-1.10	-37.68	33.97
Diaphysis surface_middle	Human	0.19	-25.87	25.62
	Neanderthal	1.45	-19.67	20.21
	Neanderthal scaled	1.66	-24.94	25.53
Diaphysis surface_distal	Human	-0.11	-27.93	27.65
	Neanderthal	-2.18	-38.96	35.89
	Neanderthal scaled	-2.77	-49.09	45.11
Neck surface	Human	15.71	-22.81	33.51
	Neanderthal	0.40	-36.17	35.28
	Neanderthal scaled	1.06	-45.23	44.44
Midshaft cross-section	Human	1.47	-19.20	19.82
	Neanderthal	3.79	-13.90	16.49
	Neanderthal scaled	4.36	-17.88	20.86
Proximal cross-section	Human	2.80	-26.62	28.22
	Neanderthal	1.75	-20.97	22.17
	Neanderthal scaled	2.20	-26.68	28.16
Distal cross-section	Human	1.05	-24.68	24.80
	Neanderthal	0.78	-25.97	26.32
	Neanderthal scaled	0.71	-32.83	33.11
Neck cross-section	Human	-9.93	-34.06	32.06
	Neanderthal	28.89	-4.35	31.02
	Neanderthal scaled	36.97	-5.93	39.97

Table 5.4 Anterior Stumble Stress Magnitudes				
Location	**Model**	**Maximum Principal Stress (Mpa)**	**Minimum Principal Stress (MPa)**	**von Mises Stress (MPa)**
Diaphysis surface_proximal	Human	-2.16	-76.49	73.19
	Neanderthal	-0.57	-59.33	55.78
	Neanderthal scaled	-0.72	-75.80	71.28
Diaphysis surface_middle	Human	1.66	-81.92	81.99
	Neanderthal	-1.81	-59.23	56.91
	Neanderthal scaled	-2.30	-75.04	72.10
Diaphysis surface_distal	Human	-0.79	-86.79	85.09
	Neanderthal	-5.47	-96.09	85.78
	Neanderthal scaled	-6.94	-121.90	108.83
Neck surface	Human	28.92	-96.74	112.74
	Neanderthal	-0.05	-69.40	68.09
	Neanderthal scaled	-0.43	-88.40	86.52
Midshaft cross-section	Human	1.57	-71.99	72.44
	Neanderthal	-0.76	-46.36	45.03
	Neanderthal scaled	-0.94	-58.73	57.05
Proximal cross-section	Human	2.75	-69.18	70.30
	Neanderthal	1.97	-47.38	48.33
	Neanderthal scaled	2.51	-60.52	61.74
Distal cross-section	Human	-1.35	-79.21	76.80
	Neanderthal	0.18	-73.68	71.25
	Neanderthal scaled	0.22	-93.36	90.27
Neck cross-section	Human	-0.47	-86.88	86.05
	Neanderthal	-0.65	-75.72	72.49
	Neanderthal scaled	-1.14	-96.35	92.02

Table 5.5 Posterior Stumble Stress Magnitudes				
Location	**Model**	**Maximum Principal Stress (Mpa)**	**Minimum Principal Stress (MPa)**	**von Mises Stress (MPa)**
Diaphysis surface_proximal	Human	-0.04	-72.46	71.20
	Neanderthal	-2.72	-60.66	53.96
	Neanderthal scaled	-3.43	-76.43	67.99
Diaphysis surface_middle	Human	15.16	-73.06	83.65
	Neanderthal	-0.54	-55.78	54.57
	Neanderthal scaled	-0.67	-70.29	68.75
Diaphysis surface_distal	Human	-0.80	-83.62	81.83
	Neanderthal	-6.30	-95.75	85.32
	Neanderthal scaled	-7.94	-120.64	107.50
Neck surface	Human	43.84	-88.37	115.85
	Neanderthal	-0.98	-67.31	60.86
	Neanderthal scaled	-1.23	-84.81	76.68
Midshaft cross-section	Human	1.72	-72.26	73.13
	Neanderthal	-1.21	-47.25	45.59
	Neanderthal scaled	-1.52	-59.54	57.44
Proximal cross-section	Human	3.04	-67.10	68.37
	Neanderthal	2.47	-45.53	46.58
	Neanderthal scaled	3.11	-57.36	58.70
Distal cross-section	Human	0.01	-75.86	74.23
	Neanderthal	0.70	-69.23	67.40
	Neanderthal scaled	0.88	-87.22	84.92
Neck cross-section	Human	8.13	-92.17	97.17
	Neanderthal	54.62	-10.15	60.00
	Neanderthal scaled	68.82	-12.80	75.60

Table 5.6 Medial Stumble Stress Magnitudes				
Location	**Model**	**Maximum Principal Stress (Mpa)**	**Minimum Principal Stress (MPa)**	**von Mises Stress (MPa)**
Diaphysis surface_proximal	Human	-1.74	-79.75	77.64
	Neanderthal	-2.64	-60.50	54.43
	Neanderthal scaled	-0.20	-82.38	76.68
Diaphysis surface_middle	Human	1.40	-83.46	84.24
	Neanderthal	2.19	-58.39	59.25
	Neanderthal scaled	2.76	-73.57	74.65
Diaphysis surface_distal	Human	-0.77	-90.68	89.12
	Neanderthal	-5.54	-99.33	90.47
	Neanderthal scaled	-6.97	-125.16	113.99
Neck surface	Human	37.77	-97.42	119.54
	Neanderthal	-2.49	-16.28	68.34
	Neanderthal scaled	-3.14	-96.60	86.10
Midshaft cross-section	Human	-0.29	-76.36	75.66
	Neanderthal	-1.07	-50.22	48.60
	Neanderthal scaled	-1.35	-63.28	61.24
Proximal cross-section	Human	3.12	-75.09	76.31
	Neanderthal	2.43	-51.71	52.78
	Neanderthal scaled	3.06	-65.15	66.50
Distal cross-section	Human	-1.03	-82.82	80.47
	Neanderthal	-0.24	-76.69	74.12
	Neanderthal scaled	-0.30	-96.63	93.39
Neck cross-section	Human	2.49	-96.62	97.74
	Neanderthal	-5.43	-73.53	66.26
	Neanderthal scaled	-6.85	-92.65	83.49

Table 5.7 Lateral Stumble Stress Magnitudes				
Location	**Model**	**Maximum Principal Stress (Mpa)**	**Minimum Principal Stress (MPa)**	**von Mises Stress (MPa)**
Diaphysis surface_proximal	Human	0.21	-67.46	66.43
	Neanderthal	-1.70	-52.12	47.39
	Neanderthal scaled	-2.14	-65.67	59.71
Diaphysis surface_middle	Human	14.13	-70.59	80.35
	Neanderthal	-0.52	-52.83	51.67
	Neanderthal scaled	-0.66	-66.56	65.11
Diaphysis surface_distal	Human	-0.96	-81.52	79.63
	Neanderthal	-6.06	-91.28	81.20
	Neanderthal scaled	-7.64	-115.01	102.32
Neck surface	Human	28.85	-104.47	119.68
	Neanderthal	-0.98	-62.36	56.32
	Neanderthal scaled	-1.24	-78.58	70.96
Midshaft cross-section	Human	1.53	-68.76	69.43
	Neanderthal	-1.01	-43.30	41.84
	Neanderthal scaled	-1.28	-54.56	52.72
Proximal cross-section	Human	0.45	-62.96	61.74
	Neanderthal	2.00	-41.10	41.95
	Neanderthal scaled	2.52	-51.79	52.86
Distal cross-section	Human	-0.44	-73.89	72.06
	Neanderthal	0.47	-66.19	64.26
	Neanderthal scaled	0.60	-83.40	80.97
Neck cross-section	Human	6.01	-83.30	86.89
	Neanderthal	3.14	-53.37	54.02
	Neanderthal scaled	3.95	-67.24	68.06

Table 5.8 Posteriorly Directed Traumatic Load Stress Magnitudes				
Location	**Model**	**Maximum Principal Stress (Mpa)**	**Minimum Principal Stress (MPa)**	**von Mises Stress (MPa)**
Diaphysis surface_proximal	Human	2.87	-27.43	29.05
	Neanderthal	2.66	-22.09	24.12
	Neanderthal scaled	3.35	-27.83	30.39
Diaphysis surface_middle	Human	1.21	-26.43	27.20
	Neanderthal	1.67	-23.66	24.74
	Neanderthal scaled	2.10	-29.81	31.17
Diaphysis surface_distal	Human	1.95	-15.50	16.92
	Neanderthal	0.02	-24.33	24.03
	Neanderthal scaled	0.03	-30.66	30.28
Neck surface	Human	15.38	-21.51	32.04
	Neanderthal	-0.30	-29.64	27.11
	Neanderthal scaled	-0.04	-37.34	34.16
Midshaft cross-section	Human	3.48	-23.37	25.65
	Neanderthal	2.59	-21.71	23.62
	Neanderthal scaled	3.26	-27.35	29.76
Proximal cross-section	Human	0.67	-25.64	25.63
	Neanderthal	1.01	-20.25	20.85
	Neanderthal scaled	1.27	-25.51	26.27
Distal cross-section	Human	4.34	-11.41	14.33
	Neanderthal	8.78	-13.89	19.74
	Neanderthal scaled	11.06	-17.50	24.88
Neck cross-section	Human	9.27	-23.35	29.09
	Neanderthal	0.35	-25.19	24.83
	Neanderthal scaled	0.44	-31.74	31.28

5.9 Medially Directed Traumatic Load Stress Magnitudes				
Location	**Model**	**Maximum Principal Stress (Mpa)**	**Minimum Principal Stress (MPa)**	**von Mises Stress (MPa)**
Diaphysis surface_proximal	Human	1.26	-14.23	14.57
	Neanderthal	-0.17	-15.85	14.92
	Neanderthal scaled	-0.21	-19.98	18.79
Diaphysis surface_middle	Human	2.34	-16.85	18.52
	Neanderthal	1.14	-10.00	10.63
	Neanderthal scaled	1.44	-12.60	13.39
Diaphysis surface_distal	Human	0.27	-18.12	18.13
	Neanderthal	-0.87	-18.55	16.79
	Neanderthal scaled	-1.10	-23.37	21.15
Neck surface	Human	6.55	-40.18	42.93
	Neanderthal	-0.10	-22.21	20.39
	Neanderthal scaled	-0.13	-27.98	25.69
Midshaft cross-section	Human	0.35	-15.47	15.28
	Neanderthal	1.45	-7.85	8.73
	Neanderthal scaled	1.83	-9.89	11.00
Proximal cross-section	Human	0.28	-9.36	9.52
	Neanderthal	1.29	-8.85	9.64
	Neanderthal scaled	1.63	-11.15	12.15
Distal cross-section	Human	-0.38	-15.82	15.34
	Neanderthal	0.73	-13.79	14.15
	Neanderthal scaled	0.92	-17.38	17.83
Neck cross-section	Human	-0.30	-36.74	33.89
	Neanderthal	0.77	-18.94	18.95
	Neanderthal scaled	0.97	-23.86	23.87

5.10 Postero-medially Directed Traumatic Load Stress Magnitudes				
Location	**Model**	**Maximum Principal Stress (Mpa)**	**Minimum Principal Stress (MPa)**	**von Mises Stress (MPa)**
Diaphysis surface_proximal	Human	-0.76	-20.88	19.74
	Neanderthal	0.48	-22.68	22.01
	Neanderthal scaled	0.60	-28.58	27.73
Diaphysis surface_middle	Human	0.88	-13.02	13.30
	Neanderthal	1.87	-18.19	19.25
	Neanderthal scaled	2.36	-22.92	24.25
Diaphysis surface_distal	Human	0.33	-12.71	12.79
	Neanderthal	1.81	-18.13	19.67
	Neanderthal scaled	2.28	-22.85	24.79
Neck surface	Human	-3.50	-40.25	35.06
	Neanderthal	0.43	-27.32	25.18
	Neanderthal scaled	0.54	-34.42	31.73
Midshaft cross-section	Human	1.07	-11.70	12.09
	Neanderthal	2.13	-15.05	16.28
	Neanderthal scaled	2.68	-18.96	20.52
Proximal cross-section	Human	0.15	-15.71	15.66
	Neanderthal	1.83	-17.40	18.53
	Neanderthal scaled	2.31	-21.93	23.35
Distal cross-section	Human	2.32	-9.90	11.20
	Neanderthal	6.86	-12.23	16.78
	Neanderthal scaled	8.65	-15.41	21.14
Neck cross-section	Human	4.67	-24.13	26.66
	Neanderthal	-1.96	-24.68	21.81
	Neanderthal scaled	-2.47	-31.09	27.48

Figure 5.1 Position of lower limb at heel-strike (a) and toe-off (b). Positions of pelvis and tibia relative to the femur were used in applying muscle forces. HFM is shown and corresponds to NFM positioning

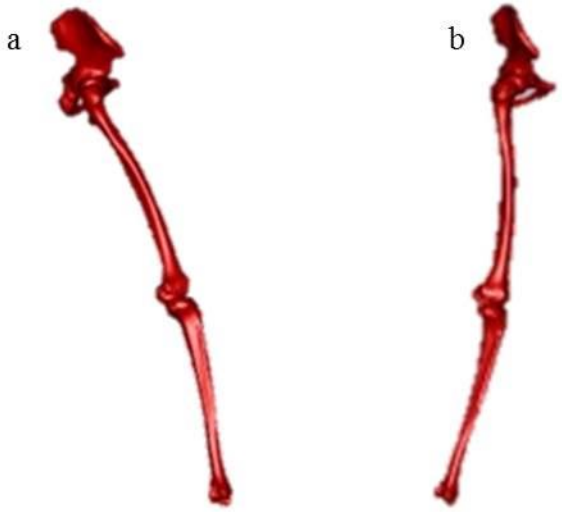

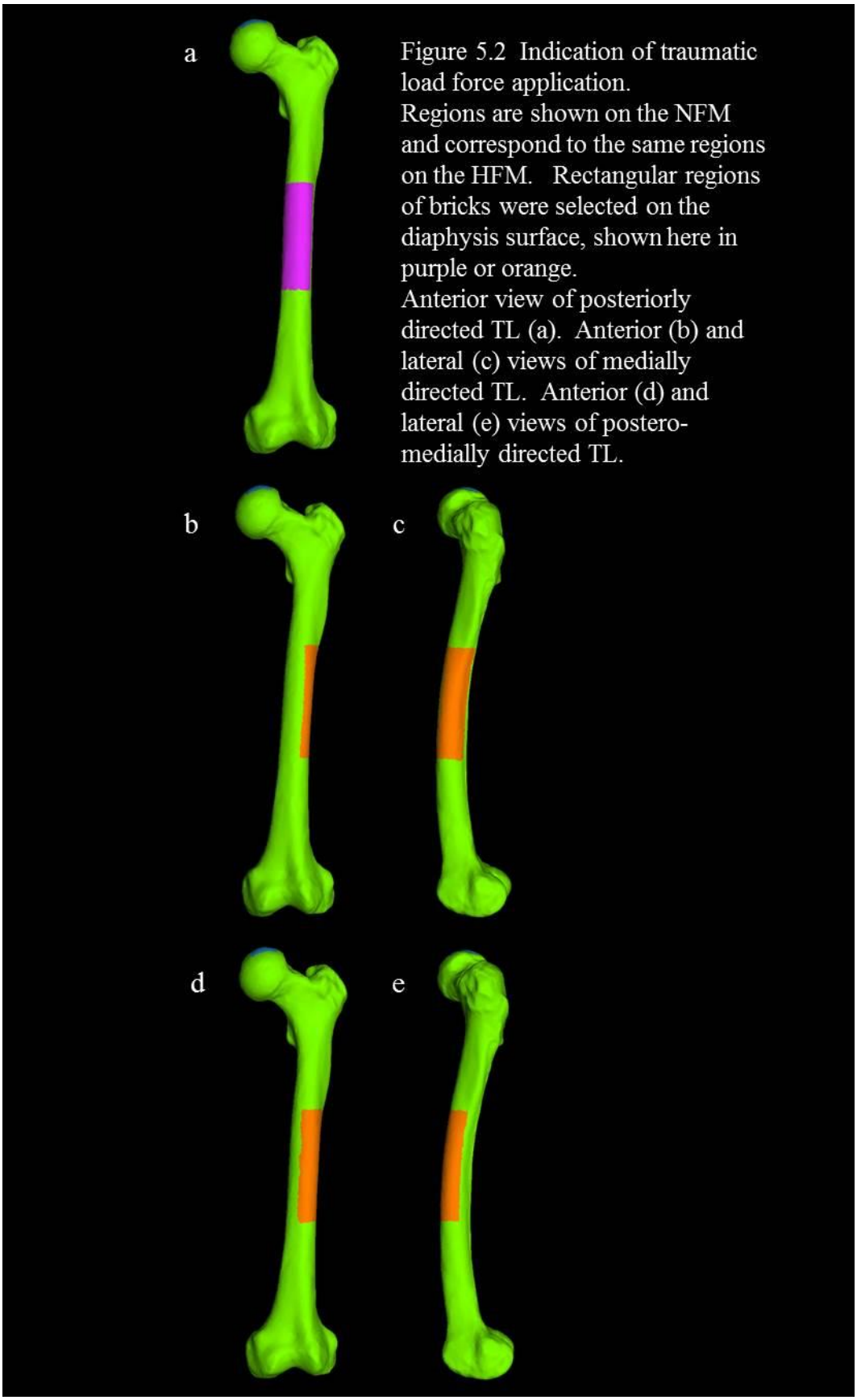

Figure 5.2 Indication of traumatic load force application.
Regions are shown on the NFM and correspond to the same regions on the HFM. Rectangular regions of bricks were selected on the diaphysis surface, shown here in purple or orange.
Anterior view of posteriorly directed TL (a). Anterior (b) and lateral (c) views of medially directed TL. Anterior (d) and lateral (e) views of postero-medially directed TL.

Figure 5.3 von Mises Stress measured at the moment of heel strike (a) and toe-off (b).

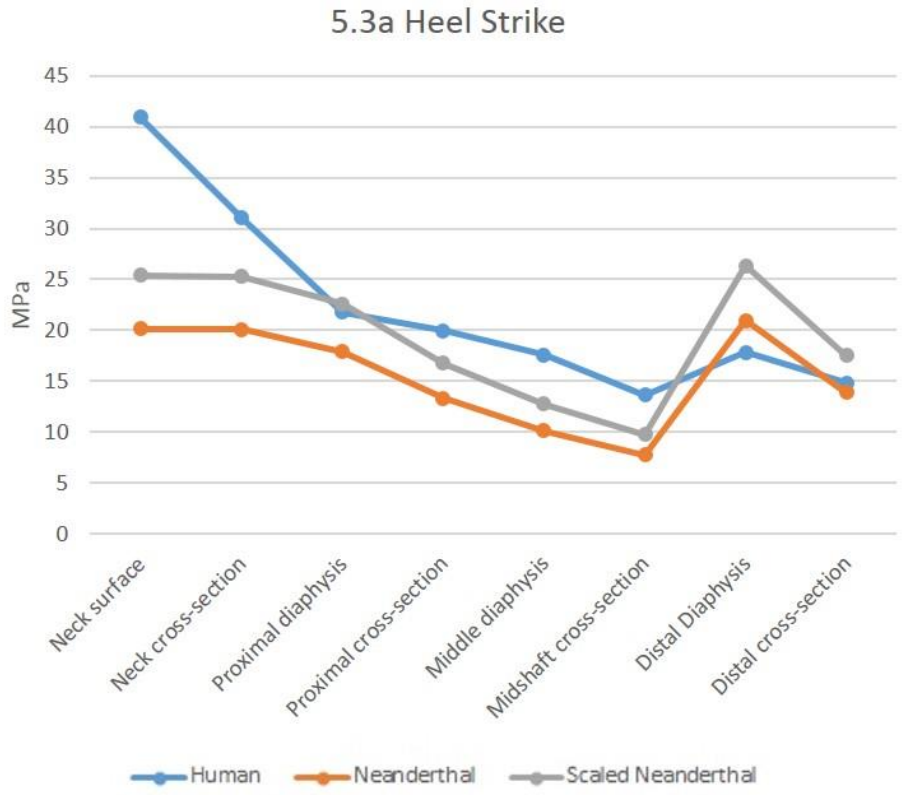

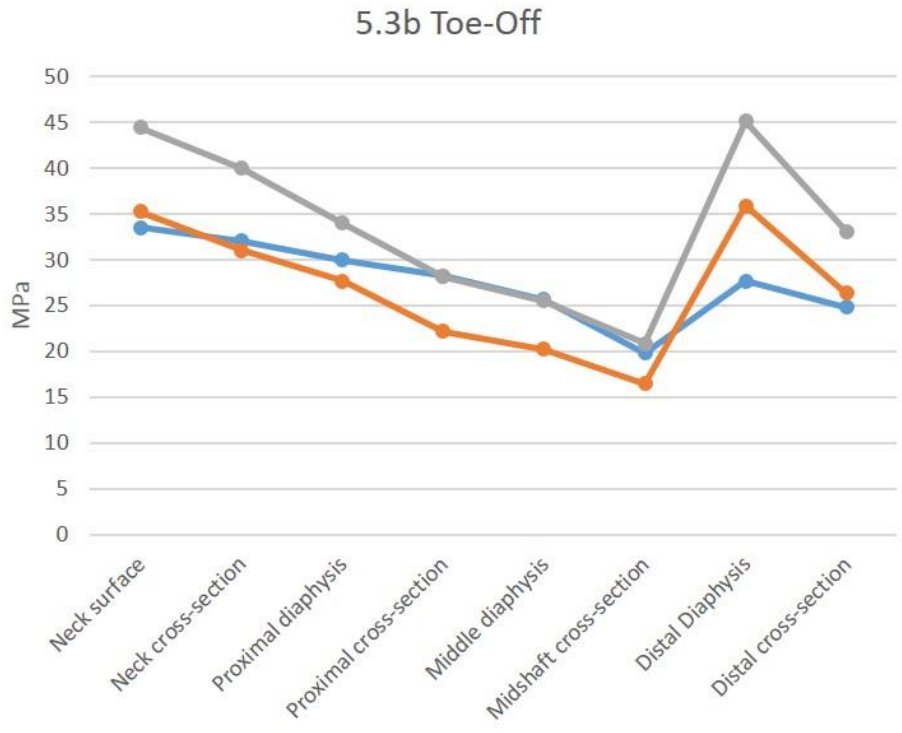

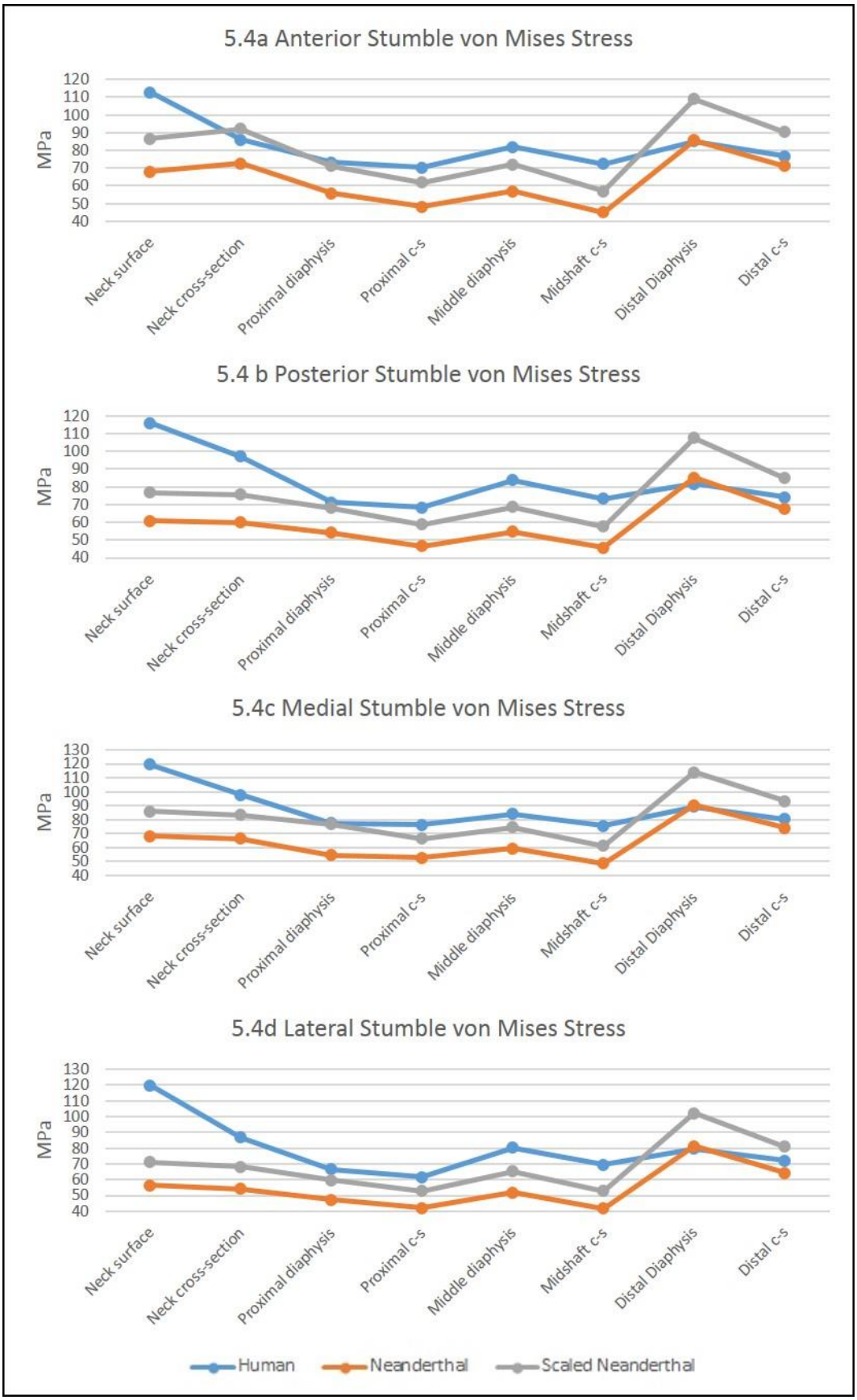
5.4a Anterior Stumble von Mises Stress
MPa
120
110
100
90
80
70
60
50
40
Neck surface
Neck cross-section
Proximal diaphysis
Proximal c-s
Middle diaphysis
Midshaft c-s
Distal Diaphysis
Distal c-s
5.4 b Posterior Stumble von Mises Stress
MPa
120
110
100
90
80
70
60
50
40
Neck surface
Neck cross-section
Proximal diaphysis
Proximal c-s
Middle diaphysis
Midshaft c-s
Distal Diaphysis
Distal c-s
5.4c Medial Stumble von Mises Stress
MPa
130
120
110
100
90
80
70
60
50
40
Neck surface
Neck cross-section
Proximal diaphysis
Proximal c-s
Middle diaphysis
Midshaft c-s
Distal Diaphysis
Distal c-s
5.4d Lateral Stumble von Mises Stress
MPa
130
120
110
100
90
80
70
60
50
40
Neck surface
Neck cross-section
Proximal diaphysis
Proximal c-s
Middle diaphysis
Midshaft c-s
Distal Diaphysis
Distal c-s
Human
Neanderthal
Scaled Neanderthal

Figure 5.5a Posteriorly Directed TL von Mises Stress

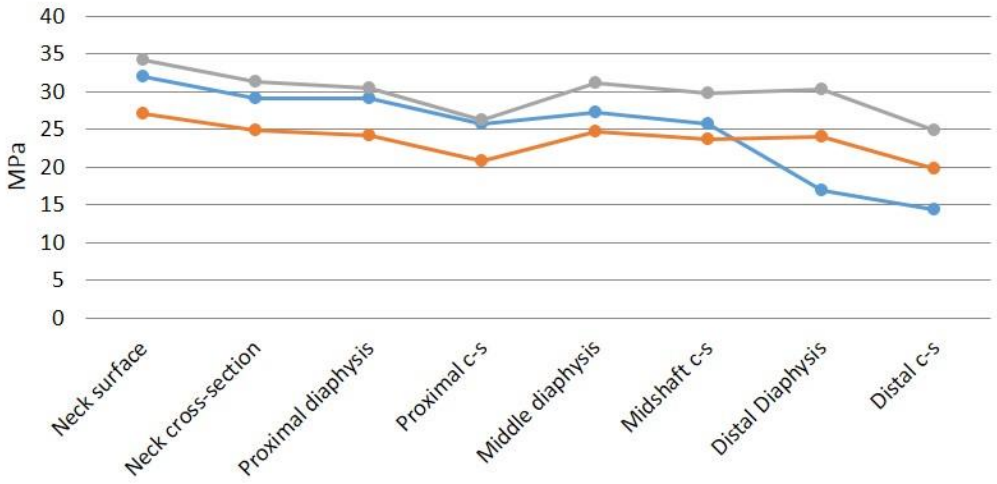

Figure 5.5b Medially Directed TL von Mises Stress

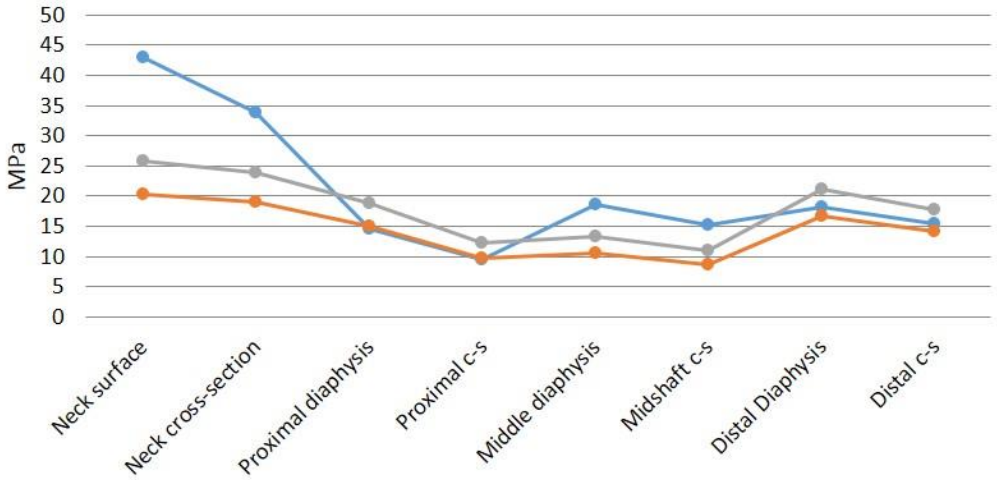

Figure 5.5c Postero-medially Directed TL von Mises Stress

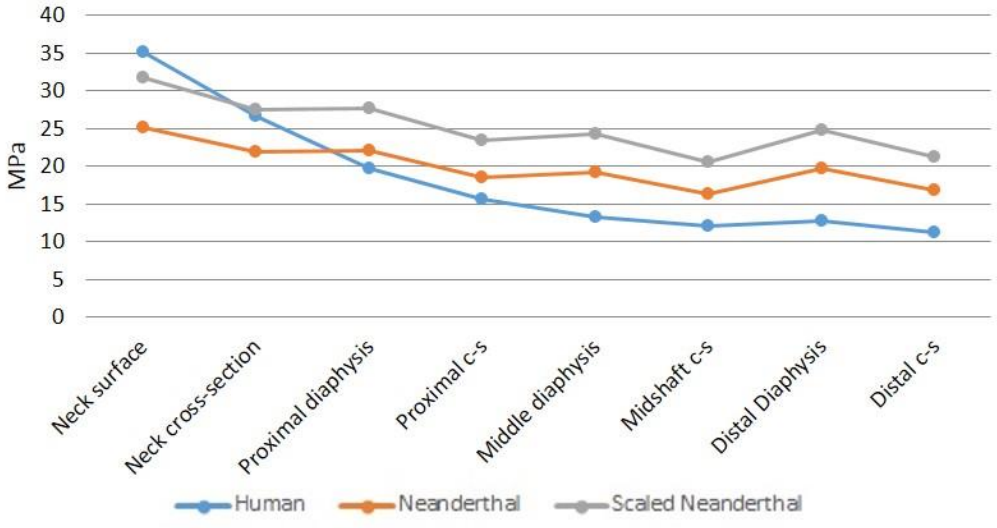

Table 5.11. Scaled Distances (mm) between Locations of peak von Mises stress

Heel-strike vs. Toe-off

Location	Human	Neanderthal
Neck surface	0.0159	0.3037
Neck cross-section	0.0571	0.1469
Proximal diaphysis	0.0797	0.0110
Proximal cross-section	0.0045	0.0142
Middle diaphysis	0.0013	0.0380
Midshaft cross-section	0.0012	0.0296
Distal Diaphysis	0.0091	0.0000
Distal cross-section	0.0041	0.0060
Total	0.1729	0.5494

Baseline (Heel-strike) vs. Anterior Stumble

	Human	Neanderthal
Neck surface	0.0000	1.6124
Neck cross-section	0.7863	9.8779
Proximal diaphysis	0.0000	0.2858
Proximal cross-section	0.1011	0.0854
Middle diaphysis	20.2271	21.0938
Midshaft cross-section	0.3497	0.7468
Distal Diaphysis	5.5339	0.0000
Distal cross-section	0.0071	0.0000
Total	27.0051	33.7021

Baseline (Heel-strike) vs. Posterior Stumble

	Human	Neanderthal
Neck surface	0.1136	0.0189
Neck cross-section	0.8153	9.1499
Proximal diaphysis	0.4532	0.4233
Proximal cross-section	0.1011	0.0854
Middle diaphysis	17.9540	21.0236
Midshaft cross-section	0.3497	0.7468
Distal Diaphysis	4.8452	0.0000
Distal cross-section	0.0071	0.0000
Total	24.6391	31.4479

Table 5.11 con't. Scaled Distances between Locations of Peak von Mises Stress

Baseline (Heel-strike) vs. Medial Stumble

	Human	Neanderthal
Neck surface	0.0000	0.0054
Neck cross-section	0.8153	9.9715
Proximal diaphysis	1.1193	0.3690
Proximal cross-section	0.1011	0.0854
Middle diaphysis	20.1245	18.5929
Midshaft cross-section	0.4035	0.7468
Distal Diaphysis	5.5339	0.0115
Distal cross-section	0.0071	0.0008
Total	28.1046	29.7834

Baseline (Heel-strike) vs. Lateral Stumble

	Human	Neanderthal
Neck surface	0.0000	0.0189
Neck cross-section	0.7863	9.7271
Proximal diaphysis	0.4532	0.1372
Proximal cross-section	0.1011	0.0854
Middle diaphysis	17.9540	21.0236
Midshaft cross-section	0.3497	0.7468
Distal Diaphysis	5.5629	0.0000
Distal cross-section	0.0071	0.0000
Total	25.2142	31.7390

Baseline (Heel-strike) vs. Posterior TL

	Human	Neanderthal
Neck surface	0.0163	0.0051
Neck cross-section	0.0425	0.1404
Proximal diaphysis	0.0898	0.1777
Proximal cross-section	0.0165	0.0251
Middle diaphysis	0.0557	0.0344
Midshaft cross-section	0.0444	0.0350
Distal Diaphysis	0.0046	0.0450
Distal cross-section	0.0284	0.0440
Total	0.2982	0.5066

Table 5.11 con't. Scaled Distances between Locations of Peak von Mises Stress

Baseline (Heel-strike) vs. Medial TL		
	Human	**Neanderthal**
Neck surface	0.0000	0.0051
Neck cross-section	0.0000	0.1410
Proximal diaphysis	0.0890	0.0059
Proximal cross-section	0.0154	0.0331
Middle diaphysis	0.1974	0.1875
Midshaft cross-section	0.0335	0.0675
Distal Diaphysis	0.2130	0.0770
Distal cross-section	0.0041	0.0000
Total	0.5523	0.5172

Baseline (Heel-strike) vs. Postero-medial TL		
	Human	**Neanderthal**
Neck surface	0.0234	0.0088
Neck cross-section	0.0429	0.1417
Proximal diaphysis	0.0874	0.0065
Proximal cross-section	0.0261	0.0331
Middle diaphysis	0.0514	0.0451
Midshaft cross-section	0.0525	0.0473
Distal Diaphysis	0.0115	0.0548
Distal cross-section	0.0172	0.0162
Total	0.3122	0.3536

Figure 5.6 Scaled distances between locations of peak von Mises Stress

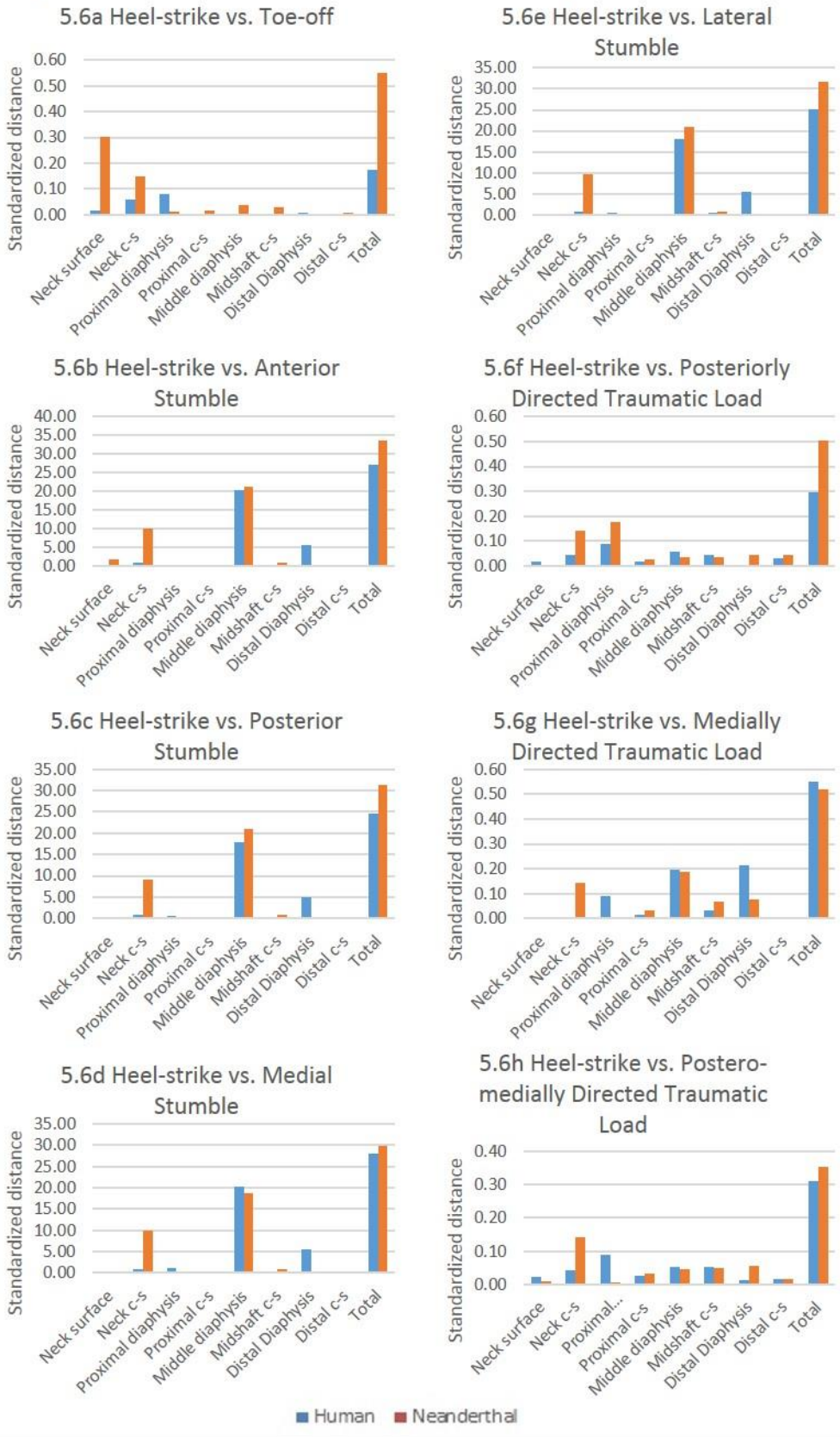

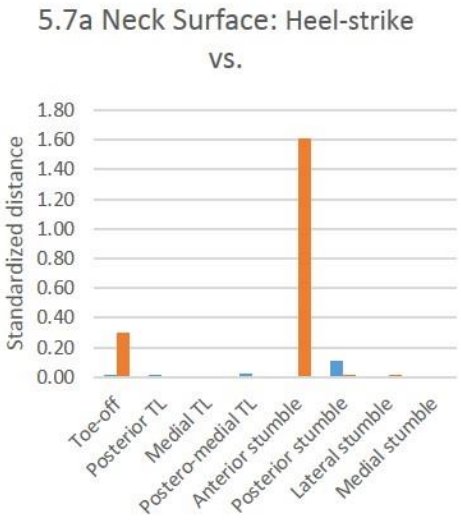

Figure 5.7 Distance between locations of peak von Mises stress within regions of interest under various loads

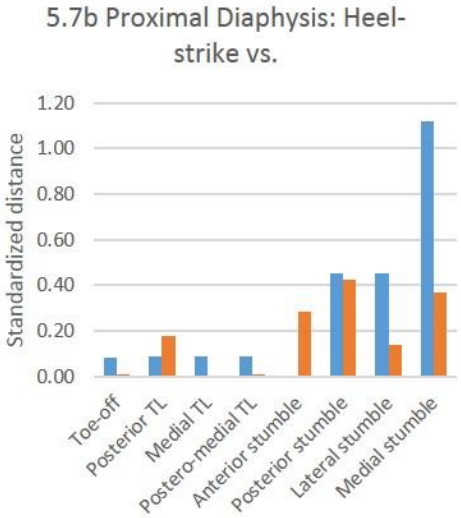

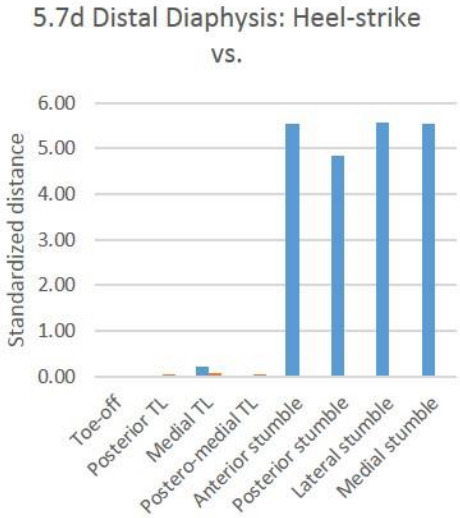

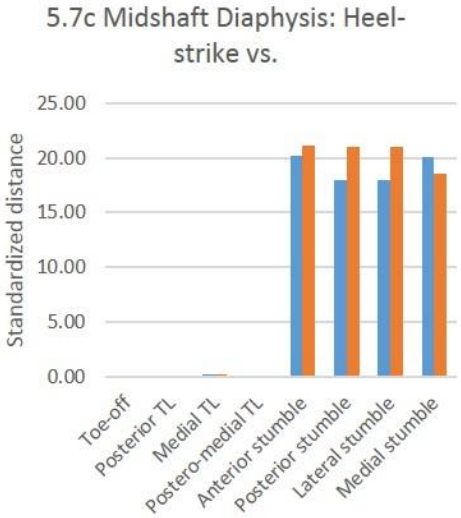

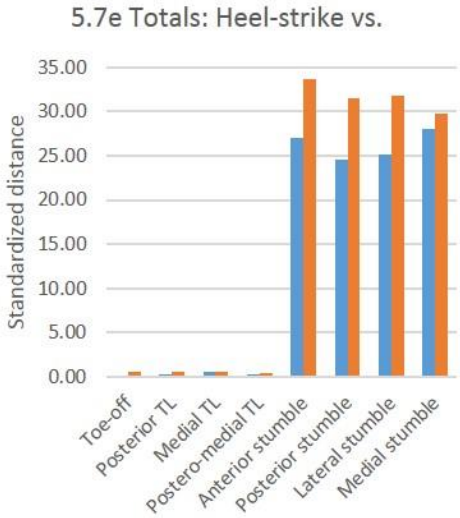

Figure 5.8 Distance between locations of peak von Mises stress within cross-sections under various loads

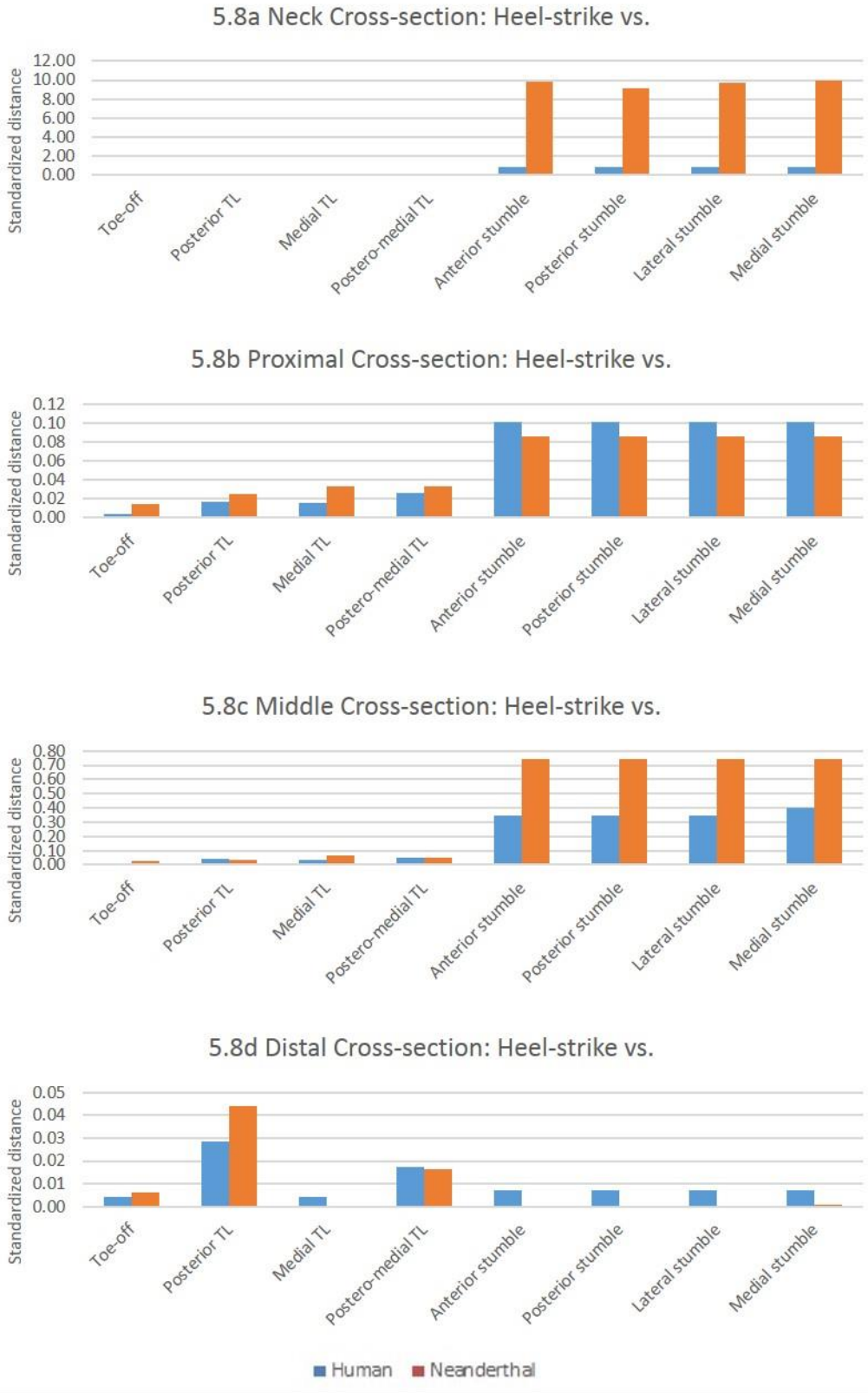

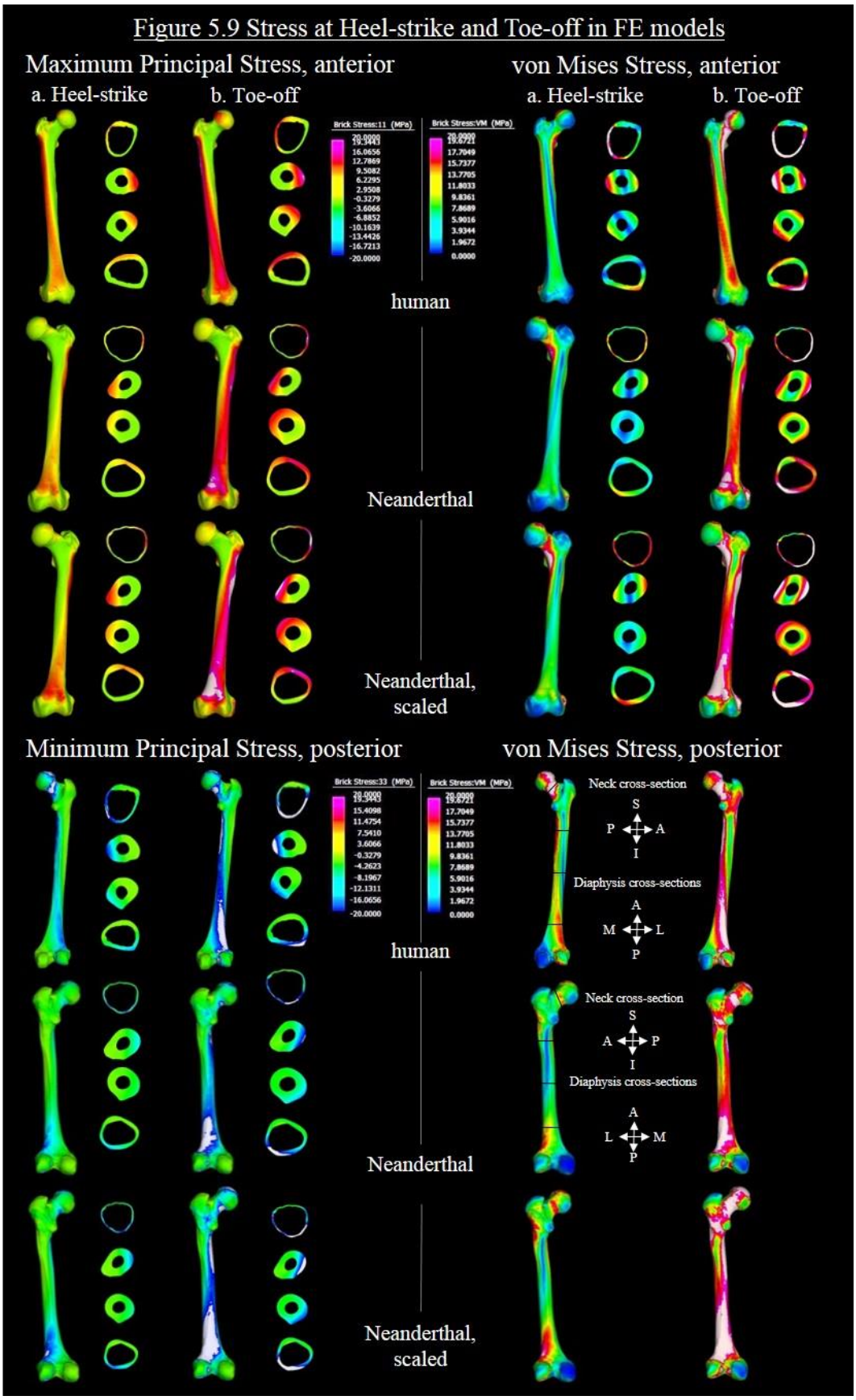
Figure 5.9 Stress at Heel-strike and Toe-off in FE models
Maximum Principal Stress, anterior
a. Heel-strike
b. Toe-off
von Mises Stress, anterior
a. Heel-strike
b. Toe-off
Brick Stress:11 (MPa)
20.0000
19.3443
16.0656
12.7869
9.5082
6.2295
2.9508
-0.3279
-3.6066
-6.8852
-10.1639
-13.4426
-16.7213
-20.0000
Brick Stress:VM (MPa)
20.0000
19.6721
17.7049
15.7377
13.7705
11.8033
9.8361
7.8689
5.9016
3.9344
1.9672
0.0000
human
Neanderthal
Neanderthal, scaled
Minimum Principal Stress, posterior
von Mises Stress, posterior
Brick Stress:33 (MPa)
20.0000
19.3443
15.4098
11.4754
7.5410
3.6066
-0.3279
-4.2623
-8.1967
-12.1311
-16.0656
-20.0000
Brick Stress:VM (MPa)
20.0000
19.6721
17.7049
15.7377
13.7705
11.8033
9.8361
7.8689
5.9016
3.9344
1.9672
0.0000
Neck cross-section
S
P
A
I
Diaphysis cross-sections
A
M
L
P
human
Neck cross-section
S
A
P
I
Diaphysis cross-sections
A
L
M
P
Neanderthal
Neanderthal, scaled

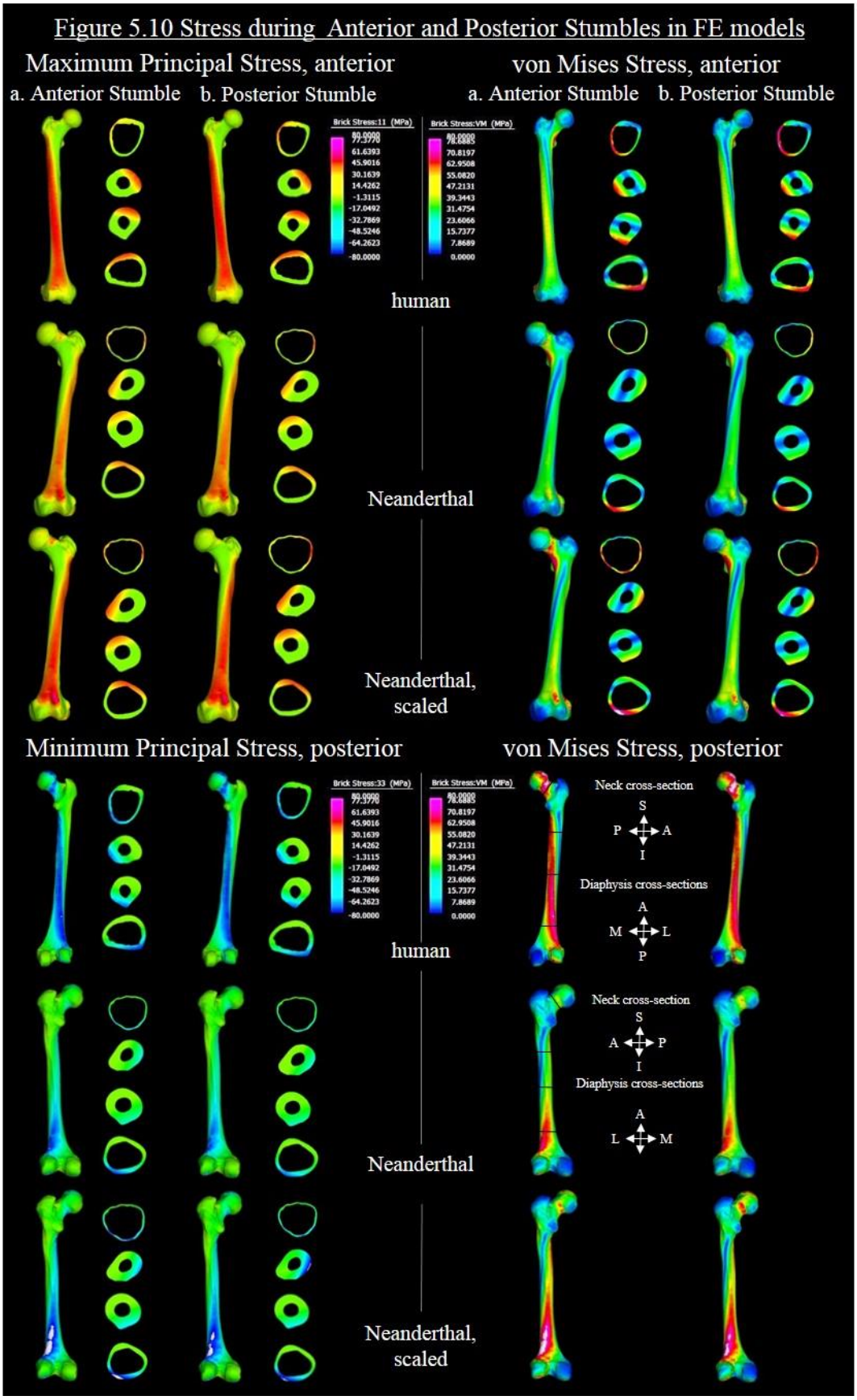
Figure 5.10 Stress during Anterior and Posterior Stumbles in FE models
Maximum Principal Stress, anterior
a. Anterior Stumble
b. Posterior Stumble
von Mises Stress, anterior
a. Anterior Stumble
b. Posterior Stumble
Brick Stress:11 (MPa)
Brick Stress:VM (MPa)
human
Neanderthal
Neanderthal, scaled
Minimum Principal Stress, posterior
von Mises Stress, posterior
Brick Stress:33 (MPa)
Neck cross-section
Diaphysis cross-sections
S
P
A
I
M
L

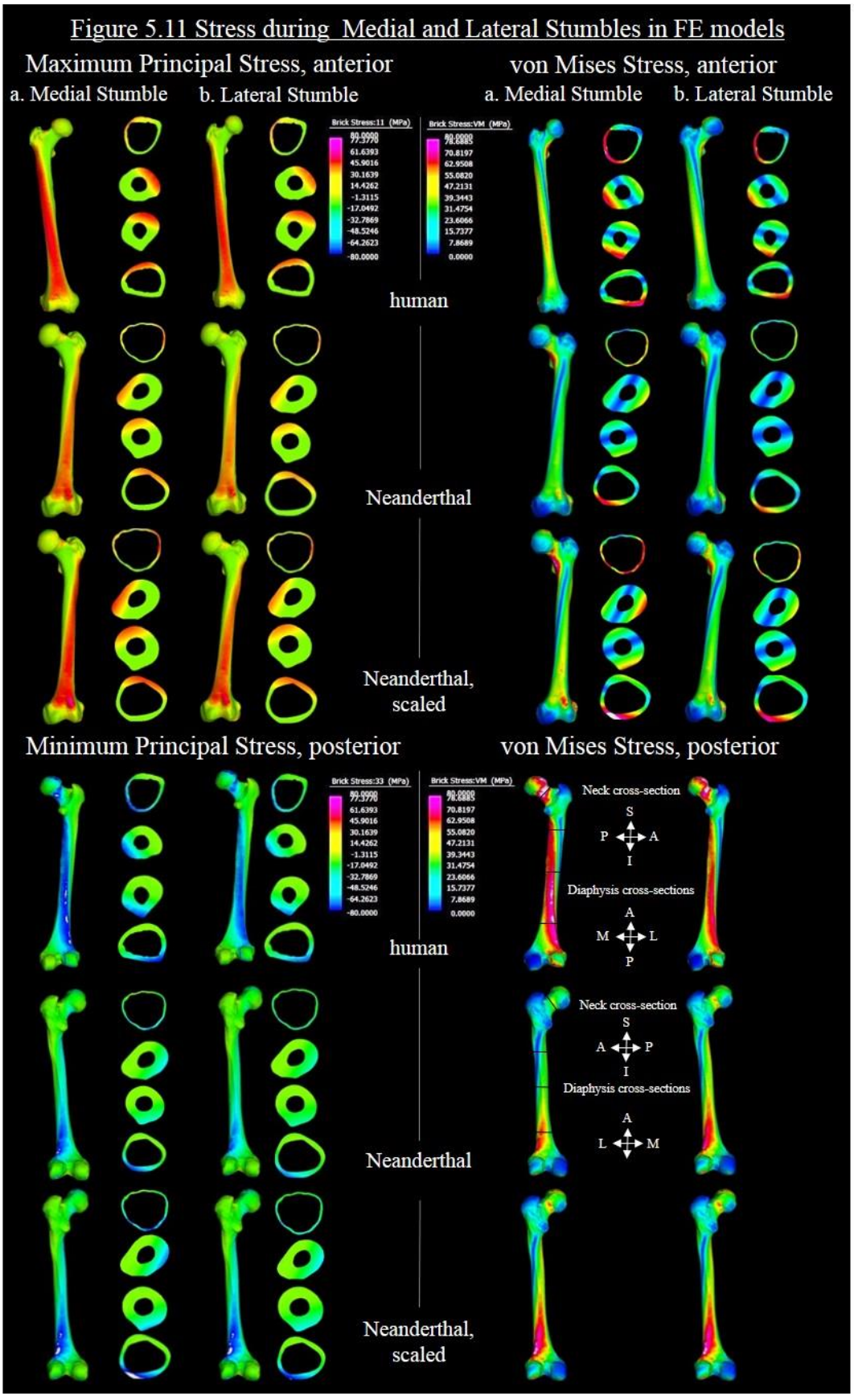
Figure 5.11 Stress during Medial and Lateral Stumbles in FE models
Maximum Principal Stress, anterior
a. Medial Stumble
b. Lateral Stumble
von Mises Stress, anterior
a. Medial Stumble
b. Lateral Stumble
Brick Stress:11 (MPa)
80.0000
77.3770
61.6393
45.9016
30.1639
14.4262
-1.3115
-17.0492
-32.7869
-48.5246
-64.2623
-80.0000
Brick Stress:VM (MPa)
90.0000
78.6885
70.8197
62.9508
55.0820
47.2131
39.3443
31.4754
23.6066
15.7377
7.8689
0.0000
human
Neanderthal
Neanderthal, scaled
Minimum Principal Stress, posterior
von Mises Stress, posterior
Brick Stress:33 (MPa)
Neck cross-section
S
P
A
I
Diaphysis cross-sections
A
M
L
P
human
Neanderthal
Neanderthal, scaled

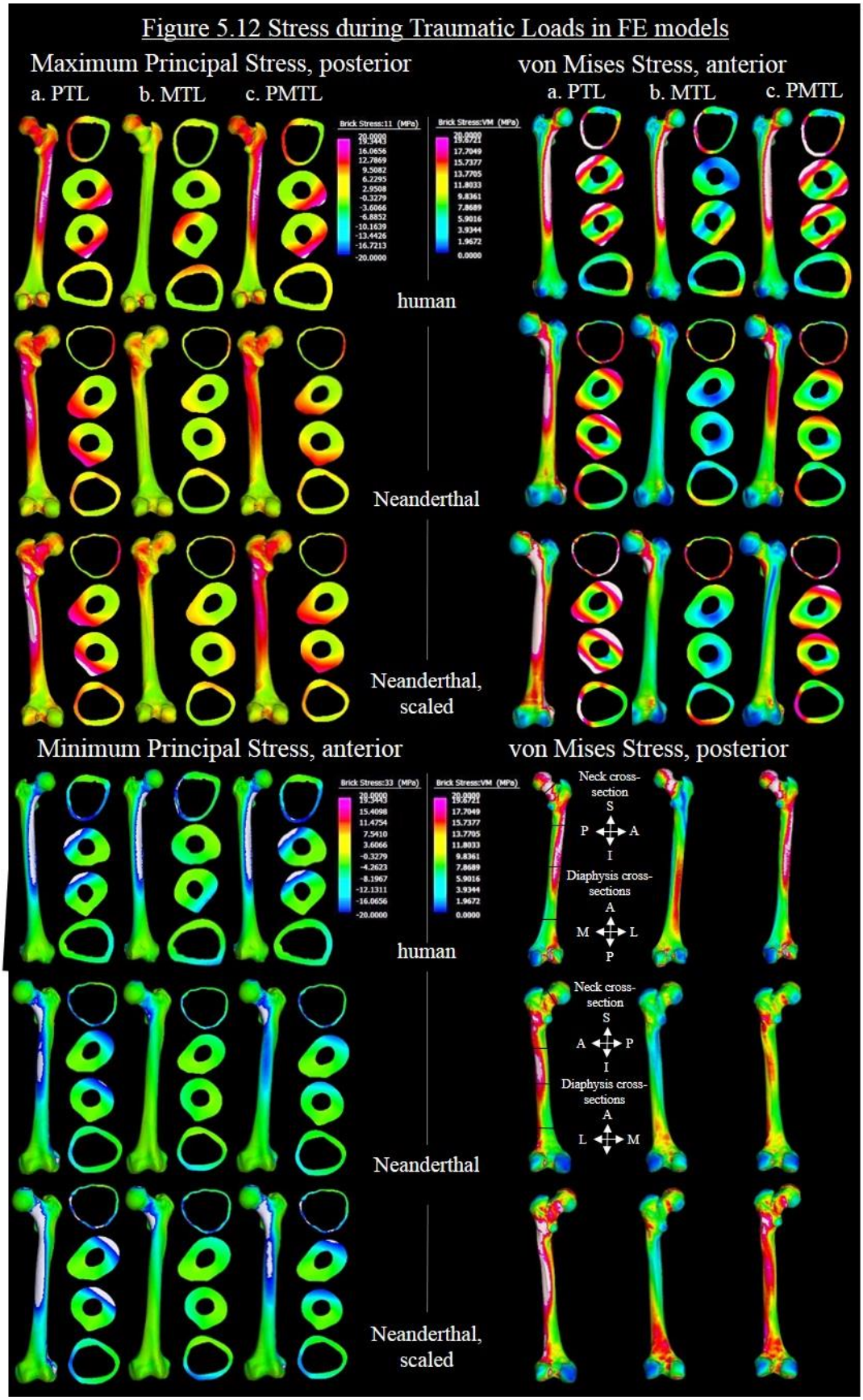
Figure 5.12 Stress during Traumatic Loads in FE models
Maximum Principal Stress, posterior
a. PTL
b. MTL
c. PMTL
Brick Stress:11 (MPa)
20.0000
18.3443
16.0656
12.7869
9.5082
6.2295
2.9508
-0.3279
-3.6066
-6.8852
-10.1639
-13.4426
-16.7213
-20.0000
Brick Stress:VM (MPa)
20.0000
19.2721
17.7049
15.7377
13.7705
11.8033
9.8361
7.8689
5.9016
3.9344
1.9672
0.0000
von Mises Stress, anterior
a. PTL
b. MTL
c. PMTL
human
Neanderthal
Neanderthal, scaled
Minimum Principal Stress, anterior
Brick Stress:33 (MPa)
20.0000
18.3443
15.4098
11.4754
7.5410
3.6066
-0.3279
-4.2623
-8.1967
-12.1311
-16.0656
-20.0000
Brick Stress:VM (MPa)
20.0000
19.2721
17.7049
15.7377
13.7705
11.8033
9.8361
7.8689
5.9016
3.9344
1.9672
0.0000
von Mises Stress, posterior
Neck cross-section
S
P
A
I
Diaphysis cross-sections
A
M
L
P
human
Neck cross-section
S
A
P
I
Diaphysis cross-sections
A
L
M
Neanderthal
Neanderthal, scaled

CHAPTER VI: CONCLUSION

The goal of this research project was to establish the biomechanical significance of two different femoral shapes that are characteristic of two separate, but related species, recent *Homo sapiens* and *Homo neanderthalensis*, and to then link the differences in each morphology's ability to dissipate stress to adaptations to specific habitual behaviors, if possible. To this end, three null hypotheses were tested according to predictions made based on extensive research about what differences in femoral morphology may mean. The first null hypothesis states that intra-generic primate species who range farther, as quantified by the ecological variable day range, would have equally robust and equally curved femora and humeri as primate species with more limited day ranges. I predicted that if the null hypothesis could be rejected, then primate species with longer day ranges would have more curved and more robust limb bones as an adaptation to improving predictability of stress transmission through the bone and to withstanding elevated loads, given that bone is an adaptive tissue and the strength of which is known to vary dependent on activity level. The sample used to test this hypothesis consisted of seven species within the genus *Cercopithecus*, commonly known as guenons; three species within the genus *Saguinus*, commonly known as tamarins; five species within the genus *Macaca*, commonly known as macaques; four species within the genus *Papio*, and one (the only) *Theropithecus*, all commonly known as baboons. Guenons, tamarins, and macaques are primarily arboreal quadrupeds, but species vary both in the amount of time spent in leaping and running, and also in their degree of terrestriality (particularly the macaques). Baboons are terrestrial quadrupeds. Total area (a measure of strength under compressive loads), second moments of area (measures of bending strength), polar moment of area (a measure of torsional strength), and section modulus (a measure of

average bending and torsional strength) were assessed on cross-sections from both humeri and femora at three levels corresponding to the proximal, midshaft, and distal portions of the bones. Antero-posterior curvature was measured on femora, and antero-posterior and medio-lateral curvature were measured on humeri. Variability in these variables was assessed using multiple regressions with body size as the covariate and day range as the independent variable.

Results from each genus prohibited the rejection of the null hypothesis. There was no pattern indicating that primates with longer day ranges had either more robust or more curved humeri/femora than primates with shorter day ranges. Others have found a significant relationship between presumed activity level and robusticity in hominin populations (Holt 2003; Holt et al. 2000; Ruff 2003; Ruff 2005; Ruff et al. 1993; Trinkaus and Ruff 1989; Trinkaus and Ruff 1999), so this result was somewhat surprising. One explanation is that these primates are quadrupedal, which means that load magnitude (body mass) is divided over four limbs rather than two. This would mean that differences in robusticity may be smaller and harder to detect. Another, and perhaps the best, explanation for the lack of significance regarding robusticity variables is that arboreal primates locomote on a compliant substrate (tree branches that sway) and that this compliancy lessens ground reaction forces (i.e. the force exerted by the ground/substrate on the body in contact with the ground/substrate) to such an extent that there is no physical need for increased robusticity as a consequence of increased loading. Biewener (1983) explored differences in the scaling of limb bones with changes in size. They found that animals across a wide range of sizes exhibit similar peak bone stress. It was proposed that the reason peak bone stress remains similar across different sized

animals is because larger animals (such as a horse) have straighter limbs, which reduces the bending moment the bones experiences. Additionally, larger animals have less curved limb bones than smaller animals. While smaller quadrupeds benefit from a crouched posture (that increases bending moments) because it allows them greater changes in momentum, larger animals benefit from decreasing bending moments, thereby reducing overall bone stress. Locomotion in an arboreal versus terrestrial setting has been shown to result in differences in cross-sectional properties indicating that multidirectional loading is favored in an arboreal environment (Carlson et al. 2006). Regarding insignificance of the curvature variable, results obtained through the FEA portion of this project suggest that cross-sectional asymmetry is a better means of increasing predictability than is increasing curvature under some loading conditions. Cross-sectional asymmetry was not directly studied in the intra-generic primate comparisons.

A potentially confounding factor within some, but not all, of these models is primate species within the same genus that have overlapping or identical day ranges. It would be interesting to explore relationships between robusticity variables and day range again, lumping primates with nearly identical day ranges together, and controlling for phylogeny in the statistical design. Scatterplots of humeral strength within the genus *Cercopithecus* suggest this might be a promising avenue of future research.

Despite a lack of significance in the intra-generic primate study, the results obtained from finite element analysis exploring strength and predictability of Neanderthal and human femur models are still valuable for the information they provide on the ability of different femoral morphologies to dissipate stress under the same loading conditions.

An important step of methods using finite element analysis is model validation. In order to ensure that a model is biologically sound, it is necessary to perform a validation study that compares the FE model's stress/strain pattern and magnitude to that of an in vivo (preferably) or in vitro study of the same type of bone. If stress/strain pattern and magnitude in both experiments show a close correspondence, then it can be assumed that the FE model behaves in a biologically realistic manner. In this study, the human FE model was compared to a cadaveric human femur in which a torque was applied to the femoral head that created antero-posterior bending. Stress was measured along the diaphysis at seven horizontal location on the cadaveric femur using strain gages. In the validation study, the human FE model which was loaded with the same torque and stress was measured at approximately the same locations at all seven horizontal levels. Stress from the cadaveric femur and FE model were compared and a close correspondence of both pattern and magnitude were observed. The largest difference was recorded at the most distal horizontal level and that is attributed to different constraints between the cadaveric and FEM femur. The author (Huiskes 1982) of the cadaveric femur analysis was vague in his description of the constraints and only stated that it was fixed in a laboratory setting. It is believed that the laboratory setting was slightly more rigid than the constraint scenario of the FEM femur. Despite this, differences were negligible and the FEM femur was judged to be biologically valid. Since the Neanderthal femur model was created using the same protocol as the human FE model, it is assumed that the Neanderthal femur is also valid. It is not possible to validate a Neanderthal femur model given the extinct nature of this hominin and the rarity of complete specimens.

After the completion of a satisfactory validation, experiments were performed with the human and Neanderthal FE models in order to test two additional null hypotheses. The second null hypothesis states that the human femur is equally as robust as the Neanderthal femur. I predicted that if the null hypothesis could be rejected, then the Neanderthal femur would be more robust given its larger size and historical description of hyper-robusticity. The third null hypothesis states that the human femur and Neanderthal femur behave equally predictably under the same loads. I predicted that if the null hypothesis could be rejected, then the Neanderthal femur would be more predictable given its more curved shape; curvature increases the predictability of stress transmission through a long bone.

In all, seven different loading experiments were carried out. In each experiment, the human femur model (HFM) and Neanderthal femur model (NFM) were loaded using the same magnitude acetabular contact forces (ACFs) and muscle forces. Additionally, muscle and ACFs were applied to the Neanderthal femur that were isometrically scaled to its volume$^{2/3}$ so that a comparison could be made between it and the HFM whose results were based strictly on shape differences rather than size *and* shape differences. Peak von Mises stress was measured at four surface locations (femoral neck, proximal, middle and distal diaphysis) and four cross-sections through each of these locations. Additionally, distance between locations (within a region) of peak von Mises stress was also calculated. Small distances between locations indicated high predictability.

Two experiments were conducted in which muscle and ACFs were applied to each FEM to simulate instances within the walking gait cycle when ACFs were highest: heel-strike and toe-off. During heel-strike the femur is slightly anterior to the pelvis and

during toe-off it is slightly posterior. These two experiments allowed a comparison of stress pattern, magnitude, and predictability in femora under loading conditions that were fairly similar in load magnitude, but quite different in orientation. Results from each indicate that the NFM is weakest along the distal diaphysis and the HFM is weakest along the neck. However, the pattern between models varies and it is apparent that the NFMs perform more poorly during toe-off than heel-strike. It was inconclusive which femur was stronger. Overall, predictability was very high on both models, but the HFM was more predictable on the neck and midshaft, whereas the NFM was more predictable on the proximal and distal diaphysis.

The next four experiments were designed to simulate irregular steps, such as might occur during a stumble. Stumbling is associated with minor changes in the orientation of ACFs, but much higher magnitudes. Accordingly, ACFs from heel-strike were tripled and rotated five degrees anteriorly, posteriorly, medially, and laterally. The same muscle forces were applied from the heel-strike experiment. Results from each experiment differed subtly, but a clear trend was evident. The HFM was always most stressed on the neck, and the NFM was most stressed at the distal diaphysis. The scaled NFM was always stronger than the HFM except at the distal diaphysis where it was less robust and at the proximal diaphysis where it was approximately equally stressed. Predictability was lowest in these experiments and the HFM was, without exception, overall more predictable in each stumbling experiment with the lowest difference between models occurring during the medial stumble. Again, the HFM was more predictable at the neck and midshaft, whereas the NFM was more predictable at the proximal and distal diaphysis.

The final three experiments were significant in that a force was applied orthogonally to the diaphysis in three directions, one each per experiment (posteriorly directed, medially directed, and postero-medially directed). Each force represented a traumatic load (TL) and yielded several interesting results. Notably the HFM performed best in the case of a postero-medially directed load, and the NFM performed best under a medially directed load. The NFM performed worst relative to the HFM in the posteriorly directed load. Stress remains high in the HFM neck and high in the distal femur of the NFMs, but relative to the other experiments, the distal diaphysis of the NFM is less stressed because the magnitude of stress increases in other regions as it also decreases in that region. The NFM is overall less predictable than the HFM in the posteriorly and postero-medially directed traumatic load cases, but not the medially directed TL. In the medially directed TL case, the HFM is overall less predictable by a scaled distance of 0.3, primarily because the NFM is highly predictable along the distal diaphysis.

Results from these experiments result in failure to reject the null hypotheses of equal robusticity during normal walking. The prediction that the Neanderthal femur is more robust was not confirmed; data were inconclusive. Regarding stumbling, the null hypothesis of equal robusticity was rejected; the NFM was stronger except at the distal diaphysis. Regarding traumatic loads, the null hypothesis of equal predictability was rejected; the HFM was as strong as, or stronger than, the NFM. The null hypothesis of equal predictability was rejected. The prediction that the Neanderthal femur was more predictable was rejected; overall, the opposite relationship was found, but within specific regions, the HFM is consistently stronger at the neck and midshaft, whereas the NFM was consistently more predictable at the proximal and distal diaphysis.

While curvature does increase bending predictability of a long bone, cross-sectional asymmetry also increases bending predictability. The antero-posteriorly elongated elliptical shape of the HFM's diaphysis provides better medio-lateral bending predictability and is influenced by the high neck-shaft angle of modern humans, while the low neck-shaft angle of Neanderthals increases medio-lateral bending. The longer femoral neck and higher neck-shaft angle in human femora result in increased stress in this region relative to the short femoral neck and smaller neck-shaft angle typical of Neanderthal femora. More curvature and a more distal point of maximum curvature in the Neanderthal femur result in increased stress along the distal diaphysis, particularly the lateral metaphysis.

A relationship could not be established between linear distance traveled (day range) and skeletal variables relating to robusticity in a diverse primate sample, probably because of the compliancy of their typical substrate. However, results from the FE study are not dependent on a quantification of mobility and if it is accurate to assume that a bone is modified to best perform its habitual function, or on a species level, to provide a level of fitness over a different morphology (be it from habitual behaviors or catastrophic events), then these results can inform inferences on behavior. One explanation for these differences is that Neanderthals retained a primitive circular cross-sectional geometry because they engaged in frequent medio-lateral movements (that modern humans did not) such that a circular shape conferred an advantage. Primate studies indicate that turning behaviors result in significantly higher medio-lateral forces compared to linear locomotion (Carlson and Judex 2007; Demes et al. 2006). Higher forces likely result in higher stress experienced by the bone, which could explain why species that incorporate

more medio-lateral movements would benefit by having bones reinforced in that dimension. Another option is that the longer femoral neck and larger neck-shaft angle in modern humans combined with differences in pelvic shape resulted in better dissipation of medio-lateral stress, a mechanism the Neanderthal femur did not have, thereby necessitating the retention of circular geometry in Neanderthals and a narrow medio-lateral dimension in modern humans. Overall, robusticity has less to do with cross-sectional geometry than with size. Early anatomically modern humans were similar to Neanderthals in their degree of robusticity and level of curvature, but different in cross-sectional geometry. This implies that the two species had differing means of increasing predictability.

Is strength or predictability more important in determining the outcome of femoral morphology? I suggest that strength is a more obvious choice as it is directly related to bone failure. However, given that early modern humans had femora that were equally robust as Neanderthals', *and* were presumably more predictable (given the results from the HFM created from a recent human femur), either early modern humans engaged in more linear long distance travel (the length of which decreased through time with increasing technological sophistication) while Neanderthals traversed terrain that necessitated frequent side-to-side movements, or the derived morphology of the human femur simply never entered the Neanderthal gene pool.

Proximal pedal phalanges in Neanderthals are proportionally wider than those of modern humans, and are overall more robust (Trinkaus and Hilton 1996), an indication that they may have been incorporating more medio-lateral movements into their locomotor repertoire perhaps due to irregular terrain or close-contact hunting with

thrusting spears that necessitated a wide stance (Churchill 1993; Shea 1990). Evidence from the foot, therefore, corroborates evidence from the femur that suggests Neanderthals and modern humans engaged in different behaviors which resulted in different patterns of stress in the lower limb.

REFERENCES

Abbott S, Trinkaus E, and Burr D. 1996. Dynamic Bone Remodeling in Later Pleistocene Fossil Hominids. American Journal of Physical Anthropology 99:585-601.

Aiello L, and Dean C. 1990. An introduction to human evolutionary anatomy. San Diego: Academic Press.

Aldrich-Blake. 1980. Long-tailed macaques, *Macaca fascicularis*. In: Chivers DJ, editor. Malayan Forest Primates: ten years' study in tropical rain forest. New York: Plenum. p 147-165.

Aldrich-Blake FPG, Bunn TK, Dunbar RIM, and Headley PM. 1971. Observations on baboons, Papio anubis, in an arid region in Ethiopia. Folia Primatologica 15:1-35.

Alexander RM. 1980. Optimum walking techniques for quadrupeds and bipeds. Journal of Zoology 197:97-117.

Alexander RM. 1984a. Stride length and speed for adults, children, and fossil hominids. American Journal of Physical Anthropology 63:23-27.

Alexander RM. 1984b. Walking and running. American Scientist 72:348-354.

Altmann SA, and Altmann J. 1970. Baboon ecology. Chicago: University of Chicago Press.

Anthony R, and Rivet P. 1907. Contribution a l'etude descriptive et morphologique de la diaphyse femorale chez l'homme et les anthropoides. Annales Des Sciences Naturelles (Zoologie). p 1-221.

Anton SC. 2003. Natural history of *Homo erectus*. Yearbook of Physical Anthropology 46:126-170.

Ballard ME, and Trudell MB. 1999. Anterior femoral curvature revisited: race assessment from the femur. Journal of Forensic Science 44(4):700-707.

Bell AL, Pedersen DR, and Brand RA. 1990. A comparision of the accuracy of several hip joint center location prediction methods. Journal of Biomechanics 23:617-621.

Berger TD, and Trinkaus E. 1995. Patterns of trauma among the Neandertals. Journal of Archaeological Science 22:841-852.

Bergmann G, Graichen F, and Rohlmann A. 1993. Hip joint loading during walking and running, measured in two patients. Journal of Biomechanics 26(8):969-990.

Bertram JEA, and Biewener AA. 1988. Bone curvature: sacrificing strength for load predictability. Journal of Theoretical Biology 131:75-92.

Bertrand M. 1969. The behavioral repertoire of the stumptailed macaque: a descriptive and comparative study. Basel: Karger.

Biewener AA. 1983. Allometry of quadrupedal locomotion: the scaling of duty factor, bone curvature and limb orientation to body size. Journal of Experimental Biology 105:147-171.

Biewener AA, and Taylor CR. 1986. Bone strain: A determinant of gait and speed? . Journal of Experimental Biology 123:383-400.

Biewener AA, Thomason J, Goodship AE, and Lanyon LE. 1983. Bone stress in the horse forelimb during locomotion at different gaits: a comparison of two experimental methods. Journal of Biomechanics 16:565-576.

Blake A. 1990a. Criteria of mechanical strength. Practical stress analysis in engineering design. 2nd ed. New York, New York: Marcel Dekker, Inc. p 43-49.

Blake A. 1990b. Stresses in shear and torsion. Practical Stress Analysis in Engineering Design. 2nd ed. New York: Marcel Dekker, Inc. p 16-28.
Boule M. 1911-1913. L'homme fossile de La Chapelle-aux-Saints. Annales de Paleontologie 6; 7; 8:111-172; 121-156, 185-192; 111-170.
Boule M, M. VH, and Verneau R. 1934. Les grottes paleolithiques des Beni Segoual (Algerie): anthropologie. Archives de l' Institut de Paleontologie Humaine 13:83-239.
Brand RA, Crowninshield RD, Wittstock CE, Pedersen DR, Clark CR, and van Krieken FM. 1982. A model of lower extremity muscular anatomy. Journal of Biomechanical Engineering 104:304-310.
Brand RA, Pedersen DR, Davy DT, Kotzar GM, Heiple KG, and Goldberg VM. 1994. Comparison of hip force calculations and measurements in the same patient. Journal of Arthroplaisy 9:45-51.
Butynski TM. 1990. Comparative ecology of blue monkeys (*Cercopithecus mitis*) in high- and low-density subpopulations. Ecological Monographs 60(1):1-26.
Carlson KJ. 2014. Linearity in the real world: an experimental assessment of nonlinearity in terrestrial locomotion. In: Carlson KJ, and Marchi D, editors. Reconstructing mobility: environmental, behavioral, and morphological determinants. New York: Springer. p 253-272.
Carlson KJ, Doran-Sheehy DM, Hunt KD, Nishida T, Yamanaka A, and Boesch C. 2006. Locomotor behavior and long bone morphology in individual free-ranging chimpanzees. Journal of Human Evolution 50:394-404.
Carlson KJ, Grine FE, and Pearson OM. 2007. Robusticity and sexual dimorphism in the postcranium of modern hunter-gatherers from Australia. American Journal of Physical Anthropology 134:9-23.
Carlson KJ, and Judex S. 2007. Increased non-linear locomotion alters diaphyseal bone shape. The Journal of Experimental Biology 210:3117-3125.
Carlson KJ, and Marchi D, editors. 2014. Reconstructing mobility: environmental, behavioral, and morphological determinants. New York: Springer. 295 p.
Castro R, and Soini P. 1977. Field studies on *Saguinus mystax* and other callitrichids in Amazonian Peru. In: Kleiman DG, editor. The biology and conservation of the Callitrichidae. Washington, D. C.: Smithsonian Institution Press. p 73-78.
Churchill SE. 1993. Weapon technology, prey size selection, and hunting methods in modern hunter-gatherers: implications for hunting in the Palaeolithic and Mesolithic. In: Peterkin GL, Bricker HM, and Mellars P, editors. Hunting and animal exploitation in the later Palaeolithic and Mesolithic of Eurasia: Archaeology Papers of the American Anthropology Association. p 11-24.
Cowgill LW. 2010. The ontogeny of Holocene and Late Pleistocene human postcranial strength. American Journal of Physical Anthropology 141:16-37.
Cowgill LW. 2014a. Femoral diaphyseal shape and mobility: an ontogenetic perspective. In: Carlson KJ, and Marchi D, editors. Reconstructing mobility: environmental, behavioral, and morphological determinants. New York: Springer. p 193-208.
Cowgill LW. 2014b. Femoral diaphyseal shape and mobility: an ontogenetic perspective. In: Marchi D, and Carlson KJ, editors. Mobility: interpreting behavior from skeletal adaptations and environmental interactions: Springer.

Cowgill LW, Warrener A, Pontzer H, and Ocobock C. 2010. Waddling and toddling: the biomechanical effects of an immature gait. American Journal of Physical Anthropology 143:52-61.
Crowninshield RD, Brand RA, and Johnston RC. 1978. The effect of walking velocity and age on hip kinematics and kinetics. Clinical Orthopedics 132:140-144.
Cullinane DM, and Einhorn TA. 2002. Biomechanics of bone. In: Bilezikian J, Riaisz L, and Rodan G, editors. Principles of bone biology. 2nd ed. San Diego: Academic Press. p 17-32.
Currey J. 2002. Bones: Structure and mechanics. Princeton: Princeton University Press.
Currey JD, Butler G, and England Y. 1975. The mechanical properties of bone tissue in children. The Journal of Bone and Joint Surgery 57-A:810-814.
Database N. 2012. Neanderthal Studies Professional Online Service.
Davy DT, Kotzar GM, Brown RH, Heiple KG, Goldberg VM, Heiple Jr. KG, Berilla J, and Burstein AH. 1988. Telemetric force measurements across the hip after total arthroplasty. Journal of Bone and Joint Surgery 70A:45-50.
Dawson GA. 1979. The use of time and space by the Panamanian tamarin, *Saguinus oedipus*. Folia Primatologica 31:253-284.
De Groote I. 2008. A comprehensive analysis of long bone curvature in Neanderthals and modern humans using 3D morphometrics. London: University College London.
Demes B, Carlson KJ, and Franz TM. 2006. Cutting corners: the dynamics of turning behaviors in two primate species. The Journal of Experimental Biology 209:927-937.
Demes B, and Jungers WL. 1993. Long bone cross-sectional dimensions, locomotor adaptations and body size in prosimian primates. Journal of Human Evolution 25:57-74.
DeVore I, and Hall KRL. 1965. Baboon ecology. In: DeVore I, editor. Primate behavior. New York: Holt, Rinehart, and Winston. p 20-52.
Duda G, Schneider E, and Chao E. 1997. Internal Forces and Moments in the Femur During Walking. Biomechanics 30(9):933-941.
Duda GN, Brand D, Freitag S, Lierse W, and Schneider E. 1996. Variability of femoral muscle attachments. Journal of Biomechanics 29(9):1185-1190.
Dumont ER, Grosse IR, and Slater GJ. 2009. Requirements for comparing the performance of finite element models of biological structures. Journal of Theoretical Biology 256(1):96-103.
Dunbar RIM, and Dunbar EP. 1974. Ecological relations and niche separation between sympatric terrestrial primates in Ethiopia. Folia Primatologica 21:36-60.
Friederich JA, and Brand RA. 1990. Muscle fiber architecture in the human lower limb. Journal of Biomechanics 23(1):91-95.
Frost HM. 1964. The laws of bone structure. Springfield: Charles C. Thomas.
Frost HM. 1987. Bone "mass" and the "mechanostat": a proposal. Anatomical Record 219:1-9.
Garber PA. 1993. Feeding ecology and behaviour of the genus *Saguinus*. In: Rylands AB, editor. Marmosets and tamarins: systematics, behaviour, and ecology. Oxford: Oxford University Press. p 273-295.
Gautier-Hion A, and Gautier J-P. 1974. Les associations polyspecifiques de Cercopitheques du Plateau de M'passa (Gabon). Folia Primatologica 22:134-177.

Gautier-Hion A, Quris R, and Gautier J-P. 1983. Nonospecific vs polyspecific life: a comparative study of foraging and antipredatory tactics in a community of *Cercopithecus* monkeys. Behavioral Ecology and Sociobiology 12:325-335.
Gautier-Hion PA, and Gautier J-P. 1978. Le Singe de Brazza: Une strategie originale. Z Tierpsychol 46:84-104.
Gilbert BM. 1976. Anterior femoral curvature: its probably basis and utility as a criterion of racial assessment. American Journal of Physical Anthropology 45(3):601-604.
Goodship AE, Lanyon LE, and MacFie H. 1979. Functional adaptation of bone to increased stress. Journal of Bone and Joint Surgery 61-A:539-546.
Grosse IR, Dumont ER, Coletta C, and Tolleson A. 2007. Techniques for modeling muscle-induced forces in finite element models of skeletal structures. Anatomical Record 290(9):1069-1088.
Harding RSO. 1976. Ranging patterns of a troop of baboons (Papio anubis) in Kenya. Folia Primatologica 25:143-185.
Haut Donahue TL, Hull ML, Rashid MM, and Jacobs CR. 2002. A finite element model of the human knee joint for the study of tibio-femoral contact. Journal of Biomechanical Engineering 124:273-280.
Heim JL. 1982. Les hommes fossiles de La Ferrassie II: les squelletes adultes (squelette des membres). Archives de l' Institut de Paleontologie Humaine 38:1-272.
Hert J, Fiala P, and Petrtyl M. 1994. Osteon orientation of the diaphysis of the long bones in man. Bone 15:269-277.
Hert J, Liskova M, and Landa J. 1971. Reaction of bone to mechanical stimuli. Part I. Continuous and intermittent loading of tibia in rabbit. Folia Morphologica 19:290-300.
Hert J, Liskova M, and Landgrot B. 1969. Influence of the long-term continuous bending on the bone. An experimental study on the tibia of the rabbit. Folia Morphologica 17:389-399.
Hert J, Pribylova E, and Liskova M. 1972. Reaction of bone to mechanical stimuli. Part 3. Microstructure of compact bone of rabbit tibia after intermittent loading. Acta Anatomica 82:218-230.
Higgins RW. 2014. The effects of terrain on long bone robusticity and cross-sectional shape in lower limb bones of bovids, Neandertals, and Upper Paleolithic modern humans. In: Carlson KJ, and Marchi D, editors. Reconstructing mobility: environmental, behavioral, and morphological determinants. New York: Springer. p 227-252.
Hildebrand M. 1995. Analysis of vertebrate structure. New York: John Wiley & Sons, Inc.
Holt BM. 2003. Mobility in Upper Paleolithic and Mesolithic Europe: evidence from the lower limb. American Journal of Physical Anthropology 122:200-215.
Holt BM, Mussi M, Churchill SE, and Formicola V. 2000. Biological and cultural trends in Upper Palaeolithic Europe. Riv Anthropol (Roma) 78:179-182.
Ivanenko YP, Poppele RE, and Lacquaniti F. 2004. Five basic muscle activation patterns account for muscle activity during human locomotion. Journal of Physiology 556(1):267-282.

Jade S, Tamvada KH, Strait DS, and Grosse IR. 2014. Finite element analysis of a femur to deconstruct the paradox of bone curvature. Journal of Theoretical Biology 341:53-63.

Jones HH, Priest JD, Hayes WC, Tichenor CC, and Nagel DA. 1977. Humeral hypertrophy in response to exercise. Journal of Bone and Joint Surgery 59A:204-208.

Kaneko TS, Bell JS, Pejcic MR, Tehranzadeh J, and Keyak JH. 2004. Mechanical properties, density, and quantitative CT scan data of trabecular bone with and without metastes. Journal of Biomechanics 37:523-530.

Kaplin BA. 2001. Ranging behavior of two species of guenons (*Cercopithecus lhoesti and C. mitis doggetti*) in the Nyungwe Forest Reserve, Rwanda. International Journal of Primatology 22(4):521-548.

Kelly RL. 1995. The foraging spectrum-diversity in hunter-gatherer lifeways. Washington: Smithsonian Institution Press.

Keyak J, and Rossi S. 2000. Prediction of femoral fracture load using finite element models: an

examination of stress- and strain-based failure models. Journal of Biomechanics 33:209-214.

Krolner B, and Toft B. 1963. Vertebral bone loss, an unheeded side effect of therapeutic bed rest. Clinical Science 64:537-540.

Kummer H. 1990. The social system of hamadryas baboons and its presumable evolution. In: de Mello MT, Whiten A, and Byrne RW, editors. Baboons: behaviour and ecology, use and care. Brazil: Brasilia. p 43-60.

Kurup GU, and Kumar A. 1993. Time budget and activity patterns of the lion-tailed macaque (*Macaca silenus*). International Journal of Primatology 14(1):27-39.

Kuruvilla GP. 1980. Ecology of the bonnet macaque (*Macaca radiata Geoffroy*) with special reference to feeding habits. Journal of Bombay Natural History Society 75:976-988.

Lanyon LE. 1980. The influence of function on the development of bone curvature. An experimental study on the rat tibia. Journal of Zoology: Proceedings of the Zoological Society of London 192:457-466.

Lanyon LE. 1987. Functional Strain In Bone Tissue As An Objective, and Controllng Stimulus for Adaptive Bone Remodelling. Biomechanics 20(11/12):1083-1093.

Lanyon LE, and Baggott DG. 1976. Mechanical function as an influence on the structure and form of bone. The Journal of Bone and Joint Surgery 58-B(4):436-443.

Lanyon LE, and Bourn S. 1979. The influence of mechanical function on the development and remodeling of the tibia: an experimental study in sheep. Journal of Bone and Joint Surgery 61:263-273.

Lanyon LE, Goodship AE, Pye CJ, and MacFie H. 1982. Mechanically adaptive bone remodeling. Journal of Biomechanics 15:141-154.

Lanyon LE, Magee PT, and Baggot DG. 1979. The relationship of functional stress and strain to the processes of bone remodeling. An experimental study on the sheep radius. Journal of Biomechanics 12:593-600.

Larsen CS. 1987. Bioarchaeological interpretations of subsistence economy and behavior from human skeletal remains. Advances in Archaeological Method and Theory 10:339-445.

Lengsfeld M, Kaminsky J, Merz B, and Franke R. 1996. Sensitivity of Femoral Strain Pattern Analysis to Resultant and Muscle Forces at Hip Joint. Medical Engineering and Physics 18(1):70-78.
Lieberman DE, Polk JD, and Demes B. 2004. Predicting long bone loading from cross-sectional geometry. American Journal of Physical Anthropology 123:156-171.
Lindburg DG. 1977. Feeding behaviour and diet of rhesus monkey (*Macaca mulatta*) in Siwalik forest of north India. In: Clutton-Brock TH, editor. Primate ecology: studies of feeding and ranging behaviour in lemurs, monkeys, and apes. London: Academic Press. p 223-250.
MacKinnon JR, and MacKinnon KS. 1980. Niche differentiation in a primate community. In: Chivers DJ, editor. Malayan Forest Primates: Ten Years' Study in Tropical Rain Forest. New York: Plenum Press. p 167-190.
Mann RA, and Hagy J. 1980. Biomechanics of walking, running, and sprinting. American Journal of Sports Medicine 8(5):345-350.
Morgan EF, and Keaveny TM. 2001. Dependence of yield strain of human trabecular bone on anatomic site. Journal of Biomechanics 34:569-577.
Neyman PF. 1977. Aspects of the ecology and social organization of free-ranging cotton-top tamarins (*Saguinus oedipus*) and the conservation status of the species. In: Kleiman DG, editor. The biology and conservation of the Callitrichidae. Washington, D. C.: Smithsonian Institution Press. p 39-71.
Nordstrom P, Thorsen K, Bergstrom E, and Lorentzon R. 1996. High bone mass and altered relationships between bone mass, muscle strength, and body constitution in adolescent boys on a high-level of physical-activity. Bone 19:189-195.
O'Brien TG, and Kinnaird MF. 1997. Behavior, diet, and movements of the Sulawesi crested black macaque (*Macaca nigra*). International Journal of Primatology 18(3):321-351.
O'Connor JA, and Lanyon LE. 1982. The influence of strain rate on adaptive bone remodelling. Journal of Biomechanics 15(10):767-781.
Patte E. 1955. Les Neanderthaliens. Paris: Masson.
Paul J. 1971a. Load Actions on the Human Femur in Walking and Some Resultant Stresses. Experimental Mechanics 11:121-125.
Paul JP. 1971b. Load actions on the human femur in walking and some resultant stresses. Experimental Mechanics 11:121-125.
Pauwels F. 1980. Biomechanics of the locomotor apparatus: contributions on the functional anatomy of the locomotor apparatus. Berlin: Springer-Verlag.
Payne J, and Francis CM. 1985. A field guide to mammals of Borneo. Sabah: Sabah Society.
Pearson OM, Petersen TR, Sparacello VS, Daneshvari SR, and Grine FE. 2014. Activity, "body shape," and cross-sectional geometry of the femur and tibia. In: Carlson KJ, and Marchi D, editors. Reconstructing mobility: environmental, behavioral, and morphological determinants. New York: Springer. p 133-152.
Peterson J, and Dechow PC. 2003. Material properties of the human cranial vault and zygoma. The Anatomical Record Part A 274A(1):785-797.
Popov EP. 1978. Mechanics of Materials. Englewood Cliffs, NJ: Prentice Hall.
Rak Y. 1991. The pelvis. In: Bar Yosef O, and Vandersmeerch B, editors. Le Squelette Mousterien de Kebara 2. Paris: Editions du C. N. R. S. p 147-156.

Rasband WS. 1997-2014. ImageJ. Bethesda, Maryland: U. S. National Institutes of Health.
Reilly DT, and Burstein AH. 1975. The elastic and ultimate properties of compact bone tissue. Journal of Biomechanics 8:393-405.
Richmond BG, Wright BW, Grosse I, Dechow PC, Ross CF, Spencer MA, and Strait DS. 2005. Finite element analysis in functional morphology. The Anatomical Record Part A 283A:259-274.
Rowell TE. 1966. Forest living baboons in Uganda. J Zool, London 149:344-364.
Rubin CT, and Lanyon LE. 1982. Limb mechanics as a function of speed and gait: a study of functional strains in the radius and tibia of horse and dog. . Journal of Experimental Biology 101:187-211.
Ruff C. 1995. Biomechanics of the hip and birth in early *Homo*. American Journal of Physical Anthropology 98:527-574.
Ruff C. 2003. Ontogenetic adaptation to bipedalism: age changes in femoral to humeral length and strength proportions in humans, with a comparison to baboons. Journal of Human Evolution 45:317-349.
Ruff C. 2005. Mechanical Determinants of Bone Form: Insights from Skeletal Remains. Muculoskelet Neutonal Interact 5(3):202-212.
Ruff C, Holt B, and Trinkaus E. 2006. Who's afraid of the big bad Wolff?: "Wolff's Law" and bone functional adaptation. American Journal of Physical Anthropology 129:484-498.
Ruff CB. 1994. Morphological adaptation to climate in modern and fossil hominids. American Journal of Physical Anthropology 19(Supplement 19):65-107.
Ruff CB. 2002. Long bone articular and diaphyseal structure in Old World monkeys and apes. I: Locomotor effects. American Journal of Physical Anthropology 119:305-342.
Ruff CB, Trinkaus E, Walker A, and Larsen CS. 1993. Postcranial robusticity in *Homo.* I: Temporal trends and mechanical interpretation. American Journal of Physical Anthropology 91:21-53.
Sawyer GJ, and Maley B. 2005. Neanderthal reconstructed. The Anatomical Record Part B: The New Anatomist 283B(1):23-31.
Schackelford LL, and Trinkaus E. 2002. Late Pleistocene human femoral diaphyseal curvature. American Journal of Physical Anthropology 118:359-370.
Schwalbe G. 1919. Studien uber das femur von Pithecanthropus erectus Dubois. Zeitschrift Fur Morphologie Und Anthropologie 21:289-360.
Shackelford LA. 2014. Variation in mobility and anatomical responses in the Late Pleistocene. In: Carlson KJ, and Marchi D, editors. Reconstructing mobility: environmental, behavioral, and morphological determinants. New York: Springer. p 153-172.
Shackelford LL, and Trinkaus E. 2002. Late Pleistocene human femoral diaphyseal curvature. American Journal of Physical Anthropology 118:359-370.
Shea J. 1990. The behavioral significance of Levantine Mousterian industrial variability: Harvard University.
Sigg H, and Stolba A. 1981. Home range and daily march in a hamadryas baboon troop. Folia Primatologica 36:40-75.

Skerry TM. 2000. Biomechanical influences on skeletal growth and development. In: O'Higgins P, and Cohn MJ, editors. Development growth and evolution: implications for the study of the hominid skeleton. San Diego: Academic Press. p 29-39.
Sladek V, E. T, Hillson SW, and Holliday TW. 2000. The people of the Pavlovian: skeletal catalogue and osteometrics of the Gravettian fossil hominids from Dolni Vestonice and Pavlov. Dolni Vestonice studies 5. Brno: Akademie ved Ceske Republicky.
Sparacello VS, Marchi D, and Shaw CN. 2014. The importance of considering fibular robusticity when inferring the mobility patterns of past populations. In: Carlson KJ, and Marchi D, editors. Reconstructing obility: environmental, behavioral, and morphological determinants. New York: Springer. p 91-110.
Stewart TD. 1962. Anterior femoral curvature: its utility for race identification. Human Biology 34:9-62.
Stock J, and Shaw C. 2007. Which measures of diaphyseal robusticity are robust? A comparison of external methods of quantifying the strength of long bone diaphyses to cross-sectional geometric properties. American Journal of Physical Anthropology 134:412-423.
Stoltz LP, and Saayman GS. 1970. Ecology and behavior of baboons in the northern Transvaal. Ann Transvaal Mus 26:99-143.
Strait DS, Wang Q, Dechow PC, Ross CF, Richmond BG, Spencer MA, and Patel BA. 2005. Modeling elastic properties in finite element analysis: how much precision is needed to produce an accurate model? Anatomical Record 283A:275-287.
Struhsaker TT. 1980. Comparison of the behaviour and ecology of red colobus and redtail monkeys in the Kibale Forest, Uganda. African Journal of Ecology 18:33-51.
Sugiyama Y. 1971. Characteristics of the social life of bonnet macaques (*Macaca radiata*). Primates 12:247-266.
Suzuki R. 1985. Human adult walking. In: Kondo S, editor. Primate morphophysiology, locomotor analysis and human bipedalism. Tokyo: University of Tokyo Press. p 3-24.
Swartz SM. 1990. Curvature of the forelimb bones of anthropoid primates: overall allometric patterns and specializations in suspensory species. American Journal of Physical Anthropology 83:477-498.
Taylor M, Tanner K, Freeman M, and Yettram A. 1996a. Stress and strain distribution within the intact femur: compression or bending? Medical Engineering and Physics 18(2):122-131.
Taylor ME, Tanner KE, Freeman MAR, and Yettram AL. 1996b. Stress and strain distribution within the intact femur: compression or bending? Med Eng Phys 18:122-131.
Terborgh J. 1983. Five New World primates: a study in comparative ecology. Princeton: Princeton University Press.
Tilton FE, Degioanni TTC, and Schneider VS. 1980. Long term follow up on Skylab bone demineralisation. Aviation, Space, and Environmental Medicine 51:209-213.
Trinkaus E. 1983. The Shanidar Neandertals. New York: Academic Press.

Trinkaus E. 1984. Neandertal pubic morphology and gestation length. Current Anthropology 25:509-514.
Trinkaus E. 1986. The Neandertals and modern human origins. Annual Review of Anthropology 15:193-218.
Trinkaus E. 1993. Femoral neck-shaft angles of the Qafzeh-Skhul early modern humans, and activity levels among immature Near Eastern Middle Paleolithic hominids. Journal of Human Evolution 25:393-416.
Trinkaus E, Churchill S, Ruff C, and Vandermeersch B. 1999a. Long Bone Shaft Robusticity and Body Proportions of the Saint-Cesaire 1 Chatelperronian Neanderthal. Archaeological Science 26:753-773.
Trinkaus E, and Hilton C. 1996. Neandertal Pedal Proximal Phalanges: Diaphyseal Loading Patterns. Journal of Human Evolution 30:399-425.
Trinkaus E, and Ruff C. 1989. Diaphyseal cross-sectional morphology and biomechanics of the Fond-de-Foret 1 femur and the Spy 2 femur and tibia. Anthropologie et Prehistoire 100:33-42.
Trinkaus E, and Ruff CB. 1999. Diaphyseal cross-sectional geometry of Near Eastern Middle Palaeolithic humans: the femur. Journal of Archaeological Science 26:409-424.
Trinkaus E, Ruff CB, and Conroy GC. 1999b. The anomalous archaic *Homo* femur from Berg Aukas, Namibia: A biomechanical assessment. American Journal of Physical Anthropology 110:379-391.
Triola MM, and Triola ME. 2006. Biostatistics for the biologial and health sciences. Boston: Pearson. 699 p.
Turner CH, Owan I, and Takano Y. 1995. Mechanotransduction in bone: role of strain-rate. American Journal of Physiology-Endocrinology and Metabolism 32:E438-E442.
Tuttle RH, Basmajian JV, and Ishida H. 1979a. Activites of pongid thigh muscles during bipedal behavior. American Journal of Physical Anthropology 50:123-136.
Tuttle RH, Cortright GW, and Buxhoeveden DP. 1979b. Anthropology on the move: progress in experimental studies of nonhuman primate positional behavior. Yearbook of Physical Anthropology 22:187-214.
Vandermeersch B. 1981. Les Hommes Fossiles de Qafzeh (Israel). Paris: Editions du C. N. R. S.
Vogt PW. 1993. Dictionary of statistics and methodology: a nontechnical guide for the social sciences. Newbury Park: Sage Publications, Inc. 253 p.
Voo L, Armand M, and Kleinberger M. 2004. Stress fracture risk analysis of the human femur based on computational biomechanics. Johns Hopkins APL Technical Digest 25(3):223-230.
Walensky NA. 1965. A study of anterior femoral curvature in man. Anatomical Record 151:559-570.
Wang Q, and Dechow PC. 2006. Elastic properties of external cortical bone in the craniofacial skeleton of the Rhesus monkey. American Journal of Physical Anthropology 131:402-415.
Wheatley BP. 1980. Feeding and ranging of east Bornean *Macaca fascicularis*. In: Lindburg DG, editor. The macaques: studies in ecology, behavior, and evolution. New York: Van Nostrand Reinhold. p 215-246.

Whitesides GH. 1989. Interspecific associations of Diana monkeys, *Cercopithecus diana*, in Sierra Leone, West Africa: biological significance or chance? Animal Behavior 37:760-776.

Wirtz CD, Schilers N, Pandorf T, Radermacher K, Weichert D, and Forst R. 2000. Critical evaluation of known bone material properties to realize anisotropic FE-simulation of the proximal femur. Journal of Biomechanics 33:1325-1330.

Woo SL-Y. 1981. The relationships of changes in stress levels on long bone remodeling. American Society of Mechanical Engineers, Applied Mechanics Division, AMD 45:107-129.

Yamanaka A, Gunji H, and Ishida H. 2005. Curvature, length, and cross-sectional geometry of the femur and humerus in anthopoid primates. American Journal of Physical Anthropology 127:46-57.

Zienkiewicz O, Taylor R, and Zhu J. 2005. The finite element method: Its basis and fundaments. Oxford: Elsevier.

APPENDIX

Within this appendix are tables containing values for robusticity and curvature as measured from cross-sections of humeri and femora as analyzed in CHAPTER III.

Abbreviations are as follows:

AMNH specimen names refer to the American Museum of Natural History. NMNH specimen names refer to the National Museum of Natural History. PC specimens names refer to the Powell-Cotton Museum. HTB specimen names refer to the Cleveland Museum of Natural History.

"DR" indicates day range and is given in kilometers. "FHD" , "MFL", "HHD", and "MHL" indicate femoral head diameter, maximum femoral length, humeral head diameter, and maximum humeral length, respectively. All values are given in millimeters. "BS.GM^3" indicates the cubed geometric mean of FHD, MFL, HHD, and MHL.

"F" and "H" abbreviations refer to the femur and humerus, respectively. "Dist", "prox", and "mid" refer to the location of the cross-section, where "dist" indicates the distal cross-section; "prox" indicates the proximal cross-section; and "mid" indicates the midshaft cross-section.

"TA" indicates total area and is given in square millimeters; "TA.s" indicates the size standardized value of total area. "Imax" indicates second moment of area along the maximum axis; "Imax.s" indicates the size standardized value of Imax. "Imin" indicates second moment of area along the minimum axis; "Imin.s" indicates the size standardized value of Imin. "J" indicates polar moment of area; "J.s" indicates the size standardized value of J. Imax, Imin, and J are given in mm^4. "Zp.Est" indicates the polar section modulus and is given in mm^3; "Zp.Est.s" indicates the size standardized Zp. "C.AP" indicates antero-posterior subtense (curvature); "C.ML" indicates medio-lateral subtense. Subtense values are given in millimeters. "MaxXrad" and "MaxYrad" refer to the maximum X and Y radii of the cross-sections and are given in millimeters.

For example, F.dist.TA.s indicates the size standardized total area of the distal femoral cross-section for the associated specimen.

Name	Species	DR	Sex	HHD	MHL	FHD	MFL	BS.GM^3
AMNH52532	C. ascanius	1.4	M	13	126	12.7	158	77193.55
AMNH52554	C. ascanius	1.4	M	13.2	122	12	162	74425.63
AMNH52563	C. ascanius	1.4	M	13.5	120.5	12.1	152.5	72116.07
AMNH55068	C. ascanius	1.4	M	13.5	120.5	12.1	152.5	72116.07
NMNH164582	C. ascanius	1.4	M	14	117	12.25	152	72982.74
NMNH452510	C. ascanius	1.4	M	15	123	13	159	86298.38
NMNH452512	C. ascanius	1.4	F	12	104	10	131	45720.86
NMNH452514	C. ascanius	1.4	M	15	129	12	157	83429.84
NMNH452517	C. ascanius	1.4	M	16	130	13	165	97077.36
NMNH218470	C. cephus	1.4	M	15	135	13	176	99864.42
PC.CAMII.360	C. cephus	1.4	M	14.2	123	12.7	156	80230.84
PC.CAMII.371	C. cephus	1.4	M	14.55	122	12.2	150	76516.56
PC.M213	C. cephus	1.4	M	15.2	117	13.7	146	81908.16
PC.M23	C. cephus	1.4	M	14.95	121	13.4	159	86985.40
PC.M230	C. cephus	1.4	M	14.1	121	12.1	156	76021.40
PC.M335	C. cephus	1.4	M	13.8	123.5	12.9	157.5	80271.66
PC.M367	C. cephus	1.4	F	16.5	145.5	14.85	178	126435.80
PC.M381	C. cephus	1.4	M	14	116	12	137	66048.94
PC.M411	C. cephus	1.4	M	16.3	131	13.65	158	99411.47
PC.M426	C. cephus	1.4	F	12.2	109	10.9	137	52899.31
PC.M536	C. cephus	1.4	M	14.7	131	12.35	158	85346.26
PC.M561	C. cephus	1.4	M	14.4	128	12.7	162.5	86133.51
PC.M618	C. cephus	1.4	M	14.7	127	12.8	163.5	87879.30
PC.M659	C. cephus	1.4	M	14.15	121	12.15	152	74984.46
PC.M688	C. cephus	1.4	M	14	127.5	12.45	165	83795.10
PC.M753	C. cephus	1.4	F	14	117.5	11.8	143	68004.55
PC.M754	C. cephus	1.4	F	12.3	109	11.3	134	53781.90
PC.M833	C. cephus	1.4	M	15	120.5	12.5	152.5	79973.04
PC.M872	C. cephus	1.4	M	14.2	121	12.4	150	75585.76
PC.M878	C. cephus	1.4	M	14.1	126	12.7	156	81262.18
PC.M94	C. cephus	1.4	M	14.6	123	12.8	163	85161.18
PC.M972	C. cephus	1.4	F	12.65	108.5	11.15	133	53887.13
NMNH477295	C. diana	1.3	F	13	129	13	164	82222.41
NMNH164832	C. mitis	1.3	F	14	121	13	148	76707.68
NMNH452530	C. mitis	1.3	M	19.5	151	15.5	184	155998.64
NMNH452531	C. mitis	1.3	F	13.5	114	12	140	64477.91
NMNH452535	C. mitis	1.3	F	14	119	12	144	69889.84
NMNH452536	C. mitis	1.3	M	16.5	138	14	170	112319.46
NMNH452537	C. mitis	1.3	F	15.5	129	13	157	90797.38
NMNH452538	C. mitis	1.3	M	17.5	146	16	180	141282.23
NMNH452545	C. mitis	1.3	M	16	142	15	176	121201.83
NMNH452546	C. mitis	1.3	F	15	120	14	151	86155.52
NMNH452547	C. mitis	1.3	M	12	144	15	184	102056.25
NMNH452549	C. mitis	1.3	F	18	125	13	146	93941.84
NMNH452550	C. mitis	1.3	F	15	121	12.5	146	77643.41
NMNH452552	C. mitis	1.3	F	14.5	118	13	138.5	73533.01
NMNH452553	C. mitis	1.3	M	18.5	148	15.5	177	143484.11
NMNH452554	C. mitis	1.3	F	15	122	13.25	148	82451.11
NMNH452556	C. mitis	1.3	F	15.5	127	12.5	155	86304.38
NMNH452557	C. mitis	1.3	F	14.5	123	12.5	150	78199.83
NMNH452559	C. mitis	1.3	F	16	123	14	154	93487.90
NMNH452568	C. mitis	1.3	F	13	118	12.5	143	67383.50
NMNH452570	C. mitis	1.3	M	16	145	15	175	122592.24
NMNH452571	C. mitis	1.3	M	15.5	139	18	162	125487.51
NMNH452574	C. mitis	1.3	M	18	146	14	177	128912.49
NMNH452578	C. mitis	1.3	F	14.5	121	12.5	141	73741.48
NMNH452581	C. mitis	1.3	F	14	121	12	152	73697.66
NMNH452586	C. mitis	1.3	M	18	137	14	164	116071.00
NMNH452587	C. mitis	1.3	M	17.5	141	14.5	171	123017.23
NMNH454554	C. mitis	1.3	F	15	122	13.25	148	82451.11
AMNH52421	C. neglectus	0.5	M	17.9	140.5	14.9	172	127918.41

Name	Species	DR	Sex	HHD	MHL	FHD	MFL	BS.GM^3
AMNH52429	C. neglectus	0.5	M	14.1	171	14.1	171	118392.13
NMNH452520	C. neglectus	0.5	F	15	119	12	140	72062.72
NMNH452522	C. neglectus	0.5	F	13	113	11.5	135	58686.75
NMNH452523	C. neglectus	0.5	M	16	134	14	159	102108.63
NMNH452524	C. neglectus	0.5	M	15.5	134	14.5	164	104769.84
NMNH452525	C. neglectus	0.5	F	12.5	108	11	128	51192.03
PC.CAMII372	C. neglectus	0.5	M	16.2	132	14	157.5	101186.64
PC.M195	C. neglectus	0.5	M	16.85	147	15	169	125435.77
PC.CF144	C. nictitans	1.8	M	16.7	140.5	14.4	179	121956.86
PC.M114	C. nictitans	1.8	M	16.7	138	14.8	181	123851.68
PC.M232	C. nictitans	1.8	M	19	147	14.9	180	143184.92
PC.M305	C. nictitans	1.8	M	16.5	138.5	14.45	170	115328.82
PC.M336	C. nictitans	1.8	M	17.8	141	14.7	178	129727.59
PC.M378	C. nictitans	1.8	M	17.6	145	16.45	195	153042.09
PC.M410	C. nictitans	1.8	F	13.5	115.5	10.3	140	58064.51
PC.M433	C. nictitans	1.8	M	17.9	140	15.35	179.5	134699.33
PC.M48	C. nictitans	1.8	M	15.8	137.5	13.5	166	103645.69
PC.M625	C. nictitans	1.8	M	15.4	121	12.9	162	87661.34
PC.M645	C. nictitans	1.8	M	17.2	145.5	14.55	179	128997.29
PC.M680	C. nictitans	1.8	M	18.2	150	15.3	190	149522.23
PC.M691	C. nictitans	1.8	F	14.4	131	12.6	163	87326.08
PC.M793	C. nictitans	1.8	F	14.9	128	13.6	154.5	89566.94
PC.M832	C. nictitans	1.8	M	16.4	140.5	13.5	172	111246.61
PC.M836	C. nictitans	1.8	M	16.1	137	13.2	174	106783.02
PC.M868	C. nictitans	1.8	F	13.7	118	11.75	136	64436.88
PC.M904	C. nictitans	1.8	M	16	148	14	185	123242.67
PC.M906	C. nictitans	1.8	M	18.1	146	14.7	185	138800.29
PC.M990	C. nictitans	1.8	F	14.7	124	12.6	154	81559.15
PC.CAMII.317	C. pogonias	1.8	M	13.5	116	12.1	149	68876.73
PC.M103	C. pogonias	1.8	F	11.4	116	10.7	138	52235.92
PC.M152	C. pogonias	1.8	F	12.2	107	10.9	131	50446.50
PC.M159	C. pogonias	1.8	M	14.5	121	12.7	155	80115.51
PC.M230	C. pogonias	1.8	M	14	127	11.7	154	75723.16
PC.M277	C. pogonias	1.8	F	12.7	109	10.6	129.5	51180.48
PC.M297	C. pogonias	1.8	M	14.5	121	12.6	149	77318.36
PC.M306	C. pogonias	1.8	M	15.5	131	12.9	160	92626.34
PC.M344	C. pogonias	1.8	M	14.5	123	12.6	153	79845.66
PC.M347	C. pogonias	1.8	F	12.9	112	11.3	130	55606.06
PC.M383	C. pogonias	1.8	M	14.7	128	13.1	157	87251.66
PC.M654	C. pogonias	1.8	M	14.9	127.5	13	157.5	87587.13
PC.M660	C. pogonias	1.8	F	13.3	115	10.9	138	59073.31
PC.M769	C. pogonias	1.8	M	14.1	120	12.5	153	76295.93
PC.M82	C. pogonias	1.8	M	15.2	133	13.1	161.5	94049.02
PC.M88	C. pogonias	1.8	F	13.5	115.5	11.7	134	61823.67
PC.M90	C. pogonias	1.8	M	14.6	120	12.7	146	76518.78
PC.M908	C. pogonias	1.8	M	15.1	130.5	12.5	152	85114.94
PC.M931	C. pogonias	1.8	M	15.1	130.5	12.7	157.5	88461.40

Name	F.dist.TA	F.dist.TA.s	F.dist.Imax	F.dist.Imax.s	F.dist.Imin
AMNH52532	78.0056	0.00101052	515.9741	4.23048E-05	460.4089
AMNH52554	75.9552	0.001020552	493.4389	4.09257E-05	427.9688
AMNH52563	77.5129	0.001074835	505.3416	4.59498E-05	453.8074
AMNH55068	NA	NA	NA	NA	NA
NMNH164582	58.4872	0.000801384	327.3281	2.95066E-05	227.2033
NMNH452510	NA	NA	NA	NA	NA
NMNH452512	45.5492	0.000996245	166.1727	2.77443E-05	164.5044
NMNH452514	NA	NA	NA	NA	NA
NMNH452517	69.088	0.00071168	433.0335	2.70346E-05	337.9817
NMNH218470	81.8886	0.000819998	618.758	3.52044E-05	463.1577
PC.CAMII.360	69.8842	0.000871039	455.2917	3.63767E-05	332.2709
PC.CAMII.371	73.4622	0.000960082	498.5337	4.34358E-05	374.0391
PC.M213	67.6483	0.000825904	402.5176	3.36593E-05	329.8867

Name	F.dist.TA	F.dist.TA.s	F.dist.lmax	F.dist.lmax.s	F.dist.lmin
PC.M23	83.7656	0.000962985	711.068	5.14124E-05	440.4749
PC.M230	75.1028	0.000987917	510.8531	4.3076E-05	394.8525
PC.M335	77.1043	0.000960542	517.9118	4.0965E-05	433.1219
PC.M367	102.785	0.000812942	998.3716	4.43611E-05	714.9937
PC.M381	64.9909	0.000983981	376.8157	4.16431E-05	301.9449
PC.M411	76.2774	0.00076729	538.1207	3.42599E-05	402.0014
PC.M426	63.473	0.001199883	358.4898	4.94659E-05	287.7296
PC.M536	59.6031	0.000698368	304.19	2.25581E-05	262.8078
PC.M561	71.2839	0.000827598	448.8575	3.20688E-05	364.5637
PC.M618	80.8956	0.000920531	616.5346	4.29095E-05	443.4931
PC.M659	76.8576	0.00102498	546.0179	4.79062E-05	405.6156
PC.M688	70.8685	0.000845736	408.6883	2.9559E-05	391.3379
PC.M753	NA	NA	NA	NA	NA
PC.M754	57.8733	0.001076074	297.9153	4.13382E-05	239.1603
PC.M833	73.3767	0.000917518	489.1914	4.01112E-05	380.7136
PC.M872	62.7302	0.000829921	343.8757	3.03298E-05	285.6605
PC.M878	57.0497	0.000702045	286.9851	2.26384E-05	234.5403
PC.M94	77.4888	0.000909908	584.8644	4.21333E-05	391.6149
PC.M972	59.4951	0.001104069	367.1547	5.12286E-05	218.0291
NMNH477295	72.8017	0.000885424	489.469	3.62987E-05	364.626
NMNH164832	60.2367	0.000785276	326.5643	2.87652E-05	257.1563
NMNH452530	NA	NA	NA	NA	NA
NMNH452531	NA	NA	NA	NA	NA
NMNH452535	NA	NA	NA	NA	NA
NMNH452536	NA	NA	NA	NA	NA
NMNH452537	NA	NA	NA	NA	NA
NMNH452538	NA	NA	NA	NA	NA
NMNH452545	NA	NA	NA	NA	NA
NMNH452546	NA	NA	NA	NA	NA
NMNH452547	109.7472	0.00107536	1039.7767	5.5371E-05	885.9981
NMNH452549	NA	NA	NA	NA	NA
NMNH452550	NA	NA	NA	NA	NA
NMNH452552	63.6538	0.000865649	368.1909	3.61527E-05	285.3639
NMNH452553	NA	NA	NA	NA	NA
NMNH452554	NA	NA	NA	NA	NA
NMNH452556	NA	NA	NA	NA	NA
NMNH452557	NA	NA	NA	NA	NA
NMNH452559	NA	NA	NA	NA	NA
NMNH452568	NA	NA	NA	NA	NA
NMNH452570	89.5519	0.000730486	779.0269	3.63121E-05	527.7358
NMNH452571	NA	NA	NA	NA	NA
NMNH452574	NA	NA	NA	NA	NA
NMNH452578	NA	NA	NA	NA	NA
NMNH452581	NA	NA	NA	NA	NA
NMNH452586	NA	NA	NA	NA	NA
NMNH452587	NA	NA	NA	NA	NA
NMNH454554	NA	NA	NA	NA	NA
AMNH52421	94.8755	0.000741688	817.1626	3.71404E-05	629.0447
AMNH52429	107.0636	0.000904313	1032.6775	5.10089E-05	808.2237
NMNH452520	60.41	0.000838298	333.9604	3.31022E-05	254.0797
NMNH452522	59.0529	0.001006239	302.2001	3.81435E-05	256.1899
NMNH452523	NA	NA	NA	NA	NA
NMNH452524	91.0577	0.000869121	791.7718	4.60808E-05	555.3147
NMNH452525	NA	NA	NA	NA	NA
PC.CAMII372	80.0204	0.00079082	596.758	3.74451E-05	439.5196
PC.M195	83.193	0.000663232	606.107	2.85918E-05	501.6027
PC.CF144	81.566	0.00066881	581.8547	2.66536E-05	484.882
PC.M114	98.3299	0.000793933	812.2429	3.62331E-05	730.3282
PC.M232	104.5135	0.00072992	1004.8845	3.89894E-05	761.7871
PC.M305	110.1647	0.000955223	1102.5972	5.6238E-05	853.2705
PC.M336	97.8533	0.000754298	853.3123	3.69535E-05	681.4306

Name	F.dist.TA	F.dist.TA.s	F.dist.lmax	F.dist.lmax.s	F.dist.lmin
PC.M378	97.3401	0.000636035	801.8313	2.68681E-05	709.797
PC.M410	63.4695	0.001093086	347.6812	4.27703E-05	297.5035
PC.M433	90.7672	0.00067385	739.5882	3.05886E-05	582.6831
PC.M48	76.9397	0.000742334	525.6231	3.05503E-05	425.1075
PC.M625	83.1812	0.000948893	653.5228	4.6019E-05	467.904
PC.M645	103.0943	0.000799197	980.1459	4.2448E-05	734.5828
PC.M680	99.6224	0.000666272	869.9238	3.06212E-05	718.3982
PC.M691	72.4303	0.000829423	464.6447	3.2643E-05	376.9412
PC.M793	73.5935	0.000821659	473.1725	3.41935E-05	398.848
PC.M832	84.2497	0.000757324	581.8353	3.04078E-05	550.252
PC.M836	79.5578	0.000745042	548.601	2.9526E-05	463.8133
PC.M868	54.041	0.000838666	255.8082	2.91905E-05	211.775
PC.M904	91.2737	0.000740601	729.4976	3.19957E-05	605.0484
PC.M906	110.7009	0.000797555	1097.7351	4.27499E-05	868.2918
PC.M990	77.1362	0.00094577	508.8398	4.05124E-05	442.6356
PC.CAMII.317	61.7189	0.000896078	317.6024	3.09475E-05	290.8827
PC.M103	56.1715	0.001075342	263.1418	3.65041E-05	239.9919
PC.M152	51.8371	0.001027566	234.973	3.55562E-05	195.2234
PC.M159	72.6577	0.000906912	469.3515	3.77964E-05	376.646
PC.M230	70.8553	0.000935715	418.2685	3.58679E-05	382.5
PC.M277	57.6247	0.001125912	282.7845	4.2666E-05	247.7623
PC.M297	68.6546	0.000887947	422.8319	3.67028E-05	336.5394
PC.M306	72.0973	0.000778367	449.2178	3.03112E-05	382.1702
PC.M344	NA	NA	NA	NA	NA
PC.M347	NA	NA	NA	NA	NA
PC.M383	65.3936	0.000749483	347.6853	2.53812E-05	333.9447
PC.M654	77.9929	0.000890461	497.9794	3.60986E-05	471.3752
PC.M660	56.9226	0.000963593	288.468	3.53857E-05	231.024
PC.M769	73.5147	0.000963547	472.7357	4.04973E-05	391.9056
PC.M82	74.7201	0.00079448	489.6918	3.22401E-05	404.0201
PC.M88	59.3894	0.000960626	292.0923	3.52582E-05	270.9023
PC.M90	65.4785	0.000855718	367.2615	3.28742E-05	317.9369
PC.M908	68.454	0.000804254	422.8555	3.26846E-05	330.3084
PC.M931	71.95	0.000813349	424.5242	3.04697E-05	401.7599

Name	F.dist.lmin.s	F.dist.MaxXrad	F.dist.MaxYrad	F.dist.J	F.dist.J.s
AMNH52532	3.775E-05	5.1424	5.1448	976.383	8.0054E-05
AMNH52554	3.550E-05	4.8436	5.194	921.4078	7.6421E-05
AMNH52563	4.126E-05	5.0184	5.2256	959.149	8.7214E-05
AMNH55068	NA	NA	NA	NA	NA
NMNH164582	2.048E-05	4.3553	4.6579	554.5314	4.9988E-05
NMNH452510	NA	NA	NA	NA	NA
NMNH452512	2.747E-05	3.8849	3.9081	330.6771	5.5210E-05
NMNH452514	NA	NA	NA	NA	NA
NMNH452517	2.110E-05	5.1308	4.6109	771.0152	4.8135E-05
NMNH218470	2.635E-05	5.6917	5.1897	1081.9157	6.1556E-05
PC.CAMII.360	2.655E-05	4.9937	4.5685	787.5626	6.2924E-05
PC.CAMII.371	3.259E-05	5.2413	4.8623	872.5728	7.6025E-05
PC.M213	2.759E-05	4.744	4.7121	732.4042	6.1245E-05
PC.M23	3.185E-05	4.7836	5.8936	1151.5429	8.3260E-05
PC.M230	3.329E-05	4.7592	5.2597	905.7055	7.6371E-05
PC.M335	3.426E-05	4.8108	5.2295	951.0337	7.5223E-05
PC.M367	3.177E-05	5.963	6.1088	1713.3653	7.6131E-05
PC.M381	3.337E-05	4.6308	4.8048	678.7606	7.5012E-05
PC.M411	2.559E-05	5.0705	5.0565	940.1221	5.9854E-05
PC.M426	3.970E-05	4.3749	4.8736	646.2194	8.9168E-05
PC.M536	1.949E-05	4.3189	4.5108	566.9978	4.2047E-05
PC.M561	2.605E-05	4.629	5.0608	813.4212	5.8115E-05
PC.M618	3.087E-05	5.0426	5.5865	1060.0277	7.3776E-05
PC.M659	3.559E-05	5.275	4.9452	951.6336	8.3494E-05
PC.M688	2.830E-05	4.8066	4.8551	800.0262	5.7863E-05
PC.M753	NA	NA	NA	NA	NA

Name	F.dist.Imin.s	F.dist.MaxXrad	F.dist.MaxYrad	F.dist.J	F.dist.J.s
PC.M754	3.319E-05	4.2984	4.3137	537.0756	7.4524E-05
PC.M833	3.122E-05	5.1644	5.2025	869.905	7.1328E-05
PC.M872	2.520E-05	4.4401	4.6992	629.5362	5.5525E-05
PC.M878	1.850E-05	4.0613	4.4896	521.5253	4.1140E-05
PC.M94	2.821E-05	5.2493	5.0423	976.4794	7.0345E-05
PC.M972	3.042E-05	4.9875	4.1346	585.1838	8.1650E-05
NMNH477295	2.704E-05	4.8221	5.0672	854.095	6.3339E-05
NMNH164832	2.265E-05	4.2988	4.775	583.7205	5.1417E-05
NMNH452530	NA	NA	NA	NA	NA
NMNH452531	NA	NA	NA	NA	NA
NMNH452535	NA	NA	NA	NA	NA
NMNH452536	NA	NA	NA	NA	NA
NMNH452537	NA	NA	NA	NA	NA
NMNH452538	NA	NA	NA	NA	NA
NMNH452545	NA	NA	NA	NA	NA
NMNH452546	NA	NA	NA	NA	NA
NMNH452547	4.718E-05	6.216	5.8474	1925.7748	1.0255E-04
NMNH452549	NA	NA	NA	NA	NA
NMNH452550	NA	NA	NA	NA	NA
NMNH452552	2.802E-05	4.6563	4.6634	653.5548	6.4173E-05
NMNH452553	NA	NA	NA	NA	NA
NMNH452554	NA	NA	NA	NA	NA
NMNH452556	NA	NA	NA	NA	NA
NMNH452557	NA	NA	NA	NA	NA
NMNH452559	NA	NA	NA	NA	NA
NMNH452568	NA	NA	NA	NA	NA
NMNH452570	2.460E-05	5.5141	5.5022	1306.7628	6.0911E-05
NMNH452571	NA	NA	NA	NA	NA
NMNH452574	NA	NA	NA	NA	NA
NMNH452578	NA	NA	NA	NA	NA
NMNH452581	NA	NA	NA	NA	NA
NMNH452586	NA	NA	NA	NA	NA
NMNH452587	NA	NA	NA	NA	NA
NMNH454554	NA	NA	NA	NA	NA
AMNH52421	2.859E-05	5.4169	5.7184	1446.2073	6.5731E-05
AMNH52429	3.992E-05	5.5297	6.3447	1840.9013	9.0931E-05
NMNH452520	2.518E-05	4.3668	4.652	588.0401	5.8287E-05
NMNH452522	3.234E-05	4.3192	4.6294	558.3901	7.0480E-05
NMNH452523	NA	NA	NA	NA	NA
NMNH452524	3.232E-05	5.1983	5.8203	1347.0865	7.8400E-05
NMNH452525	NA	NA	NA	NA	NA
PC.CAMII372	2.758E-05	5.6711	4.7924	1036.2777	6.5024E-05
PC.M195	2.366E-05	4.9298	5.4241	1107.7097	5.2254E-05
PC.CF144	2.221E-05	5.0619	5.4407	1066.7367	4.8865E-05
PC.M114	3.258E-05	5.7426	5.6312	1542.5711	6.8812E-05
PC.M232	2.956E-05	5.7241	6.1898	1766.6716	6.8547E-05
PC.M305	4.352E-05	6.2109	6.1705	1955.8677	9.9759E-05
PC.M336	2.951E-05	5.9318	5.456	1534.7429	6.6464E-05
PC.M378	2.378E-05	5.5264	5.7217	1511.6284	5.0652E-05
PC.M410	3.660E-05	4.4774	4.8151	645.1847	7.9368E-05
PC.M433	2.410E-05	5.6881	5.1859	1322.2713	5.4688E-05
PC.M48	2.471E-05	5.3592	5.0382	950.7306	5.5258E-05
PC.M625	3.295E-05	5.2923	5.5553	1121.4267	7.8967E-05
PC.M645	3.181E-05	6.1728	5.8073	1714.7287	7.4261E-05
PC.M680	2.529E-05	5.9387	5.4369	1588.322	5.5909E-05
PC.M691	2.648E-05	5.0666	4.6964	841.5859	5.9124E-05
PC.M793	2.882E-05	4.9221	5.2929	872.0205	6.3016E-05
PC.M832	2.876E-05	5.1388	5.2367	1132.0873	5.9165E-05
PC.M836	2.496E-05	5.3854	4.963	1012.4143	5.4489E-05
PC.M868	2.417E-05	4.3107	3.9214	467.5831	5.3356E-05
PC.M904	2.654E-05	5.7971	5.2685	1334.546	5.8533E-05

Name	F.dist.Imin.s	F.dist.MaxXrad	F.dist.MaxYrad	F.dist.J	F.dist.J.s
PC.M906	3.381E-05	6.3877	5.7816	1966.0269	7.6564E-05
PC.M990	3.524E-05	4.9632	5.2001	951.4755	7.5754E-05
PC.CAMII.317	2.834E-05	4.5349	4.6145	608.4851	5.9291E-05
PC.M103	3.329E-05	4.1088	4.3521	503.1338	6.9797E-05
PC.M152	2.954E-05	4.2462	3.9101	430.1964	6.5098E-05
PC.M159	3.033E-05	5.0654	4.6549	845.9975	6.8127E-05
PC.M230	3.280E-05	4.8529	4.8134	800.7685	6.8668E-05
PC.M277	3.738E-05	4.4204	4.2668	530.5468	8.0048E-05
PC.M297	2.921E-05	4.9897	4.7991	759.3712	6.5915E-05
PC.M306	2.579E-05	4.6734	5.1655	831.388	5.6098E-05
PC.M344	NA	NA	NA	NA	NA
PC.M347	NA	NA	NA	NA	NA
PC.M383	2.438E-05	4.6618	4.6282	681.6301	4.9759E-05
PC.M654	3.417E-05	5.0129	5.0142	969.3546	7.0269E-05
PC.M660	2.834E-05	4.2506	4.2328	519.492	6.3725E-05
PC.M769	3.357E-05	4.8053	4.972	864.6413	7.4070E-05
PC.M82	2.660E-05	4.9701	4.7261	893.7119	5.8840E-05
PC.M88	3.270E-05	4.4416	4.439	562.9946	6.7959E-05
PC.M90	2.846E-05	4.7773	4.5026	685.1984	6.1333E-05
PC.M908	2.553E-05	5.0159	4.7592	753.1639	5.8216E-05
PC.M931	2.884E-05	4.8261	4.9443	826.2841	5.9306E-05
Name	**F.dist.ZpEst**	**F.dist.ZpEst.s**	**F.mid.TA**	**F.mid.TA.s**	**F.mid.Imax**
AMNH52532	189.82	0.0024590762	74.1359	0.00096039	475.176
AMNH52554	183.59	0.0024667747	69.8819	0.000938949	410.611
AMNH52563	187.26	0.0025966564	73.6296	0.001020987	465.1483
AMNH55068	NA	NA	NA	NA	NA
NMNH164582	123.05	0.0016859976	58.1501	0.000796765	322.5624
NMNH452510	NA	NA	NA	NA	NA
NMNH452512	84.87	0.0018561584	45.1544	0.00098761	173.0819
NMNH452514	NA	NA	63.6214	0.000762574	342.3256
NMNH452517	158.29	0.0016305729	62.9994	0.000648961	370.4981
NMNH218470	198.86	0.0019912595	72.9799	0.00073079	495.7575
PC.CAMII.360	164.72	0.0020531275	63.2583	0.000788454	376.8666
PC.CAMII.371	172.73	0.0022573562	68.7612	0.000898645	454.5065
PC.M213	154.91	0.0018912181	64.5453	0.00078802	369.8964
PC.M23	215.70	0.0024797413	75.4595	0.000867496	565.5736
PC.M230	180.80	0.0023782698	69.5341	0.000914665	443.8359
PC.M335	189.44	0.0023600270	72.8152	0.00090711	446.0728
PC.M367	283.86	0.0022451114	95.2797	0.000753582	837.96
PC.M381	143.87	0.0021782675	59.5505	0.000901612	308.3157
PC.M411	185.67	0.0018676564	71.2828	0.000717048	419.1536
PC.M426	139.75	0.0026417313	64.3735	0.001216906	356.5601
PC.M536	128.43	0.0015048074	54.1406	0.000634364	250.7572
PC.M561	167.89	0.0019492095	70.8652	0.000822737	454.0538
PC.M618	199.46	0.0022696774	71.7318	0.000816254	469.289
PC.M659	186.23	0.0024835283	69.0739	0.000921176	446.7062
PC.M688	165.61	0.0019763416	65.646	0.000783411	350.4962
PC.M753	NA	NA	NA	NA	NA
PC.M754	124.73	0.0023191039	55.6932	0.001035538	287.1899
PC.M833	167.82	0.0020985015	70.7424	0.000884578	437.3127
PC.M872	137.76	0.0018226269	62.5976	0.000828167	344.1823
PC.M878	121.98	0.0015010842	46.9182	0.000577368	184.623
PC.M94	189.76	0.0022282737	71.9142	0.000844448	503.0544
PC.M972	128.30	0.0023809067	56.9596	0.001057017	305.3437
NMNH477295	172.73	0.0021007793	68.488	0.00083296	412.6607
NMNH164832	128.66	0.0016772851	58.2345	0.000759174	301.4231
NMNH452530	NA	NA	NA	NA	NA
NMNH452531	NA	NA	NA	NA	NA
NMNH452535	NA	NA	NA	NA	NA
NMNH452536	NA	NA	NA	NA	NA
NMNH452537	NA	NA	NA	NA	NA

Name	F.dist.ZpEst	F.dist.ZpEst.s	F.mid.TA	F.mid.TA.s	F.mid.lmax
NMNH452538	NA	NA	101.1041	0.000715618	866.0245
NMNH452545	NA	NA	NA	NA	NA
NMNH452546	NA	NA	NA	NA	NA
NMNH452547	319.28	0.0031284279	NA	NA	NA
NMNH452549	NA	NA	NA	NA	NA
NMNH452550	NA	NA	NA	NA	NA
NMNH452552	140.25	0.0019073383	NA	NA	NA
NMNH452553	NA	NA	80.1724	0.000558755	558.8303
NMNH452554	NA	NA	NA	NA	NA
NMNH452556	NA	NA	NA	NA	NA
NMNH452557	NA	NA	NA	NA	NA
NMNH452559	NA	NA	NA	NA	NA
NMNH452568	NA	NA	NA	NA	NA
NMNH452570	237.24	0.0019352097	NA	NA	NA
NMNH452571	NA	NA	NA	NA	NA
NMNH452574	NA	NA	NA	NA	NA
NMNH452578	NA	NA	NA	NA	NA
NMNH452581	NA	NA	NA	NA	NA
NMNH452586	NA	NA	NA	NA	NA
NMNH452587	NA	NA	84.2306	0.000684706	673.094
NMNH454554	NA	NA	NA	NA	NA
AMNH52421	259.75	0.0020306056	89.0597	0.000696223	683.1393
AMNH52429	310.06	0.0026189427	97.9978	0.000827739	849.3662
NMNH452520	130.40	0.0018095790	55.3094	0.000767518	279.9459
NMNH452522	124.80	0.0021265351	61.3336	0.001045101	347.1681
NMNH452523	NA	NA	NA	NA	NA
NMNH452524	244.51	0.0023337955	81.8013	0.000780771	577.924
NMNH452525	NA	NA	NA	NA	NA
PC.CAMII372	198.07	0.0019575191	76.2389	0.000753448	551.0526
PC.M195	213.97	0.0017058097	82.4516	0.000657321	597.6375
PC.CF144	203.14	0.0016656516	84.9362	0.000696445	632.3631
PC.M114	271.25	0.0021901190	89.407	0.000721888	681.1896
PC.M232	296.57	0.0020712599	91.5201	0.000639174	679.6026
PC.M305	315.94	0.0027394404	96.9936	0.000841018	815.8177
PC.M336	269.54	0.0020777508	86.6	0.000667553	643.8089
PC.M378	268.78	0.0017562445	94.0702	0.000614669	769.0442
PC.M410	138.86	0.0023915019	63.9953	0.001102141	355.159
PC.M433	243.20	0.0018054930	88.2243	0.000654972	683.8392
PC.M48	182.88	0.0017644586	80.2509	0.000774281	549.5013
PC.M625	206.76	0.0023586262	78.065	0.000890529	574.3827
PC.M645	286.26	0.0022191383	97.3685	0.00075481	852.1929
PC.M680	279.25	0.0018676198	93.0545	0.000622346	758.715
PC.M691	172.40	0.0019742457	70.7642	0.000810344	444.6537
PC.M793	170.73	0.0019062094	68.638	0.000766332	399.8827
PC.M832	218.22	0.0019616164	81.6452	0.000733912	587.4448
PC.M836	195.67	0.0018323686	78.0934	0.000731328	545.0196
PC.M868	113.60	0.0017629648	50.5593	0.000784633	226.0309
PC.M904	241.21	0.0019571652	88.3561	0.000716928	679.4429
PC.M906	323.11	0.0023278955	112.6449	0.000811561	1096.0645
PC.M990	187.24	0.0022957265	68.363	0.000838201	400.6259
PC.CAMII.317	133.01	0.0019311445	59.4358	0.00086293	298.4921
PC.M103	118.93	0.0022768145	57.5594	0.001101912	277.2966
PC.M152	105.49	0.0020910890	55.2926	0.001096064	261.5888
PC.M159	174.07	0.0021727153	73.5395	0.000917918	466.2223
PC.M230	165.68	0.0021880032	69.7053	0.000920528	433.6393
PC.M277	122.14	0.0023865442	57.434	0.001122186	271.1189
PC.M297	155.15	0.0020066518	68.1709	0.000881691	399.1859
PC.M306	169.00	0.0018245370	68.3617	0.000738037	404.6439
PC.M344	NA	NA	NA	NA	NA
PC.M347	NA	NA	NA	NA	NA
PC.M383	146.74	0.0016818581	67.8925	0.000778123	396.7636

Name	F.dist.ZpEst	F.dist.ZpEst.s	F.mid.TA	F.mid.TA.s	F.mid.lmax
PC.M654	193.35	0.0022074814	69.9918	0.000799111	430.5473
PC.M660	122.47	0.0020732306	54.1354	0.00091641	247.3488
PC.M769	176.87	0.0023181721	70.3768	0.000922419	430.8969
PC.M82	184.34	0.0019600705	70.7928	0.000752722	423.9811
PC.M88	126.79	0.0020508652	57.366	0.000927897	277.5645
PC.M90	147.67	0.0019299010	65.9346	0.000861679	364.3336
PC.M908	154.10	0.0018104748	61.0873	0.000717704	336.6538
PC.M931	169.14	0.0019120236	70.7548	0.000799838	416.3157
Name	**F.mid.lmax.s**	**F.mid.lmin**	**F.mid.lmin.s**	**F.mid.MaxXrad**	**F.mid.MaxYrad**
AMNH52532	3.89598E-05	408.2974	3.34764E-05	4.8818	4.9167
AMNH52554	3.4056E-05	369.7155	3.06641E-05	4.7047	4.9142
AMNH52563	4.22951E-05	403.2371	3.66656E-05	4.9737	5.3056
AMNH55068	NA	NA	NA	NA	NA
NMNH164582	2.9077E-05	227.5842	2.05153E-05	4.5711	4.6356
NMNH452510	NA	NA	NA	NA	NA
NMNH452512	2.88979E-05	153.1284	2.55664E-05	3.6667	4.0105
NMNH452514	2.61347E-05	305.5907	2.33302E-05	4.5431	4.7175
NMNH452517	2.31304E-05	272.682	1.70237E-05	4.8562	4.4005
NMNH218470	2.82063E-05	364.1424	2.0718E-05	4.8317	5.2209
PC.CAMII.360	3.01108E-05	272.2697	2.17537E-05	4.7126	4.7347
PC.CAMII.371	3.95998E-05	316.6046	2.75848E-05	4.9494	4.6942
PC.M213	3.09314E-05	301.533	2.52148E-05	4.9702	4.5096
PC.M23	4.08927E-05	368.1351	2.66173E-05	5.3088	5.3031
PC.M230	3.7425E-05	337.4888	2.84576E-05	5.1047	4.9686
PC.M335	3.52828E-05	400.2423	3.16578E-05	4.7211	4.9561
PC.M367	3.72334E-05	630.322	2.80074E-05	5.5515	6.3242
PC.M381	3.40729E-05	265.9122	2.93868E-05	4.5397	4.4389
PC.M411	2.66858E-05	397.4675	2.53051E-05	4.8536	4.9735
PC.M426	4.91997E-05	307.0637	4.23699E-05	4.4926	4.7215
PC.M536	1.85957E-05	217.8777	1.61574E-05	4.4828	4.176
PC.M561	3.24401E-05	354.9768	2.53615E-05	4.7991	4.8139
PC.M618	3.26615E-05	362.3725	2.52203E-05	4.7743	5.4991
PC.M659	3.91929E-05	324.6615	2.8485E-05	4.737	5.119
PC.M688	2.53502E-05	337.3125	2.43966E-05	4.5394	4.6386
PC.M753	NA	NA	NA	NA	NA
PC.M754	3.985E-05	213.2217	2.95863E-05	4.3961	4.3214
PC.M833	3.58574E-05	368.2495	3.01946E-05	5.4233	4.943
PC.M872	3.03569E-05	284.5814	2.51001E-05	4.5169	4.7245
PC.M878	1.45637E-05	166.8561	1.31622E-05	3.837	3.9785
PC.M94	3.62398E-05	338.4609	2.43826E-05	4.8014	5.3282
PC.M972	4.26042E-05	220.3065	3.07391E-05	4.6363	4.1535
NMNH477295	3.06027E-05	339.0118	2.51409E-05	4.9053	4.671
NMNH164832	2.65507E-05	243.964	2.14894E-05	4.199	4.795
NMNH452530	NA	NA	NA	NA	NA
NMNH452531	NA	NA	NA	NA	NA
NMNH452535	NA	NA	NA	NA	NA
NMNH452536	NA	NA	NA	NA	NA
NMNH452537	NA	NA	NA	NA	NA
NMNH452538	3.40542E-05	786.0081	3.09077E-05	5.9781	5.8167
NMNH452545	NA	NA	NA	NA	NA
NMNH452546	NA	NA	NA	NA	NA
NMNH452547	NA	NA	NA	NA	NA
NMNH452549	NA	NA	NA	NA	NA
NMNH452550	NA	NA	NA	NA	NA
NMNH452552	NA	NA	NA	NA	NA
NMNH452553	2.20041E-05	476.5028	1.87624E-05	5.0081	5.2346
NMNH452554	NA	NA	NA	NA	NA
NMNH452556	NA	NA	NA	NA	NA
NMNH452557	NA	NA	NA	NA	NA
NMNH452559	NA	NA	NA	NA	NA
NMNH452568	NA	NA	NA	NA	NA

Name	F.mid.lmax.s	F.mid.lmin	F.mid.lmin.s	F.mid.MaxXrad	F.mid.MaxYrad
NMNH452570	NA	NA	NA	NA	NA
NMNH452571	NA	NA	NA	NA	NA
NMNH452574	NA	NA	NA	NA	NA
NMNH452578	NA	NA	NA	NA	NA
NMNH452581	NA	NA	NA	NA	NA
NMNH452586	NA	NA	NA	NA	NA
NMNH452587	3.19973E-05	475.9021	2.26233E-05	5.8421	4.8995
NMNH454554	NA	NA	NA	NA	NA
AMNH52421	3.1049E-05	586.6788	2.66648E-05	5.7106	5.36
AMNH52429	4.19543E-05	691.5705	3.416E-05	5.525	5.7572
NMNH452520	2.77482E-05	214.6329	2.12744E-05	4.1765	4.6325
NMNH452522	4.38194E-05	261.0176	3.29455E-05	4.6147	4.6382
NMNH452523	NA	NA	NA	NA	NA
NMNH452524	3.36349E-05	492.5293	2.8665E-05	4.9535	5.2613
NMNH452525	NA	NA	NA	NA	NA
PC.CAMII372	3.45772E-05	391.0905	2.45399E-05	5.2702	4.9162
PC.M195	2.81922E-05	495.9674	2.33962E-05	5.1953	5.2334
PC.CF144	2.89672E-05	529.4656	2.42537E-05	5.1173	5.6133
PC.M114	3.0387E-05	600.3722	2.67818E-05	5.3616	5.3963
PC.M232	2.63685E-05	658.0764	2.55333E-05	5.5275	5.6014
PC.M305	4.16108E-05	699.3887	3.56724E-05	5.7231	6.2813
PC.M336	2.78808E-05	555.008	2.40352E-05	5.4599	5.0867
PC.M378	2.57695E-05	650.9828	2.18134E-05	5.5579	5.632
PC.M410	4.36902E-05	303.7186	3.73622E-05	4.5148	4.9378
PC.M433	2.82829E-05	567.8921	2.34875E-05	5.4961	5.2184
PC.M48	3.19381E-05	479.4821	2.78685E-05	5.2468	5.1714
PC.M625	4.04462E-05	419.7084	2.95546E-05	5.7229	5.3711
PC.M645	3.69066E-05	673.9893	2.9189E-05	5.6895	6.2072
PC.M680	2.67066E-05	629.9011	2.21724E-05	5.5829	5.2286
PC.M691	3.12385E-05	360.4	2.53194E-05	5.3598	4.6236
PC.M793	2.88972E-05	354.133	2.55912E-05	4.5969	4.9339
PC.M832	3.0701E-05	483.623	2.5275E-05	5.0872	5.3081
PC.M836	2.93333E-05	435.3163	2.3429E-05	5.6978	4.8314
PC.M868	2.57926E-05	183.3859	2.09263E-05	4.239	3.9041
PC.M904	2.98003E-05	577.1009	2.53116E-05	5.7743	5.4395
PC.M906	4.26849E-05	936.5545	3.6473E-05	6.1564	5.8721
PC.M990	3.18967E-05	348.0523	2.77109E-05	4.7299	4.7352
PC.CAMII.317	2.90853E-05	266.025	2.59217E-05	4.392	4.6802
PC.M103	3.84677E-05	251.3272	3.48651E-05	4.435	4.2372
PC.M152	3.95837E-05	226.5752	3.42855E-05	4.4199	4.0704
PC.M159	3.75444E-05	398.9472	3.21268E-05	4.9867	4.7508
PC.M230	3.7186E-05	349.588	2.99783E-05	5.1445	4.8427
PC.M277	4.09059E-05	255.5747	3.85606E-05	4.3492	4.1862
PC.M297	3.46502E-05	345.4614	2.99868E-05	4.7208	4.7586
PC.M306	2.73035E-05	343.9238	2.32064E-05	4.6093	4.9797
PC.M344	NA	NA	NA	NA	NA
PC.M347	NA	NA	NA	NA	NA
PC.M383	2.8964E-05	343.5253	2.50776E-05	4.6586	5.2166
PC.M654	3.12105E-05	354.6065	2.57055E-05	4.6951	4.7198
PC.M660	3.03417E-05	220.6133	2.70621E-05	4.2426	4.1731
PC.M769	3.69131E-05	363.4199	3.11326E-05	4.7693	5.1278
PC.M82	2.79138E-05	378.7431	2.49355E-05	4.8285	4.7685
PC.M88	3.35046E-05	249.0613	3.0064E-05	4.3869	4.2533
PC.M90	3.26121E-05	329.3009	2.94762E-05	4.7508	4.5234
PC.M908	2.60216E-05	263.1298	2.03386E-05	4.7426	4.272
PC.M931	2.98805E-05	382.4023	2.74464E-05	4.8162	4.6749
Name	**F.mid.J**	**F.mid.J.s**	**F.mid.ZpEst**	**F.mid.ZpEst.s**	**F.prox.TA**
AMNH52532	883.4734	7.24362E-05	180.3283	0.00233605	70.9571
AMNH52554	780.3265	6.472E-05	162.2486	0.00218001	65.4443
AMNH52563	868.3854	7.89606E-05	168.9581	0.00234286	69.0525
AMNH55068	NA	NA	NA	NA	NA

Name	F.mid.J	F.mid.J.s	F.mid.ZpEst	F.mid.ZpEst.s	F.prox.TA
NMNH164582	550.1466	4.95923E-05	119.5101	0.00163751	56.0947
NMNH452510	NA	NA	NA	NA	NA
NMNH452512	326.2103	5.44643E-05	84.9816	0.00185870	42.6477
NMNH452514	647.9163	4.9465E-05	139.9297	0.00167721	66.0882
NMNH452517	643.1802	4.01542E-05	138.9653	0.00143149	65.6084
NMNH218470	859.9	4.89243E-05	171.0801	0.00171312	63.2638
PC.CAMII.360	649.1363	5.18645E-05	137.4226	0.00171284	62.202
PC.CAMII.371	771.1111	6.71847E-05	159.9218	0.00209003	64.2587
PC.M213	671.4294	5.61462E-05	141.6548	0.00172943	67.6847
PC.M23	933.7087	6.751E-05	175.9739	0.00202303	74.1009
PC.M230	781.3246	6.58827E-05	155.1278	0.00204058	67.1425
PC.M335	846.3151	6.69406E-05	174.9091	0.00217896	71.8294
PC.M367	1468.2821	6.52408E-05	247.2750	0.00195574	86.9488
PC.M381	574.2279	6.34597E-05	127.9103	0.00193660	56.9082
PC.M411	816.6211	5.19909E-05	166.1978	0.00167182	64.0224
PC.M426	663.6237	9.15696E-05	144.0453	0.00272301	61.5933
PC.M536	468.6348	3.47531E-05	108.2447	0.00126830	54.7604
PC.M561	809.0306	5.78015E-05	168.3201	0.00195418	63.4307
PC.M618	831.6615	5.78818E-05	161.9058	0.00184237	65.5058
PC.M659	771.3677	6.76779E-05	156.5275	0.00208747	63.3427
PC.M688	687.8087	4.97468E-05	149.8820	0.00178867	66.7365
PC.M753	NA	NA	NA	NA	NA
PC.M754	500.4117	6.94363E-05	114.8062	0.00213466	49.0433
PC.M833	805.5622	6.60519E-05	155.4194	0.00194340	65.2961
PC.M872	628.7638	5.5457E-05	136.0754	0.00180028	65.9241
PC.M878	351.4791	2.77259E-05	89.9441	0.00110684	41.2077
PC.M94	841.5153	6.06223E-05	166.1498	0.00195100	67.7939
PC.M972	525.6503	7.33433E-05	119.6046	0.00221954	50.508
NMNH477295	751.6726	5.57436E-05	156.9860	0.00190929	64.4058
NMNH164832	545.3871	4.80401E-05	121.2780	0.00158104	57.376
NMNH452530	NA	NA	NA	NA	NA
NMNH452531	NA	NA	NA	NA	NA
NMNH452535	NA	NA	NA	NA	NA
NMNH452536	NA	NA	NA	NA	NA
NMNH452537	NA	NA	NA	NA	NA
NMNH452538	1652.0326	6.49619E-05	280.1290	0.00198276	99.4669
NMNH452545	NA	NA	NA	NA	NA
NMNH452546	NA	NA	NA	NA	NA
NMNH452547	NA	NA	NA	NA	90.372
NMNH452549	NA	NA	NA	NA	NA
NMNH452550	NA	NA	NA	NA	NA
NMNH452552	NA	NA	NA	NA	NA
NMNH452553	1035.3331	4.07665E-05	202.1602	0.00140894	85.0872
NMNH452554	NA	NA	NA	NA	54.8094
NMNH452556	NA	NA	NA	NA	NA
NMNH452557	NA	NA	NA	NA	NA
NMNH452559	NA	NA	NA	NA	NA
NMNH452568	NA	NA	NA	NA	NA
NMNH452570	NA	NA	NA	NA	82.5814
NMNH452571	NA	NA	NA	NA	74.8025
NMNH452574	NA	NA	NA	NA	82.8155
NMNH452578	NA	NA	NA	NA	54.5812
NMNH452581	NA	NA	NA	NA	67.8915
NMNH452586	NA	NA	NA	NA	79.8553
NMNH452587	1148.996	5.46206E-05	213.9339	0.00173906	83.7632
NMNH454554	NA	NA	NA	NA	NA
AMNH52421	1269.818	5.77138E-05	229.4036	0.00179336	85.097
AMNH52429	1540.9367	7.61142E-05	273.1625	0.00230727	97.9373
NMNH452520	494.5788	4.90227E-05	112.2894	0.00155822	58.2724
NMNH452522	608.1857	7.67648E-05	131.4584	0.00224000	63.6661
NMNH452523	NA	NA	NA	NA	NA

Name	F.mid.J	F.mid.J.s	F.mid.ZpEst	F.mid.ZpEst.s	F.prox.TA
NMNH452524	1070.4533	6.22999E-05	209.5887	0.00200047	86.593
NMNH452525	NA	NA	NA	NA	NA
PC.CAMII372	942.1431	5.91171E-05	184.9806	0.00182811	73.5103
PC.M195	1093.6048	5.15884E-05	209.7298	0.00167201	84.0941
PC.CF144	1161.8287	5.3221E-05	216.5450	0.00177559	85.435
PC.M114	1281.5618	5.71688E-05	238.2550	0.00192371	87.3072
PC.M232	1337.6789	5.19018E-05	240.3973	0.00167893	87.8853
PC.M305	1515.2064	7.72832E-05	252.4418	0.00218889	88.2145
PC.M336	1198.8169	5.19159E-05	227.3371	0.00175242	86.47
PC.M378	1420.027	4.75829E-05	253.8051	0.00165840	91.6671
PC.M410	658.8776	8.10524E-05	139.4066	0.00240089	58.6893
PC.M433	1251.7313	5.17704E-05	233.6518	0.00173462	87.7542
PC.M48	1028.9834	5.98066E-05	197.5357	0.00190588	80.8966
PC.M625	994.0911	7.00008E-05	179.2124	0.00204437	77.8669
PC.M645	1526.1822	6.60956E-05	256.5724	0.00198897	80.7047
PC.M680	1388.6161	4.88791E-05	256.8776	0.00171799	91.767
PC.M691	805.0536	5.65579E-05	161.2784	0.00184685	66.8016
PC.M793	754.0156	5.44884E-05	158.2271	0.00176658	66.0327
PC.M832	1071.0678	5.5976E-05	206.0677	0.00185235	75.2539
PC.M836	980.3359	5.27623E-05	186.2128	0.00174384	77.8929
PC.M868	409.4168	4.67189E-05	100.5555	0.00156053	50.1826
PC.M904	1256.5438	5.51118E-05	224.1067	0.00181842	81.7777
PC.M906	2032.619	7.91578E-05	337.9672	0.00243492	110.0681
PC.M990	748.6783	5.96076E-05	158.1977	0.00193967	65.7135
PC.CAMII.317	564.5171	5.5007E-05	124.4499	0.00180685	59.9132
PC.M103	528.6239	7.33328E-05	121.9123	0.00233388	56.7902
PC.M152	488.164	7.38692E-05	114.9933	0.00227951	55.8474
PC.M159	865.1695	6.96711E-05	177.6985	0.00221803	67.9707
PC.M230	783.2273	6.71643E-05	156.8462	0.00207131	65.0405
PC.M277	526.6935	7.94664E-05	123.4139	0.00241135	54.6998
PC.M297	744.6473	6.46371E-05	157.1085	0.00203197	63.5085
PC.M306	748.5678	5.05099E-05	156.1305	0.00168560	62.1218
PC.M344	NA	NA	NA	NA	NA
PC.M347	NA	NA	NA	NA	NA
PC.M383	740.2889	5.40416E-05	149.9289	0.00171835	64.4049
PC.M654	785.1538	5.69159E-05	166.7896	0.00190427	70.56
PC.M660	467.9621	5.74038E-05	111.2117	0.00188260	55.5401
PC.M769	794.3168	6.80457E-05	160.5151	0.00210385	69.3254
PC.M82	802.7242	5.28493E-05	167.2865	0.00177872	63.9122
PC.M88	526.6258	6.35686E-05	121.9013	0.00197176	53.6289
PC.M90	693.6345	6.20883E-05	149.5837	0.00195486	65.4418
PC.M908	599.7836	4.63602E-05	133.0694	0.00156341	64.0865
PC.M931	798.718	5.7327E-05	168.3088	0.00190262	68.2076

Name	F.prox.TA.s	F.prox.lmax	F.prox.lmax.s	F.prox.lmin	F.prox.lmin.s
AMNH52532	0.00091921	429.32	3.52E-05	376.6425	3.0881E-05
AMNH52554	0.000879325	379.6735	3.149E-05	306.994	2.5462E-05
AMNH52563	0.000957519	420.0594	3.81952E-05	343.0472	3.11926E-05
AMNH55068	NA	NA	NA	NA	NA
NMNH164582	0.000768602	276.8976	2.49606E-05	227.238	2.04841E-05
NMNH452510	NA	NA	NA	NA	NA
NMNH452512	0.000932784	166.0921	2.77309E-05	127.2559	2.12467E-05
NMNH452514	0.000792141	416.4362	3.17927E-05	293.1415	2.23798E-05
NMNH452517	0.000675836	386.7861	2.41473E-05	306.1931	1.91158E-05
NMNH218470	0.000633497	371.3877	2.11302E-05	274.5042	1.5618E-05
PC.CAMII.360	0.000775288	381.3609	3.04698E-05	250.8508	2.00424E-05
PC.CAMII.371	0.000839801	401.7509	3.50034E-05	272.4065	2.3734E-05
PC.M213	0.000826349	461.4496	3.85873E-05	291.1419	2.43458E-05
PC.M23	0.000851877	513.2556	3.71099E-05	374.8136	2.71002E-05
PC.M230	0.000883205	440.7016	3.71607E-05	297.1738	2.50582E-05
PC.M335	0.000894829	472.5004	3.73731E-05	357.3321	2.82637E-05
PC.M367	0.000687691	665.5526	2.95728E-05	548.8914	2.43891E-05

Name	F.prox.TA.s	F.prox.lmax	F.prox.lmax.s	F.prox.lmin	F.prox.lmin.s
PC.M381	0.000861607	307.8361	3.40199E-05	218.3409	2.41295E-05
PC.M411	0.000644014	395.5293	2.51817E-05	270.6276	1.72297E-05
PC.M426	0.00116435	335.6294	4.63116E-05	272.514	3.76026E-05
PC.M536	0.000641626	279.514	2.07282E-05	205.4372	1.52348E-05
PC.M561	0.000736423	378.8	2.70635E-05	273.6132	1.95484E-05
PC.M618	0.000745406	412.021	2.86758E-05	286.4032	1.9933E-05
PC.M659	0.000844744	390.5621	3.42669E-05	262.2131	2.30059E-05
PC.M688	0.000796425	416.7215	3.014E-05	303.677	2.19639E-05
PC.M753	NA	NA	NA	NA	NA
PC.M754	0.000911892	213.3002	2.95972E-05	172.5025	2.39362E-05
PC.M833	0.000816476	404.9224	3.32015E-05	286.7648	2.35132E-05
PC.M872	0.000872176	397.1738	3.50307E-05	302.8787	2.67139E-05
PC.M878	0.000507096	150.4575	1.18686E-05	121.5222	9.58611E-06
PC.M94	0.000796066	458.4871	3.30292E-05	292.6972	2.10858E-05
PC.M972	0.000937292	242.7752	3.38741E-05	170.4373	2.37809E-05
NMNH477295	0.000783312	382.7681	2.83858E-05	285.538	2.11753E-05
NMNH164832	0.000747982	286.5689	2.52423E-05	241.0416	2.1232E-05
NMNH452530	NA	NA	NA	NA	NA
NMNH452531	NA	NA	NA	NA	NA
NMNH452535	NA	NA	NA	NA	NA
NMNH452536	NA	NA	NA	NA	NA
NMNH452537	NA	NA	NA	NA	NA
NMNH452538	0.00070403	935.9935	3.68055E-05	673.5169	2.64843E-05
NMNH452545	NA	NA	NA	NA	NA
NMNH452546	NA	NA	NA	NA	NA
NMNH452547	0.000885512	669.598	3.5658E-05	631.2471	3.36157E-05
NMNH452549	NA	NA	NA	NA	NA
NMNH452550	NA	NA	NA	NA	NA
NMNH452552	NA	NA	NA	NA	NA
NMNH452553	0.000593008	683.7022	2.69209E-05	493.1975	1.94198E-05
NMNH452554	0.00066475	287.5613	2.35653E-05	201.9254	1.65475E-05
NMNH452556	NA	NA	NA	NA	NA
NMNH452557	NA	NA	NA	NA	NA
NMNH452559	NA	NA	NA	NA	NA
NMNH452568	NA	NA	NA	NA	NA
NMNH452570	0.000673627	593.6863	2.7673E-05	498.7096	2.32459E-05
NMNH452571	0.000596095	487.6039	2.39857E-05	409.6552	2.01513E-05
NMNH452574	0.000642416	634.0102	2.77861E-05	472.3313	2.07004E-05
NMNH452578	0.00074017	269.6835	2.59372E-05	210.7665	2.02708E-05
NMNH452581	0.000921217	387.2446	3.45691E-05	349.1986	3.11728E-05
NMNH452586	0.000687987	547.8528	2.87804E-05	472.2126	2.48068E-05
NMNH452587	0.000680906	655.9797	3.11837E-05	481.327	2.28812E-05
NMNH454554	NA	NA	NA	NA	NA
AMNH52421	0.000665244	723.7199	3.28934E-05	460.2506	2.09186E-05
AMNH52429	0.000827228	1057.1292	5.22167E-05	555.7893	2.74531E-05
NMNH452520	0.000808635	334.5953	3.31651E-05	219.1129	2.17185E-05
NMNH452522	0.001084846	433.9351	5.4771E-05	242.2962	3.05825E-05
NMNH452523	NA	NA	NA	NA	NA
NMNH452524	0.000826507	683.6375	3.97874E-05	522.5426	3.04118E-05
NMNH452525	NA	NA	NA	NA	NA
PC.CAMII372	0.000726482	590.6577	3.70623E-05	315.3272	1.9786E-05
PC.M195	0.000670416	767.0942	3.6186E-05	415.9375	1.96209E-05
PC.CF144	0.000700535	769.4072	3.5245E-05	442.0537	2.02496E-05
PC.M114	0.000704934	737.8226	3.29133E-05	499.6217	2.22875E-05
PC.M232	0.000613789	702.7725	2.72675E-05	540.0763	2.09549E-05
PC.M305	0.000764896	682.1979	3.47955E-05	565.3543	2.88359E-05
PC.M336	0.000666551	690.4795	2.99019E-05	514.6652	2.22881E-05
PC.M378	0.000598967	788.5986	2.64247E-05	573.0723	1.92028E-05
PC.M410	0.00101076	317.6467	3.90756E-05	237.823	2.9256E-05
PC.M433	0.000651482	692.0944	2.86243E-05	544.2203	2.25084E-05
PC.M48	0.000780511	573.9792	3.33608E-05	474.2396	2.75638E-05

Name	F.prox.TA.s	F.prox.lmax	F.prox.lmax.s	F.prox.lmin	F.prox.lmin.s
PC.M625	0.00088827	536.5941	3.77853E-05	437.4083	3.08009E-05
PC.M645	0.000625631	615.7117	2.66651E-05	438.1197	1.8974E-05
PC.M680	0.000613735	763.0561	2.68594E-05	592.198	2.08453E-05
PC.M691	0.000764967	409.2855	2.87538E-05	311.8628	2.19095E-05
PC.M793	0.000737244	367.2648	2.65401E-05	329.3663	2.38014E-05
PC.M832	0.00067646	557.7753	2.91504E-05	365.1615	1.9084E-05
PC.M836	0.00072945	572.5458	3.08148E-05	408.2083	2.197E-05
PC.M868	0.000778787	231.782	2.64488E-05	173.3755	1.9784E-05
PC.M904	0.00066355	567.3338	2.48832E-05	500.5881	2.19557E-05
PC.M906	0.000792996	1144.1924	4.45592E-05	824.561	3.21115E-05
PC.M990	0.000805716	408.3655	3.25129E-05	290.425	2.31228E-05
PC.CAMII.317	0.000869861	330.0784	3.21631E-05	248.6853	2.42321E-05
PC.M103	0.001087187	269.1702	3.73404E-05	245.3897	3.40414E-05
PC.M152	0.001107062	265.3317	4.01501E-05	232.5137	3.51841E-05
PC.M159	0.000848409	410.4794	3.30555E-05	331.3757	2.66853E-05
PC.M230	0.000858925	371.9702	3.18976E-05	306.5529	2.62879E-05
PC.M277	0.001068763	269.3863	4.06445E-05	212.0231	3.19896E-05
PC.M297	0.00082139	393.8422	3.41864E-05	262.6556	2.27991E-05
PC.M306	0.000670671	352.337	2.37741E-05	269.2587	1.81683E-05
PC.M344	NA	NA	NA	NA	NA
PC.M347	NA	NA	NA	NA	NA
PC.M383	0.000738151	410.1815	2.99435E-05	268.5854	1.96069E-05
PC.M654	0.000805598	447.208	3.24182E-05	352.0214	2.55181E-05
PC.M660	0.000940189	272.4076	3.34156E-05	222.2188	2.7259E-05
PC.M769	0.000908638	432.244	3.70285E-05	342.8996	2.93748E-05
PC.M82	0.000679563	399.6606	2.63126E-05	266.7341	1.75611E-05
PC.M88	0.000867449	252.0103	3.042E-05	208.4099	2.5157E-05
PC.M90	0.000855238	429.5416	3.84489E-05	271.7329	2.43232E-05
PC.M908	0.000752941	395.5344	3.05728E-05	271.8991	2.10164E-05
PC.M931	0.000771044	384.2827	2.75814E-05	358.4663	2.57285E-05

Name	F.prox.MaxXrad	F.prox.MaxYrad	F.prox.J	F.prox.J.s	F.prox.ZpEst
AMNH52532	4.8198	4.8886	805.9625	6.6081E-05	166.0341
AMNH52554	4.6842	4.6891	686.6675	5.6952E-05	146.5156
AMNH52563	4.9369	4.5681	763.1066	6.93878E-05	160.5695
AMNH55068	NA	NA	NA	NA	NA
NMNH164582	4.4982	4.0895	504.1356	4.54447E-05	117.4088
NMNH452510	NA	NA	NA	NA	NA
NMNH452512	3.7391	3.6609	293.348	4.89776E-05	79.2832
NMNH452514	4.6416	5.0219	709.5777	5.41725E-05	146.8573
NMNH452517	4.5486	4.7905	692.9791	4.32632E-05	148.4038
NMNH218470	4.5058	4.7858	645.8919	3.67482E-05	139.0271
PC.CAMII.360	4.2921	4.6009	632.2116	5.05122E-05	142.1819
PC.CAMII.371	4.7522	4.7689	674.1575	5.87374E-05	141.6134
PC.M213	5.1835	4.4108	752.5914	6.29331E-05	156.8830
PC.M23	5.0025	4.8708	888.0691	6.42101E-05	179.8931
PC.M230	5.0228	4.3886	737.8754	6.22189E-05	156.8046
PC.M335	4.9773	4.8256	829.8325	6.56368E-05	169.3035
PC.M367	5.2331	5.6239	1214.444	5.39619E-05	223.7163
PC.M381	4.0317	4.6609	526.177	5.81494E-05	121.0632
PC.M411	4.2706	4.9885	666.1569	4.24114E-05	143.8924
PC.M426	4.5635	4.5639	608.1434	8.39142E-05	133.2567
PC.M536	4.6847	3.9997	484.9512	3.5963E-05	111.6833
PC.M561	4.6284	4.6455	652.4132	4.66119E-05	140.6988
PC.M618	4.348	5.4125	698.4243	4.86088E-05	143.1124
PC.M659	4.315	4.8926	652.7752	5.72729E-05	141.7905
PC.M688	4.4197	4.8523	720.3984	5.21039E-05	155.3922
PC.M753	NA	NA	NA	NA	NA
PC.M754	3.8148	4.377	385.8027	5.35333E-05	94.1924
PC.M833	5.3459	4.3603	691.6872	5.67148E-05	142.5248
PC.M872	5.0018	4.5216	700.0526	6.17447E-05	147.0174
PC.M878	3.6239	3.6727	271.9797	2.14547E-05	74.5497

Name	F.prox.MaxXrad	F.prox.MaxYrad	F.prox.J	F.prox.J.s	F.prox.ZpEst
PC.M94	4.3228	5.206	751.1843	5.41149E-05	157.6661
PC.M972	4.1108	4.2289	413.2126	5.7655E-05	99.0953
NMNH477295	4.7635	4.3521	668.3061	4.95612E-05	146.6291
NMNH164832	4.2054	4.7579	527.6105	4.64743E-05	117.7268
NMNH452530	NA	NA	NA	NA	NA
NMNH452531	NA	NA	NA	NA	NA
NMNH452535	NA	NA	NA	NA	NA
NMNH452536	NA	NA	NA	NA	NA
NMNH452537	NA	NA	NA	NA	NA
NMNH452538	6.0174	5.6144	1609.5103	6.32898E-05	276.7431
NMNH452545	NA	NA	NA	NA	NA
NMNH452546	NA	NA	NA	NA	NA
NMNH452547	5.3661	5.5213	1300.845	6.92737E-05	238.9634
NMNH452549	NA	NA	NA	NA	NA
NMNH452550	NA	NA	NA	NA	NA
NMNH452552	NA	NA	NA	NA	NA
NMNH452553	5.4389	5.2233	1176.8998	4.63407E-05	220.7612
NMNH452554	4.3036	4.1347	489.4868	4.01128E-05	116.0155
NMNH452556	NA	NA	NA	NA	NA
NMNH452557	NA	NA	NA	NA	NA
NMNH452559	NA	NA	NA	NA	NA
NMNH452568	NA	NA	NA	NA	NA
NMNH452570	5.1969	5.4785	1092.3959	5.09189E-05	204.6567
NMNH452571	5.055	4.8294	897.2591	4.4137E-05	181.5505
NMNH452574	5.5036	5.0001	1106.3415	4.84865E-05	210.6575
NMNH452578	4.2232	4.3064	480.45	4.6208E-05	112.6548
NMNH452581	4.6802	4.5904	736.4432	6.57419E-05	158.8771
NMNH452586	5.0195	5.3833	1020.0654	5.35871E-05	196.1136
NMNH452587	6.0104	4.8897	1137.3067	5.40649E-05	208.6782
NMNH454554	NA	NA	NA	NA	NA
AMNH52421	5.9228	4.7508	1183.9705	5.3812E-05	221.8503
AMNH52429	6.0316	5.9283	1612.9184	7.96697E-05	269.7211
NMNH452520	4.081	4.8087	553.7082	5.48836E-05	124.5730
NMNH452522	4.8918	4.5551	676.2312	8.53535E-05	143.1647
NMNH452523	NA	NA	NA	NA	NA
NMNH452524	5.2575	5.5107	1206.1801	7.01992E-05	224.0263
NMNH452525	NA	NA	NA	NA	NA
PC.CAMII372	5.1468	5.1416	905.9849	5.68483E-05	176.1177
PC.M195	5.6222	5.361	1183.0317	5.58069E-05	215.4257
PC.CF144	4.9621	6.1095	1211.461	5.54945E-05	218.8412
PC.M114	5.425	5.2663	1237.4444	5.52008E-05	231.4862
PC.M232	5.2724	5.7332	1242.8489	4.82224E-05	225.8575
PC.M305	5.2326	5.8549	1247.5523	6.36315E-05	225.0376
PC.M336	5.2362	5.4472	1205.1446	5.21899E-05	225.6107
PC.M378	5.7089	5.371	1361.6709	4.56275E-05	245.7912
PC.M410	4.3385	4.6861	555.4697	6.83316E-05	123.1012
PC.M433	5.332	5.406	1236.3146	5.11327E-05	230.2691
PC.M48	4.9031	5.4137	1048.2189	6.09246E-05	203.2062
PC.M625	5.559	5.0236	974.0024	6.85862E-05	184.0762
PC.M645	4.7742	5.7107	1053.8314	4.56391E-05	201.0189
PC.M680	5.6017	5.3594	1355.2541	4.77047E-05	247.2843
PC.M691	5.1275	4.41	721.1483	5.06632E-05	151.2238
PC.M793	4.6518	4.5224	696.6311	5.03416E-05	151.8674
PC.M832	4.8181	5.3177	922.9368	4.82344E-05	182.1142
PC.M836	5.617	4.6537	980.754	5.27848E-05	190.9809
PC.M868	4.2757	3.8043	405.1575	4.62328E-05	100.2865
PC.M904	5.119	5.179	1067.9219	4.68389E-05	207.4037
PC.M906	5.9873	6.08	1968.7534	7.66707E-05	326.2956
PC.M990	4.6689	4.7199	698.7906	5.56357E-05	148.8562
PC.CAMII.317	4.2416	4.8112	578.7637	5.63952E-05	127.8640
PC.M103	4.2494	4.2716	514.5599	7.13818E-05	120.7745

Name	F.prox.MaxXrad	F.prox.MaxYrad	F.prox.J	F.prox.J.s	F.prox.ZpEst
PC.M152	4.1005	4.4044	497.8454	7.53342E-05	117.0726
PC.M159	4.7793	4.7747	741.8551	5.97408E-05	155.2973
PC.M230	4.5566	4.8261	678.5231	5.81856E-05	144.6328
PC.M277	4.1936	4.5183	481.4094	7.26341E-05	110.5177
PC.M297	4.2294	4.8808	656.4978	5.69855E-05	144.1237
PC.M306	4.3507	4.9302	621.5957	4.19424E-05	133.9516
PC.M344	NA	NA	NA	NA	NA
PC.M347	NA	NA	NA	NA	NA
PC.M383	4.2358	5.3971	678.767	4.95504E-05	140.9268
PC.M654	4.7914	4.9118	799.2293	5.79363E-05	164.7352
PC.M660	4.4862	4.2275	494.6263	6.06746E-05	113.5284
PC.M769	4.5297	5.3838	775.1436	6.64033E-05	156.3814
PC.M82	4.9089	4.547	666.3947	4.38737E-05	140.9479
PC.M88	3.9787	4.283	460.4203	5.5577E-05	111.4590
PC.M90	4.9552	4.3155	701.2745	6.27722E-05	151.2884
PC.M908	4.835	4.2023	667.4336	5.15892E-05	147.7064
PC.M931	4.7374	4.9042	742.749	5.33099E-05	154.0717
Name	**F.prox.ZpEst.s**	**H.dist.TA**	**H.dist.TA.s**	**H.dist.Imax**	**H.dist.Imax.s**
AMNH52532	0.0021509	NA	NA	NA	NA
AMNH52554	0.0019686	NA	NA	NA	NA
AMNH52563	0.0022265	NA	NA	NA	NA
AMNH55068	NA	48.0742	0.000666623	251.2467	2.89122E-05
NMNH164582	0.0016087	42.6164	0.000583924	192.3529	2.25264E-05
NMNH452510	NA	51.1168	0.000592326	274.0904	2.58218E-05
NMNH452512	0.0017341	32.2336	0.000705009	106.2478	2.23446E-05
NMNH452514	0.0017602	45.2386	0.000542235	219.7804	2.0421E-05
NMNH452517	0.0015287	47.1375	0.000485566	237.5185	1.88207E-05
NMNH218470	0.0013922	59.944	0.000600254	405.2536	3.00595E-05
PC.CAMII.360	0.0017722	42.0453	0.000524054	199.0951	2.0175E-05
PC.CAMII.371	0.0018508	42.4875	0.000555272	186.5247	1.99812E-05
PC.M213	0.0019154	43.1413	0.000526703	216.5425	2.25959E-05
PC.M23	0.0020681	48.549	0.000558128	279.1658	2.65235E-05
PC.M230	0.0020626	39.7089	0.000522338	165.6282	1.80058E-05
PC.M335	0.0021091	47.7724	0.000595134	231.9642	2.33987E-05
PC.M367	0.0017694	65.142	0.000515218	471.8438	2.56487E-05
PC.M381	0.0018329	35.342	0.000535088	138.0631	1.802E-05
PC.M411	0.0014474	47.9381	0.000482219	254.4059	1.95353E-05
PC.M426	0.0025191	44.6036	0.000843179	0.5461	9.471E-08
PC.M536	0.0013086	44.2483	0.000518456	194.4912	1.73958E-05
PC.M561	0.0016335	43.2735	0.0005024	193.9338	1.75902E-05
PC.M618	0.0016285	45.2931	0.000515401	193.2718	1.73172E-05
PC.M659	0.0018909	45.3044	0.000604184	205.0279	2.25973E-05
PC.M688	0.0018544	44.0768	0.000526007	213.1604	1.99516E-05
PC.M753	NA	43.501	0.000639678	199.1214	2.49197E-05
PC.M754	0.0017514	33.2261	0.000617793	113.6267	1.93829E-05
PC.M833	0.0017822	43.7697	0.000547306	205.4444	2.13188E-05
PC.M872	0.0019450	41.8471	0.000553637	180.2216	1.97052E-05
PC.M878	0.0009174	45.7355	0.000562814	202.5269	1.97799E-05
PC.M94	0.0018514	46.383	0.00054465	270.8323	2.58555E-05
PC.M972	0.0018389	35.59	0.000660455	127.5538	2.18162E-05
NMNH477295	0.0017833	41.3892	0.000503381	198.7652	1.87396E-05
NMNH164832	0.0015347	42.6364	0.00055583	196.0907	2.11268E-05
NMNH452530	NA	NA	NA	NA	NA
NMNH452531	NA	NA	NA	NA	NA
NMNH452535	NA	NA	NA	NA	NA
NMNH452536	NA	NA	NA	NA	NA
NMNH452537	NA	NA	NA	NA	NA
NMNH452538	0.0019588	NA	NA	NA	NA
NMNH452545	NA	NA	NA	NA	NA
NMNH452546	NA	NA	NA	NA	NA
NMNH452547	0.0023415	72.2013	0.000707466	475.6171	3.23635E-05

Name	F.prox.ZpEst.s	H.dist.TA	H.dist.TA.s	H.dist.lmax	H.dist.lmax.s
NMNH452549	NA	NA	NA	NA	NA
NMNH452550	NA	37.5306	0.000483371	138.0685	1.46962E-05
NMNH452552	NA	NA	NA	NA	NA
NMNH452553	0.0015386	NA	NA	NA	NA
NMNH452554	0.0014071	NA	NA	NA	NA
NMNH452556	NA	NA	NA	NA	NA
NMNH452557	NA	NA	NA	NA	NA
NMNH452559	NA	NA	NA	NA	NA
NMNH452568	NA	NA	NA	NA	NA
NMNH452570	0.0016694	67.1253	0.000547549	435.2206	2.44838E-05
NMNH452571	0.0014468	55.7386	0.000444176	327.475	1.87743E-05
NMNH452574	0.0016341	51.6346	0.00040054	286.0236	1.51969E-05
NMNH452578	0.0015277	34.8948	0.000473204	125.3395	1.40472E-05
NMNH452581	0.0021558	44.6852	0.000606331	224.1289	2.51338E-05
NMNH452586	0.0016896	NA	NA	NA	NA
NMNH452587	0.0016963	60.0758	0.000488353	434.7934	2.50667E-05
NMNH454554	NA	NA	NA	NA	NA
AMNH52421	0.0017343	NA	NA	NA	NA
AMNH52429	0.0022782	66.1325	0.000558589	505.735	2.49807E-05
NMNH452520	0.0017287	45.5851	0.000632575	229.4761	2.67596E-05
NMNH452522	0.0024395	38.3811	0.000653999	177.6077	2.6782E-05
NMNH452523	NA	51.9186	0.000508464	281.0989	2.05443E-05
NMNH452524	0.0021383	37.3641	0.00035663	157.4807	1.12172E-05
NMNH452525	NA	NA	NA	NA	NA
PC.CAMII372	0.0017405	52.4904	0.000518748	288.368	2.15899E-05
PC.M195	0.0017174	57.188	0.000455915	367.6668	1.99396E-05
PC.CF144	0.0017944	68.0337	0.000557851	484.7743	2.82916E-05
PC.M114	0.0018691	74.273	0.000599693	562.1116	3.28883E-05
PC.M232	0.0015774	74.3101	0.00051898	622.4037	2.95704E-05
PC.M305	0.0019513	60.6126	0.000525563	392.9748	2.46024E-05
PC.M336	0.0017391	72.8073	0.000561232	633.4089	3.46284E-05
PC.M378	0.0016060	85.8516	0.000560967	868.0989	3.91192E-05
PC.M410	0.0021201	37.9691	0.000653912	137.4664	2.04976E-05
PC.M433	0.0017095	73.1455	0.000543028	584.4612	3.09929E-05
PC.M48	0.0019606	54.018	0.000521179	304.5934	2.13731E-05
PC.M625	0.0020999	58.2458	0.000664441	339.3932	3.1997E-05
PC.M645	0.0015583	73.6408	0.000570871	626.4956	3.33791E-05
PC.M680	0.0016538	69.8951	0.000467456	497.9107	2.22001E-05
PC.M691	0.0017317	42.8052	0.000490177	218.4708	1.90976E-05
PC.M793	0.0016956	60.411	0.000674479	339.6153	2.9623E-05
PC.M832	0.0016370	61.1877	0.000550019	344.4388	2.20368E-05
PC.M836	0.0017885	NA	NA	NA	NA
PC.M868	0.0015564	39.1384	0.000607391	156.7787	2.06191E-05
PC.M904	0.0016829	77.1106	0.000625681	531.8685	2.91596E-05
PC.M906	0.0023508	73.6713	0.000530772	546.1344	2.69498E-05
PC.M990	0.0018251	47.2469	0.000579296	224.0273	2.21517E-05
PC.CAMII.317	0.0018564	44.3473	0.000643865	200.5146	2.50966E-05
PC.M103	0.0023121	40.5937	0.000777122	165.0843	2.72445E-05
PC.M152	0.0023207	35.0411	0.000694619	124.1472	2.29997E-05
PC.M159	0.0019384	59.1838	0.000738731	456.0535	4.7045E-05
PC.M230	0.0019100	54.9198	0.000725271	320.5353	3.33306E-05
PC.M277	0.0021594	30.9595	0.000604908	137.4198	2.46331E-05
PC.M297	0.0018640	52.2683	0.000676014	267.1257	2.85527E-05
PC.M306	0.0014462	52.6173	0.00056806	287.6425	2.37054E-05
PC.M344	NA	45.183	0.000565879	226.3704	2.30496E-05
PC.M347	NA	32.9449	0.00059247	113.0406	1.81507E-05
PC.M383	0.0016152	49.2803	0.000564806	286.157	2.56225E-05
PC.M654	0.0018808	60.2761	0.000688184	393.9774	3.52794E-05
PC.M660	0.0019218	43.4127	0.000734895	184.8741	2.72137E-05
PC.M769	0.0020497	46.7416	0.000612636	231.3168	2.52653E-05
PC.M82	0.0014987	61.1257	0.000649934	417.3777	3.33675E-05

Name	F.prox.ZpEst.s	H.dist.TA	H.dist.TA.s	H.dist.lmax	H.dist.lmax.s
PC.M88	0.0018029	35.4534	0.00057346	113.9826	1.59625E-05
PC.M90	0.0019771	47.426	0.000619796	240.5608	2.61985E-05
PC.M908	0.0017354	57.0949	0.000670798	355.7035	3.20237E-05
PC.M931	0.0017417	50.1755	0.000567202	255.9268	2.21693E-05
Name	**H.dist.lmin**	**H.dist.lmin.s**	**H.dist.MaxXrad**	**H.dist.MaxYrad**	**H.dist.J**
AMNH52532	NA	NA	NA	NA	NA
AMNH52554	NA	NA	NA	NA	NA
AMNH52563	NA	NA	NA	NA	NA
AMNH55068	137.4375	1.58156E-05	3.6466	4.5586	388.6842
NMNH164582	110.1316	1.28975E-05	3.4792	4.2779	302.4844
NMNH452510	160.6046	1.51304E-05	3.6992	4.615	434.695
NMNH452512	65.1197	1.36951E-05	2.9048	3.7488	171.3675
NMNH452514	122.377	1.13707E-05	4.7036	3.3583	342.1575
NMNH452517	135.1913	1.07124E-05	4.5317	4.0597	372.7098
NMNH218470	204.8681	1.5196E-05	5.4087	3.7911	610.1217
PC.CAMII.360	104.6828	1.06079E-05	4.7025	3.3705	303.7779
PC.CAMII.371	113.7891	1.21895E-05	4.1934	3.4275	300.3138
PC.M213	103.9608	1.08482E-05	3.3453	4.5387	320.5034
PC.M23	129.9883	1.23502E-05	4.8974	3.435	409.1541
PC.M230	99.8116	1.08508E-05	4.4692	3.7757	265.4398
PC.M335	143.5757	1.44828E-05	4.6038	3.5587	375.5399
PC.M367	258.4516	1.4049E-05	5.6227	4.3894	730.2954
PC.M381	74.0333	9.66281E-06	3.293	4.1712	212.0964
PC.M411	132.7385	1.01927E-05	3.5123	4.5771	387.1444
PC.M426	0.1078	1.86957E-08	4.1335	4.5792	0.6539
PC.M536	129.1931	1.15554E-05	3.5739	4.2775	323.6842
PC.M561	120.8023	1.0957E-05	3.7704	4.4409	314.7361
PC.M618	142.2351	1.27443E-05	3.9559	3.8411	335.5068
PC.M659	132.7147	1.46272E-05	4.318	3.5733	337.7426
PC.M688	114.9337	1.07577E-05	4.3443	3.4627	328.0941
PC.M753	115.4399	1.44471E-05	3.3247	4.3024	314.5613
PC.M754	69.5339	1.18613E-05	3.8694	3.1629	183.1606
PC.M833	116.1272	1.20505E-05	4.3792	3.4817	321.5715
PC.M872	109.1988	1.19397E-05	3.356	4.0651	289.4203
PC.M878	139.0976	1.3585E-05	4.2922	3.6837	341.6245
PC.M94	113.7436	1.08588E-05	3.4904	4.5754	384.576
PC.M972	83.7303	1.43208E-05	3.4771	3.3333	211.2841
NMNH477295	94.7027	8.92858E-06	3.1421	4.367	293.4678
NMNH164832	109.8397	1.18341E-05	3.3951	4.5862	305.9304
NMNH452530	NA	NA	NA	NA	NA
NMNH452531	NA	NA	NA	NA	NA
NMNH452535	NA	NA	NA	NA	NA
NMNH452536	NA	NA	NA	NA	NA
NMNH452537	NA	NA	NA	NA	NA
NMNH452538	NA	NA	NA	NA	NA
NMNH452545	NA	NA	NA	NA	NA
NMNH452546	NA	NA	NA	NA	NA
NMNH452547	364.3138	2.47898E-05	4.6034	5.2212	839.9309
NMNH452549	NA	NA	NA	NA	NA
NMNH452550	91.8519	9.77683E-06	3.7648	3.6734	229.9204
NMNH452552	NA	NA	NA	NA	NA
NMNH452553	NA	NA	NA	NA	NA
NMNH452554	NA	NA	NA	NA	NA
NMNH452556	NA	NA	NA	NA	NA
NMNH452557	NA	NA	NA	NA	NA
NMNH452559	NA	NA	NA	NA	NA
NMNH452568	NA	NA	NA	NA	NA
NMNH452570	303.2259	1.70583E-05	4.8353	4.4832	738.4465
NMNH452571	189.2798	1.08515E-05	4.7544	3.9291	516.7549
NMNH452574	159.5475	8.477E-06	3.7839	4.7485	445.571
NMNH452578	77.0916	8.63992E-06	3.1734	3.9254	202.4311

Name	H.dist.lmin	H.dist.lmin.s	H.dist.MaxXrad	H.dist.MaxYrad	H.dist.J
NMNH452581	115.9893	1.30071E-05	4.4231	4.1308	340.1182
NMNH452586	NA	NA	NA	NA	NA
NMNH452587	199.6099	1.15079E-05	3.9807	5.358	634.4033
NMNH454554	NA	NA	NA	NA	NA
AMNH52421	NA	NA	NA	NA	NA
AMNH52429	259.2497	1.28056E-05	5.6522	4.4488	764.9846
NMNH452520	124.8011	1.45533E-05	4.7363	3.6573	354.2772
NMNH452522	81.599	1.23046E-05	3.7646	4.4462	259.2067
NMNH452523	169.2285	1.23682E-05	3.9296	4.8746	450.3273
NMNH452524	83.1015	5.91927E-06	4.1916	3.314	240.5822
NMNH452525	NA	NA	NA	NA	NA
PC.CAMII372	178.3525	1.33531E-05	4.7679	4.7476	466.7206
PC.M195	194.4254	1.05442E-05	4.2082	5.227	562.0922
PC.CF144	287.4349	1.67748E-05	5.4008	4.3142	772.2092
PC.M114	357.0301	2.08893E-05	5.4402	4.8815	919.1417
PC.M232	320.9544	1.52486E-05	5.9875	4.401	943.3581
PC.M305	224.3436	1.40451E-05	4.1314	5.1923	617.3184
PC.M336	287.0976	1.56956E-05	4.2097	5.7684	920.5065
PC.M378	411.5585	1.85461E-05	6.1562	4.7828	1279.6574
PC.M410	97.6641	1.45627E-05	3.9849	3.4248	235.1305
PC.M433	328.0787	1.73974E-05	5.3727	4.8948	912.5399
PC.M48	179.2971	1.25811E-05	3.7687	4.767	483.8905
PC.M625	218.6724	2.06158E-05	5.0194	4.1362	558.0656
PC.M645	301.4403	1.60605E-05	4.3897	5.9566	927.9359
PC.M680	312.8715	1.39498E-05	4.3791	5.427	810.7821
PC.M691	109.6457	9.58465E-06	4.9785	3.5007	328.1165
PC.M793	257.5224	2.24625E-05	4.541	4.8392	597.1377
PC.M832	261.2815	1.67165E-05	4.2706	4.9825	605.7203
PC.M836	NA	NA	NA	NA	NA
PC.M868	98.2819	1.29258E-05	3.444	4.0066	255.0606
PC.M904	427.4094	2.34326E-05	5.3888	5.326	959.2778
PC.M906	347.687	1.71572E-05	4.9262	5.4782	893.8213
PC.M990	145.8127	1.44179E-05	4.3215	3.6899	369.84
PC.CAMII.317	126.3277	1.58113E-05	4.3898	3.5109	326.8423
PC.M103	105.1092	1.73466E-05	3.3017	4.0894	270.1935
PC.M152	78.6143	1.45642E-05	3.9189	3.1024	202.7615
PC.M159	177.7599	1.83371E-05	5.25	4.1409	633.8134
PC.M230	187.6852	1.95163E-05	5.0441	3.7819	508.2205
PC.M277	43.491	7.79594E-06	4.4005	2.8865	180.9108
PC.M297	182.7799	1.95371E-05	4.2809	3.9182	449.9056
PC.M306	175.7383	1.44831E-05	4.2742	4.5209	463.3807
PC.M344	125.2033	1.27485E-05	4.5497	3.6512	351.5738
PC.M347	67.5479	1.08461E-05	3.8375	2.9279	180.5885
PC.M383	136.0389	1.21809E-05	3.8509	4.9231	422.1959
PC.M654	223.257	1.99919E-05	5.0419	4.182	617.2344
PC.M660	126.7834	1.86626E-05	4.1533	3.9958	311.6576
PC.M769	132.811	1.45061E-05	4.5086	3.4025	364.1278
PC.M82	222.7988	1.78118E-05	5.5056	3.9735	640.1765
PC.M88	90.2917	1.26448E-05	3.6528	3.6847	204.2742
PC.M90	135.9095	1.48013E-05	3.8665	4.5473	376.4703
PC.M908	190.5666	1.71566E-05	4.7846	4.1704	546.2701
PC.M931	164.7777	1.42736E-05	4.056	4.7473	420.7045

Name	H.dist.J.s	H.dist.ZpEst	H.dist.ZpEst.s	H.mid.TA	H.mid.TA.s
AMNH52532	NA	NA	NA	NA	NA
AMNH52554	NA	NA	NA	NA	NA
AMNH52563	NA	NA	NA	NA	NA
AMNH55068	4.47278E-05	94.74	0.00131373	53.2583	0.000738508
NMNH164582	3.54239E-05	77.99	0.00106860	47.9743	0.000657338
NMNH452510	4.09522E-05	104.57	0.00121169	55.9303	0.000648104
NMNH452512	3.60397E-05	51.51	0.00112665	35.0023	0.000765565
NMNH452514	3.17918E-05	84.88	0.00101741	53.3402	0.000639342

Name	H.dist.J.s	H.dist.ZpEst	H.dist.ZpEst.s	H.mid.TA	H.mid.TA.s
NMNH452517	2.95331E-05	86.76	0.00089376	54.3534	0.000559898
NMNH218470	4.52556E-05	132.64	0.00132818	61.1214	0.000612044
PC.CAMII.360	3.07829E-05	75.26	0.00093802	48.7428	0.000607532
PC.CAMII.371	3.21707E-05	78.81	0.00103002	44.8678	0.00058638
PC.M213	3.34441E-05	81.30	0.00099263	50.0162	0.000610638
PC.M23	3.88736E-05	98.21	0.00112902	58.0333	0.000667161
PC.M230	2.88566E-05	64.39	0.00084698	46.8318	0.000616034
PC.M335	3.78815E-05	92.02	0.00114631	50.7603	0.000632356
PC.M367	3.96977E-05	145.88	0.00115381	69.4082	0.00054896
PC.M381	2.76828E-05	56.83	0.00086043	41.0237	0.000621111
PC.M411	2.9728E-05	95.72	0.00096283	52.4026	0.000527128
PC.M426	1.13406E-07	0.15	0.00000284	48.1488	0.000910197
PC.M536	2.89511E-05	82.45	0.00096610	44.6901	0.000523633
PC.M561	2.85473E-05	76.66	0.00089001	48.232	0.000559968
PC.M618	3.00615E-05	86.06	0.00097930	50.7336	0.00057731
PC.M659	3.72245E-05	85.60	0.00114155	45.5319	0.000607218
PC.M688	3.07093E-05	84.05	0.00100306	46.7897	0.000558382
PC.M753	3.93667E-05	82.49	0.00121294	47.2323	0.000694546
PC.M754	3.12442E-05	52.09	0.00096856	37.0796	0.000689444
PC.M833	3.33693E-05	81.82	0.00102304	49.4167	0.000617917
PC.M872	3.16449E-05	78.00	0.00103193	43.1534	0.00057092
PC.M878	3.33649E-05	85.66	0.00105417	47.1605	0.00058035
PC.M94	3.67143E-05	95.36	0.00111976	55.7633	0.000654797
PC.M972	3.6137E-05	62.05	0.00115143	35.9515	0.000667163
NMNH477295	2.76682E-05	78.16	0.00095063	47.2797	0.000575022
NMNH164832	3.29609E-05	76.66	0.00099940	45.9733	0.000599331
NMNH452530	NA	NA	NA	NA	NA
NMNH452531	NA	NA	NA	NA	NA
NMNH452535	NA	NA	NA	NA	NA
NMNH452536	NA	NA	NA	NA	NA
NMNH452537	NA	NA	NA	NA	NA
NMNH452538	NA	NA	NA	NA	NA
NMNH452545	NA	NA	NA	NA	NA
NMNH452546	NA	NA	NA	NA	NA
NMNH452547	5.71533E-05	170.99	0.00167540	83.9228	0.000822319
NMNH452549	NA	NA	NA	NA	NA
NMNH452550	2.4473E-05	61.82	0.00079622	NA	NA
NMNH452552	NA	NA	NA	NA	NA
NMNH452553	NA	NA	NA	NA	NA
NMNH452554	NA	NA	NA	NA	NA
NMNH452556	NA	NA	NA	NA	NA
NMNH452557	NA	NA	NA	NA	NA
NMNH452559	NA	NA	NA	NA	NA
NMNH452568	NA	NA	NA	NA	NA
NMNH452570	4.15421E-05	158.49	0.00129283	64.6131	0.000527057
NMNH452571	2.96257E-05	119.02	0.00094846	NA	NA
NMNH452574	2.36739E-05	104.44	0.00081018	63.8011	0.000494918
NMNH452578	2.26872E-05	57.03	0.00077341	37.8353	0.00051308
NMNH452581	3.81409E-05	79.52	0.00107905	47.4342	0.000643632
NMNH452586	NA	NA	NA	NA	NA
NMNH452587	3.65747E-05	135.87	0.00110444	69.1622	0.000562216
NMNH454554	NA	NA	NA	NA	NA
AMNH52421	NA	NA	NA	NA	NA
AMNH52429	3.77862E-05	151.47	0.00127937	75.0334	0.00063377
NMNH452520	4.13129E-05	84.42	0.00117142	53.7963	0.000746521
NMNH452522	3.90866E-05	63.14	0.00107585	42.246	0.000719856
NMNH452523	3.29125E-05	102.30	0.00100186	62.4674	0.000611774
NMNH452524	1.71365E-05	64.11	0.00061189	45.5008	0.000434293
NMNH452525	NA	NA	NA	NA	NA
PC.CAMII372	3.4943E-05	98.10	0.00096947	60.066	0.000593616
PC.M195	3.04838E-05	119.15	0.00094987	66.6596	0.000531424

Name	H.dist.J.s	H.dist.ZpEst	H.dist.ZpEst.s	H.mid.TA	H.mid.TA.s
PC.CF144	4.50664E-05	158.97	0.00130351	73.806	0.000605181
PC.M114	5.37776E-05	178.10	0.00143800	75.6248	0.000610608
PC.M232	4.4819E-05	181.62	0.00126840	79.9651	0.000558474
PC.M305	3.86475E-05	132.42	0.00114819	68.6267	0.000595052
PC.M336	5.0324E-05	184.51	0.00142225	75.599	0.000582752
PC.M378	5.76653E-05	233.96	0.00152875	104.7128	0.000684209
PC.M410	3.50603E-05	63.47	0.00109302	37.6265	0.000648012
PC.M433	4.83903E-05	177.75	0.00131963	77.3861	0.00057451
PC.M48	3.39542E-05	113.38	0.00109392	58.3881	0.000563343
PC.M625	5.26128E-05	121.91	0.00139066	63.8812	0.000728727
PC.M645	4.94395E-05	179.38	0.00139054	84.2923	0.000653442
PC.M680	3.61499E-05	165.36	0.00110594	83.2794	0.00055697
PC.M691	2.86822E-05	77.39	0.00088626	47.7478	0.000546776
PC.M793	5.20855E-05	127.32	0.00142149	63.9369	0.000713845
PC.M832	3.87533E-05	130.92	0.00117687	74.5282	0.000669937
PC.M836	NA	NA	NA	NA	NA
PC.M868	3.35449E-05	68.47	0.00106255	40.6799	0.000631314
PC.M904	5.25922E-05	179.06	0.00145288	80.5239	0.000653377
PC.M906	4.4107E-05	171.82	0.00123787	82.4318	0.000593888
PC.M990	3.65695E-05	92.33	0.00113204	52.2376	0.000640487
PC.CAMII.317	4.0908E-05	82.74	0.00120124	50.7569	0.000736924
PC.M103	4.4591E-05	73.11	0.00139967	41.7887	0.000799999
PC.M152	3.75639E-05	57.76	0.00114490	37.0068	0.000733585
PC.M159	6.53822E-05	134.98	0.00168487	60.1041	0.000750218
PC.M230	5.28469E-05	115.16	0.00152086	58.0973	0.000767233
PC.M277	3.2429E-05	49.65	0.00097016	32.7308	0.000639517
PC.M297	4.80898E-05	109.75	0.00141939	62.9112	0.000813664
PC.M306	3.81885E-05	105.37	0.00113761	58.864	0.0006355
PC.M344	3.57981E-05	85.74	0.00107383	50.9158	0.000637678
PC.M347	2.89968E-05	53.39	0.00096007	35.7372	0.000642685
PC.M383	3.78034E-05	96.24	0.00110299	56.3336	0.000645645
PC.M654	5.52713E-05	133.83	0.00152801	65.4985	0.00074781
PC.M660	4.58763E-05	76.49	0.00129481	49.1306	0.000831689
PC.M769	3.97714E-05	92.05	0.00120655	54.1222	0.000709372
PC.M82	5.11792E-05	135.07	0.00143618	77.8655	0.000827925
PC.M88	2.86073E-05	55.68	0.00090062	40.1118	0.00064881
PC.M90	4.09998E-05	89.49	0.00116950	49.7694	0.000650421
PC.M908	4.91803E-05	122.00	0.00143340	62.8436	0.000738338
PC.M931	3.64429E-05	95.58	0.00108046	56.1042	0.000634222

Name	H.mid.lmax	H.mid.lmax.s	H.mid.lmin	H.mid.lmin.s	H.mid.MaxXrad
AMNH52532	NA	NA	NA	NA	NA
AMNH52554	NA	NA	NA	NA	NA
AMNH52563	NA	NA	NA	NA	NA
AMNH55068	281.6731	3.24135E-05	185.2934	2.13226E-05	4.3345
NMNH164582	244.7493	2.86626E-05	140.8571	1.64958E-05	4.1638
NMNH452510	308.7206	2.90842E-05	204.291	1.9246E-05	4.2345
NMNH452512	133.2395	2.80211E-05	73.6787	1.54951E-05	3.2906
NMNH452514	294.8466	2.73959E-05	175.1021	1.62697E-05	4.5451
NMNH452517	284.4314	2.2538E-05	200.7913	1.59105E-05	4.323
NMNH218470	444.5839	3.29769E-05	201.4102	1.49395E-05	5.217
PC.CAMII.360	225.2506	2.28255E-05	168.3399	1.70585E-05	4.4531
PC.CAMII.371	225.6735	2.41749E-05	121.7765	1.30451E-05	4.4339
PC.M213	263.979	2.75459E-05	156.5475	1.63355E-05	3.9888
PC.M23	347.3709	3.30036E-05	214.0375	2.03357E-05	4.9554
PC.M230	234.7814	2.55236E-05	134.8037	1.46548E-05	4.8268
PC.M335	258.5252	2.6078E-05	168.0387	1.69504E-05	4.842
PC.M367	564.2219	3.06702E-05	275.7092	1.49871E-05	5.5973
PC.M381	176.022	2.29743E-05	105.19	1.37294E-05	3.6501
PC.M411	263.9161	2.02655E-05	185.6131	1.42528E-05	4.3956
PC.M426	249.4362	4.32596E-05	140.6068	2.43854E-05	4.3913
PC.M536	198.9233	1.77922E-05	132.191	1.18235E-05	4.1717

Name	H.mid.lmax	H.mid.lmax.s	H.mid.lmin	H.mid.lmin.s	H.mid.MaxXrad
PC.M561	230.0528	2.08663E-05	150.86	1.36833E-05	4.1707
PC.M618	270.9434	2.42766E-05	157.1932	1.40846E-05	4.2514
PC.M659	207.0917	2.28248E-05	134.0506	1.47745E-05	4.3288
PC.M688	248.1209	2.32239E-05	129.3993	1.21116E-05	4.3329
PC.M753	230.5361	2.88511E-05	139.1162	1.74101E-05	4.0143
PC.M754	123.7002	2.11012E-05	98.2307	1.67565E-05	3.6766
PC.M833	275.5541	2.85941E-05	141.3525	1.46681E-05	4.4144
PC.M872	185.1426	2.02433E-05	120.7456	1.32022E-05	3.7466
PC.M878	213.2051	2.08228E-05	148.6377	1.45168E-05	4.2529
PC.M94	361.1003	3.44732E-05	184.2144	1.75864E-05	4.31
PC.M972	147.0631	2.51529E-05	76.6939	1.31173E-05	3.6164
NMNH477295	240.4194	2.26668E-05	136.8939	1.29064E-05	3.8318
NMNH164832	225.6083	2.4307E-05	136.9994	1.47603E-05	4.059
NMNH452530	NA	NA	NA	NA	NA
NMNH452531	NA	NA	NA	NA	NA
NMNH452535	NA	NA	NA	NA	NA
NMNH452536	NA	NA	NA	NA	NA
NMNH452537	NA	NA	NA	NA	NA
NMNH452538	NA	NA	NA	NA	NA
NMNH452545	NA	NA	NA	NA	NA
NMNH452546	NA	NA	NA	NA	NA
NMNH452547	698.9985	4.75635E-05	455.303	3.09812E-05	4.9269
NMNH452549	NA	NA	NA	NA	NA
NMNH452550	NA	NA	NA	NA	NA
NMNH452552	NA	NA	NA	NA	NA
NMNH452553	NA	NA	NA	NA	NA
NMNH452554	NA	NA	NA	NA	NA
NMNH452556	NA	NA	NA	NA	NA
NMNH452557	NA	NA	NA	NA	NA
NMNH452559	NA	NA	NA	NA	NA
NMNH452568	NA	NA	NA	NA	NA
NMNH452570	459.0315	2.58233E-05	251.8464	1.41679E-05	5.4739
NMNH452571	NA	NA	NA	NA	NA
NMNH452574	429.5224	2.28212E-05	271.8855	1.44457E-05	4.8465
NMNH452578	150.0174	1.6813E-05	90.0463	1.00918E-05	3.5351
NMNH452581	253.1895	2.83927E-05	132.2758	1.48334E-05	4.6403
NMNH452586	NA	NA	NA	NA	NA
NMNH452587	557.8747	3.21626E-05	273.0528	1.57421E-05	4.7735
NMNH454554	NA	NA	NA	NA	NA
AMNH52421	NA	NA	NA	NA	NA
AMNH52429	602.5471	2.97627E-05	354.8811	1.75293E-05	5.7494
NMNH452520	289.3876	3.3746E-05	200.4259	2.3372E-05	4.9341
NMNH452522	208.433	3.14303E-05	102.3835	1.54387E-05	4.626
NMNH452523	402.1642	2.93925E-05	259.0011	1.89293E-05	5.2507
NMNH452524	200.2462	1.42634E-05	145.8104	1.0386E-05	4.3473
NMNH452525	NA	NA	NA	NA	NA
PC.CAMII372	399.63	2.992E-05	219.0832	1.64026E-05	4.0493
PC.M195	436.5858	2.36772E-05	333.8159	1.81037E-05	5.4483
PC.CF144	560.3594	3.27027E-05	347.7056	2.02922E-05	5.6922
PC.M114	547.7366	3.20473E-05	384.7287	2.25099E-05	5.3749
PC.M232	673.7238	3.20086E-05	398.2779	1.89222E-05	5.8863
PC.M305	532.7651	3.3354E-05	270.6164	1.69421E-05	4.6161
PC.M336	591.9502	3.23619E-05	362.3347	1.98088E-05	5.0022
PC.M378	1105.9675	4.98383E-05	730.1908	3.29047E-05	7.14
PC.M410	144.791	2.15898E-05	89.7622	1.33845E-05	4.0601
PC.M433	645.7689	3.42439E-05	371.4397	1.96968E-05	5.4499
PC.M48	377.7338	2.65053E-05	202.4692	1.42071E-05	4.2709
PC.M625	418.892	3.9492E-05	257.6953	2.42948E-05	4.9902
PC.M645	702.3128	3.74186E-05	472.6904	2.51845E-05	5.4122
PC.M680	678.1967	3.02384E-05	472.5847	2.10709E-05	5.5859
PC.M691	256.3523	2.2409E-05	135.9038	1.188E-05	4.712

Name	H.mid.lmax	H.mid.lmax.s	H.mid.lmin	H.mid.lmin.s	H.mid.MaxXrad
PC.M793	377.7082	3.29457E-05	299.7159	2.61428E-05	5.0184
PC.M832	548.4609	3.50899E-05	360.5931	2.30704E-05	4.7881
PC.M836	NA	NA	NA	NA	NA
PC.M868	160.7015	2.11351E-05	112.3496	1.47759E-05	3.6405
PC.M904	665.1413	3.64662E-05	415.8286	2.27977E-05	5.9697
PC.M906	677.2336	3.34191E-05	468.4358	2.31157E-05	5.286
PC.M990	313.1181	3.09609E-05	159.0815	1.57299E-05	4.8842
PC.CAMII.317	255.7269	3.20071E-05	172.1691	2.15489E-05	4.4277
PC.M103	189.2849	3.12384E-05	105.4982	1.74108E-05	3.9286
PC.M152	128.4347	2.3794E-05	94.2137	1.74542E-05	3.6191
PC.M159	413.1642	4.26207E-05	210.1961	2.16832E-05	5.4421
PC.M230	377.6022	3.92647E-05	193.1772	2.00874E-05	4.9791
PC.M277	127.3433	2.28268E-05	58.2019	1.04329E-05	3.9485
PC.M297	422.5394	4.51647E-05	240.0023	2.56535E-05	4.8299
PC.M306	359.6408	2.9639E-05	220.6326	1.81829E-05	5.1525
PC.M344	274.3368	2.79336E-05	170.5643	1.73673E-05	4.4196
PC.M347	130.3947	2.09373E-05	79.8839	1.28268E-05	3.8521
PC.M383	326.2908	2.9216E-05	206.4485	1.84854E-05	4.3389
PC.M654	460.1226	4.12025E-05	265.3742	2.37634E-05	5.148
PC.M660	211.8394	3.1183E-05	179.2535	2.63863E-05	4.1802
PC.M769	302.9683	3.30914E-05	184.6713	2.01705E-05	4.8727
PC.M82	638.0575	5.10098E-05	383.4155	3.06523E-05	5.6576
PC.M88	152.5482	2.13634E-05	108.096	1.51382E-05	3.9532
PC.M90	236.4119	2.57466E-05	166.4181	1.81239E-05	4.3074
PC.M908	357.6261	3.21968E-05	284.0593	2.55736E-05	4.8908
PC.M931	292.9029	2.53723E-05	218.6878	1.89435E-05	4.6608
Name	**H.mid.MaxYrad**	**H.mid.J**	**H.mid.J.s**	**H.mid.ZpEst**	**H.mid.ZpEst.s**
AMNH52532	NA	NA	NA	NA	NA
AMNH52554	NA	NA	NA	NA	NA
AMNH52563	NA	NA	NA	NA	NA
AMNH55068	4.5174	466.9664	5.37362E-05	105.51	0.001463009
NMNH164582	4.5002	385.6064	4.51584E-05	89.01	0.001219651
NMNH452510	4.7604	513.0115	4.83303E-05	114.07	0.001321777
NMNH452512	3.9626	206.9181	4.35162E-05	57.06	0.001247913
NMNH452514	3.8368	469.9488	4.36656E-05	112.13	0.001344054
NMNH452517	4.811	485.2227	3.84485E-05	106.25	0.001094440
NMNH218470	4.1415	645.9941	4.79164E-05	138.06	0.001382425
PC.CAMII.360	4.1762	393.5905	3.9884E-05	91.22	0.001136993
PC.CAMII.371	3.9114	347.4499	3.722E-05	83.27	0.001088240
PC.M213	4.6393	420.5265	4.38814E-05	97.48	0.001190093
PC.M23	4.1878	561.4084	5.33393E-05	122.80	0.001411771
PC.M230	3.5416	369.5851	4.01785E-05	88.33	0.001161893
PC.M335	4.1709	426.5638	4.30284E-05	94.66	0.001179199
PC.M367	4.8317	839.9311	4.56573E-05	161.08	0.001273975
PC.M381	4.142	281.212	3.67037E-05	72.18	0.001092807
PC.M411	4.5944	449.5291	3.45184E-05	100.01	0.001005985
PC.M426	4.269	390.043	6.7645E-05	90.08	0.001702784
PC.M536	3.9454	331.1143	2.96157E-05	81.58	0.000955922
PC.M561	3.9141	380.9129	3.45496E-05	94.23	0.001093992
PC.M618	4.3963	428.1367	3.83612E-05	99.02	0.001126744
PC.M659	3.5823	341.1423	3.75992E-05	86.24	0.001150158
PC.M688	4.1198	377.5201	3.53355E-05	89.33	0.001065997
PC.M753	4.2222	369.6523	4.62613E-05	89.76	0.001319905
PC.M754	3.5125	221.9309	3.78578E-05	61.74	0.001147987
PC.M833	4.1075	416.9066	4.32622E-05	97.84	0.001223457
PC.M872	4.1785	305.8882	3.34455E-05	77.19	0.001021287
PC.M878	3.9507	361.8428	3.53395E-05	88.22	0.001085568
PC.M94	4.9947	545.3147	5.20596E-05	117.21	0.001376364
PC.M972	3.8218	223.757	3.82703E-05	60.16	0.001116487
NMNH477295	4.632	377.3133	3.55731E-05	89.16	0.001084368
NMNH164832	4.443	362.6077	3.90672E-05	85.30	0.001112006

Name	H.mid.MaxYrad	H.mid.J	H.mid.J.s	H.mid.ZpEst	H.mid.ZpEst.s
NMNH452530	NA	NA	NA	NA	NA
NMNH452531	NA	NA	NA	NA	NA
NMNH452535	NA	NA	NA	NA	NA
NMNH452536	NA	NA	NA	NA	NA
NMNH452537	NA	NA	NA	NA	NA
NMNH452538	NA	NA	NA	NA	NA
NMNH452545	NA	NA	NA	NA	NA
NMNH452546	NA	NA	NA	NA	NA
NMNH452547	5.9959	1154.3015	7.85447E-05	211.36	0.002070979
NMNH452549	NA	NA	NA	NA	NA
NMNH452550	NA	NA	NA	NA	NA
NMNH452552	NA	NA	NA	NA	NA
NMNH452553	NA	NA	NA	NA	NA
NMNH452554	NA	NA	NA	NA	NA
NMNH452556	NA	NA	NA	NA	NA
NMNH452557	NA	NA	NA	NA	NA
NMNH452559	NA	NA	NA	NA	NA
NMNH452568	NA	NA	NA	NA	NA
NMNH452570	4.8556	710.8778	3.99912E-05	137.64	0.001122749
NMNH452571	NA	NA	NA	NA	NA
NMNH452574	5.4428	701.408	3.72669E-05	136.34	0.001057596
NMNH452578	4.1318	240.0637	2.69048E-05	62.62	0.000849229
NMNH452581	4.1583	385.4653	4.32261E-05	87.62	0.001188907
NMNH452586	NA	NA	NA	NA	NA
NMNH452587	5.826	830.9274	4.79047E-05	156.79	0.001274506
NMNH454554	NA	NA	NA	NA	NA
AMNH52421	NA	NA	NA	NA	NA
AMNH52429	5.0964	957.4282	4.7292E-05	176.55	0.001491255
NMNH452520	4.6255	489.8135	5.7118E-05	102.48	0.001422035
NMNH452522	3.7666	310.8165	4.6869E-05	74.07	0.001262111
NMNH452523	5.0906	661.1653	4.83218E-05	127.87	0.001252283
NMNH452524	4.309	346.0566	2.46494E-05	79.95	0.000763148
NMNH452525	NA	NA	NA	NA	NA
PC.CAMII372	5.5967	618.7131	4.63225E-05	128.28	0.001267795
PC.M195	5.3053	770.4017	4.1781E-05	143.28	0.001142278
PC.CF144	4.7975	908.065	5.29949E-05	173.13	0.001419638
PC.M114	4.9623	932.4653	5.45572E-05	180.41	0.001456659
PC.M232	5.1614	1072.0017	5.09308E-05	194.07	0.001355365
PC.M305	5.5544	803.3815	5.02961E-05	157.98	0.001369846
PC.M336	5.7391	954.2849	5.21707E-05	177.69	0.001369679
PC.M378	5.7233	1836.1582	8.2743E-05	285.49	0.001865421
PC.M410	3.4916	234.5533	3.49743E-05	62.12	0.001069833
PC.M433	5.6877	1017.2086	5.39407E-05	182.66	0.001356073
PC.M48	5.1015	580.2029	4.07123E-05	123.81	0.001194560
PC.M625	4.7587	676.5873	6.37867E-05	138.80	0.001583398
PC.M645	6.2729	1175.0032	6.2603E-05	201.11	0.001559036
PC.M680	5.9885	1150.7814	5.13093E-05	198.85	0.001329899
PC.M691	3.9955	392.2561	3.4289E-05	90.10	0.001031721
PC.M793	5.0675	677.4242	5.90885E-05	134.33	0.001499783
PC.M832	5.176	909.054	5.81603E-05	182.47	0.001640192
PC.M836	NA	NA	NA	NA	NA
PC.M868	3.8686	273.0511	3.5911E-05	72.73	0.001128630
PC.M904	4.6435	1080.9699	5.9264E-05	203.70	0.001652860
PC.M906	5.7912	1145.6693	5.65348E-05	206.85	0.001490284
PC.M990	4.1979	472.1996	4.66908E-05	103.98	0.001274960
PC.CAMII.317	4.1601	427.896	5.35559E-05	99.65	0.001446818
PC.M103	4.0003	294.7831	4.86492E-05	74.36	0.001423477
PC.M152	3.574	222.6485	4.12482E-05	61.91	0.001227164
PC.M159	4.0219	623.3604	6.43039E-05	131.73	0.001644288
PC.M230	4.1733	570.7794	5.93521E-05	124.73	0.001647155
PC.M277	2.9225	185.5452	3.32597E-05	54.01	0.001055250

Name	H.mid.MaxYrad	H.mid.J	H.mid.J.s	H.mid.ZpEst	H.mid.ZpEst.s
PC.M297	4.8749	662.5417	7.08183E-05	136.54	0.001765932
PC.M306	4.2732	580.2735	4.78219E-05	123.13	0.001329274
PC.M344	4.4198	444.9011	4.53009E-05	100.66	0.001260722
PC.M347	3.2356	210.2786	3.37641E-05	59.34	0.001067082
PC.M383	5.0341	532.7393	4.77014E-05	113.68	0.001302844
PC.M654	4.8875	725.4968	6.49658E-05	144.59	0.001650769
PC.M660	4.2638	391.0929	5.75693E-05	92.63	0.001568088
PC.M769	4.0285	487.6396	5.32619E-05	109.57	0.001436081
PC.M82	5.6657	1021.473	8.16622E-05	180.42	0.001918358
PC.M88	3.4122	260.6442	3.65015E-05	70.78	0.001144793
PC.M90	4.0107	402.8301	4.38705E-05	96.86	0.001265784
PC.M908	4.6407	641.6855	5.77705E-05	134.65	0.001581922
PC.M931	4.4315	511.5907	4.43158E-05	112.53	0.001272111
Name	**H.prox.TA**	**H.prox.TA.s**	**H.prox.lmax**	**H.prox.lmax.s**	**H.prox.lmin**
AMNH52532	NA	NA	NA	NA	NA
AMNH52554	NA	NA	NA	NA	NA
AMNH52563	NA	NA	NA	NA	NA
AMNH55068	66.5034	0.000922172	398.5078	4.58583E-05	369.3813
NMNH164582	60.208	0.000824962	360.614	4.22315E-05	270.4766
NMNH452510	65.9626	0.000764355	409.9339	3.86195E-05	366.139
NMNH452512	38.2601	0.000836819	139.3699	2.93104E-05	107.1853
NMNH452514	65.4005	0.000783898	425.2434	3.95118E-05	283.8606
NMNH452517	68.414	0.000704737	463.6366	3.67381E-05	365.9413
NMNH218470	72.6681	0.000727668	524.1375	3.88777E-05	359.3479
PC.CAMII.360	59.6904	0.000743983	393.8653	3.99118E-05	280.5357
PC.CAMII.371	52.7203	0.000689005	288.2646	3.08799E-05	223.486
PC.M213	64.9189	0.000792582	391.4872	4.08512E-05	348.9451
PC.M23	73.0877	0.00084023	479.5693	4.55638E-05	454.235
PC.M230	62.1219	0.000817163	391.0721	4.25144E-05	276.4131
PC.M335	59.7688	0.000744582	359.664	3.628E-05	266.8628
PC.M367	76.4221	0.000604434	583.9936	3.1745E-05	419.8378
PC.M381	52.0912	0.000788676	278.1766	3.63075E-05	210.2399
PC.M411	64.4094	0.000647907	396.5804	3.04525E-05	330.2383
PC.M426	52.7508	0.000997193	299.6667	5.19711E-05	195.7182
PC.M536	51.6794	0.000605526	282.1757	2.52385E-05	187.3472
PC.M561	56.3407	0.000654109	298.652	2.70884E-05	246.7941
PC.M618	52.9435	0.000602457	306.9667	2.75043E-05	182.2502
PC.M659	61.9091	0.000825626	359.606	3.96342E-05	288.3093
PC.M688	53.2813	0.000635852	290.7527	2.72142E-05	212.3833
PC.M753	49.9531	0.000734555	238.3379	2.98275E-05	174.8716
PC.M754	42.3828	0.00078805	165.136	2.81695E-05	139.9467
PC.M833	61.9012	0.000774026	382.3917	3.96806E-05	280.8807
PC.M872	47.8724	0.000633352	232.1933	2.53878E-05	149.623
PC.M878	62.7524	0.000772221	370.392	3.61745E-05	320.7949
PC.M94	66.9732	0.000786429	496.5133	4.74006E-05	284.3139
PC.M972	40.8852	0.000758719	195.1719	3.33812E-05	104.3181
NMNH477295	58.4177	0.000710484	355.4351	3.35105E-05	254.587
NMNH164832	56.5869	0.000737695	324.0091	3.49086E-05	237.8028
NMNH452530	NA	NA	NA	NA	NA
NMNH452531	NA	NA	NA	NA	NA
NMNH452535	NA	NA	NA	NA	NA
NMNH452536	NA	NA	NA	NA	NA
NMNH452537	NA	NA	NA	NA	NA
NMNH452538	NA	NA	NA	NA	NA
NMNH452545	NA	NA	NA	NA	NA
NMNH452546	NA	NA	NA	NA	NA
NMNH452547	97.7056	0.00095737	824.2827	5.60885E-05	724.6138
NMNH452549	NA	NA	NA	NA	NA
NMNH452550	50.4788	0.000650136	274.3834	2.92057E-05	180.2773
NMNH452552	NA	NA	NA	NA	NA
NMNH452553	NA	NA	NA	NA	NA

Name	H.prox.TA	H.prox.TA.s	H.prox.lmax	H.prox.lmax.s	H.prox.lmin
NMNH452554	NA	NA	NA	NA	NA
NMNH452556	NA	NA	NA	NA	NA
NMNH452557	NA	NA	NA	NA	NA
NMNH452559	NA	NA	NA	NA	NA
NMNH452568	NA	NA	NA	NA	NA
NMNH452570	74.3874	0.000606787	543.5298	3.05768E-05	438.2263
NMNH452571	74.7144	0.000595393	598.6485	3.43207E-05	373.3177
NMNH452574	81.7797	0.000634382	688.2294	3.65667E-05	577.5017
NMNH452578	46.8224	0.000634953	220.5361	2.47162E-05	158.8342
NMNH452581	55.925	0.000758844	290.422	3.2568E-05	246.6884
NMNH452586	NA	NA	NA	NA	NA
NMNH452587	88.3537	0.000718222	834.0795	4.80864E-05	565.8186
NMNH454554	NA	NA	NA	NA	NA
AMNH52421	NA	NA	NA	NA	NA
AMNH52429	92.3283	0.000779852	957.7475	4.73077E-05	617.614
NMNH452520	62.3233	0.000864848	364.6277	4.25199E-05	320.6517
NMNH452522	50.2747	0.000856662	303.427	4.57547E-05	174.963
NMNH452523	75	0.000734512	588.8542	4.30369E-05	452.3545
NMNH452524	58.6413	0.000559715	357.2936	2.54498E-05	254.5041
NMNH452525	NA	NA	NA	NA	NA
PC.CAMII372	71.0823	0.000702487	585.1422	4.38091E-05	356.2979
PC.M195	74.2341	0.00059181	550.428	2.98512E-05	491.5879
PC.CF144	84.9401	0.000696477	682.3281	3.98209E-05	603.8849
PC.M114	89.7356	0.000724541	772.0941	4.51741E-05	578.7587
PC.M232	94.6297	0.000660892	833.1541	3.95832E-05	733.0899
PC.M305	86.1001	0.000746562	803.7577	5.03196E-05	492.2422
PC.M336	90.8371	0.000700214	771.3604	4.21702E-05	640.9909
PC.M378	109.0787	0.000712737	1078.2887	4.8591E-05	897.1425
PC.M410	42.4584	0.000731228	166.3425	2.48034E-05	133.6158
PC.M433	90.1396	0.000669191	750.3939	3.9792E-05	663.8677
PC.M48	68.5519	0.000661406	489.737	3.43644E-05	350.1875
PC.M625	74.8605	0.000853974	600.648	5.66274E-05	376.1618
PC.M645	103.6488	0.000803496	1000.8741	5.33256E-05	824.7736
PC.M680	110.3535	0.000738041	1192.603	5.31739E-05	933.6179
PC.M691	55.5158	0.00063573	348.2622	3.04433E-05	214.1004
PC.M793	74.5659	0.000832516	537.5863	4.68911E-05	445.9064
PC.M832	78.3553	0.000704339	627.1227	4.01226E-05	422.8212
PC.M836	NA	NA	NA	NA	NA
PC.M868	48.8955	0.000758812	202.7194	2.66611E-05	199.4613
PC.M904	95.7616	0.000777017	924.1761	5.06678E-05	688.3582
PC.M906	108.4523	0.000781355	1125.5868	5.55438E-05	1046.2883
PC.M990	61.5705	0.000754918	413.4059	4.08773E-05	273.4049
PC.CAMII.317	61.2701	0.000889562	331.3615	4.14736E-05	318.0447
PC.M103	45.0678	0.000862774	215.7951	3.56135E-05	134.537
PC.M152	41.8321	0.000829237	165.7504	3.07072E-05	128.0481
PC.M159	64.9821	0.000811105	390.0004	4.02312E-05	365.9026
PC.M230	64.4732	0.000851433	435.6528	4.5301E-05	281.3444
PC.M277	40.2367	0.000786173	152.0925	2.72632E-05	117.8731
PC.M297	69.9959	0.000905295	512.2977	5.47589E-05	331.6324
PC.M306	66.9747	0.000723063	472.1583	3.89118E-05	307.9667
PC.M344	66.5651	0.000833672	468.3026	4.76837E-05	327.1469
PC.M347	40.7282	0.000732442	157.6071	2.53067E-05	120.4189
PC.M383	68.7642	0.000788113	449.2825	4.02287E-05	378.6829
PC.M654	84.0083	0.00095914	621.436	5.56475E-05	591.6904
PC.M660	59.8099	0.001012469	366.4909	5.39478E-05	245.1416
PC.M769	69.5493	0.000911573	461.2113	5.03753E-05	386.5756
PC.M82	80.4804	0.000855728	600.8418	4.80346E-05	488.6526
PC.M88	45.6082	0.000737714	187.4847	2.6256E-05	163.6357
PC.M90	63.6134	0.000831344	344.6844	3.75381E-05	342.74
PC.M908	77.3234	0.000908459	531.9324	4.78895E-05	450.8299
PC.M931	65.9545	0.000745574	392.6191	3.401E-05	336.8858

Name	H.prox.Imin.s	H.prox.MaxXrad	H.prox.MaxYrad	H.prox.J	H.prox.J.s
AMNH52532	NA	NA	NA	NA	NA
AMNH52554	NA	NA	NA	NA	NA
AMNH52563	NA	NA	NA	NA	NA
AMNH55068	4.25065E-05	5.73	5.8276	767.8891	8.83648E-05
NMNH164582	3.16755E-05	5.2281	5.5221	631.0906	7.3907E-05
NMNH452510	3.44936E-05	5.8789	5.9822	776.0729	7.3113E-05
NMNH452512	2.25417E-05	3.9111	3.7562	246.5551	5.18521E-05
NMNH452514	2.63751E-05	4.6907	4.9005	709.104	6.58869E-05
NMNH452517	2.89968E-05	6.3204	5.5097	829.5778	6.57349E-05
NMNH218470	2.66545E-05	4.9887	5.4685	883.4854	6.55322E-05
PC.CAMII.360	2.84277E-05	6.0412	5.8537	674.401	6.83395E-05
PC.CAMII.371	2.39406E-05	5.1078	5.6195	511.7506	5.48205E-05
PC.M213	3.6412E-05	5.576	5.7	740.4323	7.72631E-05
PC.M23	4.31568E-05	5.9599	6.0766	933.8043	8.87205E-05
PC.M230	3.00495E-05	5.1283	4.8894	667.4852	7.25639E-05
PC.M335	2.6919E-05	5.1116	4.9883	626.5267	6.3199E-05
PC.M367	2.28217E-05	5.7991	6.2168	1003.8314	5.45667E-05
PC.M381	2.74405E-05	4.7571	4.8751	488.4165	6.3748E-05
PC.M411	2.53583E-05	5.6618	5.4198	726.8187	5.58108E-05
PC.M426	3.39433E-05	5.2403	5.0339	495.3849	8.59145E-05
PC.M536	1.67568E-05	5.273	4.2984	469.5229	4.19953E-05
PC.M561	2.23848E-05	5.0801	5.6537	545.4461	4.94732E-05
PC.M618	1.63297E-05	4.6607	5.3079	489.217	4.3834E-05
PC.M659	3.17762E-05	5.6261	5.283	647.9152	7.14104E-05
PC.M688	1.98789E-05	5.4804	5.0427	503.136	4.7093E-05
PC.M753	2.18848E-05	4.583	4.2093	413.2095	5.17124E-05
PC.M754	2.38726E-05	3.8995	4.6696	305.0826	5.20421E-05
PC.M833	2.91468E-05	5.0381	5.6527	663.2724	6.88274E-05
PC.M872	1.63596E-05	4.4199	4.5189	381.8164	4.17474E-05
PC.M878	3.13306E-05	5.8339	5.2098	691.187	6.75051E-05
PC.M94	2.71426E-05	5.5845	5.4214	780.8272	7.45432E-05
PC.M972	1.78421E-05	3.9969	4.9128	299.4899	5.12233E-05
NMNH477295	2.40025E-05	5.1276	5.0783	610.0221	5.7513E-05
NMNH164832	2.56208E-05	5.2345	4.5383	561.8119	6.05294E-05
NMNH452530	NA	NA	NA	NA	NA
NMNH452531	NA	NA	NA	NA	NA
NMNH452535	NA	NA	NA	NA	NA
NMNH452536	NA	NA	NA	NA	NA
NMNH452537	NA	NA	NA	NA	NA
NMNH452538	NA	NA	NA	NA	NA
NMNH452545	NA	NA	NA	NA	NA
NMNH452546	NA	NA	NA	NA	NA
NMNH452547	4.93065E-05	6.1201	5.9307	1548.8965	0.000105395
NMNH452549	NA	NA	NA	NA	NA
NMNH452550	1.91889E-05	4.6548	4.5968	454.6607	4.83947E-05
NMNH452552	NA	NA	NA	NA	NA
NMNH452553	NA	NA	NA	NA	NA
NMNH452554	NA	NA	NA	NA	NA
NMNH452556	NA	NA	NA	NA	NA
NMNH452557	NA	NA	NA	NA	NA
NMNH452559	NA	NA	NA	NA	NA
NMNH452568	NA	NA	NA	NA	NA
NMNH452570	2.46529E-05	6.8338	5.6727	981.7561	5.52297E-05
NMNH452571	2.14024E-05	6.4498	5.5972	971.9661	5.57232E-05
NMNH452574	3.06835E-05	6.8883	6.1585	1265.731	6.72502E-05
NMNH452578	1.78011E-05	4.7532	4.3751	379.3703	4.25173E-05
NMNH452581	2.76637E-05	4.9465	4.9865	537.1104	6.02316E-05
NMNH452586	NA	NA	NA	NA	NA
NMNH452587	3.26206E-05	7.0691	6.2868	1399.8981	8.0707E-05
NMNH454554	NA	NA	NA	NA	NA
AMNH52421	NA	NA	NA	NA	NA

Name	H.prox.Imin.s	H.prox.MaxXrad	H.prox.MaxYrad	H.prox.J	H.prox.J.s
AMNH52429	3.05069E-05	7.0754	6.6527	1575.3614	7.78146E-05
NMNH452520	3.73918E-05	5.9849	5.4305	685.2794	7.99116E-05
NMNH452522	2.63832E-05	4.9234	5.669	478.39	7.21379E-05
NMNH452523	3.30607E-05	5.9405	7.0297	1041.2087	7.60975E-05
NMNH452524	1.81282E-05	5.5252	5.3626	611.7977	4.35779E-05
NMNH452525	NA	NA	NA	NA	NA
PC.CAMII372	2.66757E-05	6.248	6.0454	941.44	7.04848E-05
PC.M195	2.66601E-05	6.1574	7.1384	1042.0158	5.65113E-05
PC.CF144	3.52429E-05	7.1876	6.3076	1286.2129	7.50638E-05
PC.M114	3.38623E-05	5.9916	6.4145	1350.8529	7.90364E-05
PC.M232	3.48291E-05	7.137	6.8758	1566.2439	7.44123E-05
PC.M305	3.08171E-05	6.0185	6.1006	1295.9999	8.11367E-05
PC.M336	3.50429E-05	6.658	6.9456	1412.3513	7.72132E-05
PC.M378	4.0428E-05	6.8328	6.4812	1975.4312	8.90191E-05
PC.M410	1.99235E-05	4.1155	4.1069	299.9582	4.47268E-05
PC.M433	3.52037E-05	7.0561	6.41	1414.2615	7.49957E-05
PC.M48	2.45724E-05	5.6787	5.9718	839.9245	5.89368E-05
PC.M625	3.54635E-05	5.6878	6.5221	976.8098	9.20909E-05
PC.M645	4.39431E-05	6.8211	7.3478	1825.6477	9.72688E-05
PC.M680	4.16267E-05	8.2769	7.1533	2126.2209	9.48007E-05
PC.M691	1.87155E-05	5.5475	5.4592	562.3625	4.91588E-05
PC.M793	3.88943E-05	6.3368	5.2914	983.4926	8.57854E-05
PC.M832	2.70516E-05	5.85	5.1655	1049.9439	6.71743E-05
PC.M836	NA	NA	NA	NA	NA
PC.M868	2.62326E-05	4.5918	4.7372	402.1807	5.28938E-05
PC.M904	3.77391E-05	6.4555	6.1955	1612.5343	8.84069E-05
PC.M906	5.16307E-05	7.7051	6.3856	2171.8751	0.000107175
PC.M990	2.70341E-05	6.0119	5.4021	686.8108	6.79114E-05
PC.CAMII.317	3.98068E-05	4.9003	5.4284	649.4061	8.12804E-05
PC.M103	2.22031E-05	4.711	4.4758	350.3321	5.78166E-05
PC.M152	2.37224E-05	3.8645	4.643	293.7985	5.44296E-05
PC.M159	3.77454E-05	4.8973	5.3713	755.903	7.79766E-05
PC.M230	2.92554E-05	4.8972	5.583	716.9972	7.45564E-05
PC.M277	2.11292E-05	3.8097	3.8619	269.9656	4.83924E-05
PC.M297	3.54478E-05	5.3376	6.1032	843.9301	9.02066E-05
PC.M306	2.53804E-05	5.5524	5.562	780.125	6.42922E-05
PC.M344	3.33109E-05	5.3923	6.2225	795.4496	8.09946E-05
PC.M347	1.93355E-05	3.8549	4.4364	278.026	4.46422E-05
PC.M383	3.39072E-05	5.3	6.4735	827.9654	7.41359E-05
PC.M654	5.29839E-05	6.5339	5.967	1213.1264	0.000108631
PC.M660	3.60851E-05	4.1812	5.6398	611.6325	9.00329E-05
PC.M769	4.22233E-05	5.5616	5.7028	847.7869	9.25985E-05
PC.M82	3.90656E-05	5.4498	6.182	1089.4944	8.71002E-05
PC.M88	2.29161E-05	4.1052	4.3154	351.1204	4.91722E-05
PC.M90	3.73264E-05	4.5897	5.4867	687.4244	7.48645E-05
PC.M908	4.05879E-05	5.0687	5.8486	982.7624	8.84774E-05
PC.M931	2.91822E-05	5.2063	5.5869	729.5049	6.31923E-05

Name	H.prox.ZpEst	H.prox.ZpEst.s	F.C.AP	H.C.AP	H.C.ML
AMNH52532	NA	NA	7.00	7.18	5.08
AMNH52554	NA	NA	5.38	3.67	6.55
AMNH52563	NA	NA	7.32	5.33	6.07
AMNH55068	132.88	0.00184259	5.04	6.68	3.79
NMNH164582	117.41	0.00160874	6.37	7.12	4.88
NMNH452510	130.86	0.00151637	7.33	6.47	5.33
NMNH452512	64.31	0.00140665	6.01	3.46	4.78
NMNH452514	147.87	0.00177233	6.26	5.32	6.85
NMNH452517	140.25	0.00144471	7.33	5.93	4.68
NMNH218470	168.97	0.00169201	8.10	7.59	7.00
PC.CAMII.360	113.39	0.00141334	6.25	7.23	7.85
PC.CAMII.371	95.41	0.00124693	8.13	5.23	6.98
PC.M213	131.33	0.00160337	7.02	4.84	4.89

Name	H.prox.ZpEst	H.prox.ZpEst.s	F.C.AP	H.C.AP	H.C.ML
PC.M23	155.16	0.00178377	7.02	5.24	8.92
PC.M230	133.26	0.00175294	6.13	5.66	6.06
PC.M335	124.07	0.00154558	5.14	6.98	3.48
PC.M367	167.08	0.00132149	7.24	4.11	7.95
PC.M381	101.41	0.00153543	7.33	7.17	5.29
PC.M411	131.18	0.00131952	7.13	6.26	6.49
PC.M426	96.43	0.00182295	6.07	4.91	7.24
PC.M536	98.11	0.00114955	7.26	5.63	7.59
PC.M561	101.63	0.00117993	7.59	6.56	4.34
PC.M618	98.15	0.00111689	8.11	6.18	6.44
PC.M659	118.78	0.00158412	7.42	5.68	4.35
PC.M688	95.63	0.00114118	6.59	6.68	4.67
PC.M753	93.99	0.00138216	NA	3.63	5.24
PC.M754	71.21	0.00132396	5.32	5.58	5.00
PC.M833	124.08	0.00155156	7.39	5.66	6.73
PC.M872	85.43	0.00113023	6.28	5.29	5.40
PC.M878	125.17	0.00154036	5.63	5.54	5.58
PC.M94	141.89	0.00166616	9.10	4.98	8.56
PC.M972	67.23	0.00124757	5.31	5.21	5.20
NMNH477295	119.54	0.00145390	6.26	7.27	6.36
NMNH164832	114.97	0.00149887	6.54	6.10	5.91
NMNH452530	NA	NA	8.76	5.80	5.89
NMNH452531	NA	NA	6.59	5.04	6.63
NMNH452535	NA	NA	7.60	5.26	5.63
NMNH452536	NA	NA	7.46	4.93	5.78
NMNH452537	NA	NA	7.13	6.40	4.82
NMNH452538	NA	NA	7.79	5.59	6.19
NMNH452545	NA	NA	7.85	7.47	6.36
NMNH452546	NA	NA	NA	7.08	5.55
NMNH452547	257.06	0.00251882	7.32	6.55	8.29
NMNH452549	NA	NA	7.04	5.19	6.44
NMNH452550	98.29	0.00126589	7.07	5.95	4.27
NMNH452552	NA	NA	7.70	4.01	6.38
NMNH452553	NA	NA	9.07	6.54	6.62
NMNH452554	NA	NA	7.09	6.36	7.42
NMNH452556	NA	NA	5.90	6.92	8.62
NMNH452557	NA	NA	7.08	NA	NA
NMNH452559	NA	NA	7.88	4.93	5.14
NMNH452568	NA	NA	5.23	5.86	7.62
NMNH452570	157.00	0.001280663	6.47	5.93	6.19
NMNH452571	161.36	0.001285884	6.02	5.53	7.35
NMNH452574	194.03	0.001505124	7.78	8.28	5.68
NMNH452578	83.12	0.001127176	6.12	5.15	3.71
NMNH452581	108.15	0.001467437	6.56	5.58	6.71
NMNH452586	NA	NA	8.74	NA	NA
NMNH452587	209.63	0.001704070	7.82	6.70	6.53
NMNH454554	NA	NA	NA	NA	NA
AMNH52421	NA	NA	7.18	NA	NA
AMNH52429	229.51	0.001938550	6.12	7.98	7.52
NMNH452520	120.06	0.001666080	6.03	4.96	5.66
NMNH452522	90.33	0.001539138	5.83	6.10	7.79
NMNH452523	160.55	0.001572384	6.97	9.35	7.39
NMNH452524	112.38	0.001072658	7.57	7.82	6.48
NMNH452525	NA	NA	5.33	5.37	6.19
PC.CAMII372	153.16	0.001513657	8.85	9.52	9.45
PC.M195	156.74	0.001249593	7.52	6.95	8.47
PC.CF144	190.62	0.001562994	8.24	6.99	8.66
PC.M114	217.77	0.001758332	6.75	3.69	7.01
PC.M232	223.54	0.001561231	7.86	6.63	7.42
PC.M305	213.88	0.001854500	7.44	5.55	6.77
PC.M336	207.64	0.001600614	8.55	6.85	7.67

Name	H.prox.ZpEst	H.prox.ZpEst.s	F.C.AP	H.C.AP	H.C.ML
PC.M378	296.74	0.001938976	7.62	7.71	11.13
PC.M410	72.96	0.001256555	5.27	4.55	5.73
PC.M433	210.05	0.001559382	6.27	6.62	8.11
PC.M48	144.19	0.001391152	5.61	5.80	6.87
PC.M625	160.00	0.001825239	6.04	6.00	6.16
PC.M645	257.70	0.001997700	8.31	6.25	8.13
PC.M680	275.59	0.001843152	7.53	7.79	7.98
PC.M691	102.19	0.001170160	7.33	6.22	6.02
PC.M793	169.16	0.001888604	5.10	5.79	5.88
PC.M832	190.63	0.001713583	10.31	8.96	5.91
PC.M836	NA	NA	7.62	6.27	6.08
PC.M868	86.22	0.00133808	5.14	4.88	4.92
PC.M904	254.93	0.00206849	6.96	5.12	6.78
PC.M906	308.27	0.00222097	6.81	5.26	6.91
PC.M990	120.35	0.00147556	7.21	5.99	5.33
PC.CAMII.317	125.75	0.00182569	5.56	6.85	6.10
PC.M103	76.27	0.00146008	6.18	4.19	5.34
PC.M152	69.07	0.00136914	4.30	4.57	4.45
PC.M159	147.23	0.00183767	8.17	6.76	6.53
PC.M230	136.83	0.00180696	6.41	5.79	5.25
PC.M277	70.38	0.00137514	5.90	4.33	4.36
PC.M297	147.53	0.00190808	8.43	5.87	5.76
PC.M306	140.38	0.00151556	7.39	7.03	6.28
PC.M344	136.97	0.00171546	5.76	7.36	5.60
PC.M347	67.06	0.00120606	5.35	4.51	4.34
PC.M383	140.65	0.00161199	6.05	6.32	5.74
PC.M654	194.09	0.00221592	5.55	8.38	6.49
PC.M660	124.56	0.00210850	5.00	4.39	3.39
PC.M769	150.52	0.00197291	5.74	6.37	4.11
PC.M82	187.33	0.00199184	5.55	6.93	7.29
PC.M88	83.40	0.00134893	5.44	5.17	3.19
PC.M90	136.44	0.00178312	5.00	3.74	5.79
PC.M908	180.04	0.00211523	4.44	4.98	5.27
PC.M931	135.18	0.00152811	6.42	6.12	5.32

Name	Species	DR	Sex	HHD	MHL	FHD	MFL	BS.GM^3
NMNH238258	S. fuscicollis	1.3	M	6.5	49	5	59	5366.592131
NMNH336299	S. fuscicollis	1.3	F	6	47	5	58	4835.989282
NMNH337331	S. fuscicollis	1.3	F	5.5	45	5	56	4271.200178
NMNH461267	S. fuscicollis	1.3	M	6.5	51	5	63	5808.922266
AMNH188173	S. mystax	1.6	M	6.1	49	5.3	62	5548.110544
AMNH188176	S. mystax	1.6	F	5.7	41.5	4.8	57.5	4084.360109
AMNH188177	S. mystax	1.6	M	5.9	41.5	4.7	57	4098.780076
AMNH188178	S. mystax	1.6	F	5.8	50.5	5	61	5167.308709
AMNH188179	S. mystax	1.6	M	6.1	47	4.9	59	4884.913057
NMNH543485	S. mystax	1.6	M	7.25	55	6.5	72	8978.626625
NMNH543486	S. mystax	1.6	F	8	57	6.75	73	10320.33053
NMNH543487	S. mystax	1.6	F	6.5	53	6	69.5	7378.939693
NMNH543489	S. mystax	1.6	F	7	50.5	6	67	7319.166106
NMNH543490	S. mystax	1.6	M	7	56	6	71	8260.793188
NMNH544381	S. mystax	1.6	F	7.5	56	6.5	75	9625.381082
NMNH544382	S. mystax	1.6	M	7	57.5	6.25	74	8962.067619
NMNH544383	S. mystax	1.6	F	7.5	58	6.75	77	10368.42561
NMNH501080	S. oedipus	1.7	M	6.5	50	6	66	6794.913151
NMNH501082	S. oedipus	1.7	F	6.5	52	6	67	7077.128236
NMNH501084	S. oedipus	1.7	F	6.5	51	6	61	6500.899671
NMNH501085	S. oedipus	1.7	M	6.25	50	5	63	5557.384323
NMNH501088	S. oedipus	1.7	M	7	53	6	67.5	7631.707198
NMNH501091	S. oedipus	1.7	F	7	51	6.5	65	7653.695801
NMNH501092	S. oedipus	1.7	F	6.5	50.5	5.5	63	6193.42639
NMNH501093	S. oedipus	1.7	M	6.5	50	5.5	63	6147.378444
NMNH501094	S. oedipus	1.7	M	6.5	53	6	67	7178.958776
NMNH501097	S. oedipus	1.7	M	6.75	50	5.5	65	6473.846049
NMNH501099	S. oedipus	1.7	F	7.5	53	6	66	7902.677136
NMNH501100	S. oedipus	1.7	F	6.5	52	6	66	6997.757923
NMNH501102	S. oedipus	1.7	F	7	56	6.5	70	8679.068134
NMNH501103	S. oedipus	1.7	M	5	47	5.5	60	4647.146371
NMNH501105	S. oedipus	1.7	M	7	51	6	67	7373.44936
NMNH501106	S. oedipus	1.7	F	6	50	5	64.5	5485.778023
NMNH501107	S. oedipus	1.7	M	6.5	50	6	63	6561.926637
NMNH501108	S. oedipus	1.7	M	6.5	50	6	66	6794.913151

Name	F.dist.TA	F.dist.TA.s	F.dist.lmax	F.dist.lmax.s	F.dist.lmin
NMNH238258	12.2517	0.002283	14.2974	0.0000451551	10.0342
NMNH336299	11.149	0.002305	12.1802	0.0000434251	8.1028
NMNH337331	11.8344	0.002771	16.168	0.0000675956	7.6992
NMNH461267	13.9284	0.002398	19.3967	0.0000530019	12.4608
AMNH188173	13.0594	0.002354	17.7722	0.0000516659	10.3924
AMNH188176	11.311	0.002769	11.7973	0.0000502332	8.8286
AMNH188177	NA	NA	NA	NA	NA
AMNH188178	11.1138	0.002151	10.4383	0.0000331158	9.2848
AMNH188179	12.0842	0.002474	14.6897	0.0000509688	9.2283
NMNH543485	15.2101	0.001694	21.142	0.0000327042	16.1077
NMNH543486	NA	NA	NA	NA	NA
NMNH543487	16.1627	0.00219	24.4867	0.0000477476	17.754
NMNH543489	17.0502	0.00233	26.088	0.0000531991	20.8008
NMNH543490	NA	NA	NA	NA	NA
NMNH544381	NA	NA	NA	NA	NA
NMNH544382	19.8575	0.002216	34.77	0.0000524282	28.541
NMNH544383	NA	NA	NA	NA	NA
NMNH501080	12.9194	0.001901	17.0787	0.0000380826	10.4573
NMNH501082	NA	NA	NA	NA	NA
NMNH501084	13.8207	0.002126	17.7147	0.0000446715	13.1828
NMNH501085	11.0486	0.001988	11.0181	0.0000314699	8.6044
NMNH501088	15.2361	0.001996	22.8143	0.0000442876	15.1381
NMNH501091	12.9858	0.001697	15.309	0.0000307725	11.8979
NMNH501092	13.2183	0.002134	15.9476	0.0000408718	12.2174
NMNH501093	11.7581	0.001913	12.1153	0.0000312827	10.0887

Name	F.dist.TA	F.dist.TA.s	F.dist.lmax	F.dist.lmax.s	F.dist.lmin
NMNH501094	13.8838	0.001934	18.5147	0.0000384929	12.8951
NMNH501097	13.3136	0.002057	15.9615	0.0000379313	12.5163
NMNH501099	NA	NA	NA	NA	NA
NMNH501100	15.0695	0.002153	20.0991	0.0000435185	16.3315
NMNH501102	NA	NA	NA	NA	NA
NMNH501103	12.0218	0.002587	13.2584	0.0000475503	9.9923
NMNH501105	NA	NA	NA	NA	NA
NMNH501106	NA	NA	NA	NA	NA
NMNH501107	13.3279	0.002031	16.751	0.0000405199	11.9708
NMNH501108	14.1072	0.002076	18.5609	0.0000413877	13.5671
Name	**F.dist.lmin.s**	**F.dist.MaxXrad**	**F.dist.MaxYrad**	**F.dist.J**	**F.dist.J.s**
NMNH238258	0.000031691	2.0901	1.9489	24.3316	0.0000768
NMNH336299	0.000028888	1.795	2.1081	20.283	0.0000723
NMNH337331	0.000032189	2.1644	1.8849	23.8672	0.0000998
NMNH461267	0.000034049	2.072	2.3577	31.8575	0.0000871
AMNH188173	0.000030212	2.3376	1.898	28.1645	0.0000819
AMNH188176	0.000037592	1.9619	1.8315	20.6259	0.0000878
AMNH188177	NA	NA	NA	NA	NA
AMNH188178	0.000029456	1.8612	2.0054	19.7231	0.0000626
AMNH188179	0.000032019	1.8534	2.1689	23.918	0.0000830
NMNH543485	0.000024917	2.4047	2.14	37.2496	0.0000576
NMNH543486	NA	NA	NA	NA	NA
NMNH543487	0.000034619	2.1432	2.5447	42.2406	0.0000824
NMNH543489	0.000042417	2.2916	2.5905	46.8888	0.0000956
NMNH543490	NA	NA	NA	NA	NA
NMNH544381	NA	NA	NA	NA	NA
NMNH544382	0.000043036	2.5362	2.7348	63.311	0.0000955
NMNH544383	NA	NA	NA	NA	NA
NMNH501080	0.000023318	2.3772	1.8949	27.536	0.0000614
NMNH501082	NA	NA	NA	NA	NA
NMNH501084	0.000033243	1.9805	2.4045	30.8975	0.0000779
NMNH501085	0.000024576	1.8586	1.9268	19.6225	0.0000560
NMNH501088	0.000029386	2.458	2.1018	37.9524	0.0000737
NMNH501091	0.000023916	2.136	2.0212	27.2068	0.0000547
NMNH501092	0.000031312	1.9976	2.274	28.165	0.0000722
NMNH501093	0.000026050	1.9383	2.1264	22.2039	0.0000573
NMNH501094	0.000026809	2.0203	2.3622	31.4097	0.0000653
NMNH501097	0.000029744	2.241	1.9942	28.4778	0.0000677
NMNH501099	NA	NA	NA	NA	NA
NMNH501100	0.000035361	2.381	2.1328	36.4306	0.0000789
NMNH501102	NA	NA	NA	NA	NA
NMNH501103	0.000035837	2.1311	1.8457	23.2507	0.0000834
NMNH501105	NA	NA	NA	NA	NA
NMNH501106	NA	NA	NA	NA	NA
NMNH501107	0.000028957	2.2911	1.9449	28.7218	0.0000695
NMNH501108	0.000030252	2.3296	2.0086	32.128	0.0000716
Name	**F.dist.ZpEst**	**F.dist.ZpEst.s**	**F.mid.TA**	**F.mid.TA.s**	**F.mid.lmax**
NMNH238258	12.04832879	0.0022451	12.195	0.0022724	13.1472
NMNH336299	10.39327714	0.0021492	10.9588	0.0022661	11.0215
NMNH337331	11.78830909	0.0027600	10.4216	0.0024400	10.0223
NMNH461267	14.38359257	0.0024761	11.9888	0.0020639	11.9631
AMNH188173	13.2989423	0.0023970	13.1283	0.0023663	14.9204
AMNH188176	10.87462435	0.0026625	11.2589	0.0027566	10.5175
AMNH188177	NA	NA	NA	NA	NA
AMNH188178	10.20177934	0.0019743	11.6341	0.0022515	11.4578
AMNH188179	11.89269821	0.0024346	12.3415	0.0025265	13.1382
NMNH543485	16.39254516	0.0018257	14.5122	0.0016163	17.1301
NMNH543486	NA	NA	NA	NA	NA
NMNH543487	18.0211182	0.0024422	15.9825	0.0021660	22.6636
NMNH543489	19.20845538	0.0026244	15.4694	0.0021135	20.136
NMNH543490	NA	NA	NA	NA	NA

Name	F.dist.ZpEst	F.dist.ZpEst.s	F.mid.TA	F.mid.TA.s	F.mid.lmax
NMNH544381	NA	NA	NA	NA	NA
NMNH544382	24.02238664	0.0026805	18.6749	0.0020838	29.7136
NMNH544383	NA	NA	NA	NA	NA
NMNH501080	12.89108401	0.0018972	12.4918	0.0018384	14.7369
NMNH501082	NA	NA	NA	NA	NA
NMNH501084	14.09236032	0.0021678	11.9628	0.0018402	12.9917
NMNH501085	10.36746447	0.0018655	10.1418	0.0018249	8.6645
NMNH501088	16.64651958	0.0021812	13.1998	0.0017296	15.2251
NMNH501091	13.08900221	0.0017102	10.8212	0.0014139	10.5496
NMNH501092	13.18709617	0.0021292	12.6106	0.0020361	13.6974
NMNH501093	10.92523433	0.0017772	10.8766	0.0017693	9.9101
NMNH501094	14.33414718	0.0019967	11.3883	0.0015863	11.6086
NMNH501097	13.44814885	0.0020773	12.3619	0.0019095	13.5952
NMNH501099	NA	NA	NA	NA	NA
NMNH501100	16.14187602	0.0023067	13.3395	0.0019063	14.8781
NMNH501102	NA	NA	NA	NA	NA
NMNH501103	11.69317039	0.0025162	10.3957	0.0022370	8.9511
NMNH501105	NA	NA	NA	NA	NA
NMNH501106	NA	NA	NA	NA	NA
NMNH501107	13.56081209	0.0020666	11.6669	0.0017780	11.7082
NMNH501108	14.81167304	0.0021798	13.2119	0.0019444	15.145

Name	F.mid.lmax.s	F.mid.lmin	F.mid.lmin.s	F.mid.MaxXrad	F.mid.MaxYrad
NMNH238258	0.00004152	10.6719	0.0000337048	1.9619	2.0814
NMNH336299	0.00003929	8.3413	0.0000297386	1.8265	2.0461
NMNH337331	0.00004190	7.4924	0.0000313244	1.94	1.9115
NMNH461267	0.00003269	11.0488	0.0000301911	1.9197	2.0522
AMNH188173	0.00004338	12.6302	0.0000367175	2.166	2.0196
AMNH188176	0.00004478	9.695	0.0000412815	1.9622	1.9111
AMNH188177	NA	NA	NA	NA	NA
AMNH188178	0.00003635	10.2194	0.0000324214	2.0172	2.0038
AMNH188179	0.00004559	11.2179	0.0000389227	1.9394	2.1076
NMNH543485	0.00002650	16.5108	0.0000255403	2.2246	2.1748
NMNH543486	NA	NA	NA	NA	NA
NMNH543487	0.00004419	18.3054	0.0000356944	2.1951	2.3958
NMNH543489	0.00004106	18.1153	0.0000369410	2.2603	2.364
NMNH543490	NA	NA	NA	NA	NA
NMNH544381	NA	NA	NA	NA	NA
NMNH544382	0.00004480	26.2164	0.0000395306	2.5847	2.6175
NMNH544383	NA	NA	NA	NA	NA
NMNH501080	0.00003286	10.5631	0.0000235539	2.2223	1.9366
NMNH501082	NA	NA	NA	NA	NA
NMNH501084	0.00003276	10.0449	0.0000253304	1.8835	2.1054
NMNH501085	0.00002475	7.7702	0.0000221933	1.7958	1.9002
NMNH501088	0.00002956	12.6656	0.0000245867	2.0734	2.0825
NMNH501091	0.00002121	8.3281	0.0000167402	1.8756	1.9025
NMNH501092	0.00003510	11.7668	0.0000301569	1.937	2.1163
NMNH501093	0.00002559	9.0363	0.0000233324	1.9114	2.0656
NMNH501094	0.00002413	9.2939	0.0000193224	1.8476	2.0833
NMNH501097	0.00003231	10.9946	0.0000261279	2.0702	1.9545
NMNH501099	NA	NA	NA	NA	NA
NMNH501100	0.00003221	13.5748	0.0000293921	2.1489	2.082
NMNH501102	NA	NA	NA	NA	NA
NMNH501103	0.00003210	8.2919	0.0000297383	1.8677	1.8186
NMNH501105	NA	NA	NA	NA	NA
NMNH501106	NA	NA	NA	NA	NA
NMNH501107	0.00002832	10.1015	0.0000244351	2.0197	1.8859
NMNH501108	0.00003377	12.7885	0.0000285162	2.156	2.021

Name	F.mid.J	F.mid.J.s	F.mid.ZpEst	F.mid.ZpEst.s	F.prox.TA
NMNH238258	23.8191	0.000075227	11.78	0.002195062	13.7799
NMNH336299	19.3628	0.000069033	10	0.002067829	10.0181
NMNH337331	17.5147	0.000073226	9.1	0.002130549	10.6178

Name	F.mid.J	F.mid.J.s	F.mid.ZpEst	F.mid.ZpEst.s	F.prox.TA
NMNH461267	23.0118	0.000062880	11.59	0.001995207	NA
AMNH188173	27.5507	0.000080093	13.16	0.002371979	12.5044
AMNH188176	20.2125	0.000086065	10.44	0.002556092	10.3389
AMNH188177	NA	NA	NA	NA	NA
AMNH188178	21.6772	0.000068772	10.78	0.002086192	12.343
AMNH188179	24.3561	0.000084508	12.04	0.002464732	11.7479
NMNH543485	33.6409	0.000052039	15.29	0.001702933	15.4791
NMNH543486	NA	NA	NA	NA	NA
NMNH543487	40.969	0.000079887	17.85	0.002419047	14.1906
NMNH543489	38.2513	0.000078003	16.54	0.002259820	15.4177
NMNH543490	NA	NA	NA	NA	NA
NMNH544381	NA	NA	NA	NA	NA
NMNH544382	55.93	0.000084334	21.5	0.002399000	17.9926
NMNH544383	NA	NA	NA	NA	NA
NMNH501080	25.3	0.000056415	12.17	0.001791046	11.8853
NMNH501082	NA	NA	NA	NA	NA
NMNH501084	23.0367	0.000058092	11.55	0.001776677	11.1884
NMNH501085	16.4347	0.000046941	8.89	0.001599673	10.0907
NMNH501088	27.8907	0.000054142	13.42	0.001758453	12.4069
NMNH501091	18.8778	0.000037946	9.99	0.001305252	10.1456
NMNH501092	25.4642	0.000065262	12.56	0.002027957	11.5873
NMNH501093	18.9463	0.000048921	9.53	0.001550254	10.4923
NMNH501094	20.9025	0.000043457	10.63	0.001480716	11.182
NMNH501097	24.5898	0.000058436	12.22	0.001887595	11.4985
NMNH501099	NA	NA	NA	NA	NA
NMNH501100	28.4529	0.000061606	13.45	0.001922044	12.2392
NMNH501102	NA	NA	NA	NA	NA
NMNH501103	17.243	0.000061841	9.36	0.002014139	9.9766
NMNH501105	NA	NA	NA	NA	NA
NMNH501106	NA	NA	NA	NA	NA
NMNH501107	21.8097	0.000052757	11.17	0.001702244	11.4798
NMNH501108	27.9335	0.000062287	13.37	0.001967648	12.0739

Name	F.prox.TA.s	F.prox.lmax	F.prox.lmax.s	F.prox.lmin	F.prox.lmin.s
NMNH238258	0.002567719	16.5197	0.000052174	13.8697	0.0000438043
NMNH336299	0.002071572	9.1298	0.000032550	7.0396	0.0000250977
NMNH337331	0.002485905	9.8018	0.000040980	8.2578	0.0000345244
NMNH461267	NA	NA	NA	NA	NA
AMNH188173	0.002253812	16.7984	0.000048835	9.2684	0.0000269444
AMNH188176	0.002531339	9.6776	0.000041207	7.5192	0.0000320169
AMNH188177	NA	NA	NA	NA	NA
AMNH188178	0.002388671	15.039	0.000047712	9.9625	0.0000316063
AMNH188179	0.002404935	13.5974	0.000047179	8.9687	0.0000311186
NMNH543485	0.001723994	23.2195	0.000035918	15.8917	0.0000245826
NMNH543486	NA	NA	NA	NA	NA
NMNH543487	0.001923122	17.2197	0.000033577	14.9256	0.0000291040
NMNH543489	0.002106483	20.8655	0.000042549	17.358	0.0000353967
NMNH543490	NA	NA	NA	NA	NA
NMNH544381	NA	NA	NA	NA	NA
NMNH544382	0.002007639	32.1767	0.000048518	20.7429	0.0000312773
NMNH544383	NA	NA	NA	NA	NA
NMNH501080	0.001749147	13.6815	0.000030507	9.3455	0.0000208389
NMNH501082	NA	NA	NA	NA	NA
NMNH501084	0.001721054	11.9831	0.000030218	8.2978	0.0000209247
NMNH501085	0.001815728	8.9254	0.000025493	7.3853	0.0000210939
NMNH501088	0.001625704	15.1497	0.000029409	9.9253	0.0000192672
NMNH501091	0.001325582	10.2476	0.000020599	6.5526	0.0000131713
NMNH501092	0.001870903	12.7481	0.000032672	8.9679	0.0000229837
NMNH501093	0.001706793	10.227	0.000026407	7.5423	0.0000194748
NMNH501094	0.001557607	11.2171	0.000023321	8.8548	0.0000184095
NMNH501097	0.001776147	12.4989	0.000029703	8.8894	0.0000211250
NMNH501099	NA	NA	NA	NA	NA

Name	F.prox.TA.s	F.prox.lmax	F.prox.lmax.s	F.prox.lmin	F.prox.lmin.s
NMNH501100	0.001749017	13.5721	0.000029386	10.554	0.0000228515
NMNH501102	NA	NA	NA	NA	NA
NMNH501103	0.002146823	8.6223	0.000030923	7.2927	0.0000261548
NMNH501105	NA	NA	NA	NA	NA
NMNH501106	NA	NA	NA	NA	NA
NMNH501107	0.001749456	11.2663	0.000027253	9.804	0.0000237155
NMNH501108	0.001776903	13.7276	0.000030610	9.8319	0.0000219235
Name	**F.prox.MaxXrad**	**F.prox.MaxYrad**	**F.prox.J**	**F.prox.J.s**	**F.prox.ZpEst**
NMNH238258	2.1108	2.2112	30.3894	0.000095978	14.06265618
NMNH336299	1.7981	1.903	16.1694	0.000057648	8.737618546
NMNH337331	2.004	1.8534	18.0596	0.000075504	9.363612796
NMNH461267	NA	NA	NA	NA	NA
AMNH188173	2.2147	1.9973	26.0668	0.000075779	12.37739791
AMNH188176	2.0474	1.7646	17.1967	0.000073224	9.022402938
AMNH188177	NA	NA	NA	NA	NA
AMNH188178	2.2425	1.9029	25.0015	0.000079318	12.06228591
AMNH188179	2.1343	1.9295	22.5661	0.000078297	11.10591072
NMNH543485	2.168	2.4074	39.1112	0.000060500	17.09629759
NMNH543486	NA	NA	NA	NA	NA
NMNH543487	2.0671	2.2079	32.1453	0.000062681	15.03873684
NMNH543489	2.2652	2.4931	38.2235	0.000077946	16.06603199
NMNH543490	NA	NA	NA	NA	NA
NMNH544381	NA	NA	NA	NA	NA
NMNH544382	2.6734	2.231	52.9196	0.000079795	21.58045836
NMNH544383	NA	NA	NA	NA	NA
NMNH501080	2.1413	1.9414	23.027	0.000051346	11.28028021
NMNH501082	NA	NA	NA	NA	NA
NMNH501084	1.8516	2.043	20.2809	0.000051143	10.41488214
NMNH501085	1.7864	1.9189	16.3107	0.000046587	8.803983483
NMNH501088	1.9332	2.0835	25.075	0.000048676	12.48537357
NMNH501091	1.7603	1.9022	16.8002	0.000033770	9.174170648
NMNH501092	1.8792	2.0823	21.716	0.000055656	10.96352392
NMNH501093	2.0463	1.7303	17.7692	0.000045881	9.410157284
NMNH501094	1.8853	2.0046	20.0719	0.000041730	10.32000823
NMNH501097	1.9555	1.8904	21.3883	0.000050828	11.12265009
NMNH501099	NA	NA	NA	NA	NA
NMNH501100	1.9948	2.0345	24.1261	0.000052238	11.9753307
NMNH501102	NA	NA	NA	NA	NA
NMNH501103	1.7967	1.8154	15.9151	0.000057078	8.812103762
NMNH501105	NA	NA	NA	NA	NA
NMNH501106	NA	NA	NA	NA	NA
NMNH501107	1.8642	1.9868	21.0703	0.000050968	10.94276811
NMNH501108	2.0308	1.9299	23.5595	0.000052534	11.89663443
Name	**F.prox.ZpEst.s**	**H.dist.TA**	**H.dist.TA.s**	**H.dist.lmax**	**H.dist.lmax.s**
NMNH238258	0.002620407	NA	NA	NA	NA
NMNH336299	0.001806790	7.2998	0.0015095	5.3698	0.000023625
NMNH337331	0.002192267	9.057	0.0021205	7.0459	0.000036658
NMNH461267	NA	NA	NA	NA	NA
AMNH188173	0.002230921	9.0106	0.0016241	8.4184	0.000030966
AMNH188176	0.002209013	NA	NA	NA	NA
AMNH188177	NA	6.7375	0.0016438	3.9776	0.000023384
AMNH188178	0.002334346	8.8184	0.0017066	6.8322	0.000026182
AMNH188179	0.002273512	10.0632	0.0020601	11.0959	0.000048329
NMNH543485	0.001904111	12.1329	0.0013513	15.5391	0.000031467
NMNH543486	NA	NA	NA	NA	NA
NMNH543487	0.002038062	13.6411	0.0018487	17.8969	0.000045762
NMNH543489	0.002195063	NA	NA	NA	NA
NMNH543490	NA	NA	NA	NA	NA
NMNH544381	NA	11.892	0.0012355	14.3137	0.000026555
NMNH544382	0.002407978	12.3811	0.0013815	18.6439	0.000036179
NMNH544383	NA	12.2613	0.0011826	16.0381	0.000026669

Name	F.prox.ZpEst.s	H.dist.TA	H.dist.TA.s	H.dist.lmax	H.dist.lmax.s
NMNH501080	0.001660107	9.685	0.0014253	9.5317	0.000028055
NMNH501082	NA	NA	NA	NA	NA
NMNH501084	0.001602068	10.0788	0.0015504	12.0501	0.000036345
NMNH501085	0.001584196	NA	NA	NA	NA
NMNH501088	0.001635987	10.7321	0.0014063	14.705	0.000036355
NMNH501091	0.001198659	8.4875	0.0011089	8.3481	0.000021387
NMNH501092	0.001770187	NA	NA	NA	NA
NMNH501093	0.001530759	8.9537	0.0014565	9.5486	0.000031066
NMNH501094	0.001437536	10.2359	0.0014258	11.9734	0.000031469
NMNH501097	0.001718090	9.9208	0.0015324	10.8808	0.000033615
NMNH501099	NA	NA	NA	NA	NA
NMNH501100	0.001711310	10.6372	0.0015201	12.8341	0.000035270
NMNH501102	NA	12.0333	0.0013865	15.9742	0.000032867
NMNH501103	0.001896240	8.466	0.0018218	6.8471	0.000031349
NMNH501105	NA	NA	NA	NA	NA
NMNH501106	NA	NA	NA	NA	NA
NMNH501107	0.001667615	10.3912	0.0015836	11.3757	0.000034672
NMNH501108	0.001750815	12.393	0.0018239	16.1375	0.000047499
Name	**H.dist.lmin**	**H.dist.lmin.s**	**H.dist.MaxXrad**	**H.dist.MaxYrad**	**H.dist.J**
NMNH238258	NA	NA	NA	NA	NA
NMNH336299	3.5315	0.000015537	1.5968	2.1174	8.9013
NMNH337331	6.1855	0.000032182	1.723	1.9386	13.2314
NMNH461267	NA	NA	NA	NA	NA
AMNH188173	5.0188	0.000018461	1.7137	1.9367	13.4372
AMNH188176	NA	NA	NA	NA	NA
AMNH188177	3.3413	0.000019643	1.5752	1.5631	7.3189
AMNH188178	5.6495	0.000021650	1.7282	1.6663	12.4817
AMNH188179	5.9204	0.000025787	1.6857	2.149	17.0164
NMNH543485	9.4118	0.000019059	1.9285	2.4007	24.9509
NMNH543486	NA	NA	NA	NA	NA
NMNH543487	12.6306	0.000032296	2.2177	2.15	30.5275
NMNH543489	NA	NA	NA	NA	NA
NMNH543490	NA	NA	NA	NA	NA
NMNH544381	9.2653	0.000017189	2.1113	2.0681	23.579
NMNH544382	8.2849	0.000016077	1.8728	2.5145	26.9288
NMNH544383	9.3908	0.000015616	1.8763	2.597	25.4289
NMNH501080	6.252	0.000018402	1.9553	2.1371	15.7836
NMNH501082	NA	NA	NA	NA	NA
NMNH501084	5.9197	0.000017855	2.0757	1.8597	17.9698
NMNH501085	NA	NA	NA	NA	NA
NMNH501088	6.3013	0.000015579	1.8286	2.7004	21.0063
NMNH501091	4.2786	0.000010961	1.6624	2.1716	12.6267
NMNH501092	NA	NA	NA	NA	NA
NMNH501093	4.8172	0.000015672	1.5896	2.4846	14.3658
NMNH501094	6.1982	0.000016290	2.5333	1.6793	18.1716
NMNH501097	6.261	0.000019342	2.0502	1.9158	17.1418
NMNH501099	NA	NA	NA	NA	NA
NMNH501100	6.7528	0.000018558	2.0587	1.8425	19.5869
NMNH501102	8.9542	0.000018423	2.4665	1.9746	24.9284
NMNH501103	4.8443	0.000022179	1.6864	1.7184	11.6914
NMNH501105	NA	NA	NA	NA	NA
NMNH501106	NA	NA	NA	NA	NA
NMNH501107	6.9488	0.000021179	2.0439	1.8688	18.3245
NMNH501108	9.6862	0.000028510	2.5964	1.9704	25.8237
Name	**H.dist.J.s**	**H.dist.ZpEst**	**H.dist.ZpEst.s**	**H.mid.TA**	**H.mid.TA.s**
NMNH238258	NA	NA	NA	NA	NA
NMNH336299	0.0000391625	4.79	0.0009905	7.5107	0.001553085
NMNH337331	0.0000688404	7.23	0.0016927	8.2188	0.001924237
NMNH461267	NA	NA	NA	NA	NA
AMNH188173	0.0000494274	7.36	0.0013266	9.7616	0.001759446
AMNH188176	NA	NA	NA	NA	NA

Name	H.dist.J.s	H.dist.ZpEst	H.dist.ZpEst.s	H.mid.TA	H.mid.TA.s
AMNH188177	0.0000430272	4.66	0.0011369	6.1414	0.001498348
AMNH188178	0.0000478319	7.35	0.0014224	9.9475	0.001925083
AMNH188179	0.0000741162	8.87	0.0018158	9.6103	0.001967343
NMNH543485	0.0000505258	11.53	0.0012842	12.1889	0.001357546
NMNH543486	NA	NA	NA	NA	NA
NMNH543487	0.0000780587	13.98	0.0018946	14.1971	0.001924003
NMNH543489	NA	NA	NA	NA	NA
NMNH543490	NA	NA	NA	NA	NA
NMNH544381	0.0000437441	11.28	0.0011719	11.8049	0.001226435
NMNH544382	0.0000522566	12.28	0.0013698	14.5213	0.001620307
NMNH544383	0.0000422850	11.37	0.0010966	13.5109	0.001303081
NMNH501080	0.0000464571	7.71	0.0011347	9.8196	0.001445140
NMNH501082	NA	NA	NA	NA	NA
NMNH501084	0.0000542000	9.13	0.0014044	10.742	0.001652387
NMNH501085	NA	NA	NA	NA	NA
NMNH501088	0.0000519340	9.28	0.0012160	10.987	0.001439652
NMNH501091	0.0000323481	6.59	0.0008610	9.2283	0.001205731
NMNH501092	NA	NA	NA	NA	NA
NMNH501093	0.0000467380	7.05	0.0011468	8.9015	0.001448016
NMNH501094	0.0000477591	8.63	0.0012021	10.1561	0.001414704
NMNH501097	0.0000529571	8.64	0.0013346	10.0087	0.001546021
NMNH501099	NA	NA	NA	NA	NA
NMNH501100	0.0000538274	10.04	0.0014347	11.8298	0.001690513
NMNH501102	0.0000512901	11.23	0.0012939	12.6111	0.001453048
NMNH501103	0.0000535282	6.87	0.0014783	8.3768	0.001802569
NMNH501105	NA	NA	NA	NA	NA
NMNH501106	NA	NA	NA	NA	NA
NMNH501107	0.0000558510	9.37	0.0014279	9.7624	0.001487734
NMNH501108	0.0000760089	11.31	0.0016645	12.2512	0.001802996

Name	H.mid.lmax	H.mid.lmax.s	H.mid.lmin	H.mid.lmin.s	H.mid.MaxXrad
NMNH238258	NA	NA	NA	NA	NA
NMNH336299	4.8816	0.000021477	4.2085	0.0000185159	1.5585
NMNH337331	5.7799	0.000030072	5.1052	0.0000265614	1.6691
NMNH461267	NA	NA	NA	NA	NA
AMNH188173	8.2338	0.000030287	7.0753	0.0000260258	1.8899
AMNH188176	NA	NA	NA	NA	NA
AMNH188177	3.5465	0.000020850	2.546	0.0000149677	1.357
AMNH188178	8.5797	0.000032879	7.2698	0.0000278591	1.7241
AMNH188179	9.3678	0.000040802	5.8105	0.0000253081	1.7608
NMNH543485	12.6321	0.000025580	11.1335	0.0000225455	2.0866
NMNH543486	NA	NA	NA	NA	NA
NMNH543487	17.6967	0.000045250	14.6655	0.0000374996	2.225
NMNH543489	NA	NA	NA	NA	NA
NMNH543490	NA	NA	NA	NA	NA
NMNH544381	12.4564	0.000023109	9.8996	0.0000183659	1.975
NMNH544382	18.9558	0.000036785	14.9246	0.0000289619	2.2683
NMNH544383	15.5852	0.000025916	13.6787	0.0000227459	2.1777
NMNH501080	9.5771	0.000028189	6.2663	0.0000184441	2.0757
NMNH501082	NA	NA	NA	NA	NA
NMNH501084	9.6069	0.000028976	8.8248	0.0000266171	1.9354
NMNH501085	NA	NA	NA	NA	NA
NMNH501088	9.8549	0.000024364	9.5452	0.0000235987	1.9727
NMNH501091	7.982	0.000020449	5.8779	0.0000150585	1.8621
NMNH501092	NA	NA	NA	NA	NA
NMNH501093	6.9901	0.000022742	5.9321	0.0000192996	1.8684
NMNH501094	8.5646	0.000022510	8.1135	0.0000213241	1.8751
NMNH501097	9.8858	0.000030541	6.535	0.0000201889	2.0683
NMNH501099	NA	NA	NA	NA	NA
NMNH501100	11.997	0.000032969	10.5762	0.0000290648	2.0835
NMNH501102	13.8129	0.000028420	11.7885	0.0000242548	2.1297
NMNH501103	6.2764	0.000028736	5.0095	0.0000229356	1.6877

Name	H.mid.lmax	H.mid.lmax.s	H.mid.lmin	H.mid.lmin.s	H.mid.MaxXrad
NMNH501105	NA	NA	NA	NA	NA
NMNH501106	NA	NA	NA	NA	NA
NMNH501107	8.3556	0.000025467	7.1167	0.0000216909	1.9434
NMNH501108	13.4605	0.000039619	10.7044	0.0000315071	1.9436
Name	**H.mid.MaxYrad**	**H.mid.J**	**H.mid.J.s**	**H.mid.ZpEst**	**H.mid.ZpEst.s**
NMNH238258	NA	NA	NA	NA	NA
NMNH336299	1.7089	9.0901	0.000039993	5.56	0.00114971
NMNH337331	1.694	10.8851	0.000056633	6.47	0.00151480
NMNH461267	NA	NA	NA	NA	NA
AMNH188173	1.8674	15.3091	0.000056313	8.15	0.00146897
AMNH188176	NA	NA	NA	NA	NA
AMNH188177	1.5042	6.0926	0.000035818	4.26	0.00103933
AMNH188178	1.9009	15.8495	0.000060738	8.74	0.00169140
AMNH188179	1.9456	15.1783	0.000066110	8.19	0.00167659
NMNH543485	1.9198	23.7656	0.000048126	11.86	0.00132091
NMNH543486	NA	NA	NA	NA	NA
NMNH543487	2.2786	32.3622	0.000082750	14.37	0.00194743
NMNH543489	NA	NA	NA	NA	NA
NMNH543490	NA	NA	NA	NA	NA
NMNH544381	1.9714	22.356	0.000041475	11.33	0.00117710
NMNH544382	2.1023	33.8804	0.000065746	15.5038	0.00172993
NMNH544383	2.0676	29.2639	0.000048662	13.79	0.00133000
NMNH501080	1.6885	15.8434	0.000046633	8.42	0.00123916
NMNH501082	NA	NA	NA	NA	NA
NMNH501084	1.8164	18.4317	0.000055593	9.83	0.00151210
NMNH501085	NA	NA	NA	NA	NA
NMNH501088	1.9086	19.4002	0.000047963	10	0.00131032
NMNH501091	1.8333	13.8599	0.000035507	7.5	0.00097992
NMNH501092	NA	NA	NA	NA	NA
NMNH501093	1.8118	12.9222	0.000042041	7.02	0.00114195
NMNH501094	1.907	16.6781	0.000043834	8.82	0.00122859
NMNH501097	1.7484	16.4208	0.000050730	8.6	0.00132842
NMNH501099	NA	NA	NA	NA	NA
NMNH501100	2.0388	22.5732	0.000062034	10.95	0.00156479
NMNH501102	2.0775	25.6014	0.000052675	12.17	0.00140222
NMNH501103	1.739	11.2859	0.000051672	6.59	0.00141807
NMNH501105	NA	NA	NA	NA	NA
NMNH501106	NA	NA	NA	NA	NA
NMNH501107	1.8655	15.4723	0.000047158	8.12	0.00123744
NMNH501108	2.1766	24.1649	0.000071126	11.73	0.00172629
Name	**H.prox.TA**	**H.prox.TA.s**	**H.prox.lmax**	**H.prox.lmax.s**	**H.prox.lmin**
NMNH238258	NA	NA	NA	NA	NA
NMNH336299	11.3069	0.002338074	12.7357	0.0000560325	9.2663
NMNH337331	11.9757	0.002803826	12.6879	0.0000660127	10.7847
NMNH461267	NA	NA	NA	NA	NA
AMNH188173	13.747	0.002477780	19.6241	0.0000721853	12.4819
AMNH188176	NA	NA	NA	NA	NA
AMNH188177	7.1024	0.001732808	5.2248	0.0000307162	3.1799
AMNH188178	13.8646	0.002683138	19.1959	0.0000735619	13.5743
AMNH188179	12.1757	0.002492511	18.5085	0.0000806151	7.8847
NMNH543485	15.9362	0.001774904	29.1785	0.0000590868	15.6183
NMNH543486	NA	NA	NA	NA	NA
NMNH543487	18.0288	0.002443278	38.2785	0.0000978780	19.6694
NMNH543489	NA	NA	NA	NA	NA
NMNH543490	NA	NA	NA	NA	NA
NMNH544381	17.0898	0.001775493	33.1365	0.0000614753	17.4565
NMNH544382	18.0393	0.002012850	39.4097	0.0000764763	18.3806
NMNH544383	18.1646	0.001751915	34.8349	0.0000579260	22.2931
NMNH501080	13.4188	0.001974830	17.7702	0.0000523044	12.2982
NMNH501082	NA	NA	NA	NA	NA
NMNH501084	13.5344	0.002081927	18.6253	0.0000561771	12.065

Name	H.prox.TA	H.prox.TA.s	H.prox.lmax	H.prox.lmax.s	H.prox.lmin
NMNH501085	NA	NA	NA	NA	NA
NMNH501088	14.2056	0.001861392	19.466	0.0000481259	14.047
NMNH501091	12.3137	0.001608857	15.9871	0.0000409570	9.5882
NMNH501092	NA	NA	NA	NA	NA
NMNH501093	11.5991	0.001886837	13.1257	0.0000427034	9.2377
NMNH501094	12.7483	0.001775787	15.4924	0.0000407175	11.4091
NMNH501097	14.8397	0.002292254	24.4941	0.0000756709	13.285
NMNH501099	NA	NA	NA	NA	NA
NMNH501100	14.291	0.002042226	22.0506	0.0000605980	12.7908
NMNH501102	16.3268	0.001881170	28.3664	0.0000583637	17.9775
NMNH501103	11.1647	0.002402485	13.0631	0.0000598084	7.8393
NMNH501105	NA	NA	NA	NA	NA
NMNH501106	NA	NA	NA	NA	NA
NMNH501107	13.1077	0.001997538	17.7302	0.0000540396	11.2377
NMNH501108	15.4339	0.002271390	25.5575	0.0000752254	15.1198

Name	H.prox.lmin.s	H.prox.MaxXrad	H.prox.MaxYrad	H.prox.J	H.prox.J.s
NMNH238258	NA	NA	NA	NA	NA
NMNH336299	0.000040768	2.0315	2.0858	22.002	0.000096801
NMNH337331	0.000056111	1.9919	2.2247	23.4726	0.000122123
NMNH461267	NA	NA	NA	NA	NA
AMNH188173	0.000045913	2.2072	2.3261	32.106	0.000118099
AMNH188176	NA	NA	NA	NA	NA
AMNH188177	0.000018694	1.8179	1.5327	8.4047	0.000049411
AMNH188178	0.000052019	2.3221	2.7583	32.7703	0.000125581
AMNH188179	0.000034342	2.539	1.9838	26.3931	0.000114957
NMNH543485	0.000031627	3.0955	2.231	44.7968	0.000090714
NMNH543486	NA	NA	NA	NA	NA
NMNH543487	0.000050295	2.5973	3.2886	57.9479	0.000148173
NMNH543489	NA	NA	NA	NA	NA
NMNH543490	NA	NA	NA	NA	NA
NMNH544381	0.000032386	2.9715	2.5418	50.593	0.000093861
NMNH544382	0.000035668	3.28	2.2027	57.7904	0.000112145
NMNH544383	0.000037071	3.0131	2.2777	57.1279	0.000094996
NMNH501080	0.000036198	2.3325	2.1371	30.0683	0.000088502
NMNH501082	NA	NA	NA	NA	NA
NMNH501084	0.000036390	2.3306	2.379	30.6903	0.000092567
NMNH501085	NA	NA	NA	NA	NA
NMNH501088	0.000034728	2.709	2.145	33.513	0.000082854
NMNH501091	0.000024564	2.1627	1.9649	25.5753	0.000065521
NMNH501092	NA	NA	NA	NA	NA
NMNH501093	0.000030054	2.3682	1.9033	22.3634	0.000072758
NMNH501094	0.000029986	2.0873	2.4317	26.9014	0.000070703
NMNH501097	0.000041042	2.6102	2.4087	37.7791	0.000116713
NMNH501099	NA	NA	NA	NA	NA
NMNH501100	0.000035151	2.2494	2.7683	34.8414	0.000095749
NMNH501102	0.000036989	2.6276	2.9826	46.3439	0.000095352
NMNH501103	0.000035892	2.1075	2.1066	20.9024	0.000095700
NMNH501105	NA	NA	NA	NA	NA
NMNH501106	NA	NA	NA	NA	NA
NMNH501107	0.000034251	2.1491	2.5651	28.9679	0.000088291
NMNH501108	0.000044503	2.0505	2.6496	40.6773	0.000119729

Name	H.prox.ZpEst	H.prox.ZpEst.s	F.C.AP
NMNH238258	NA	NA	1.54
NMNH336299	10.69	0.002	NA
NMNH337331	11.13	0.003	1.66
NMNH461267	NA	NA	2.34
AMNH188173	14.16	0.003	2.14
AMNH188176	NA	NA	1.88
AMNH188177	5.02	0.001	NA
AMNH188178	12.9	0.002	NA
AMNH188179	11.67	0.002	2.16

Name	H.prox.ZpEst	H.prox.ZpEst.s	F.C.AP
NMNH543485	16.82	0.002	2.26
NMNH543486	NA	NA	2.24
NMNH543487	19.69	0.003	2.08
NMNH543489	NA	NA	2.06
NMNH543490	NA	NA	1.98
NMNH544381	18.35	0.002	1.87
NMNH544382	21.08	0.002	1.84
NMNH544383	21.6	0.002	NA
NMNH501080	13.45	0.002	2.09
NMNH501082	NA	NA	2.33
NMNH501084	13.03	0.002	1.85
NMNH501085	NA	NA	1.87
NMNH501088	13.81	0.002	1.29
NMNH501091	12.39	0.002	1.68
NMNH501092	NA	NA	1.91
NMNH501093	10.47	0.002	2.43
NMNH501094	11.91	0.002	2.34
NMNH501097	15.05	0.002	2.77
NMNH501099	NA	NA	2.5
NMNH501100	13.89	0.002	2.06
NMNH501102	16.52	0.002	2.42
NMNH501103	9.92	0.002	1.37
NMNH501105	NA	NA	2.4
NMNH501106	NA	NA	2.03
NMNH501107	12.29	0.002	1.49
NMNH501108	17.31	0.003	1.98

Name	Species	DR	Sex	HHD	MHL	FHD	MFL	BS.GM^3
AMNH30620	M. fascicularis	1.3	F	12.6	111	11.7	128	55057.57
AMNH30622	M. fascicularis	1.3	F	12.9	116	11.8	129	58632.66
NMNH344989	M. fascicularis	1.3	F	13.5	122	11.5	130	62158.58
AMNH103654	M. fascicularis	1.3	F	11.9	115.5	11.2	129	52899.61
AMNH103659	M. fascicularis	1.3	M	14.1	125	12.4	141	73549.11
NMNH173813	M. mulatta	1.4	M	22.5	157	18	183	199229.81
NMNH241160	M. mulatta	1.4	F	20	147	16	170	150378.99
NMNH399285	M. mulatta	1.4	F	18	140	15.5	170	130808.47
AMNH28256	M. nemestrina	2	M	21.8	196	18.4	222	270030.31
HTB0337	M. nemestrina	2	M	18.5	161	18	196	184563.00
NMNH305069	M. nemestrina	2	F	19	156	16	172	152631.78
NMNHA49691	M. nemestrina	2	M	21.5	189	18	224	257522.74
NMNHA49696	M. nemestrina	2	M	14	131	18	145	102336.34
NMNHA49874	M. nemestrina	2	M	23.5	174	18.5	197	239850.87
AMNH106563	M. nemestrina	2	M	23	198	20.2	236	318047.73
AMNH106564	M. nemestrina	2	M	23.9	192	18.4	128	188492.98
AMNH30597	M. nigra	2.4	F	15.9	133	14.1	148	96282.46
HTB1160	M. silenus	1.7	M	17	174	18	193	181497.64

Name	F.dist.TA	F.dist.TA.s	F.dist.lmax	F.dist.lmax.s	F.dist.lmin
AMNH30620	40.4249	0.00073423	137.7387	1.95447E-05	122.8654
AMNH30622	39.926	0.000680952	133.0855	1.75955E-05	121.0518
NMNH344989	51.6923	0.00083162	271.1458	3.35551E-05	167.4398
AMNH103654	46.6909	0.000882632	185.3069	2.7155E-05	162.6058
AMNH103659	NA	NA	NA	NA	NA
NMNH173813	154.5302	0.000775638	2162.5419	5.93143E-05	1699.7325
NMNH241160	93.4776	0.000621613	751.0717	2.93796E-05	646.7454
NMNH399285	102.1623	0.000781007	959.4324	4.31449E-05	728.8596
AMNH28256	135.1204	0.00050039	1463.71	2.44168E-05	1445.1728
HTB0337	158.7449	0.000860112	2221.1742	6.14019E-05	1830.9673
NMNH305069	97.4883	0.000638716	843.5366	3.21315E-05	680.5962
NMNHA49691	111.9279	0.000434633	1100.8102	1.90831E-05	903.379
NMNHA49696	73.6672	0.000719854	477.2601	3.21631E-05	393.0072
NMNHA49874	112.2888	0.000468161	1073.6079	2.27216E-05	941.0171
AMNH106563	170.7626	0.000536909	2438.5752	3.24887E-05	2228.5282
AMNH106564	160.8816	0.000853515	2108.9042	8.74081E-05	2015.0086
AMNH30597	85.4252	0.000887235	623.6096	4.37627E-05	542.9174
HTB1160	99.8989	0.000550414	825.3902	2.3563E-05	765.8068

Name	F.dist.lmin.s	F.dist.MaxXrad	F.dist.MaxYrad	F.dist.J	F.dist.J.s
AMNH30620	1.74342E-05	3.696	3.6276	260.6041	3.69789E-05
AMNH30622	1.60045E-05	3.6928	3.5289	254.1372	3.36E-05
NMNH344989	2.07212E-05	4.7259	3.7871	438.5856	5.42763E-05
AMNH103654	2.38283E-05	3.7602	3.9978	347.9127	5.09833E-05
AMNH103659	NA	NA	NA	NA	NA
NMNH173813	4.66203E-05	7.3483	7.667	3862.2744	0.000105935
NMNH241160	2.52986E-05	5.7612	5.4793	1397.8171	5.46782E-05
NMNH399285	3.27762E-05	5.6706	6.2311	1688.292	7.59211E-05
AMNH28256	2.41076E-05	6.6663	6.6919	2908.8828	4.85245E-05
HTB0337	5.06151E-05	7.0612	7.7226	4052.1415	0.000112017
NMNH305069	2.59248E-05	5.3142	5.9745	1524.1328	5.80563E-05
NMNHA49691	1.56605E-05	6.27	5.851	2004.1892	3.47436E-05
NMNHA49696	2.64852E-05	4.7272	5.4189	870.2673	5.86482E-05
NMNHA49874	1.99154E-05	5.9561	6.1511	2014.6251	4.2637E-05
AMNH106563	2.96902E-05	7.2826	7.5142	4667.1034	6.21789E-05
AMNH106564	8.35164E-05	7.1841	7.2128	4123.9127	0.000170924
AMNH30597	3.81E-05	5.4781	5.2244	1166.527	8.18627E-05
HTB1160	2.18621E-05	5.7773	5.6408	1591.197	4.54251E-05

Name	F.dist.ZpEst	F.dist.ZpEst.s	F.mid.TA	F.mid.TA.s	F.mid.lmax
AMNH30620	71.17	0.00129262	38.5287	0.000699789	129.4044
AMNH30622	70.38	0.00120038	39.3637	0.000671361	131.9877
NMNH344989	103.04	0.00165768	50.2343	0.000808164	231.4248
AMNH103654	89.69	0.00169550	48.6479	0.000919627	209.6591

Name	F.dist.ZpEst	F.dist.ZpEst.s	F.mid.TA	F.mid.TA.s	F.mid.lmax
AMNH103659	NA	NA	NA	NA	NA
NMNH173813	514.45	0.00258217	147.6243	0.000740975	1808.7667
NMNH241160	248.71	0.00165389	92.2687	0.000613574	726.704
NMNH399285	283.71	0.00216887	102.0496	0.000780145	882.4628
AMNH28256	435.52	0.00161286	141.0859	0.000522482	1681.1139
HTB0337	548.19	0.00297019	138.3772	0.000749756	1670.6356
NMNH305069	270.03	0.00176915	90.7505	0.000594571	685.6746
NMNHA49691	330.70	0.00128415	110.6892	0.000429823	1101.9448
NMNHA49696	171.55	0.00167631	68.5338	0.000669692	418.6115
NMNHA49874	332.80	0.00138752	106.3063	0.000443218	934.4246
AMNH106563	630.83	0.00198343	159.4504	0.000501341	2232.8313
AMNH106564	572.89	0.00303931	149.908	0.000795298	1934.4537
AMNH30597	210.2931	0.00218413	77.5764	0.000805717	504.7884
HTB1160	278.71	0.00153564	93.4939	0.000515125	719.9219
Name	**F.mid.lmax.s**	**F.mid.lmin**	**F.mid.lmin.s**	**F.mid.MaxXrad**	**F.mid.MaxYrad**
AMNH30620	1.83621E-05	107.9142	1.53127E-05	3.5322	3.5718
AMNH30622	1.74504E-05	115.4246	1.52605E-05	3.6339	3.4995
NMNH344989	2.86395E-05	175.3056	2.16946E-05	4.2958	3.8097
AMNH103654	3.07236E-05	170.1115	2.49282E-05	3.9333	4.2672
AMNH103659	NA	NA	NA	NA	NA
NMNH173813	4.96109E-05	1684.2303	4.61951E-05	6.9326	7.3022
NMNH241160	2.84264E-05	633.9482	2.47981E-05	5.5589	5.4334
NMNH399285	3.96837E-05	798.0807	3.58891E-05	6.1604	5.6006
AMNH28256	2.80435E-05	1507.8334	2.51529E-05	7.3417	6.6248
HTB0337	4.61829E-05	1394.6454	3.85534E-05	6.9289	6.6296
NMNH305069	2.61183E-05	633.941	2.41477E-05	5.3374	5.4517
NMNHA49691	1.91028E-05	866.3478	1.50186E-05	6.3488	5.6853
NMNHA49696	2.82107E-05	335.5998	2.26164E-05	4.3791	5.2162
NMNHA49874	1.97759E-05	871.1243	1.84363E-05	5.8154	5.999
AMNH106563	2.97476E-05	1860.7905	2.4791E-05	7.7812	7.1273
AMNH106564	8.01776E-05	1662.0851	6.88887E-05	6.8017	7.0846
AMNH30597	3.54242E-05	456.323	3.20231E-05	5.0829	4.9249
HTB1160	2.05521E-05	674.0913	1.92438E-05	5.5889	5.45
Name	**F.mid.J**	**F.mid.J.s**	**F.mid.ZpEst**	**F.mid.ZpEst.s**	**F.prox.TA**
AMNH30620	237.3186	3.36748E-05	66.81	0.001213506	36.8873
AMNH30622	247.4123	3.27109E-05	69.37	0.001183083	35.8444
NMNH344989	406.7304	5.03341E-05	100.36	0.001614566	46.6025
AMNH103654	379.7706	5.56518E-05	92.62	0.001750889	45.9876
AMNH103659	NA	NA	NA	NA	NA
NMNH173813	3492.997	9.5806E-05	490.77	0.002463330	141.8279
NMNH241160	1360.6522	5.32244E-05	247.56	0.001646271	93.1797
NMNH399285	1680.5435	7.55727E-05	285.78	0.002184739	90.7969
AMNH28256	3188.9472	5.31963E-05	456.66	0.001691131	136.7942
HTB0337	3065.281	8.47363E-05	452.16	0.002449875	128.4512
NMNH305069	1319.6156	5.0266E-05	244.62	0.001602682	84.14
NMNHA49691	1968.2926	3.41213E-05	327.12	0.001270254	102.7436
NMNHA49696	754.2113	5.08271E-05	157.20	0.001536153	73.4242
NMNHA49874	1805.5489	3.82122E-05	305.65	0.001274343	104.7791
AMNH106563	4093.6218	5.45385E-05	549.17	0.001726678	161.7254
AMNH106564	3596.5388	0.000149066	518.00	0.002748103	152.5423
AMNH30597	961.1114	6.74473E-05	186.26	0.001934529	70.7854
HTB1160	1394.0133	3.97959E-05	252.56	0.001391554	99.3099
Name	**F.prox.TA.s**	**F.prox.lmax**	**F.prox.lmax.s**	**F.prox.lmin**	**F.prox.lmin.s**
AMNH30620	0.000669977	126.5363	1.79551E-05	92.9776	1.31932E-05
AMNH30622	0.000611339	116.6518	1.54228E-05	90.1672	1.19212E-05
NMNH344989	0.000749736	194.2237	2.40358E-05	156.1045	1.93184E-05
AMNH103654	0.000869337	187.6892	2.75041E-05	153.2464	2.24568E-05
AMNH103659	NA	NA	NA	NA	NA
NMNH173813	0.000711881	1696.528	4.65324E-05	1518.2282	4.1642E-05
NMNH241160	0.000619632	799.4805	3.12732E-05	602.2311	2.35574E-05
NMNH399285	0.000694121	747.863	3.36308E-05	584.1223	2.62675E-05

Name	F.prox.TA.s	F.prox.lmax	F.prox.lmax.s	F.prox.lmin	F.prox.lmin.s
AMNH28256	0.000506588	1884.9589	3.14439E-05	1206.7519	2.01304E-05
HTB0337	0.000695975	1510.0479	4.17436E-05	1146.7981	3.1702E-05
NMNH305069	0.000551261	611.9961	2.33118E-05	529.702	2.01771E-05
NMNHA49691	0.000398969	943.2017	1.63509E-05	762.0486	1.32105E-05
NMNHA49696	0.000717479	507.806	3.42216E-05	370.5256	2.49701E-05
NMNHA49874	0.000436851	1023.8466	2.16684E-05	758.5122	1.6053E-05
AMNH106563	0.000508494	2663.3837	3.54837E-05	1652.6205	2.20175E-05
AMNH106564	0.000809273	2059.2908	8.53518E-05	1687.8563	6.99569E-05
AMNH30597	0.000735185	443.7456	3.11405E-05	362.929	2.54691E-05
HTB1160	0.000547169	921.4246	2.63046E-05	681.8341	1.94648E-05
Name	**F.prox.MaxXrad**	**F.prox.MaxYrad**	**F.prox.J**	**F.prox.J.s**	**F.prox.ZpEst**
AMNH30620	3.8788	3.2893	219.5139	3.11483E-05	61.25
AMNH30622	3.2888	3.7101	206.819	2.73439E-05	59.10
NMNH344989	4.0994	3.8614	350.3282	4.33541E-05	88.01
AMNH103654	4.2346	3.8266	340.9357	4.99609E-05	84.59
AMNH103659	NA	NA	NA	NA	NA
NMNH173813	6.8677	7.2145	3214.7562	8.81744E-05	456.57
NMNH241160	5.7844	5.2981	1401.7116	5.48305E-05	252.96
NMNH399285	5.5887	5.6525	1331.9853	5.98983E-05	236.98
AMNH28256	8.0567	6.2997	3091.7108	5.15743E-05	430.71
HTB0337	6.2622	6.7396	2656.846	7.34456E-05	408.69
NMNH305069	5.1714	5.5008	1141.6982	4.34888E-05	213.96
NMNHA49691	5.7496	6.3707	1705.2503	2.95614E-05	281.39
NMNHA49696	4.9	5.0613	878.3316	5.91917E-05	176.35
NMNHA49874	5.7945	6.2414	1782.3588	3.77214E-05	296.17
AMNH106563	8.2859	6.7948	4316.0042	5.75013E-05	572.39
AMNH106564	6.9662	7.3567	3747.1471	0.000155309	523.24
AMNH30597	5.25	4.7811	806.6746	5.66095E-05	160.83
HTB1160	6.0848	5.5055	1603.2587	4.57694E-05	276.66
Name	**F.prox.ZpEst.s**	**H.dist.TA**	**H.dist.TA.s**	**H.dist.lmax**	**H.dist.lmax.s**
AMNH30620	0.00111243	33.2105	0.000603196	106.5565	1.74357E-05
AMNH30622	0.00100798	30.7939	0.000525201	93.0605	1.36826E-05
NMNH344989	0.00141595	38.63	0.000621475	147.8679	1.9499E-05
AMNH103654	0.00159901	33.1875	0.000627368	95.956	1.5705E-05
AMNH103659	NA	41.8824	0.000569448	200.9099	2.18531E-05
NMNH173813	0.00229168	96.3545	0.000483635	1048.6993	3.35272E-05
NMNH241160	0.00168215	NA	NA	NA	NA
NMNH399285	0.00181168	67.1274	0.000513173	446.7478	2.43949E-05
AMNH28256	0.00159504	121.8787	0.000451352	1467.8543	2.77341E-05
HTB0337	0.00221436	111.8821	0.0006062	1376.5714	4.63264E-05
NMNH305069	0.00140179	75.2965	0.000493321	565.9635	2.37694E-05
NMNHA49691	0.00109267	101.0856	0.000392531	908.6024	1.86679E-05
NMNHA49696	0.00172323	63.3126	0.000618672	412.2795	3.07532E-05
NMNHA49874	0.00123482	92.016	0.000383638	870.4423	2.08569E-05
AMNH106563	0.00179969	174.2776	0.000547961	3755.7685	5.96405E-05
AMNH106564	0.00277590	156.5679	0.00083063	3078.8066	8.50719E-05
AMNH30597	0.00167045	53.4791	0.00055544	281.4593	2.19794E-05
HTB1160	0.00152429	96.8503	0.000533617	956.293	3.0281E-05
Name	**H.dist.lmin**	**H.dist.lmin.s**	**H.dist.MaxXrad**	**H.dist.MaxYrad**	**H.dist.J**
AMNH30620	75.7772	1.23993E-05	3.7754	3.315	182.3336
AMNH30622	66.295	9.74728E-06	3.5582	3.8681	159.3555
NMNH344989	98.1203	1.29389E-05	3.4073	3.9559	245.9882
AMNH103654	83.682	1.36961E-05	3.2906	3.434	179.6381
AMNH103659	107.5366	1.16968E-05	3.8395	4.9866	308.4465
NMNH173813	547.3433	1.74987E-05	5.1376	7.5319	1596.0426
NMNH241160	NA	NA	NA	NA	NA
NMNH399285	309.3295	1.68911E-05	4.5962	5.0636	756.0773
AMNH28256	1012.6045	1.91325E-05	6.7439	7.4597	2480.4588
HTB0337	773.6253	2.60352E-05	6.9697	6.7966	2150.1967
NMNH305069	385.2524	1.61799E-05	5.8868	4.8306	951.2159
NMNHA49691	772.781	1.58774E-05	7.1579	6.08	1681.3834

Name	H.dist.lmin	H.dist.lmin.s	H.dist.MaxXrad	H.dist.MaxYrad	H.dist.J
NMNHA49696	263.7347	1.96728E-05	4.4427	5.3457	676.0143
NMNHA49874	551.8094	1.3222E-05	5.2175	6.4622	1422.2517
AMNH106563	1690.2688	2.6841E-05	9.7833	7.163	5446.0373
AMNH106564	1366.4542	3.77571E-05	6.8597	9.9164	4445.2608
AMNH30597	191.8341	1.49805E-05	5.0176	4.368	473.2935
HTB1160	621.5942	1.96828E-05	6.0352	5.7855	1577.8872
Name	**H.dist.J.s**	**H.dist.ZpEst**	**H.dist.ZpEst.s**	**H.mid.TA**	**H.mid.TA.s**
AMNH30620	2.9835E-05	51.43	0.000934134	35.2783	0.000640753
AMNH30622	2.34298E-05	42.92	0.000731956	34.1051	0.000581674
NMNH344989	3.24379E-05	66.82	0.001074921	38.8035	0.000624266
AMNH103654	2.94011E-05	53.43	0.001009972	35.6063	0.000673092
AMNH103659	3.355E-05	69.89	0.000950306	40.5708	0.000551615
NMNH173813	5.10259E-05	251.95	0.001264622	102.3392	0.000513674
NMNH241160	NA	NA	NA	NA	NA
NMNH399285	4.1286E-05	156.54	0.001196719	81.7414	0.000624894
AMNH28256	4.68666E-05	349.27	0.001293454	147.2496	0.000545308
HTB0337	7.23615E-05	312.39	0.001692569	116.4043	0.000630702
NMNH305069	3.99493E-05	177.51	0.001162987	76.3886	0.000500476
NMNHA49691	3.45453E-05	254.03	0.000986420	100.3519	0.000389682
NMNHA49696	5.0426E-05	138.13	0.001349722	66.8124	0.000652871
NMNHA49874	3.40789E-05	243.54	0.001015391	99.1678	0.000413456
AMNH106563	8.64815E-05	642.74	0.002020893	203.1393	0.000638707
AMNH106564	0.000122829	529.95	0.002811519	168.1787	0.000892228
AMNH30597	3.696E-05	100.86	0.001047493	60.4937	0.000628294
HTB1160	4.99638E-05	266.97	0.001470929	85.4894	0.000471022
Name	**H.mid.lmax**	**H.mid.lmax.s**	**H.mid.lmin**	**H.mid.lmin.s**	**H.mid.MaxXrad**
AMNH30620	124.2324	2.0328E-05	80.2929	1.31382E-05	3.8434
AMNH30622	126.7039	1.86291E-05	68.0523	1.00056E-05	3.9759
NMNH344989	187.7382	2.47566E-05	78.5237	1.03548E-05	3.3021
AMNH103654	130.4689	2.13537E-05	80.6523	1.32003E-05	3.4938
AMNH103659	176	1.91437E-05	99.9236	1.08688E-05	4.2666
NMNH173813	1046.8331	3.34675E-05	671.1319	2.14563E-05	5.9788
NMNH241160	NA	NA	NA	NA	NA
NMNH399285	734.289	4.00962E-05	391.9661	2.14035E-05	5.2888
AMNH28256	1943.8261	3.67273E-05	1549.0338	2.92679E-05	7.2741
HTB0337	1316.1197	4.4292E-05	892.1426	3.00237E-05	6.7638
NMNH305069	605.1286	2.54143E-05	361.8202	1.51958E-05	5.4266
NMNHA49691	846.09	1.73836E-05	778.4243	1.59933E-05	5.6809
NMNHA49696	446.8181	3.33296E-05	285.5004	2.12964E-05	4.6046
NMNHA49874	964.9852	2.31223E-05	641.2659	1.53655E-05	5.8597
AMNH106563	3702.5409	5.87953E-05	2982.0879	4.73547E-05	8.9896
AMNH106564	2464.1895	6.80891E-05	2097.9233	5.79686E-05	7.3852
AMNH30597	405.1605	3.16394E-05	213.0444	1.66369E-05	5.2943
HTB1160	632.7916	2.00374E-05	538.3485	1.70468E-05	5.353
Name	**H.mid.MaxYrad**	**H.mid.J**	**H.mid.J.s**	**H.mid.ZpEst**	**H.mid.ZpEst.s**
AMNH30620	3.4519	204.5253	3.34662E-05	56.070	0.0000091747
AMNH30622	2.8598	194.7562	2.86348E-05	56.982	0.0000083780
NMNH344989	4.433	266.2619	3.51114E-05	68.845	0.0000090785
AMNH103654	3.8717	211.1212	3.45539E-05	57.327	0.0000093826
AMNH103659	3.2884	275.9236	3.00124E-05	73.044	0.0000079451
NMNH173813	6.0292	1717.965	5.49238E-05	286.137	0.0000091479
NMNH241160	NA	NA	NA	NA	NA
NMNH399285	5.9192	1126.2552	6.14997E-05	200.973	0.0000109742
AMNH28256	6.4642	3492.8599	6.59952E-05	508.485	0.0000096075
HTB0337	5.4915	2208.2623	7.43156E-05	360.377	0.0000121279
NMNH305069	5.1259	966.9488	4.06101E-05	183.264	0.0000076968
NMNHA49691	6.0911	1624.5143	3.33769E-05	275.996	0.0000056706
NMNHA49696	5.1011	732.3185	5.46259E-05	150.905	0.0000112565
NMNHA49874	6.1756	1606.2511	3.84878E-05	266.923	0.0000063958
AMNH106563	8.5167	6684.6288	0.00010615	763.683	0.0000121271
AMNH106564	7.6069	4562.1128	0.000126058	608.602	0.0000168166

Name	H.mid.MaxYrad	H.mid.J	H.mid.J.s	H.mid.ZpEst	H.mid.ZpEst.s
AMNH30597	3.9471	618.2049	4.82763E-05	133.790	0.0000104478
HTB1160	5.5808	1171.1401	3.70842E-05	214.224	0.0000067834
Name	**H.prox.TA**	**H.prox.TA.s**	**H.prox.lmax**	**H.prox.lmax.s**	**H.prox.lmin**
AMNH30620	44.6543	0.000811047	185.4025	3.03372E-05	152.0538
AMNH30622	40.429	0.00068953	183.6677	2.70044E-05	100.4462
NMNH344989	48.4554	0.000779545	248.9259	3.28253E-05	157.2372
AMNH103654	37.3874	0.000706761	148.6906	2.4336E-05	92.3482
AMNH103659	56.1614	0.00076359	323.4678	3.51839E-05	252.5114
NMNH173813	136.0969	0.000683115	1920.4719	6.1398E-05	1362.4302
NMNH241160	NA	NA	NA	NA	NA
NMNH399285	97.9455	0.00074877	996.4003	5.44089E-05	701.7126
AMNH28256	177.079	0.000655775	3084.4832	5.82792E-05	2293.7476
HTB0337	144.6013	0.000783479	2141.9375	7.20836E-05	1539.811
NMNH305069	95.2891	0.000624307	949.3177	3.98696E-05	616.6156
NMNHA49691	125.5895	0.000487683	1586.2759	3.25913E-05	1202.5389
NMNHA49696	73.0557	0.000713878	509.6066	3.80132E-05	422.0314
NMNHA49874	122.789	0.000511939	1448.4551	3.47068E-05	1140.9884
AMNH106563	278.4079	0.000875365	7737.0287	0.000122862	5553.7786
AMNH106564	214.4681	0.001137804	4780.1323	0.000132082	3377.3502
AMNH30597	66.4432	0.000690086	445.7597	3.48098E-05	310.9899
HTB1160	103.7763	0.000571778	1184.3721	3.75032E-05	696.3795
Name	**H.prox.lmin.s**	**H.prox.MaxXrad**	**H.prox.MaxYrad**	**H.prox.J**	**H.prox.J.s**
AMNH30620	2.48804E-05	4.8677	4.3821	337.4563	5.52176E-05
AMNH30622	1.47685E-05	4.5578	3.3602	284.1139	4.17729E-05
NMNH344989	2.07345E-05	4.477	4.5454	406.1632	5.35599E-05
AMNH103654	1.51145E-05	3.6297	4.1177	241.0389	3.94505E-05
AMNH103659	2.74659E-05	5.1877	5.0306	575.9792	6.26498E-05
NMNH173813	4.35572E-05	9.0381	7.3392	3282.902	0.000104955
NMNH241160	NA	NA	NA	NA	NA
NMNH399285	3.83173E-05	7.6717	6.1088	1698.113	9.27262E-05
AMNH28256	4.33388E-05	8.0222	8.9431	5378.2308	0.000101618
HTB0337	5.18199E-05	7.9151	8.3656	3681.7485	0.000123904
NMNH305069	2.58967E-05	5.9359	6.9559	1565.9333	6.57663E-05
NMNHA49691	2.47071E-05	8.0136	7.0046	2788.8148	5.72984E-05
NMNHA49696	3.14806E-05	6.5761	5.5959	931.638	6.94938E-05
NMNHA49874	2.73395E-05	7.9272	6.8067	2589.4435	6.20463E-05
AMNH106563	8.81924E-05	10.1565	12.1122	13290.8073	0.000211054
AMNH106564	9.33211E-05	9.124	10.9712	8157.4825	0.000225403
AMNH30597	2.42855E-05	5.3936	4.8347	756.7496	5.90954E-05
HTB1160	2.20509E-05	5.6162	7.9877	1880.7516	5.9554E-05
Name	**H.prox.ZpEst**	**H.prox.ZpEst.s**	**F.C.AP**	**H.C.AP**	**H.C.ML**
AMNH30620	72.97	0.00132525	6.37	6.89	2.54
AMNH30622	71.76	0.00122396	5.34	5.76	2.57
NMNH344989	90.03	0.00144846	5.26	6.35	4.59
AMNH103654	62.22	0.00117627	4.76	4.91	2.98
AMNH103659	112.73	0.00153278	6.59	7.74	5.41
NMNH173813	400.91	0.00201229	6.82	7.40	5.30
NMNH241160	NA	NA	8.61	8.49	6.14
NMNH399285	246.45	0.00188406	8.39	8.44	6.31
AMNH28256	634.03	0.00234799	9.22	9.85	6.40
HTB0337	452.28	0.00245057	10.06	10.92	6.49
NMNH305069	242.93	0.00159164	6.49	8.03	5.82
NMNHA49691	371.39	0.00144217	9.01	8.76	7.58
NMNHA49696	153.08	0.00149584	5.34	NA	4.83
NMNHA49874	351.49	0.00146547	7.50	NA	6.38
AMNH106563	1193.68	0.00375314	6.80	13.49	6.82
AMNH106564	811.88	0.00430724	5.91	16.79	8.18
AMNH30597	147.97	0.00153685	5.09	6.76	3.49
HTB1160	276.50	0.00152345	10.68	8.97	5.34

Name	Species	DR	Sex	HHD	MHL	FHD	MFL	BS.GM^3
NMNH23976	P. anubis	3.6	M	32	236	26	267	616112.3906
NMNH162899	P. anubis	3.6	M	28.5	232.5	25	200.5	437513.6953
NMNH354984	P. anubis	3.6	F	26.5	224	24	266	482992.1563
NMNH354987	P. anubis	3.6	M	27.5	228.5	24	266	504061.8539
NMNH354988	P. anubis	3.6	M	28	229	24	263	507423.2679
NMNH354989	P. anubis	3.6	M	26.5	227.5	23	264	470618.8068
NMNH354992	P. anubis	3.6	F	21	187	20	212	260657.4057
NMNH354993	P. anubis	3.6	M	28	235	25.5	280.5	568230.0601
NMNH384223	P. anubis	3.6	M	31	229	26	265	584873.977
NMNH384227	P. anubis	3.6	F	26	204	23	223	376683.989
NMNH384228	P. anubis	3.6	F	27.5	204	23	232	404700.7522
NMNH384229	P. anubis	3.6	M	29	226	25.5	252.5	523577.53
NMNH384235	P. anubis	3.6	F	25	201	22	227	354558.9504
NMNH384238	P. anubis	3.6	F	23	200	21	229	322559.2173
NMNH395440	P. anubis	3.6	M	29.5	229.5	25	263	544973.453
NMNH395441	P. anubis	3.6	F	22.5	186	20.5	213	279493.489
PC.C212	P. anubis	3.6	M	29.4	237	26.9	261	584946.7708
PC.CAMII.160	P. anubis	3.6	M	30.9	237	27.3	276.5	641096.5741
NMNH384238	P. cynocephalus	5.9	F	22	187	20	217	274672.7102
NMNH384239	P. cynocephalus	5.9	F	22.5	188.5	18.5	219	266889.9909
NMNH452508	P. cynocephalus	5.9	F	24.5	184	19.5	200	271510.3476
NMNH452509	P. cynocephalus	5.9	M	27	233	24	254	487330.3762
HTB0889	P. hamadryas	10.7	F	19	186	19	201	222670.2274
HTB0890	P. hamadryas	10.7	M	21	213	20.5	230	311214.9465
HTB0900	P. hamadryas	10.7	M	20.5	214	20	230	301088.4525
HTB1025	P. hamadryas	10.7	M	20	214	20	230	295563.7721
HTB1027	P. hamadryas	10.7	F	17	175	18	198	185809.75
HTB1028	P. hamadryas	10.7	F	15.5	182.5	17.5	201	177162.3795
HTB1043	P. hamadryas	10.7	M	21	222	21	241	338537.2444
HTB1503	P. hamadryas	10.7	F	16	183	17.5	200	181125.3916
PC.SUDANII.26	P. hamadryas	10.7	M	28.4	212	22.6	233	422511.8762
HTB0828	P. ursinus	7.2	M	22.5	209	26	241	399934.9847
NMNH337250	P. ursinus	7.2	M	26	216	22	253	418049.5168
NMNH337253	P. ursinus	7.2	M	25	217	21	251	391038.5457
HTB0891	T. gelada	0.6	M	20.5	202	21	213	282343.6966
HTB1207	T. gelada	0.6	M	18.5	208	20	220.5	264396.2186

Name	F.dist.TA	F.dist.TA.s	F.dist.lmax	F.dist.lmax.s	F.dist.lmin
NMNH23976	301.2198	0.000488904	7920.437	4.8148E-05	6633.7913
NMNH162899	NA	NA	NA	NA	NA
NMNH354984	270.5505	0.000560155	5937.4724	4.62147E-05	5746.9456
NMNH354987	230.655	0.000457593	5052.4221	3.7682E-05	3579.2935
NMNH354988	276.7583	0.000545419	6513.8002	4.88099E-05	5747.0783
NMNH354989	246.8944	0.000524617	4986.5747	4.01355E-05	4767.6974
NMNH354992	166.8041	0.000639936	2515.801	4.55271E-05	1977.0855
NMNH354993	328.9313	0.00057887	10023.0547	6.28844E-05	7402.2442
NMNH384223	281.0688	0.000480563	6839.2089	4.41263E-05	5837.6538
NMNH384227	206.1282	0.000547218	3836.8473	4.56765E-05	3000.5255
NMNH384228	224.0783	0.000553689	4310.7921	4.59129E-05	3739.9266
NMNH384229	NA	NA	NA	NA	NA
NMNH384235	198.4843	0.000559806	3713.0753	4.61338E-05	2668.2304
NMNH384238	172.2228	0.000533926	2570.8291	3.48039E-05	2177.0261
NMNH395440	277.3879	0.000508993	6287.1187	4.38652E-05	6008.2189
NMNH395441	160.2329	0.000573297	2115.099	3.55287E-05	1981.7078
PC.C212	284.0815	0.000485654	6779.5204	4.4406E-05	6096.992
PC.CAMII.160	336.2293	0.00052446	9307.534	5.25069E-05	8791.7518
NMNH384238	152.487	0.000555159	2089.5348	3.5057E-05	1664.1061
NMNH384239	145.3109	0.00054446	1974.5027	3.37817E-05	1435.9035
NMNH452508	NA	NA	NA	NA	NA
NMNH452509	195.2489	0.00040065	3479.342	2.81086E-05	2646.9336
HTB0889	165.8678	0.000744903	2596.9367	5.80234E-05	1854.4941
HTB0890	170.5718	0.000548084	2772.3148	3.87306E-05	1952.9709

Name	F.dist.TA	F.dist.TA.s	F.dist.lmax	F.dist.lmax.s	F.dist.lmin
HTB0900	184.8474	0.000613931	3163.026	4.56752E-05	2361.0052
HTB1025	175.9909	0.000595441	2504.4683	3.68414E-05	2435.5485
HTB1027	124.2669	0.000668786	1419.9077	3.85946E-05	1066.6933
HTB1028	NA	NA	NA	NA	NA
HTB1043	NA	NA	NA	NA	NA
HTB1503	NA	NA	NA	NA	NA
PC.SUDANII.26	186.5879	0.000441616	3050.6403	3.09882E-05	2524.859
HTB0828	223.3717	0.00055852	4641.9166	4.81605E-05	3422.2637
NMNH337250	221.8124	0.000530589	4096.4963	3.87315E-05	3768.921
NMNH337253	177.0432	0.000452751	2715.5673	2.76673E-05	2316.6586
HTB0891	187.0817	0.000662603	3062.9212	5.09305E-05	2544.7847
HTB1207	NA	NA	NA	NA	NA
Name	**F.dist.lmin.s**	**F.dist.MaxXrad**	**F.dist.MaxYrad**	**F.dist.J**	**F.dist.J.s**
NMNH23976	4.0327E-05	10.5539	9.9015	14554.2283	8.84745E-05
NMNH162899	NA	NA	NA	NA	NA
NMNH354984	4.4732E-05	9.2932	9.7247	11684.418	9.09464E-05
NMNH354987	2.6695E-05	8.5474	9.5777	8631.7157	6.43771E-05
NMNH354988	4.3065E-05	10.1619	9.3453	12260.8785	9.18746E-05
NMNH354989	3.8374E-05	9.167	9.2566	9754.2721	7.85094E-05
NMNH354992	3.5778E-05	8.2079	7.3134	4492.8865	8.13054E-05
NMNH354993	4.6442E-05	9.9587	10.9182	17425.2989	0.000109326
NMNH384223	3.7664E-05	9.9129	9.4496	12676.8627	8.17906E-05
NMNH384227	3.5720E-05	8.4246	8.1538	6837.3728	8.13968E-05
NMNH384228	3.9833E-05	8.9651	8.653	8050.7187	8.57458E-05
NMNH384229	NA	NA	NA	NA	NA
NMNH384235	3.3152E-05	8.8841	7.4782	6381.3057	7.92858E-05
NMNH384238	2.9473E-05	7.4068	7.9577	4747.8551	6.42765E-05
NMNH395440	4.1919E-05	9.7036	10.0124	12295.3376	8.57846E-05
NMNH395441	3.3288E-05	7.381	7.059	4096.8068	6.88168E-05
PC.C212	3.9935E-05	9.3759	9.8218	12876.5124	8.43415E-05
PC.CAMII.160	4.9597E-05	10.4809	10.7722	18099.2858	0.000102104
NMNH384238	2.7919E-05	7.7175	6.9219	3753.6409	6.29763E-05
NMNH384239	2.4567E-05	7.5572	6.3575	3410.4063	5.83485E-05
NMNH452508	NA	NA	NA	NA	NA
NMNH452509	2.1384E-05	8.2619	7.8089	6126.2755	4.94925E-05
HTB0889	4.1435E-05	8.0654	6.7817	4451.4308	9.94584E-05
HTB0890	2.7284E-05	7.9147	7.4335	4725.2857	6.60146E-05
HTB0900	3.4094E-05	7.5768	8.1873	5524.0311	7.9769E-05
HTB1025	3.5828E-05	7.6984	7.4621	4940.0168	7.2669E-05
HTB1027	2.8994E-05	6.2697	6.6397	2486.601	6.75884E-05
HTB1028	NA	NA	NA	NA	NA
HTB1043	NA	NA	NA	NA	NA
HTB1503	NA	NA	NA	NA	NA
PC.SUDANII.26	2.5647E-05	7.9544	7.6646	5575.4993	5.66355E-05
HTB0828	3.5506E-05	9.425	8.1461	8064.1802	8.36669E-05
NMNH337250	3.5634E-05	8.8616	8.526	7865.4173	7.43658E-05
NMNH337253	2.3603E-05	8.1009	7.4894	5032.2259	5.12704E-05
HTB0891	4.2315E-05	7.8362	8.0615	5607.7059	9.32454E-05
HTB1207	NA	NA	NA	NA	NA
Name	**F.dist.ZpEst**	**F.dist.ZpEst.s**	**F.mid.TA**	**F.mid.TA.s**	**F.mid.lmax**
NMNH23976	1423.02	0.0023097	280.8254	0.000455802	6857.7634
NMNH162899	NA	NA	NA	NA	NA
NMNH354984	1228.78	0.0025441	237.1999	0.000491105	4690.6855
NMNH354987	952.46	0.0018896	203.1152	0.000402957	3593.131
NMNH354988	1257.06	0.0024773	252.8457	0.000498293	5760.8419
NMNH354989	1058.89	0.0022500	249.5342	0.000530226	5565.0776
NMNH354992	578.93	0.0022210	144.2325	0.000553341	1755.7957
NMNH354993	1669.34	0.0029378	272.3408	0.000479279	6468.1407
NMNH384223	1309.42	0.0022388	245.1417	0.000419136	5452.4158
NMNH384227	824.85	0.0021898	197.9207	0.000525429	3381.5152
NMNH384228	913.91	0.0022582	213.7634	0.000528201	3897.5228

Name	F.dist.ZpEst	F.dist.ZpEst.s	F.mid.TA	F.mid.TA.s	F.mid.lmax
NMNH384229	NA	NA	NA	NA	NA
NMNH384235	780.00	0.0021999	177.8369	0.000501572	2860.6895
NMNH384238	618.03	0.0019160	161.0278	0.000499219	2153.9988
NMNH395440	1247.24	0.0022886	249.8315	0.000458429	5278.9975
NMNH395441	567.42	0.0020302	144.4523	0.000516836	1783.6065
PC.C212	1341.46	0.0022933	246.7612	0.000421852	5176.0715
PC.CAMII.160	1703.21	0.0026567	315.0836	0.000491476	8442.5454
NMNH384238	512.81	0.0018670	137.9696	0.000502305	1580.1611
NMNH384239	490.19	0.0018367	146.1744	0.000547695	1796.7397
NMNH452508	NA	NA	NA	NA	NA
NMNH452509	762.41	0.0015645	184.249	0.000378078	3063.637
HTB0889	599.64	0.0026929	148.7881	0.000668199	1962.7454
HTB0890	615.74	0.0019785	172.5819	0.000554542	2603.7959
HTB0900	700.84	0.0023277	187.5105	0.000622775	3098.0881
HTB1025	651.70	0.0022049	160.1216	0.00054175	2197.9987
HTB1027	385.24	0.0020733	132.2584	0.000711795	1586.4467
HTB1028	NA	NA	NA	NA	NA
HTB1043	NA	NA	NA	NA	NA
HTB1503	NA	NA	NA	NA	NA
PC.SUDANII.26	713.94	0.0016897	183.9772	0.000435437	3003.0573
HTB0828	917.89	0.0022951	199.6686	0.000499253	3240.1715
NMNH337250	904.72	0.0021641	187.1842	0.000447756	2870.1119
NMNH337253	645.56	0.0016509	175.7788	0.000449518	2532.572
HTB0891	705.47	0.0024986	172.9053	0.000612393	2502.9953
HTB1207	NA	NA	NA	NA	NA

Name	F.mid.lmax.s	F.mid.lmin	F.mid.lmin.s	F.mid.MaxXrad	F.mid.MaxYrad
NMNH23976	4.1688E-05	5793.6391	3.52193E-05	9.9789	9.4614
NMNH162899	NA	NA	NA	NA	NA
NMNH354984	3.6510E-05	4329.8071	3.37013E-05	8.8023	9.0458
NMNH354987	2.6798E-05	3052.485	2.27661E-05	8.4603	8.4924
NMNH354988	4.3168E-05	4537.7919	3.40031E-05	10.0704	8.9447
NMNH354989	4.4792E-05	4516.6714	3.63534E-05	8.8851	9.9381
NMNH354992	3.1774E-05	1586.0887	2.87026E-05	7.1942	6.6777
NMNH354993	4.0581E-05	5406.0016	3.39171E-05	9.2312	9.7767
NMNH384223	3.5179E-05	4270.1223	2.75507E-05	9.0051	8.8542
NMNH384227	4.0256E-05	2890.0634	3.44053E-05	8.2702	8.0349
NMNH384228	4.1511E-05	3441.5007	3.66544E-05	8.9719	8.2999
NMNH384229	NA	NA	NA	NA	NA
NMNH384235	3.5543E-05	2262.5444	2.81114E-05	8.3381	7.3651
NMNH384238	2.9161E-05	1999.7691	2.70729E-05	7.1768	7.577
NMNH395440	3.6832E-05	4721.1709	3.29396E-05	9.2065	9.7749
NMNH395441	2.9960E-05	1562.9515	2.62539E-05	7.0123	6.7208
PC.C212	3.3903E-05	4578.6959	2.99906E-05	8.7803	10.0035
PC.CAMII.160	4.7627E-05	7485.8582	4.22302E-05	10.2689	10.2961
NMNH384238	2.6511E-05	1485.0484	2.49153E-05	6.9464	7.1171
NMNH384239	3.0740E-05	1615.2478	2.76352E-05	6.9259	6.571
NMNH452508	NA	NA	NA	NA	NA
NMNH452509	2.4750E-05	2394.9399	1.93481E-05	8.4619	7.3267
HTB0889	4.3854E-05	1594.6581	3.56295E-05	7.3546	6.8508
HTB0890	3.6376E-05	2206.9546	3.08322E-05	7.9955	7.6242
HTB0900	4.4738E-05	2548.7308	3.68046E-05	7.9616	7.9533
HTB1025	3.2333E-05	1914.3834	2.81611E-05	7.4465	7.5751
HTB1027	4.3121E-05	1226.459	3.33364E-05	6.8809	6.6232
HTB1028	NA	NA	NA	NA	NA
HTB1043	NA	NA	NA	NA	NA
HTB1503	NA	NA	NA	NA	NA
PC.SUDANII.26	3.0505E-05	2428.6408	2.467E-05	7.6791	8.2851
HTB0828	3.3617E-05	3129.8419	3.24725E-05	8.1913	8.2715
NMNH337250	2.7136E-05	2719.7976	2.57151E-05	7.7695	7.636
NMNH337253	2.5803E-05	2408.3797	2.45376E-05	7.5944	7.7013
HTB0891	4.1620E-05	2271.3894	3.77689E-05	7.6754	7.4483

Name	F.mid.lmax.s	F.mid.lmin	F.mid.lmin.s	F.mid.MaxXrad	F.mid.MaxYrad
HTB1207	NA	NA	NA	NA	NA
Name	**F.mid.J**	**F.mid.J.s**	**F.mid.ZpEst**	**F.mid.ZpEst.s**	**F.prox.TA**
NMNH23976	12651.4025	7.69073E-05	1301.56	0.00211254	272.9101
NMNH162899	NA	NA	NA	NA	NA
NMNH354984	9020.4925	7.02115E-05	1010.81	0.00209280	221.2021
NMNH354987	6645.616	4.95644E-05	784.02	0.00155540	216.1514
NMNH354988	10298.6338	7.71709E-05	1083.21	0.00213472	222.9369
NMNH354989	10081.749	8.11452E-05	1071.20	0.00227616	251.0704
NMNH354992	3341.8844	6.04763E-05	481.82	0.00184848	135.8727
NMNH354993	11874.1423	7.44981E-05	1249.39	0.00219874	279.8742
NMNH384223	9722.5381	6.27295E-05	1088.79	0.00186159	251.4364
NMNH384227	6271.5786	7.46612E-05	769.28	0.00204224	185.1376
NMNH384228	7339.0235	7.81657E-05	849.83	0.00209989	206.7517
NMNH384229	NA	NA	NA	NA	NA
NMNH384235	5123.2339	6.36546E-05	652.51	0.00184034	172.4393
NMNH384238	4153.7679	5.62338E-05	563.08	0.00174566	155.1831
NMNH395440	10000.1684	6.97712E-05	1053.68	0.00193345	262.5475
NMNH395441	3346.5581	5.62143E-05	487.37	0.00174377	142.9909
PC.C212	9754.7674	6.3894E-05	1038.64	0.00177561	248.2675
PC.CAMII.160	15928.4036	8.98574E-05	1549.08	0.00241630	309.4477
NMNH384238	3065.2095	5.14263E-05	435.91	0.00158702	133.584
NMNH384239	3411.9874	5.83756E-05	505.60	0.00189440	150.1009
NMNH452508	NA	NA	NA	NA	118.3011
NMNH452509	5458.5769	4.40983E-05	691.46	0.00141887	193.9952
HTB0889	3557.4035	7.94831E-05	500.85	0.00224930	148.7922
HTB0890	4810.7505	6.72086E-05	615.99	0.00197929	165.6188
HTB0900	5646.8189	8.15421E-05	709.63	0.00235687	172.9278
HTB1025	4112.382	6.04943E-05	547.53	0.00185249	151.0113
HTB1027	2812.9057	7.64577E-05	416.60	0.00224208	129.8808
HTB1028	NA	NA	NA	NA	NA
HTB1043	NA	NA	NA	NA	NA
HTB1503	NA	NA	NA	NA	116.399
PC.SUDANII.26	5431.698	5.51748E-05	680.48	0.00161057	188.6062
HTB0828	6370.0134	6.60897E-05	773.87	0.00193498	198.2262
NMNH337250	5589.9095	5.28514E-05	725.70	0.00173593	169.9305
NMNH337253	4940.9516	5.03405E-05	646.06	0.00165216	167.5186
HTB0891	4774.3847	7.93889E-05	631.38	0.00223620	165.7107
HTB1207	NA	NA	NA	NA	NA
Name	**F.prox.TA.s**	**F.prox.lmax**	**F.prox.lmax.s**	**F.prox.lmin**	**F.prox.lmin.s**
NMNH23976	0.000442955	7064.6575	4.29457E-05	5044.0282	3.06624E-05
NMNH162899	NA	NA	NA	NA	NA
NMNH354984	0.000457983	4323.5333	3.36525E-05	3521.0367	2.74062E-05
NMNH354987	0.000428819	4606.2302	3.43542E-05	3045.7632	2.27159E-05
NMNH354988	0.000439351	4676.3528	3.50414E-05	3416.8145	2.56033E-05
NMNH354989	0.00053349	6258.779	5.03752E-05	4053.771	3.26277E-05
NMNH354992	0.000521269	1643.4116	2.974E-05	1331.2724	2.40913E-05
NMNH354993	0.000492537	7193.2013	4.513E-05	5434.9011	3.40984E-05
NMNH384223	0.000429898	6796.8765	4.38532E-05	3785.9612	2.44269E-05
NMNH384227	0.000491493	3043.2918	3.62294E-05	2459.106	2.92749E-05
NMNH384228	0.000510876	3896.07	4.14959E-05	3000.7736	3.19603E-05
NMNH384229	NA	NA	NA	NA	NA
NMNH384235	0.000486349	2723.8166	3.38426E-05	2078.4127	2.58236E-05
NMNH384238	0.0004811	2165.0401	2.93104E-05	1716.6113	2.32395E-05
NMNH395440	0.000481762	6566.1171	4.58118E-05	4597.3508	3.20757E-05
NMNH395441	0.000511607	1908.8153	3.20636E-05	1400.4856	2.35249E-05
PC.C212	0.000424428	5741.7424	3.76086E-05	4232.8188	2.77251E-05
PC.CAMII.160	0.000482685	8984.7242	5.06858E-05	6491.5955	3.66212E-05
NMNH384238	0.000486339	1649.5093	2.76745E-05	1236.5081	2.07454E-05
NMNH384239	0.000562407	2115.0033	3.61855E-05	1524.0056	2.60742E-05
NMNH452508	0.000435715	1326.1029	2.44209E-05	945.8442	1.74182E-05
NMNH452509	0.000398077	3938.4283	3.18175E-05	2289.8302	1.84989E-05

Name	F.prox.TA.s	F.prox.Imax	F.prox.Imax.s	F.prox.Imin	F.prox.Imin.s
HTB0889	0.000668218	2013.6171	4.49903E-05	1551.3296	3.46614E-05
HTB0890	0.000532169	2584.5067	3.61068E-05	1886.9008	2.63609E-05
HTB0900	0.000574342	2896.5231	4.18268E-05	1960.1576	2.83054E-05
HTB1025	0.000510926	2132.8551	3.13749E-05	1562.8101	2.29894E-05
HTB1027	0.000698999	1631.8816	4.43563E-05	1113.2253	3.02586E-05
HTB1028	NA	NA	NA	NA	NA
HTB1043	NA	NA	NA	NA	NA
HTB1503	0.000642643	1349.4099	3.72507E-05	869.5173	2.40032E-05
PC.SUDANII.26	0.000446393	3516.9019	3.57244E-05	2286.4376	2.32255E-05
HTB0828	0.000495646	3420.4763	3.54879E-05	2876.4794	2.98438E-05
NMNH337250	0.000406484	2521.5581	2.38408E-05	2110.1363	1.99509E-05
NMNH337253	0.000428394	2559.7902	2.60802E-05	1977.3829	2.01464E-05
HTB0891	0.000586911	2490.1019	4.14056E-05	1930.9121	3.21074E-05
HTB1207	NA	NA	NA	NA	NA
Name	**F.prox.MaxXrad**	**F.prox.MaxYrad**	**F.prox.J**	**F.prox.J.s**	**F.prox.ZpEst**
NMNH23976	9.6004	9.1989	12108.6858	7.36081E-05	1288.21
NMNH162899	NA	NA	NA	NA	NA
NMNH354984	8.5638	8.5414	7844.5701	6.10587E-05	917.21
NMNH354987	8.6326	8.0978	7651.9934	5.70702E-05	914.74
NMNH354988	10.2151	8.5926	8093.1673	6.06446E-05	860.62
NMNH354989	8.9841	9.2917	10312.5499	8.30028E-05	1128.55
NMNH354992	7.1137	6.5107	2974.684	5.38313E-05	436.67
NMNH354993	9.1889	10.124	12628.1024	7.92284E-05	1307.74
NMNH384223	9.9837	8.7391	10582.8378	6.82801E-05	1130.48
NMNH384227	8.4527	7.4992	5502.3977	6.55043E-05	689.87
NMNH384228	8.4916	8.1384	6896.8437	7.34562E-05	829.45
NMNH384229	NA	NA	NA	NA	NA
NMNH384235	7.8771	7.3319	4802.2293	5.96662E-05	631.50
NMNH384238	7.0262	7.0791	3881.6514	5.25499E-05	550.38
NMNH395440	8.6797	9.7239	11163.4679	7.78875E-05	1213.18
NMNH395441	7.1997	6.5044	3309.3009	5.55885E-05	482.97
PC.C212	8.7531	9.7778	9974.5612	6.53337E-05	1076.53
PC.CAMII.160	9.7273	10.5084	15476.3196	8.7307E-05	1529.61
NMNH384238	6.9372	6.3722	2886.0175	4.84199E-05	433.68
NMNH384239	7.155	6.6323	3639.0089	6.22597E-05	527.88
NMNH452508	5.8219	6.5061	2271.947	4.1839E-05	368.58
NMNH452509	9.135	7.4616	6228.2585	5.03164E-05	750.55
HTB0889	7.169	6.7903	3564.9467	7.96517E-05	510.76
HTB0890	8.5451	7.1524	4471.4075	6.24678E-05	569.70
HTB0900	8.5256	6.9258	4856.6807	7.01322E-05	628.64
HTB1025	7.0753	7.0088	3695.6652	5.43643E-05	524.80
HTB1027	7.3066	6.1365	2745.1069	7.46149E-05	408.40
HTB1028	NA	NA	NA	NA	NA
HTB1043	NA	NA	NA	NA	NA
HTB1503	6.9685	5.9119	2218.9272	6.12539E-05	344.54
PC.SUDANII.26	7.3762	8.3181	5803.3395	5.89499E-05	739.55
HTB0828	7.9905	8.1983	6296.9557	6.53317E-05	777.94
NMNH337250	7.7599	7.3113	4631.6945	4.37917E-05	614.64
NMNH337253	7.646	7.3331	4537.1731	4.62266E-05	605.80
HTB0891	7.0698	7.5023	4421.014	7.3513E-05	606.78
HTB1207	NA	NA	NA	NA	NA
Name	**F.prox.ZpEst.s**	**H.dist.TA**	**H.dist.TA.s**	**H.dist.Imax**	**H.dist.Imax.s**
NMNH23976	0.00209086	248.3716	0.000403127	5914.8438	4.06791E-05
NMNH162899	NA	NA	NA	NA	NA
NMNH354984	0.00189903	182.0131	0.000376845	3824.3467	3.53484E-05
NMNH354987	0.00181474	162.3357	0.000322055	2787.5043	2.42017E-05
NMNH354988	0.00169606	191.6364	0.000377666	3955.9064	3.4044E-05
NMNH354989	0.00239801	204.7016	0.000434963	4481.0175	4.18529E-05
NMNH354992	0.00167526	101.1844	0.000388189	1005.1747	2.0622E-05
NMNH354993	0.00230142	192.956	0.000339574	3629.4652	2.71801E-05
NMNH384223	0.00193285	193.8216	0.00033139	3911.0332	2.92007E-05

Name	F.prox.ZpEst.s	H.dist.TA	H.dist.TA.s	H.dist.lmax	H.dist.lmax.s
NMNH384227	0.00183144	150.746	0.000400192	2255.5582	2.93526E-05
NMNH384228	0.00204953	161.3969	0.000398806	2732.1759	3.30936E-05
NMNH384229	NA	173.1515	0.000330708	3099.346	2.61927E-05
NMNH384235	0.00178108	132.0414	0.00037241	1756.1346	2.46418E-05
NMNH384238	0.00170630	119.3616	0.000370046	1544.0599	2.39345E-05
NMNH395440	0.00222613	201.9424	0.000370555	4057.8214	3.2444E-05
NMNH395441	0.00172800	110.7355	0.000396201	1252.5717	2.40945E-05
PC.C212	0.00184039	224.1758	0.000383241	5010.7909	3.61444E-05
PC.CAMII.160	0.00238592	228.4189	0.000356294	4849.1852	3.19152E-05
NMNH384238	0.00157890	106.8641	0.00038906	1221.3765	2.37789E-05
NMNH384239	0.00197789	122.7347	0.00045987	1523.5399	3.02838E-05
NMNH452508	0.00135753	119.956	0.00044181	1535.6973	3.07398E-05
NMNH452509	0.00154012	149.7179	0.000307221	2134.1252	1.87949E-05
HTB0889	0.00229381	NA	NA	NA	NA
HTB0890	0.00183056	139.092	0.000446932	1967.8612	2.96862E-05
HTB0900	0.00208789	137.0673	0.000455239	1817.7158	2.8211E-05
HTB1025	0.00177559	141.6811	0.000479359	1864.0021	2.94701E-05
HTB1027	0.00219797	NA	NA	NA	NA
HTB1028	NA	92.4627	0.000521909	783.1742	2.42228E-05
HTB1043	NA	149.8273	0.000442573	2169.961	2.8873E-05
HTB1503	0.00190224	89.7625	0.000495582	769.1409	2.32047E-05
PC.SUDANII.26	0.00175036	167.6565	0.000396809	2875.6066	3.21037E-05
HTB0828	0.00194517	175.2915	0.0004383	3312.9504	3.9635E-05
NMNH337250	0.00147026	150.4037	0.000359775	2056.5575	2.27751E-05
NMNH337253	0.00154921	134.1349	0.000343022	1641.5758	1.93456E-05
HTB0891	0.00214908	134.8978	0.000477779	1720.5728	3.01678E-05
HTB1207	NA	111.4493	0.000421524	1415.5013	2.5739E-05

Name	H.dist.lmin	H.dist.lmin.s	H.dist.MaxXrad	H.dist.MaxYrad	H.dist.J
NMNH23976	4406.009	3.03021E-05	10.3818	9.4018	10320.8528
NMNH162899	NA	NA	NA	NA	NA
NMNH354984	2013.2263	1.86082E-05	10.3444	7.7625	5837.573
NMNH354987	1691.1109	1.46826E-05	8.3889	8.1254	4478.6152
NMNH354988	2267.0268	1.95097E-05	9.6229	7.6656	6222.9332
NMNH354989	2602.9005	2.43112E-05	10.5736	7.9198	7083.9181
NMNH354992	698.2317	1.43248E-05	5.5788	6.8095	1703.4064
NMNH354993	2617.9658	1.96052E-05	8.9582	8.0241	6247.431
NMNH384223	2535.6312	1.89316E-05	8.1922	10.3496	6446.6644
NMNH384227	1533.4275	1.99552E-05	7.7194	8.2596	3788.9857
NMNH384228	1644.3101	1.99168E-05	8.1605	7.977	4376.486
NMNH384229	2112.0612	1.78491E-05	9.1406	7.7914	5211.4073
NMNH384235	1142.7536	1.6035E-05	6.4295	7.4626	2898.8882
NMNH384238	931.4711	1.44388E-05	7.4593	6.1049	2475.531
NMNH395440	2700.7458	2.15936E-05	8.0065	9.1246	6758.5672
NMNH395441	796.1145	1.53141E-05	5.7005	6.8134	2048.6862
PC.C212	3460.1786	2.49594E-05	9.6564	9.3679	8470.9695
PC.CAMII.160	3759.2457	2.47417E-05	9.6929	8.8935	8608.4309
NMNH384238	731.1289	1.42343E-05	6.8702	5.8584	1952.5054
NMNH384239	975.6205	1.93927E-05	7.0637	6.2846	2499.1604
NMNH452508	910.8835	1.8233E-05	6.1026	7.3937	2446.5808
NMNH452509	1542.6014	1.35855E-05	6.9185	7.9918	3676.7266
HTB0889	NA	NA	NA	NA	NA
HTB0890	1294.3245	1.95255E-05	6.7692	8.5517	3262.1857
HTB0900	1284.2335	1.99313E-05	7.4244	6.9318	3101.9493
HTB1025	1433.7458	2.26677E-05	6.9895	7.7868	3297.7479
HTB1027	NA	NA	NA	NA	NA
HTB1028	618.1198	1.91178E-05	5.4645	5.9433	1401.294
HTB1043	1537.0756	2.0452E-05	7.1148	7.7395	3707.0366
HTB1503	562.4251	1.69681E-05	5.9296	5.2928	1331.566
PC.SUDANII.26	1877.6527	2.09624E-05	8.7928	7.2123	4753.2593
HTB0828	1942.9104	2.32443E-05	9.6385	7.3536	5255.8608
NMNH337250	1658.8457	1.83706E-05	7.2725	7.4529	3715.4032

Name	H.dist.lmin	H.dist.lmin.s	H.dist.MaxXrad	H.dist.MaxYrad	H.dist.J
NMNH337253	1326.6401	1.56341E-05	7.725	7.1309	2968.2158
HTB0891	1251.0736	2.19358E-05	6.7253	7.2535	2971.6464
HTB1207	760.7021	1.38324E-05	6.7568	6.3109	2176.2034
Name	**H.dist.J.s**	**H.dist.ZpEst**	**H.dist.ZpEst.s**	**H.mid.TA**	**H.mid.TA.s**
NMNH23976	7.09812E-05	1043.37	0.00169348	284.5189	0.000461797
NMNH162899	NA	NA	NA	NA	NA
NMNH354984	5.39566E-05	644.79	0.00133499	191.2969	0.000396066
NMNH354987	3.88842E-05	542.39	0.00107604	169.0683	0.000335412
NMNH354988	5.35537E-05	719.89	0.00141872	216.6733	0.000427007
NMNH354989	6.61642E-05	766.10	0.00162786	207.098	0.000440055
NMNH354992	3.49467E-05	275.00	0.00105503	122.2432	0.00046898
NMNH354993	4.67853E-05	735.76	0.00129482	206.5037	0.000363416
NMNH384223	4.81324E-05	695.37	0.00118892	223.5123	0.000382155
NMNH384227	4.93078E-05	474.25	0.00125900	166.4283	0.000441825
NMNH384228	5.30104E-05	542.40	0.00134025	179.4955	0.000443526
NMNH384229	4.40419E-05	615.57	0.00117570	188.9917	0.000360962
NMNH384235	4.06768E-05	417.34	0.00117708	149.4358	0.00042147
NMNH384238	3.83733E-05	365.01	0.00113160	134.5321	0.000417077
NMNH395440	5.40377E-05	789.04	0.00144785	204.3746	0.000375018
NMNH395441	3.94086E-05	327.43	0.00117150	110.0757	0.00039384
PC.C212	6.11038E-05	890.54	0.00152243	220.7343	0.000377358
PC.CAMII.160	5.66568E-05	926.32	0.00144489	239.698	0.000373888
NMNH384238	3.80133E-05	306.79	0.00111693	105.1932	0.000382977
NMNH384239	4.96764E-05	374.45	0.00140303	126.9284	0.000475583
NMNH452508	4.89728E-05	362.56	0.00133533	136.3964	0.000502362
NMNH452509	3.23804E-05	493.18	0.00101200	154.642	0.000317325
HTB0889	NA	NA	NA	NA	NA
HTB0890	4.92117E-05	425.85	0.00136834	147.144	0.000472805
HTB0900	4.81423E-05	432.14	0.00143526	155.0532	0.000514976
HTB1025	5.21378E-05	446.36	0.00151019	157.5635	0.000533095
HTB1027	NA	NA	NA	NA	NA
HTB1028	4.33406E-05	245.67	0.00138671	97.7734	0.000551886
HTB1043	4.9325E-05	499.12	0.00147434	158.8736	0.000469294
HTB1503	4.01728E-05	237.31	0.00131017	87.1888	0.000481373
PC.SUDANII.26	5.3066E-05	593.97	0.00140580	182.6139	0.00043221
HTB0828	6.28794E-05	618.62	0.00154681	175.2245	0.000438132
NMNH337250	4.11457E-05	504.63	0.00120709	156.5738	0.000374534
NMNH337253	3.49797E-05	399.60	0.00102190	136.1935	0.000348287
HTB0891	5.21036E-05	425.16	0.00150584	150.2521	0.00053216
HTB1207	3.95714E-05	333.07	0.00125972	113.9132	0.000430843
Name	**H.mid.lmax**	**H.mid.lmax.s**	**H.mid.lmin**	**H.mid.lmin.s**	**H.mid.MaxXrad**
NMNH23976	8468.8833	5.82444E-05	4984.6436	3.42817E-05	9.51
NMNH162899	NA	NA	NA	NA	NA
NMNH354984	4013.2856	3.70947E-05	2155.6865	1.9925E-05	7.7523
NMNH354987	3139.654	2.72591E-05	1662.4876	1.44341E-05	8.6331
NMNH354988	4877.7613	4.19773E-05	2919.1783	2.5122E-05	8.5743
NMNH354989	4754.1815	4.44043E-05	2464.5849	2.30194E-05	7.4674
NMNH354992	1658.3278	3.40219E-05	859.0409	1.76239E-05	6.2275
NMNH354993	4722.0225	3.53619E-05	2477.9727	1.85569E-05	8.5138
NMNH384223	5356.5447	3.99933E-05	2983.3681	2.22746E-05	9.8863
NMNH384227	2949.5171	3.83834E-05	1654.3115	2.15283E-05	8.376
NMNH384228	3413.3876	4.13449E-05	1937.4642	2.34676E-05	8.9088
NMNH384229	3948.9693	3.33729E-05	2068.7145	1.74828E-05	8.8641
NMNH384235	2322.447	3.25883E-05	1367.0724	1.91826E-05	7.5835
NMNH384238	1720.2633	2.66659E-05	1215.0853	1.88351E-05	6.5686
NMNH395440	4271.6497	3.41537E-05	2632.2184	2.10457E-05	8.902
NMNH395441	1178.3838	2.26674E-05	791.5448	1.52262E-05	6.0762
PC.C212	4875.5036	3.51686E-05	3115.6296	2.2474E-05	9.6884
PC.CAMII.160	5781.5827	3.80518E-05	3665.7386	2.41262E-05	9.0384
NMNH384238	1075.3081	2.09351E-05	725.73	1.41292E-05	6.1466
NMNH384239	1611.3982	3.20302E-05	1023.8579	2.03515E-05	6.4428

Name	H.mid.lmax	H.mid.lmax.s	H.mid.lmin	H.mid.lmin.s	H.mid.MaxXrad
NMNH452508	1775.5402	3.55407E-05	1242.7508	2.4876E-05	6.7108
NMNH452509	2455.18	2.16224E-05	1490.4364	1.3126E-05	7.5818
HTB0889	NA	NA	NA	NA	NA
HTB0890	2305.0089	3.47722E-05	1317.9415	1.98818E-05	7.8292
HTB0900	2490.163	3.86474E-05	1476.2064	2.29107E-05	6.1698
HTB1025	2436.2077	3.85167E-05	1615.652	2.55436E-05	7.8757
HTB1027	NA	NA	NA	NA	NA
HTB1028	926.8259	2.86658E-05	627.4518	1.94064E-05	5.6272
HTB1043	2621.3082	3.48786E-05	1562.7145	2.07931E-05	7.6662
HTB1503	815.3892	2.46E-05	453.2425	1.36741E-05	5.4513
PC.SUDANII.26	3180.3631	3.5506E-05	2234.7522	2.49491E-05	7.6079
HTB0828	3309.8479	3.95979E-05	1807.0082	2.16184E-05	7.2746
NMNH337250	2494.9462	2.76299E-05	1536.548	1.70163E-05	7.8682
NMNH337253	1948.9683	2.29681E-05	1131.2312	1.33313E-05	7.7003
HTB0891	2312.687	4.05497E-05	1407.0893	2.46713E-05	7.8156
HTB1207	1225.8086	2.22897E-05	878.485	1.59741E-05	6.3374
Name	**H.mid.MaxYrad**	**H.mid.J**	**H.mid.J.s**	**H.mid.ZpEst**	**H.mid.ZpEst.s**
NMNH23976	11.0369	13453.5268	9.25261E-05	1309.54	0.00212549
NMNH162899	NA	NA	NA	NA	NA
NMNH354984	9.1288	6168.972	5.70197E-05	730.87	0.00151322
NMNH354987	6.5317	4802.1416	4.16932E-05	633.33	0.00125645
NMNH354988	9.5453	7796.9396	6.70993E-05	860.61	0.00169604
NMNH354989	9.2466	7218.7664	6.74237E-05	863.80	0.00183545
NMNH354992	7.0703	2517.3687	5.16458E-05	378.61	0.00145254
NMNH354993	9.1916	7199.9952	5.39188E-05	813.31	0.00143131
NMNH384223	7.8719	8339.9128	6.22678E-05	939.27	0.00160594
NMNH384227	6.1852	4603.8286	5.99117E-05	632.34	0.00167871
NMNH384228	6.6968	5350.8518	6.48125E-05	685.76	0.00169449
NMNH384229	8.0332	6017.6837	5.08557E-05	712.27	0.00136038
NMNH384235	6.9679	3689.5194	5.17708E-05	507.10	0.00143023
NMNH384238	6.6147	2935.3486	4.55009E-05	445.31	0.00138056
NMNH395440	7.9645	6903.8682	5.51994E-05	818.65	0.00150218
NMNH395441	6.2152	1969.9285	3.78936E-05	320.54	0.00114685
PC.C212	8.1686	7991.1332	5.76426E-05	895.01	0.00153008
PC.CAMII.160	9.7147	9447.3213	6.2178E-05	1007.55	0.00157160
NMNH384238	5.709	1801.0381	3.50643E-05	303.83	0.00110615
NMNH384239	6.6137	2635.2562	5.23817E-05	403.67	0.00151249
NMNH452508	6.788	3018.2909	6.04167E-05	447.19	0.00164706
NMNH452509	6.8385	3945.6165	3.47485E-05	547.23	0.00112292
HTB0889	NA	NA	NA	NA	NA
HTB0890	6.3499	3622.9504	5.4654E-05	511.03	0.00164204
HTB0900	7.8725	3966.3694	6.15581E-05	564.92	0.00187625
HTB1025	6.6153	4051.8597	6.40604E-05	559.22	0.00189206
HTB1027	NA	NA	NA	NA	NA
HTB1028	5.9943	1554.2777	4.80722E-05	267.48	0.00150982
HTB1043	6.8563	4184.0227	5.56717E-05	576.21	0.00170207
HTB1503	5.4131	1268.6316	3.82741E-05	233.54	0.00128938
PC.SUDANII.26	8.0688	5415.1153	6.04551E-05	690.85	0.00163510
HTB0828	7.9859	5116.8562	6.12164E-05	670.60	0.00167678
NMNH337250	7.271	4031.4942	4.46462E-05	532.59	0.00127399
NMNH337253	6.5493	3080.1995	3.62994E-05	432.32	0.00110557
HTB0891	6.2592	3719.7763	6.5221E-05	528.57	0.00187209
HTB1207	6.1934	2104.2936	3.82638E-05	335.86	0.00127029
Name	**H.prox.TA**	**H.prox.TA.s**	**H.prox.lmax**	**H.prox.lmax.s**	**H.prox.lmin**
NMNH23976	321.8133	0.000522329	10944.0289	7.52671E-05	7207.7448
NMNH162899	NA	NA	NA	NA	NA
NMNH354984	204.0577	0.000422487	4876.2946	4.50715E-05	2404.0576
NMNH354987	213.0699	0.000422706	5065.002	4.39754E-05	2844.3256
NMNH354988	246.883	0.000486543	6419.577	5.5246E-05	4164.3845
NMNH354989	263.2002	0.000559264	7123.4878	6.65338E-05	4788.5311
NMNH354992	136.5992	0.000524056	1862.5903	3.82125E-05	1355.2156

Name	H.prox.TA	H.prox.TA.s	H.prox.lmax	H.prox.lmax.s	H.prox.lmin
NMNH354993	236.9501	0.000416997	5939.2621	4.44775E-05	3634.6701
NMNH384223	266.7272	0.000456042	8354.5972	6.23775E-05	4338.7126
NMNH384227	190.8166	0.000506569	3968.3071	5.16414E-05	2275.6868
NMNH384228	205.6375	0.000508122	4377.9881	5.30286E-05	3009.3287
NMNH384229	235.6426	0.000450062	6290.3381	5.31599E-05	3444.9398
NMNH384235	177.5429	0.000500743	3374.6336	4.73524E-05	2086.1738
NMNH384238	150.4166	0.000466322	2247.7549	3.48425E-05	1615.3278
NMNH395440	222.5169	0.000408308	4937.2627	3.94756E-05	3493.2478
NMNH395441	121.7359	0.000435559	1470.562	2.82878E-05	1036.7835
PC.C212	256.8173	0.000439044	7017.9487	5.06227E-05	4560.6797
PC.CAMII.160	273.0493	0.00042591	7905.8087	5.20325E-05	5106.2786
NMNH384238	122.0469	0.000444336	1540.4071	2.99901E-05	1033.8789
NMNH384239	130.4962	0.000488951	1776.8061	3.5318E-05	1081.4395
NMNH452508	168.9137	0.000622126	2482.3863	4.96896E-05	2220.8866
NMNH452509	188.2298	0.000386247	3436.7971	3.02674E-05	2565.0851
HTB0889	NA	NA	NA	NA	NA
HTB0890	166.9362	0.000536402	3030.377	4.57148E-05	1919.35
HTB0900	169.527	0.000563047	3111.8244	4.82956E-05	1840.26
HTB1025	173.9788	0.000588634	3102.9033	4.90573E-05	2100.5106
HTB1027	NA	NA	NA	NA	NA
HTB1028	114.3874	0.000645664	1370.3499	4.23835E-05	875.3948
HTB1043	173.5461	0.000512635	3242.1644	4.31395E-05	2037.1175
HTB1503	98.179	0.00054205	1000.5222	3.01854E-05	626.7637
PC.SUDANII.26	195.7049	0.000463194	3514.7064	3.92387E-05	2998.2749
HTB0828	187.8616	0.00046973	3923.8892	4.69441E-05	2161.848
NMNH337250	195.3932	0.000467392	4389.9683	4.86161E-05	2535.8945
NMNH337253	153.3611	0.000392189	2631.3561	3.10099E-05	1474.1063
HTB0891	146.527	0.000518967	2377.3759	4.16839E-05	1365.2126
HTB1207	117.4223	0.000444115	1423.1437	2.5878E-05	925.6249

Name	H.prox.lmin.s	H.prox.MaxXrad	H.prox.MaxYrad	H.prox.J	H.prox.J.s
NMNH23976	4.9571E-05	11.2094	13.7855	18151.7737	0.000124838
NMNH162899	NA	NA	NA	NA	NA
NMNH354984	2.22207E-05	7.7439	9.9993	7280.3522	6.72921E-05
NMNH354987	2.4695E-05	9.5398	9.5102	7909.3276	6.86704E-05
NMNH354988	3.58381E-05	9.3861	11.885	10583.9615	9.10841E-05
NMNH354989	4.47251E-05	11.0209	10.6287	11912.0189	0.000111259
NMNH354992	2.78033E-05	8.8031	7.1236	3217.806	6.60158E-05
NMNH354993	2.7219E-05	9.6092	11.1439	9573.9322	7.16966E-05
NMNH384223	3.23939E-05	13.1988	9.6478	12693.3098	9.47714E-05
NMNH384227	2.96146E-05	8.8243	7.6028	6243.9939	8.12559E-05
NMNH384228	3.64507E-05	9.3972	9.1623	7387.3167	8.94793E-05
NMNH384229	2.91134E-05	9.1077	11.7569	9735.2779	8.22733E-05
NMNH384235	2.92729E-05	10.3245	7.5395	5460.8074	7.66253E-05
NMNH384238	2.50392E-05	7.5723	8.7595	3863.0827	5.98818E-05
NMNH395440	2.793E-05	10.511	9.0688	8430.5104	6.74056E-05
NMNH395441	1.99436E-05	8.1462	6.371	2507.3455	4.82314E-05
PC.C212	3.28977E-05	10.7571	11.2326	11578.6283	8.35204E-05
PC.CAMII.160	3.36072E-05	10.0662	12.4429	13012.0873	8.56397E-05
NMNH384238	2.01286E-05	7.0162	7.8611	2574.286	5.01187E-05
NMNH384239	2.1496E-05	6.6147	8.0586	2858.2456	5.68141E-05
NMNH452508	4.44552E-05	8.7468	8.2935	4703.2728	9.41447E-05
NMNH452509	2.25903E-05	9.2318	8.7355	6001.8822	5.28577E-05
HTB0889	NA	NA	NA	NA	NA
HTB0890	2.89544E-05	9.2059	8.2427	4949.727	7.46691E-05
HTB0900	2.85609E-05	7.7304	9.2336	4952.0844	7.68564E-05
HTB1025	3.32093E-05	8.519	8.3328	5203.4139	8.22666E-05
HTB1027	NA	NA	NA	NA	NA
HTB1028	2.70751E-05	8.1563	6.3145	2245.7446	6.94586E-05
HTB1043	2.71055E-05	9.3653	7.6584	5279.2819	7.0245E-05
HTB1503	1.89092E-05	6.0407	6.8326	1627.2859	4.90946E-05
PC.SUDANII.26	3.34732E-05	8.7532	9.3854	6512.9813	7.27118E-05

Name	H.prox.Imin.s	H.prox.MaxXrad	H.prox.MaxYrad	H.prox.J	H.prox.J.s
HTB0828	2.58636E-05	7.8982	9.4962	6085.7372	7.28077E-05
NMNH337250	2.80834E-05	11.5758	8.6996	6925.8628	7.66995E-05
NMNH337253	1.7372E-05	7.5521	8.9907	4105.4624	4.83819E-05
HTB0891	2.39371E-05	8.0218	7.3925	3742.5885	6.5621E-05
HTB1207	1.68313E-05	6.3949	8.0043	2348.7686	4.27092E-05
Name	**H.prox.ZpEst**	**H.prox.ZpEst.s**	**F.C.AP**	**H.C.AP**	**H.C.ML**
NMNH23976	1452.44	0.00235742	13.12	16.76	7.35
NMNH162899	NA	NA	12.11	13.48	6.55
NMNH354984	820.64	0.00169907	11.10	9.26	7.49
NMNH354987	830.38	0.00164737	10.53	7.61	8.59
NMNH354988	995.15	0.00196118	12.83	14.19	7.52
NMNH354989	1100.44	0.00233828	10.37	11.01	8.18
NMNH354992	404.08	0.00155022	10.35	10.80	5.22
NMNH354993	922.65	0.00162373	NA	12.46	10.25
NMNH384223	1111.18	0.00189986	12.78	13.39	8.53
NMNH384227	760.21	0.00201815	7.65	10.83	7.16
NMNH384228	796.07	0.00196705	6.88	9.57	4.60
NMNH384229	933.19	0.00178233	10.91	14.83	7.05
NMNH384235	611.38	0.00172433	9.21	11.03	7.70
NMNH384238	473.07	0.00146663	9.38	9.48	7.36
NMNH395440	861.14	0.00158016	10.03	8.01	9.63
NMNH395441	345.43	0.00123592	10.38	7.66	6.43
PC.C212	1053.10	0.00180033	12.12	13.96	6.58
PC.CAMII.160	1156.16	0.00180341	8.25	11.33	5.45
NMNH384238	346.07	0.00125993	8.83	8.11	6.89
NMNH384239	389.58	0.00145972	9.30	8.70	7.58
NMNH452508	552.02	0.00203314	9.91	NA	NA
NMNH452509	668.09	0.00137092	7.66	8.56	7.61
HTB0889	NA	NA	8.10	7.71	4.51
HTB0890	567.35	0.00182301	6.61	12.93	5.71
HTB0900	583.83	0.00193908	10.50	12.67	3.70
HTB1025	617.55	0.00208940	10.39	11.83	5.89
HTB1027	NA	NA	6.00	8.96	5.89
HTB1028	310.38	0.00175197	7.25	9.74	4.17
HTB1043	620.23	0.00183208	9.19	13.15	5.23
HTB1503	252.82	0.00139580	6.98	10.62	3.97
PC.SUDANII.26	718.13	0.00169968	8.60	13.09	6.96
HTB0828	699.74	0.00174962	8.15	11.59	6.71
NMNH337250	683.18	0.00163421	10.83	11.81	4.70
NMNH337253	496.34	0.00126930	10.20	12.32	7.02
HTB0891	485.60	0.00171989	8.62	11.53	3.75
HTB1207	326.24	0.00123389	8.71	12.16	2.67